Zeitschrift: IABSE congress report = Rapport du congrès AIPC = IVBH Kongressbericht

Band: 8 (1968)

Rubrik: Prepared discussion

DISCUSSION PRÉPARÉE / VORBEREITETE DISKUSSION / PREPARED DISCUSSION

Dynamic Behaviour of Structures and Dynamic Modeling

Le comportement dynamique des constructions et la simulation dynamique

Das dynamische Verhalten von Bauwerken und dynamische Simulation

JOSEPH G. ILLÉSSY
C.E., E.E.
Hungary

The constructions are due to the corpuscular nature of matter mechanical systems with large degree of freedom. The equations of motions can be derived from the equilibrium of the forces: in case of linear systems this whould lead - however only theoretically - to the very compact matrix-formulated set of the differential-equationsystem

$$\underline{\underline{M}}\,\ddot{\underline{x}} + \underline{\underline{C}}\,\dot{\underline{x}} + \underline{\underline{K}}\,\underline{x} = \underline{G} \qquad /1/$$

with N simultaneous equations [1],[2].

To overcome the difficulties caused by the very large, but nevertheless finite number $1 \ll N < \infty$, there are two different ways possible. The infinite increase of the degree of freedom results models of continuously distributed parameters, dealt mathematically by partial differential equations. Conversely the decrease of the degree is equivalent with the concentrating of the properties to $1 \leq n < N$ discret points: models with concentrated parameters. In praxis only the first dominating particular solutions of Eq./1/ are of interest, being characteristic for the total dynamic behaviour of the structure. From this point of view both type of models can be adapted equivalently; to that method is given preference, that optimally secures suitable results for the adapter.

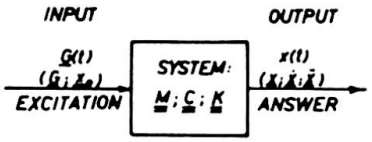

Fig.1.

The dynamical behaviour of a system /$\underline{\underline{M}}$,$\underline{\underline{C}}$,$\underline{\underline{K}}$/ with excitation $\underline{G}$, namely $\underline{F}$ force- and/or $\underline{x}$ displacement-excitation is characterized by the response $\underline{x}$,$\dot{\underline{x}}$,$\ddot{\underline{x}}$ /Fig.1/. This means methematically the transform of Eq./1/ to its explicite form. The modern high-speed electronic compu-

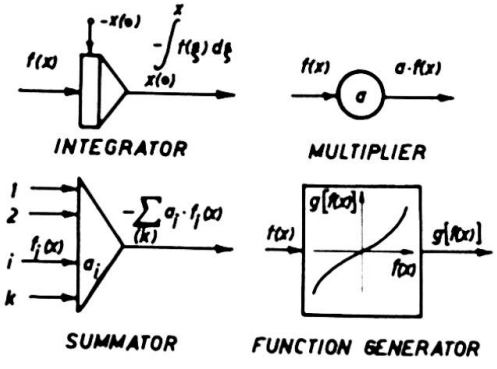

Fig.2.

ters offer due to the rapid flow of information an easy possibility for solving Eq./1/. In digital computers the simultaneous integration is produced by stepwise iteration. In possession of the elements of the analogue computers /Fig.2./ the mathematical Eq./1/ can be simulated electrically by a "laboratory model"; the several differential-equations represent in the logic block-diagram product-sums based on integrating chains and are easily realizable by means of electric circuits.

The internal mass, damping- and spring-forces of a nonlinear vibrator of unique degree of freedom are in equilibrium with the external forces of excitation:

$$F_m + F_c + F_k = m\ddot{x} + F_c/\dot{x}/ + F_k/x/ = F_G = G \qquad /2'/$$

or after mathematical rearrangement - without altering the physical information-content -

$$\ddot{x}/t/ = \frac{1}{m}\left[c\left(-\int_o^t x/\tau/d\tau - k\int_o^t x/\tau/d\tau + G/t/\right)\right] \qquad /2''/$$

The logic block-structure of Eq./2/, Fig.3, is in addition the principal programing plan and switching graph of the equivalent simulating model, the analogue computer.

One of the simplest mind-model of a springed vehicle with one degree of freedom is to be seen on Fig.4. /by ignoring the pitching component of the movement/. Jumpes of the two axes at a velocity v_o can be represented in the model by twin pulses. In case of linear system the matrices of Eq./1/ have the actual form:

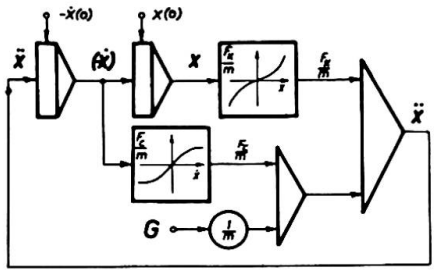

Fig.3.

$$\underline{\underline{M}} = \begin{bmatrix} m & o \\ o & o \end{bmatrix};\quad \underline{\underline{C}} = \begin{bmatrix} c & -c \\ -c & c \end{bmatrix};\quad \underline{\underline{K}} = \begin{bmatrix} k & -k \\ -k & k \end{bmatrix};$$

$$\text{and } \underline{G} = \begin{bmatrix} mg \\ o \end{bmatrix} \qquad /3'/$$

if time-dependent force-excitation is missing. Expressing the derivatives of the highest order by the other terms:

$$x = \frac{c}{m}\left(-\dot{x}\right) - \frac{c}{m}\left(-\dot{x}_o\right) - \frac{k}{m}\left(-x_o\right) + g \qquad /3''/$$

$$-x_o = \left(-\dot{x}\right) - \frac{k}{c}x - \frac{k}{c}\left(-x_o\right)$$

Fig.9.a illustrates the logic block-diagram of Eq./3/.

Constructions loaded by space- and time-variable moving loads get their new, deformed shape of equilibrium only after the decay of transient oscillations; the final shape however can be derived by well-known statical treatments too. As mentioned above, in praxis the interesting modes of maximal amplitudes /that of the lowest natural frequencies/ dominate and are characteristic for the dynamical behaviour of the structure. The reduction of the degree of freedom is to be carried out in such a manner, that these modes of technical interest should be included by the selected model.

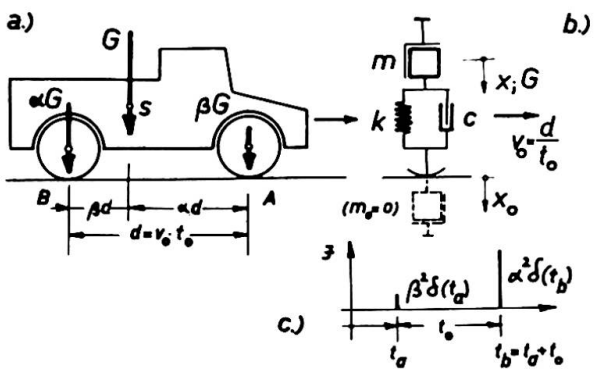

Fig. 4.

For illustration let us take a special archstiffened sing-

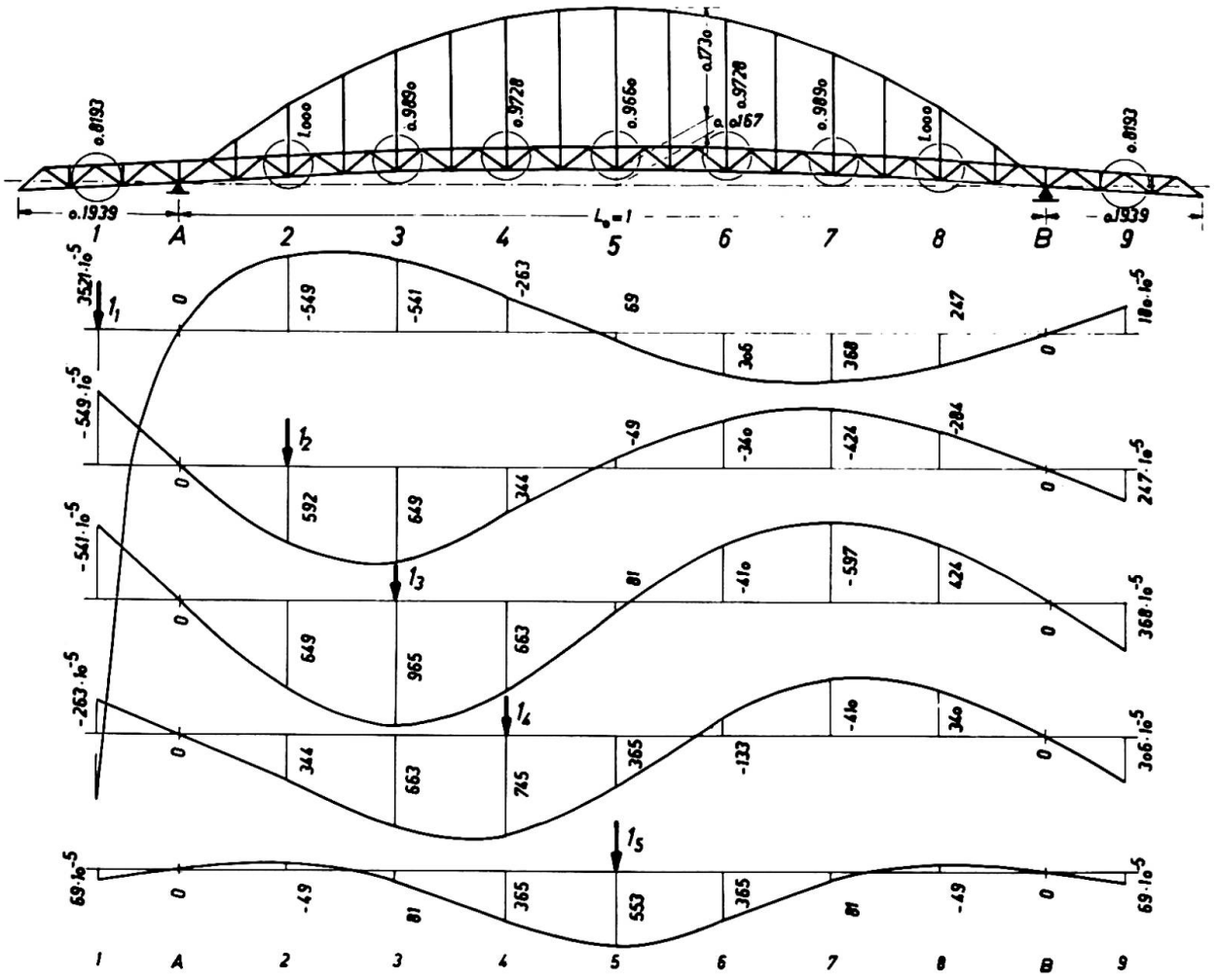

Fig. 5.

le span bridge construction: a Gerber-truss /Fig.5/, the two side-extensions of which being cantilevers; only the last secondary longitudional girders of the deck-plate are on both sides pin-connected with the bridge and the abutments, respectively. The total statical informations are involved in the matrix of the displacement influence-line ordinates; for dynamical behaviour the mass- and the damping-distributions are needed too.

The derivation of the mass-matrix $\underline{\underline{M}}$ implies principally no difficulties. For the actual damping conditions are hardly to be seized exactly, consequently for simpler numerical algorithms it is assumed, that the damping-matrix $\underline{\underline{C}}$ is diagonal /physically: presence of only grounded dampers/. The direct determination of the spring-matrix $\underline{\underline{K}}$ is often quite troublesome indeed; but in statics convenient methods are available for the computation of the displacement-influence-lines $[\eta_{kl}] = \underline{\underline{H}}$, the inversion of $\underline{\underline{H}}$ being a submatrix of $\underline{\underline{K}}$:

$$\underline{\underline{H}}^{-1} = \underline{\underline{K}}_R \qquad /4/$$

The missing elements are to be determined by the reciprocity-law of Maxwell /$k_{ij}=k_{ji}$/, the equilibrium of the forces embodied in $\underline{k}_j$, fundamental relation: $\sum_{i=1}^{n} k_{ij} = o$, respectively.

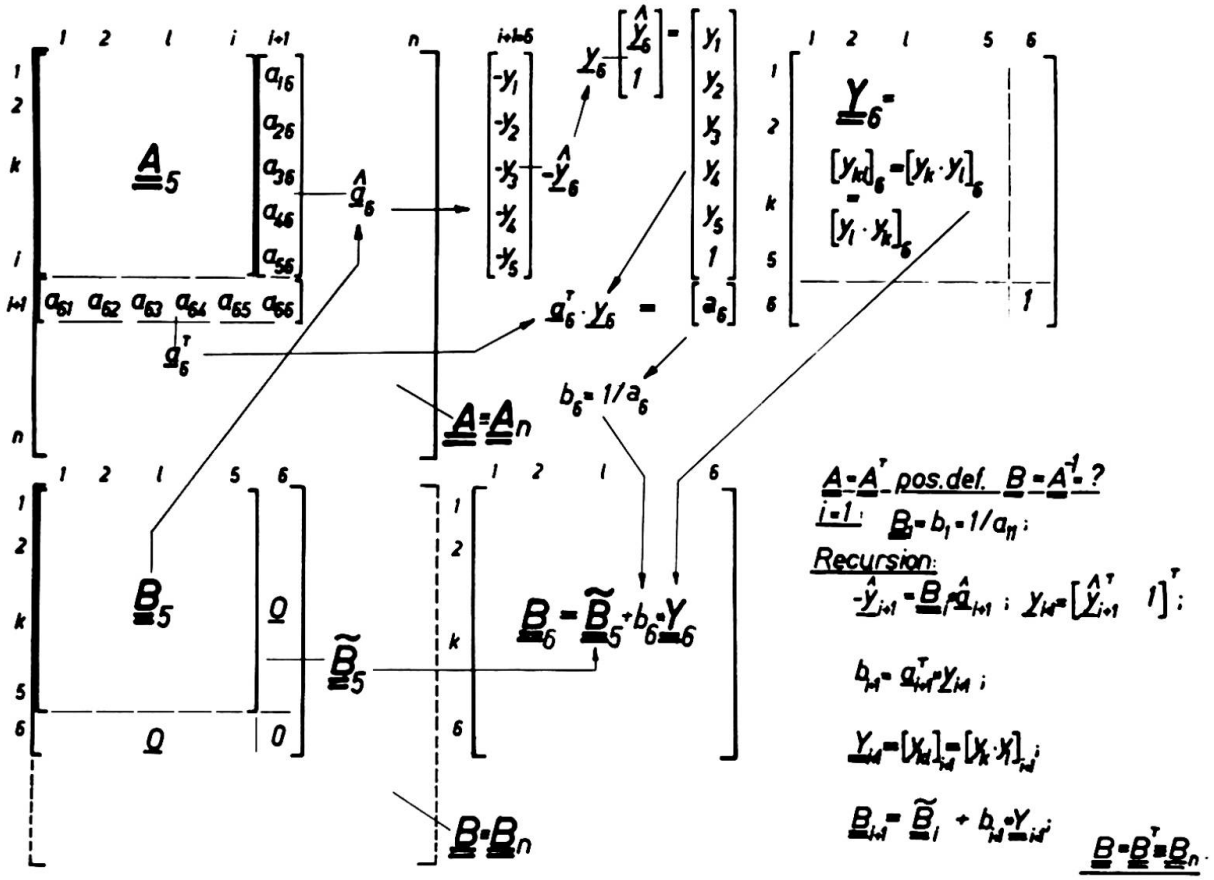

Fig. 6.

Fig.6. gives a recoursive procedure for matrix-inversion like Eq./4/ for symmetrical and positively definite matrices, common in linear structural engineering. Among others, the given method has the advantage, that all mathematical steps can be interpreted mechanically too[3].

For symmetrical constructions all asymmetrical effects can be resolved into symmetrical and antimetrical components; applying this to Eq./1/ :

$$\underline{\underline{M}}_S \ddot{\underline{y}} + \underline{\underline{C}}_S \dot{\underline{y}} + \underline{\underline{K}}_S \underline{y} = \frac{1}{2} \underline{\underline{E}} \underline{Y} + \frac{1}{2} \underline{\underline{K}}_{RS} \underline{y}_R \qquad /5'/$$

$$\underline{\underline{M}}_A \ddot{\underline{z}} + \underline{\underline{C}}_A \dot{\underline{z}} + \underline{\underline{K}}_A \underline{z} = \frac{1}{2} \underline{\underline{E}} \underline{Z} + \frac{1}{2} \underline{\underline{K}}_{RA} \underline{z}_R$$

where

$\underline{F} = \underline{Y} + \underline{Z}$ means the force-excitation,

$\underline{x}_R = \underline{y}_R + \underline{z}_R$ the displacement-excitation,

$\underline{x} = \underline{y} + \underline{z}$ the output displacement-vector, while

$$\underline{\underline{A}}_S = [a_{ik}]_S = a_{ik} + a_{n-(i-1),k}$$
$$\underline{\underline{A}}_A = [a_{ik}]_A = a_{ik} - a_{n-(i-1),k} \qquad /5''/$$

are the new matrices of the symmetric and antimetric components. Let us express the accelerations in terms of the other elements:

$$\underline{\underline{E}} \ddot{\underline{y}} = \underline{\underline{M}}^{-1} \left[\underline{\underline{C}} (-\dot{\underline{y}}) - \underline{\underline{K}}_S \underline{y} + \frac{1}{2} \underline{\underline{E}} \underline{Y} + \frac{1}{2} \underline{\underline{K}}_{RS} \underline{y}_R \right]$$
$$\underline{\underline{E}} \ddot{\underline{z}} = \underline{\underline{M}}^{-1} \left[\underline{\underline{C}} (-\dot{\underline{z}}) - \underline{\underline{K}}_A \underline{z} + \frac{1}{2} \underline{\underline{E}} \underline{Z} + \frac{1}{2} \underline{\underline{K}}_{RA} \underline{z}_R \right] \qquad /5'''/$$

These new equations represent the programing of the analogue computer, the simulation-equations of the analogue dynamic model [2].

a./

$$\begin{bmatrix} 0.8193 & & & & & & & & \\ & 1.0000 & & & & & & & \\ & & 0.9890 & & & & & & \\ & & & 0.9728 & & & & & \\ & & & & 0.9660 & & & & \\ & & & & & 0.9728 & & & \\ & & & & & & 0.9890 & & \\ & & & & & & & 1.0000 & \\ & & & & & & & & 0.8193 \end{bmatrix} \cdot \begin{bmatrix} \ddot{x}_1 \\ \ddot{x}_2 \\ \ddot{x}_3 \\ \ddot{x}_4 \\ \ddot{x}_5 \\ \ddot{x}_6 \\ \ddot{x}_7 \\ \ddot{x}_8 \\ \ddot{x}_9 \end{bmatrix} + \begin{bmatrix} 1.046 & & & & & & & & \\ & 5.993 & & & & & & & \\ & & 6.896 & & & & & & \\ & & & 6.966 & & & & & \\ & & & & 6.972 & & & & \\ & & & & & 6.966 & & & \\ & & & & & & 6.896 & & \\ & & & & & & & 5.993 & \\ & & & & & & & & 1.046 \end{bmatrix} \cdot \begin{bmatrix} \dot{x}_1 \\ \dot{x}_2 \\ \dot{x}_3 \\ \dot{x}_4 \\ \dot{x}_5 \\ \dot{x}_6 \\ \dot{x}_7 \\ \dot{x}_8 \\ \dot{x}_9 \end{bmatrix} +$$

$$+ \begin{bmatrix} +33.38 & +40.99 & -10.75 & +2.67 & -0.86 & -0.17 & +0.95 & -1.82 & -0.41 \\ +40.99 & +898.01 & -795.22 & +367.60 & -84.55 & +47.19 & +14.91 & +2.81 & -1.82 \\ -10.75 & -795.22 & +1202.06 & -890.79 & +404.87 & -102.70 & +46.96 & +14.91 & +0.95 \\ +2.67 & +367.60 & -890.79 & +1247.18 & -917.07 & +417.93 & -102.70 & -47.19 & +0.17 \\ -0.86 & -84.55 & +404.87 & -917.07 & +1258.06 & -917.07 & +404.87 & -84.55 & -0.86 \\ -0.17 & +47.19 & -102.70 & +417.93 & -917.07 & +1247.18 & -890.79 & +367.60 & +2.67 \\ +0.95 & +14.91 & +46.96 & -102.70 & +404.87 & -890.79 & +1202.06 & -795.22 & -10.75 \\ -1.82 & +2.81 & +14.91 & +47.19 & -84.55 & +367.60 & -795.22 & +898.01 & +40.99 \\ -0.41 & -1.82 & +0.95 & -0.17 & -0.86 & +2.67 & -10.75 & +40.99 & +33.38 \end{bmatrix} \cdot \begin{bmatrix} x_1 \\ x_2 \\ x_3 \\ x_4 \\ x_5 \\ x_6 \\ x_7 \\ x_8 \\ x_9 \end{bmatrix} =$$

$$= \begin{bmatrix} F_1 \\ F_2 \\ F_3 \\ F_4 \\ F_5 \\ F_6 \\ F_7 \\ F_8 \\ F_9 \end{bmatrix} + \begin{bmatrix} -65.66 & +1.68 \\ -443.74 & -46.18 \\ +185.37 & -55.66 \\ -114.40 & -57.44 \\ -31.42 & -31.42 \\ -57.44 & -114.40 \\ -55.66 & +185.37 \\ -46.18 & -443.74 \\ +1.68 & -65.66 \end{bmatrix} \cdot \begin{bmatrix} x_A \\ x_B \end{bmatrix}$$

b./

$$\ddot{\underline{x}} = \begin{bmatrix} +1.277 \\ +5.993 \\ +6.973 \\ +7.161 \\ +7.217 \end{bmatrix} \cdot (-\ddot{\underline{z}}) + \begin{bmatrix} -40.24 & -47.81 & +11.98 & -3.05 & +1.05 \\ -39.17 & -900.82 & +780.31 & -414.79 & +84.55 \\ +9.91 & +788.99 & -1262.91 & +1004.54 & -409.37 \\ -2.57 & -426.39 & +1021.27 & -1711.67 & +942.71 \\ +1.78 & +175.05 & -838.24 & +1898.70 & -1302.34 \end{bmatrix} \cdot \underline{x} + \begin{bmatrix} 0.6102 \\ 0.5000 \\ 0.5056 \\ 0.5140 \\ 0.5176 \end{bmatrix} \cdot \underline{\ddot{x}} + \begin{bmatrix} -39.04 \\ -244.96 \\ +65.58 \\ -88.32 \\ -32,53 \end{bmatrix} \cdot \ddot{x}_R$$

$$\ddot{\underline{z}} = \begin{bmatrix} +1.277 \\ +5.993 \\ +6.973 \\ +7.161 \\ 0 \end{bmatrix} \cdot (-\ddot{\underline{z}}) + \begin{bmatrix} -41.24 & -52.25 & +14.28 & -3.47 & 0 \\ -42.81 & -895.20 & +810.13 & -320.41 & 0 \\ +11.83 & +819.14 & -1167.94 & +796.85 & 0 \\ -2.92 & -329.37 & +810.12 & -852.44 & 0 \\ 0 & 0 & 0 & 0 & 0 \end{bmatrix} \cdot \underline{z} + \begin{bmatrix} 0.6102 \\ 0.5000 \\ 0.5056 \\ 0.5140 \\ 0 \end{bmatrix} \cdot \underline{\ddot{z}} + \begin{bmatrix} -41.10 \\ -198.78 \\ +121.86 \\ -29.28 \\ 0 \end{bmatrix} \cdot \ddot{z}_R$$

Table 1.

Table 1. gives the actual values of the selected illustrative problem of Fig.5. The values are in the normed form of Eq./1/ and Eq./5/, respectively, with the units of m_e = 60 kp s^2/cm; k_e = 114,6 kp/cm; x_e = 1 cm; t_e = 0.724 s; F_e = 114.6 kp; ω_e = 1.382 r/s; f_e =0.220 c/s.

The logic block-diagram of the above equations is to be seen in the lower part of Fig 9 b.

If a moving vehicle is crossing a bridge, the wheel-forces excite vibrations in the bridge-construction, which conversely generates the displacement-excitations of the vehicle /Fig.7/, the mutual feedback varying with the position of the load nonlinearily,

even if the separate systems are linear. The several components of the excitation are on one hand the dead-load weights and the eventual centrifugal forces caused by the rotating excentricities of the motor, the forced movement of the roling load along the vertival trace of the deckplate. On the other hand there may be dead loads or vibrators located at fixed points of the construction; wind- and earthquake-forces are of this kind.

The difficulties caused by the continuous space-variation of the load in a model of discrete concentration of parameters can be removed by the adaptation of the well-known lever-law approximately, explained in Fig.8.

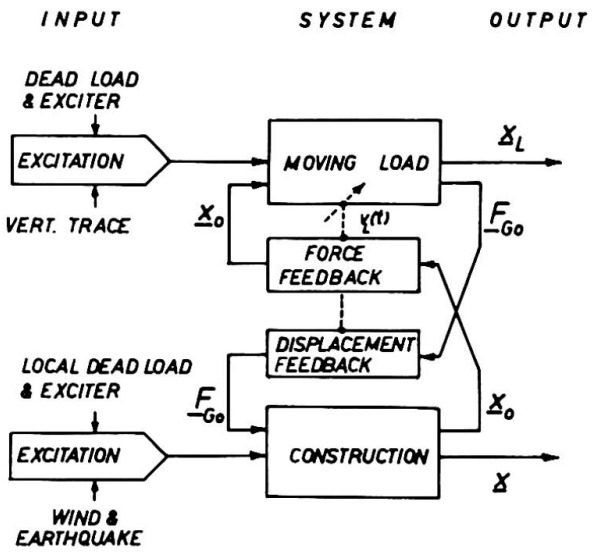

Fig.7.

Should all effects of possible excitations taken simultaneously into consideration, then the model is to be build up by the principles shown in Fig.9 a. and b. The variable, nonlinear feedback-systems are based on the application of the lever-rule, mentioned above and can be easily realised electrically by means of sliding potentiometers. The sliding contacts are to be moved with such a relative velocity, that the actual vehicle under consideration may have; research studies on motor accelerations, as well as brakings can be made without difficulties. If the model of the moving vehicle has several degrees of freedom, the feedback-systems are of multichannel type, of course.

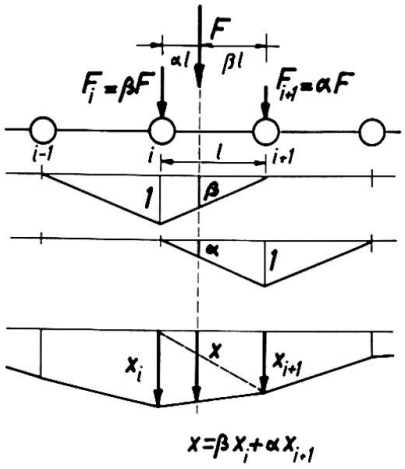

Fig.8.

In practice the several effects can be studied naturally separately too, but it is always to be kept in mind, that the systems with space-variable loads are nonlinear and the linear law of superposition is not yet valid.

For practical purposes often only the eigenvalues of the unloaded structure are of technical interest, being characteristic parameters of the total dynamical behaviour. The spring-matrix may be generally given in form of displacement-influenceline ordinates. In this case even the matrix-inversion of $\underline{\underline{H}}^{-1} = \underline{\underline{K}}_R$ is redundant. Pre-multiplying Eq./1/ by $\underline{\underline{K}}^{-1} = \underline{\underline{H}}$, we get another mathematical form of the Eq./1/:

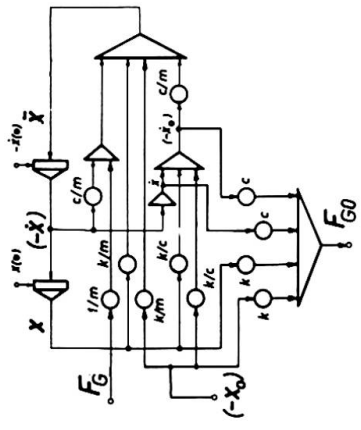

Fig. 9 a.

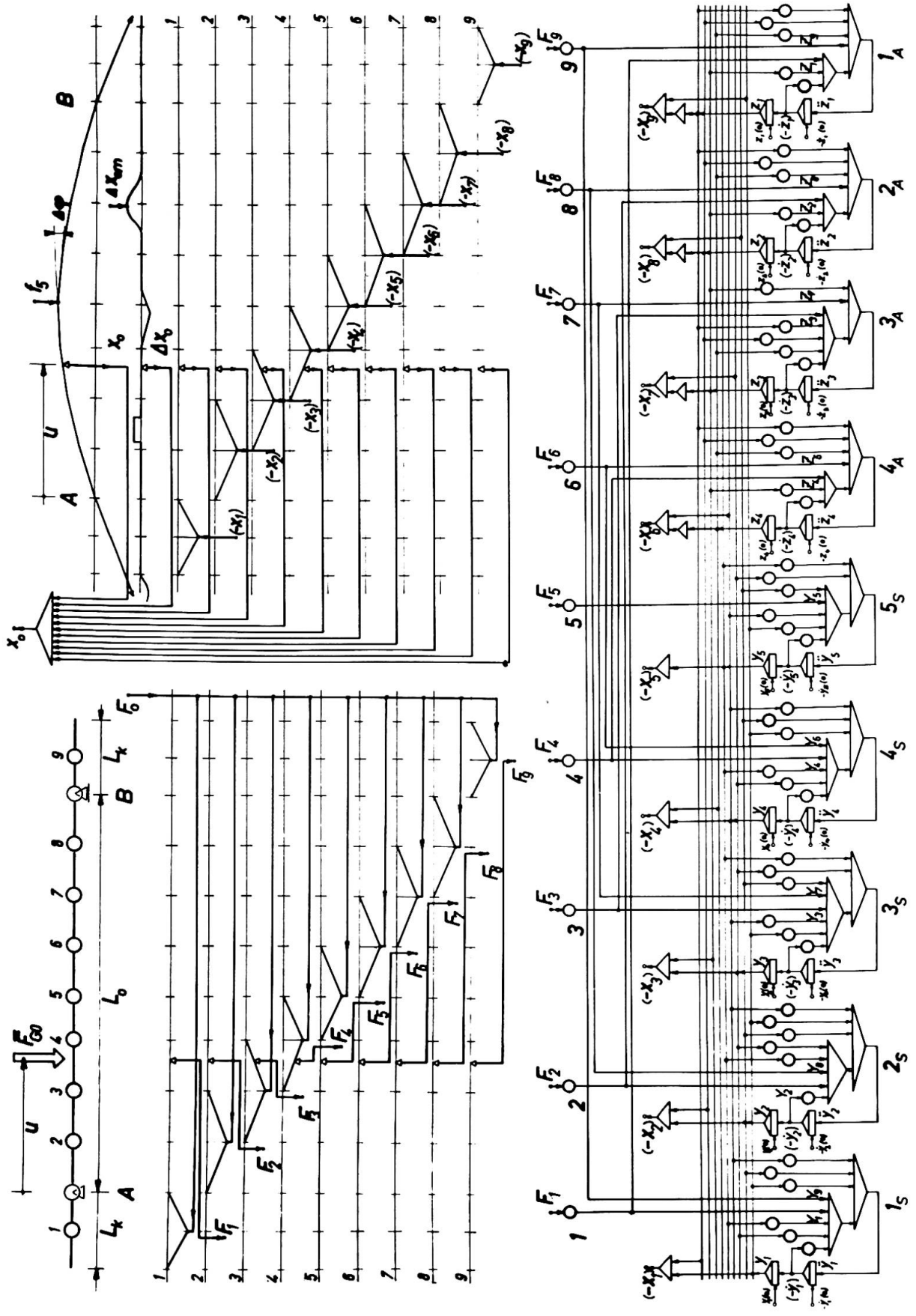

Fig. 9 b.

$$\underline{\underline{H}}\,\underline{\underline{M}}\,\ddot{\underline{x}} + \underline{\underline{K}}_R^{-1}\underline{\underline{C}}\,\dot{\underline{x}} + \underline{\underline{E}}\,\underline{x} = \underline{\underline{A}}\,\ddot{\underline{x}} + \underline{\underline{D}}\,\dot{\underline{x}} + \underline{\underline{E}}\,\underline{x} = \underline{o} \qquad /6'/$$

Developing the accelerations to the main diagonal $\langle \underline{\underline{A}}_{Tr} \rangle$ of $\underline{\underline{A}}$:

$$\underline{\underline{E}}\,\ddot{\underline{x}} = \langle \underline{\underline{A}}_{Tr} \rangle^{-1} \left[-\left(\underline{\underline{A}} - \langle \underline{\underline{A}}_{Tr} \rangle \right) \ddot{\underline{x}} - D\,\underline{x} - \underline{\underline{E}}\,\underline{x} \right] \qquad /6''/$$

only grounded dampings are assumed again.

Resolving Eq./6/ again into symmetric and antimetric components, the logical block-diagram decomposes into two independent separate parts; for the illustrative problem shown in Fig.1o.

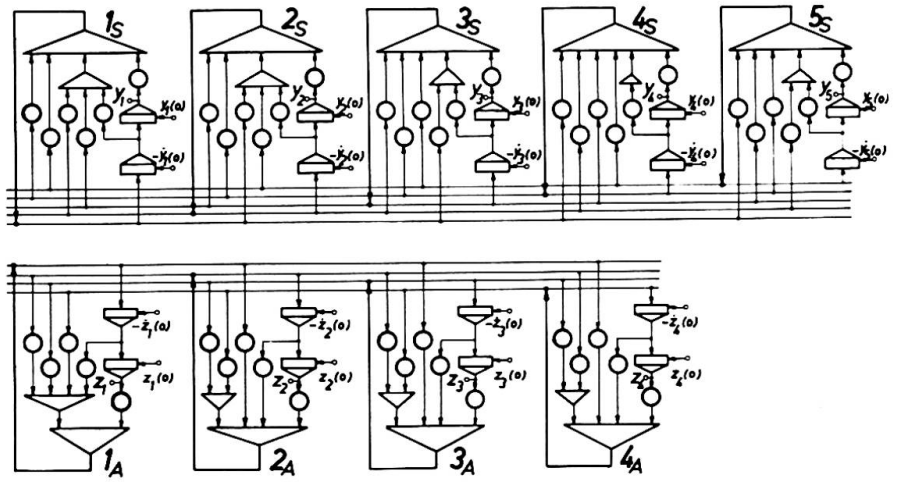

Fig. 1o.

The numerical determination of the natural frequencies leads to the roots of a polinomial with a degree - in our case of the illustrative problem - n = 9 with relative differences in the coefficients of 437 dB /namely from the numerical order of the extreme $1o^{22}$!/ The relative order of the roots however are only yet about 64 dB, /namely $1o^{3}$/ . But the technically interesting naturally frequencies varies only in the range of f_n = 1 - 15 c/s /See Fig. 11/.

With respect to the eigenvalues in analogue computation, only the approximative shape $\underline{x}_n'$ of the exact natural mode $\underline{x}_n$ is needed, but not the value of the natural frequency. Giving to the simulating dynamic model the initial conditions $\underline{x}(o) = \underline{x}_n'$ and $\dot{\underline{x}}(o) = \underline{o}$, then dominant oscillations with the natural frequency f_n occurs, superposed by decaying transients of the other harmonics.For the exact, accurate natural mode $\underline{x}_n$ /ini-

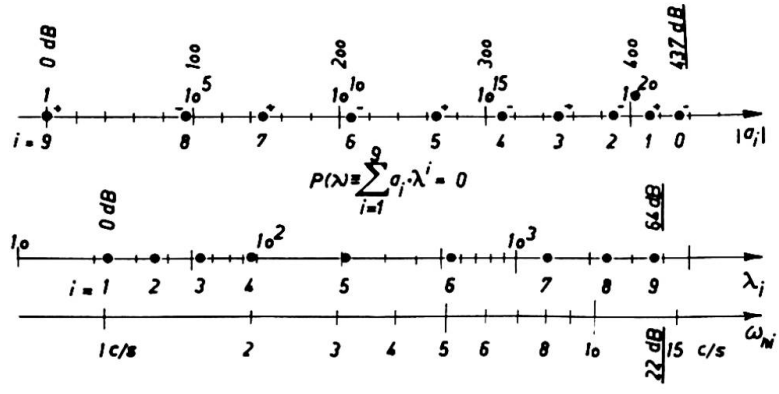

Fig.11.

tial conditions: $\underline{x}(o) = \underline{x}_n$ and $\dot{\underline{x}}(o) = \underline{o}$/ the system-oscillations are

$$\underline{x}(t) = \underline{x}_{no}\, e^{-\beta t} \cos\left(2\pi f_n\right)t$$

without any other harmonic transients. This procedure can be used for the very easy and very rapid iterative detemination of the unknown eigenvalues: both modes and shapes.

The dynamic behaviour of a structure can be characterized by the answer given to ideal Dirac-pulses $\delta_i(t)$

$$J = \int_o^T F\,dt = m_i \int_o^T \ddot{x}_i(t)dt = m_i\left[\dot{x}_i(T) - \dot{x}_i(o)\right] = m_i \Delta \dot{x}_i$$

The application of ideal pulses of the same intensity J at the mass m_i can be expressed mathematically by the initial conditions: $\underline{x}(o) = \underline{o}$; $\dot{\underline{x}}(o) = \left[o, o, \ldots, \dot{x}_i(o) = J/m_i, \ldots, o\right]^T$. The answer functions $\underline{x}(t)$, the weight-functions contain all the eigenvalues and thus several natural frequencies can be determined from the diagrams of $\underline{x}(t)$too.

Applying a constant force F_{io} suddenly to the mass m_i is equivalent with the excitation caused by the step-function $F_{io} \cdot 1(t)$; initial conditions: $\underline{x}(o) = \underline{o}$; $\dot{\underline{x}}(o) = \underline{o}$, and generating vector: $G(t) = \left[o, o, \ldots, G_i(t) = F_{io} \cdot 1(t), \ldots, o\right]^T$; oscillations with decaying transients occur, having the asymptotes

$$\underline{x}(\infty) = F_{oi}\underline{\eta}_i = F_{oi}\left[\eta_{1i}, \eta_{2i}, \ldots, \eta_{ii}, \ldots, \eta_{ni}\right]^T .$$

This procedure offers simultaneously an easy and very suitable testprogram, controling totally the entire modeling, both the developed mathematical equations Eq./5/, both their electrical realization.

The possibility of solving Eq./1/ for general optional excitations necessitates an analogue computer with suitable capacity, but offers the great advantage of analysing the dynamical behaviour by laboratory measurements; cumbersome site measurements are

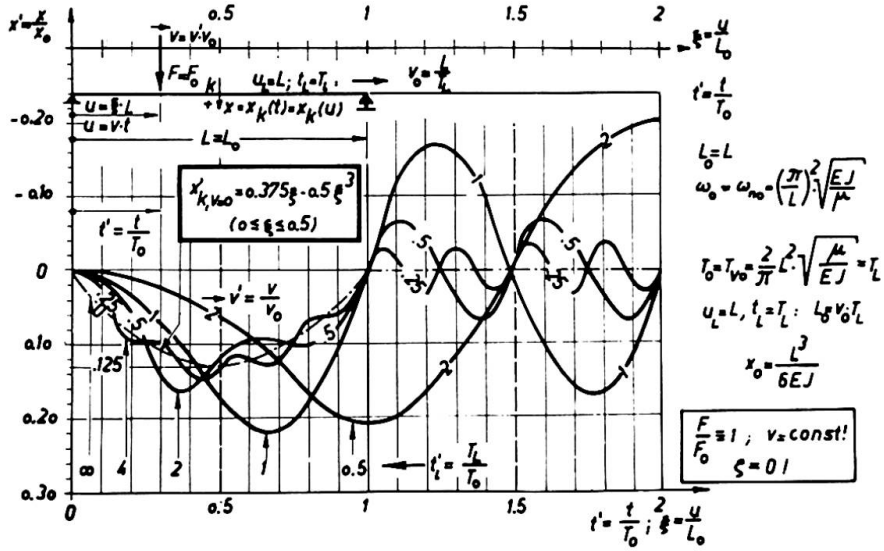

Fig.12.

to be made only to verify the theoretical results gained by dynamic modeling.

Such a pure theortical result is the dynamical effect of a unique - massless force rolling with different, but constant velocity over a simply supported beam [4],[5]. The results of elaborate digital calculations are to be verified easily by analogue modeling. The several functions of oscillations can be gained instantly in grafical manner /Fig.12/. Such methods give sharp inside views into an important, but nevertheless very complex problem, covered in statics by the concept of the so called "impact factor" [6].

If diagrams of the stochastic variations of wind- or earthquake effects are available, then these can be considered as the input force and displacement generation of the structure under discussion. Dynamic modeling conversely gives the response by simple recording of the output.

A c k n o l e d g e m e n t s.

The necessity of the method outlined grew out and was based on researches and nondestructive site investigations, made on the iniciative of the Council of the Hungarian Capital Budapest and the Hungarian Ministry of Post and Communication. Considerable help in assistance was given in analogue computation of the developed equations by Mr. G á b o r L a d á n y i, E.E. /Department for Process Control, Technical University,Budapest/ and in digital computing by Mr. G y ö r g y P o p p e r /Computing Centre of the Ministry of Heavy Industries/. Site investigations were made on the authority of the Ministry of Post and Communications and the Council of Budapest in assistance of the Institute for Quality Control of Building Materials and Constructions.

R e f e r e n c e s.

[1] . S. F A L K: Numerical Methods in Technical Mechanics. /Manuscript in German/.

[2] . J.G. I L L É S S Y: Dynamical Behaviour of Suspension Bridge Systems. /International Symposium on Suspension Bridges, Proceedings Paper No.6. Lisbon, Portugal, 1966/.

[3] . J.G. I L L É S S Y: Tabulated Solution of the Equations of statically Indetermined Structures. /In Hungarian/ Mélyépitéstudományi Szemle, /Scientific Review of Civil Engineering/ Budapest 1952.II./2-3.

[4] . J.F. F L E M I N G - J.P. R O M U A L D I: Dynamic Response of Highway Bridges. Proceedings of the A.S.C.E., Journal of the Str. Div. Vol.87. No.ST 7. October 1961.

[5] . R.K. W E N - T.T O R D I S : Dynamical Bahaviour of Cantilever Bridges. /Proc.A.S.C.E., Journ. of the Str.Div. Vol.88. No.EM4. August 1962./

[6] . F.V. F I L H O: Dynamic Influence Lines of Beams and Frames. /Proc.A.S.C.E., Journ. of the Str.Div. Vol.92. No. ST2. April 1966/.

SUMMARY

The electric simulation of mechanical systems by means of analogue computers makes laboratory researches of the actual dynamic behaviour of structures possible. The influence of space- and timevariable coupling of load and structure, changes and steps in vertical trace before or on the bridge, wind and earthquake effects respectively can be analysed separately or simultaneously.

RÉSUMÉ

La simulation électrique de systèmes mécaniques à l'aide de calculateurs analogiques permet l'étude au laboratoire du comportement dynamique réel des structures. Ainsi l'on peut analyser séparément ou simultanément l'influence d'un accouplement (variable dans l'espace et dans le temps) des vibrations de la charge et de celles de la structure, les changements ou les gradins dans le tracé vertical avant ou sur le pont, les effets du vent et de tremblements de terre.

ZUSAMMENFASSUNG

Durch die elektrische Simulierung mechanischer Systeme mit Hilfe von Analogrechner kann das wirkliche dynamische Verhalten von Bauwerken im Labor untersucht werden. Dabei können die Einflüsse der im Raum und Zeit veränderlichen Kopplung der Belastung und der des Bauwerkes, Gradientenänderungen, Sprünge in der Fahrbahn, vor und auf der Brücke, sowie Wind- und Erdbebenwirkungen gesondert, oder simultan untersucht werden.

Leere Seite
Blank page
Page vide

VI

A Model for the Study of Soil-Structure Inetaction

Modèle pour l'étude de l'interaction dans les composantes du sol

Ein Modell zur Betrachtung von Wechselwirkungen im Boden

M.E. AGABEIN
Lecturer, Civil Engineering Department
University of Khartoum, Khartoum, Sudan

R.A. PARMELEE
Associate Professor of
Civil Engineering

S.L. LEE
Professor of
Civil Engineering

Northwestern University, Evanston, Illinois, U.S.A.

1. Introduction

The seismic response of a multi-story building based on the assumption that the building rests on a rigid foundation has been considered by several investigators [1,2]. Observations [3] and studies [4] allowing for the flexibility of the foundation indicated that the influence of the flexible foundation on the dynamic response is significant and recently this dynamic coupling gained considerable attention [5,6,7,8].

One way to analyze soil-structure interaction phenomena is accomplished by utilizing the solutions for the steady state vibration of a rigid plate on the elastic half space [7,8]. However, the application of this approach to the analysis of the transient response of the system presents fundamental difficulties because of the frequency dependent nature of the parameters which characterize the foundation medium [8].

The object of this study is to investigate the transient response of a long building resting on an elastic half space using a mathematically consistent lumped-parameter model [9] of finite size to represent the semi-infinite foundation medium. Appropriate damping elements are introduced at the boundaries to account for the energy dissipation and to reduce wave reflection. In the construction of the model, the solutions to the harmonic horizontal translation and rocking vibrations of an infinitely long rigid rectangular body on an elastic half space presented by Karasudhi, Keer and Lee [10] are used as a basis for the determination of the properties of the damping elements. In spite of its simplicity the model provides a phenomenologically satisfactory representation of the elastic half plane, as evidenced by a comparison of the results for steady state motion obtained by the model with the analytical solutions [10].

Also included is a parametric study of the interaction between elastic multiple-story shear buildings and the flexible elastic foundation media as compared to the response of the same structures on rigid foundation when the systems are subjected to a strong motion earthquake.

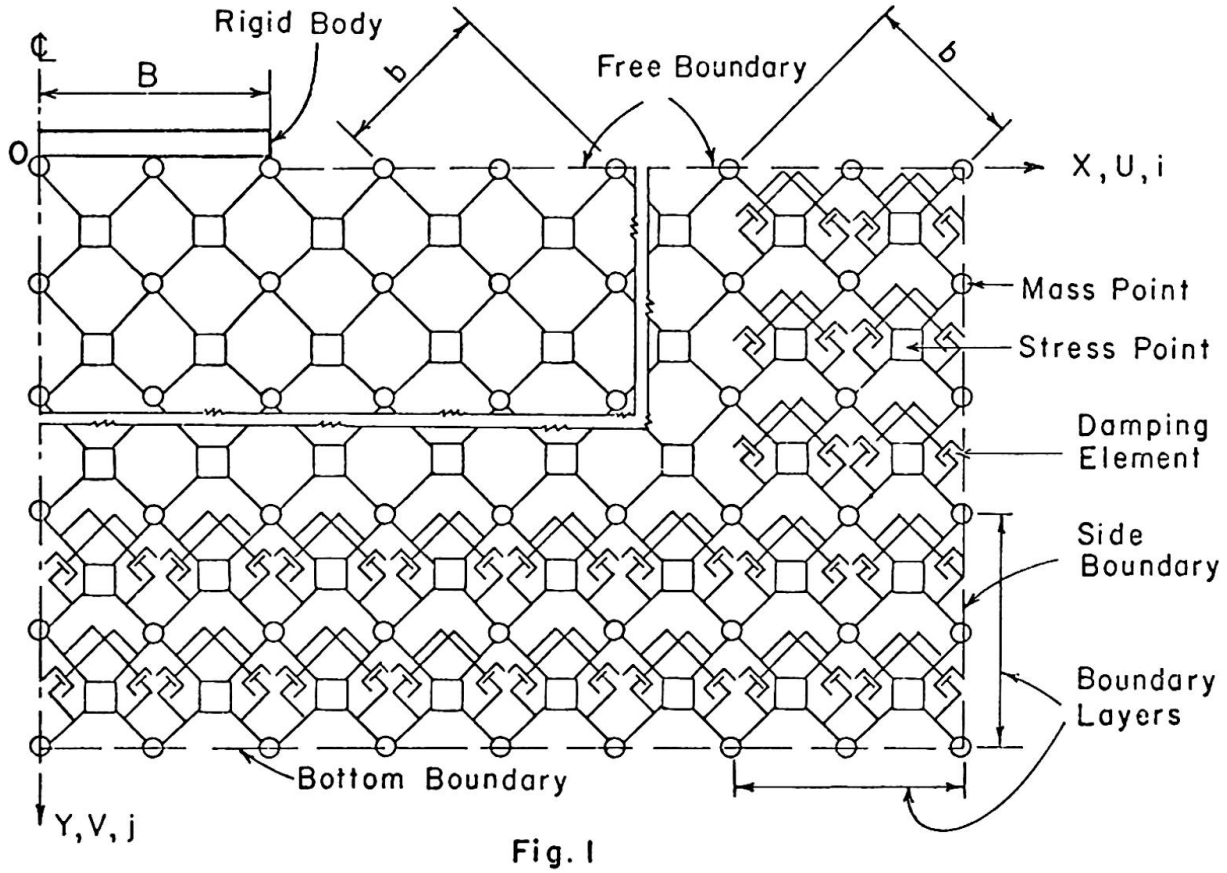

Fig. 1

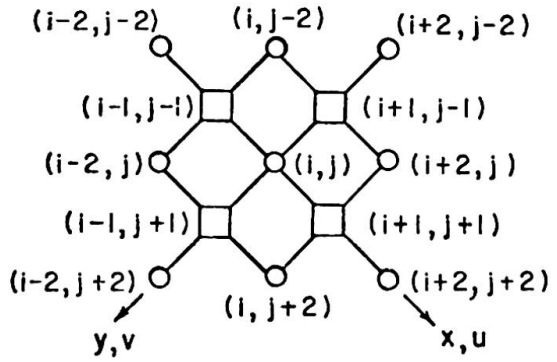

Fig. 2

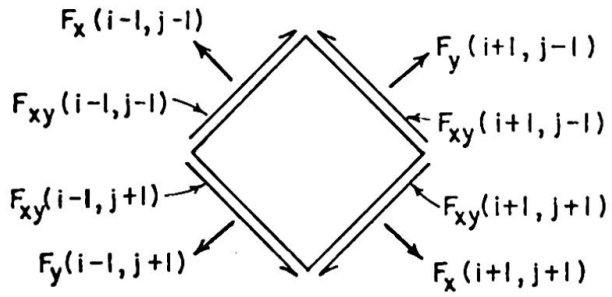

Fig. 3

2. Formulation of the Model

The lumped-parameter model for plane strain problems introduced by Ang and Harper [9] is used to represent the foundation medium which is assumed to be elastic, homogeneous and isotropic. The model consists essentially of mass points and stress points arranged as shown in Fig. 1, where the boundaries of the model and the reference coordinates, X- and Y-axes, are indicated.

A typical interior mass point shown in Fig. 2 contains the mass $m = \rho b^2/2$ of the foundation medium, where b is the mesh size of the model in the x- and y-axes and ρ is the mass density of the medium. The displacement, velocities and accelerations are defined at the mass points. The average stresses and

strains are defined at the stress points, which are assumed to be in a state of homogeneous stress and strain. The strains at a stress point are determined from the displacements of adjacent mass points, and the forces acting on a mass point are calculated from the stresses at adjacent stress points (Fig. 3).

For small deformation and plane strain conditions, the strain-displacement relationships for a typical interior stress point (i+1,j+1), as shown in Fig. 2, take the form

$$\begin{aligned}
\epsilon_x\,(i+1,j+1) &= \frac{u(i+2,j+2) - u(i,j)}{b} \\
\epsilon_y\,(i+1,j+1) &= \frac{v(i,j+2) - v(i+2,j)}{b} \\
\epsilon_{xy}\,(i+1,j+1) &= \frac{1}{2b}\left[u(i,j+2) - u(i+2,j) + v(i+2,j+2) - v(i,j)\right]
\end{aligned} \tag{1}$$

In these equations, ϵ_x, ϵ_y and ϵ_{xy} denote the strain components and u and v the displacements along the x- and y-axes respectively.

The forces acting on an interior mass point (i,j) are shown in Fig. 3. The normal forces F_x and F_y and the shearing force F_{xy} exerted by the adjacent stress points are equal to the products of the corresponding average stresses and the effective area on which they act and are given by

$$\begin{aligned}
F_x\,(i+1,j+1) &= \frac{b}{2}\,\sigma_x\,(i+1,j+1) \\
F_y\,(i+1,j+1) &= \frac{b}{2}\,\sigma_y\,(i+1,j+1) \\
F_{xy}(i+1,j+1) &= \frac{b}{2}\,\sigma_{xy}\,(i+1,j+1)
\end{aligned} \tag{2}$$

in which σ_x, σ_y and σ_{xy} are the normal and shearing stresses along the x- and y-axes.

From Fig. 3, the equations of motion for a typical interior mass point (i,j) along the x and y directions are, in view of (2),

$$\begin{aligned}
\frac{\sigma_x(i+1,j+1) - \sigma_x(i-1,j-1)}{b} + \frac{\sigma_{xy}(i-1,j+1) - \sigma_{xy}(i+1,j-1)}{b} &= \rho\ddot{u}(i,j) \\
\frac{\sigma_y(i-j,j+1) - \sigma_y(i+1,j-1)}{b} + \frac{\sigma_{xy}(i+1,j+1) - \sigma_{xy}(i-1,j-1)}{b} &= \rho\ddot{v}(i,j)
\end{aligned} \tag{3}$$

Applying Hooke's law to (3) and substituting for the strains from (1), the resulting equations of motion of a typical interior mass point in terms of the displacements are

$$\begin{aligned}
&\frac{G}{b^2}\left[u(i+2,j+2) + u(i-2,j+2) - 4u(i,j) + u(i-2,j-2) + u(i+2,j-2)\right] \\
&+ \frac{\lambda+G}{b^2}\left[u(i+2,j+2) - 2u(i,j) + u(i-2,j-2) - v(i-2,j) + v(i,j-2)\right. \\
&\qquad \left. - v(i+2,j) + v(i,j+2)\right] = \rho\,\ddot{u}\,(i,j)
\end{aligned} \tag{4}$$

$$\frac{G}{b^2}\left[v(i-2,j+2) + v(i-2,j-2) - 4v(i,j) + v(i+2,j-2) + v(i+2,j+2)\right] +$$

$$+\frac{\lambda+G}{b^2}\Big[v(i-2,j+2) - 2v(i,j) + v(i+2,j-2) + u(i,j+2) - u(i-2,j) + u(i,j-2) - u(i+2,j)\Big] = \rho\,\ddot{v}\,(i,j) \qquad (4)$$

in which $\lambda = 2\nu G/(1-2\nu)$, G is the shear modulus and ν the Poisson's ratio.

It is interesting to note that (1) and (4) are the central finite difference analogue of the corresponding differential equations for the continuum. On the free surface, applied stresses are defined at fictitious stress points adjacent to the boundary, while boundary displacements are defined at the boundary mass points.

3. Model Size and Damping

To develop the model, the harmonic rocking of an infinitely long rigid rectangular body on an elastic half space is considered. The rigid body is of width 2B with mass M per unit length and the elastic half space is approximated by the lumped-parameter model as shown in Fig. 1. The boundary conditions are such that the vertical displacement of the five mass points in contact with the rigid body is ΨX, where Ψ is the angle of rotation of the body, the free surface beyond the rigid body is stress free, the surface of contact between the base of the rigid body and the semi-infinite medium is smooth, and the displacements of the mass points on the side and bottom boundaries are assumed to vanish.

The equation of motion that governs the harmonic rocking of the rigid body takes the form

$$\begin{aligned} m(5 + 16\,\bar{J})\frac{B\ddot{\Psi}}{\sqrt{2}} + G\Big[\frac{10}{\sqrt{2}}B\Psi - 2v(6,0) - 2v(6,2) - v(4,2) \\ - 2v(2,2) - 2u(0,0) - 4u(2,0) + 2u(4,0) + 2u(6,0) - 2u(6,2) \\ - u(4,2) - 2u(2,2)\Big] + (\lambda+G)\Big[\frac{7}{\sqrt{2}}B\Psi + 2v(6,0) - 2v(4,2) \\ - 3v(2,2) + u(0,0) + 2u(2,0) - u(4,0) - 2u(6,2) - 3u(4,2) \\ - u(2,2) + u(0,2)\Big] = 2\sqrt{2}\;T\,e^{i\omega t}/B \end{aligned} \qquad (5)$$

in which $\bar{J} = J/\rho B^4$ is the non-dimensional inertia, J is the polar inertia of the body, T and ω are respectively the amplitude of the applied torque and frequency of excitation, and t denotes time.

The optimum size of the model with rigid boundaries is established by varying the dimensions of the model and solving the system of equations by a high-speed digital computer for the static case, i.e., $\omega = 0$. For each model size the static rotational stiffness T/Ψ is determined and compared with the analytical value [10] given by $T/\Psi = \pi GB^2/2(1-\nu)$. It is found that the larger the dimensions of the model, the closer is the agreement; however the computer time required becomes excessive. The model size X = 4B (i = 16, b = B / $\sqrt{2}$) and Y = 3.5 B (j = 14) yields a static stiffness with 5% accuracy and requires reasonable computational time, hence it will be used in the following study. For this model size, observing the condition of antisymmetry and the boundary conditions, the model has 104 degrees of freedom.

Next the system of equations for harmonic rocking is solved and the results obtained showed, as expected, infinitely large amplitudes at resonant frequencies. This is of course physically incorrect since in the infinite medium the

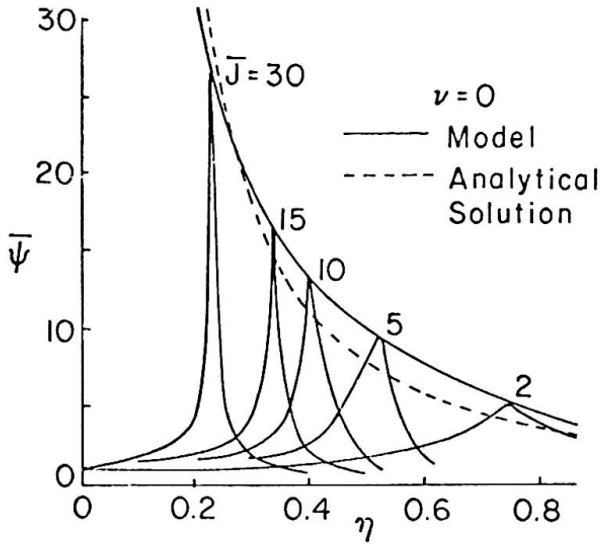

Fig. 4

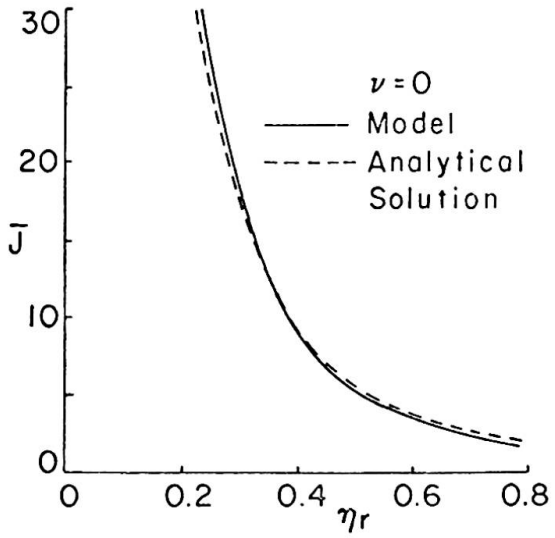

Fig. 5

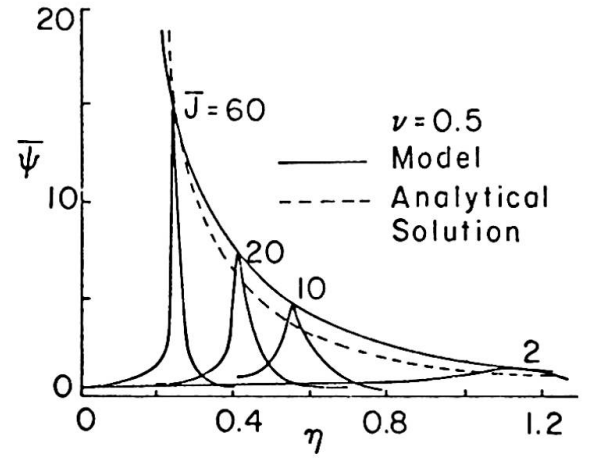

Fig. 6

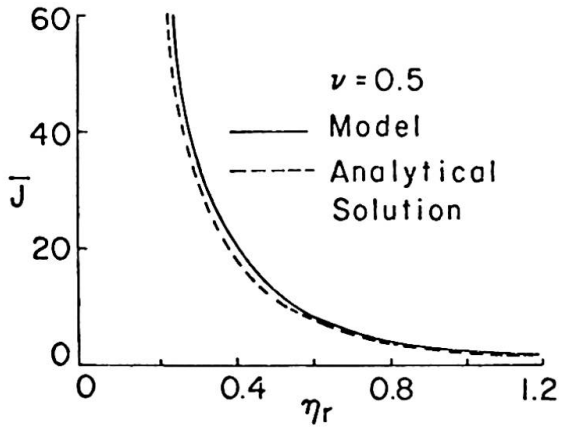

Fig. 7

energy is dissipated by the dispersion of the elastic waves far from the source of disturbance. This dissipation of energy produces a damping effect which limits the amplitudes at resonant frequencies. To build this damping effect into the finite-size model, damping elements are placed in parallel to the stress points along the two boundary layers adjacent to the side and bottom boundaries, as shown in Fig. 1. Thus the equations of motion for the boundary mass points contain damping terms which serve the purpose of dissipating the energy and reducing the reflection of waves from the boundaries. The damping coefficient c of these elements is determined by matching the amplitudes at resonant frequencies with the analytical solution [10] and depends not only on the properties of the medium and the size of the model, but also on the frequency. The value of the non-dimensional damping factor $\bar{c} = c/\rho B V_s$, where $V_s = \sqrt{G/\rho}$ is the shear wave velocity, given by

$$\bar{c} = 9 - 10\,\nu \tag{6}$$

is found to give reasonably good results for the frequency range of interest.

Using the values of $\bar{c}$ defined by (6), the results for $\nu = 0$ are shown in Figs. 4,5 and those for $\nu = 0.5$ in Figs. 6,7. In Figs. 4,6 the non-dimensional amplitude $\bar{\Psi} = \pi G B^2 \, |\Psi| \, / \, 2T$ is plotted versus the frequency factor $\eta = B\omega/V_s$ for

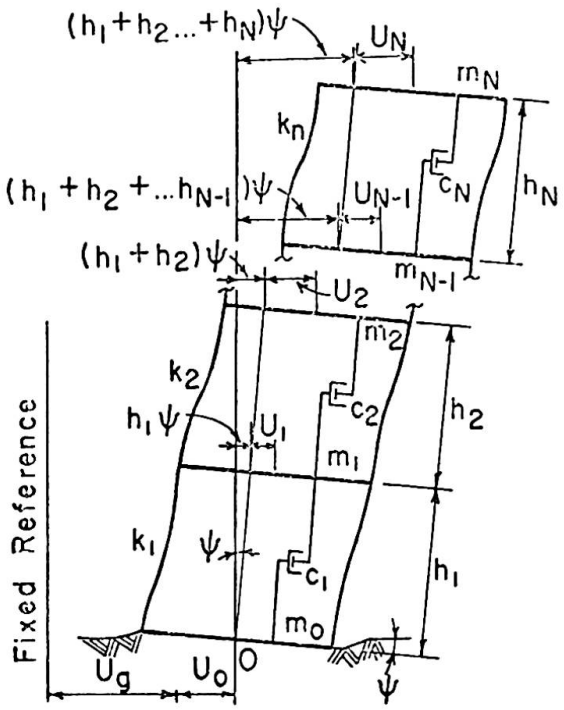

Fig. 8

various values of the non-dimensional inertia $\bar{J}$. In Figs. 5,7 the non-dimensional inertia $\bar{J}$ is plotted versus the resonant frequency factor $\eta_r = B\omega_r/V_s$, where ω_r is the resonant frequency. It can be seen that the approximation of the stiffness and damping characteristics of the elastic half space by the model give, for practical purposes, results which are in satisfactory agreement with those obtained by the analytical solution [10] especially in the lower frequency range which is of primary importance in the seismic response of soil-structure interaction systems.

4. Multiple-Story Building on Flexible Foundation

A dynamic model for an elastic N-story shear building resting on the elastic half space is shown in Fig. 8 in the deformed state. Both interaction rotation Ψ and horizontal translation U_o of the base mass m_o are allowed in contrast to rigid foundation. The interfloor damping coefficient c_n, taken as a percentage of the critical damping in the first mode of vibration of the structure supported on a rigid foundation, is assumed to be proportional to the flexural stiffness k_n of story n to eliminate the dynamic coupling between the various modes.

The soil-structure interaction system is represented by placing the building in Fig. 8 on the foundation model in Fig. 1, where the base mass of the building replaces the rigid body. No slippage is allowed in this instance. Thus the five mass points at the surface of contact undergo the same displacement as the base mass, i.e.,

$$\begin{aligned} V(i,0) &= \Psi X_i \\ U(0,0) &= U(2,0) = U(4,0) = U_o \end{aligned} \tag{7}$$

In view of (7) the degree of freedom of the foundation model is 102 and that of the interaction system for N stories is (N + 102). The (N + 2) equations of motion for the building shown in Fig. 8 are

$$\ddot{U}_o\left(\frac{5}{2}\alpha + \sum_{n=0}^{N}\alpha_n\right) + \ddot{\Psi}\sum_{n=1}^{N}\alpha_n\bar{h}_n + \sum_{n=1}^{N}\alpha_n\ddot{U}_n + \frac{G}{\sqrt{2}\,m_N}\left[\frac{10}{\sqrt{2}}U_o - u(6,0) - u(6,2) - u(4,2) - 2u(2,2) - 2u(0,2) - \frac{2}{\sqrt{2}}B\Psi - v(6,0) + v(6,2) + v(4,2) + 2v(2,2)\right.$$

$$+\frac{\lambda+G}{\sqrt{2}\,m_N}\left[\frac{1}{\sqrt{2}}U_o - u(6,2) + \frac{B}{\sqrt{2}}\Psi + v(6,0) - v(4,2)\right] = -\ddot{U}_g\sum_{n=0}^{N}\alpha_n$$

$$\ddot{U}_o\sum_{n=1}^{N}\alpha_n\bar{h}_n + \ddot{\Psi}\left[\frac{5}{4}\alpha B^2 + \frac{B^2}{3}\sum_{n=0}^{N}\alpha_n + \sum_{n=1}^{N}\alpha_n\bar{h}_n^2\right] + \sum_{n=1}^{N}\alpha_n\bar{h}_n\ddot{U}_n \qquad (8)$$

$$+\frac{GB}{\sqrt{2}\,m_N}\left[\frac{5}{\sqrt{2}}B\Psi - v(6,0) - v(6,2) - \tfrac{1}{2}v(4,2) - v(2,2) - \frac{2}{\sqrt{2}}U_o + u(6,0) -\right.$$

$$\left. - u(6,2) - \tfrac{1}{2}u(4,2) - u(2,2)\right] + \frac{(\lambda+G)B}{\sqrt{2}\,m_N}\left[\frac{7}{2\sqrt{2}}B\Psi + v(6,0) - v(4,2) - \frac{3}{2}v(2,2)+\right.$$

$$\left. + \frac{1}{\sqrt{2}}U_o - u(6,2) - \frac{3}{2}u(4,2) - \tfrac{1}{2}u(2,2) + \tfrac{1}{2}u(0,2)\right] = -\ddot{U}_g\sum_{n=1}^{N}\alpha_n\bar{h}_n$$

$$\alpha_n\ddot{U}_o + \alpha_n\bar{h}_n\ddot{\Psi} + \alpha_n\ddot{U}_n - \frac{c_{n+1}}{m_N}\dot{U}_{n+1} + \frac{(c_n + c_{n+1})}{m_N}\dot{U}_n - \frac{c_n}{m_N}\dot{U}_{n-1} - \frac{k_{n+1}}{m_N}U_{n+1} +$$

$$+\frac{(k_n + k_{n+1})}{m_N}U_n - \frac{k_n}{m_N}U_{n-1} = -\ddot{U}_g\alpha_n \qquad (n = 1,2,\ldots N)$$

in which

$$\alpha_n = m_n/m_N\,,\quad \alpha_o = m_o/m_N\,,\quad \alpha = m/m_N\,,\quad \bar{h}_n = \sum_{i=1}^{n} h_i$$

$$c_1\dot{U}_o = k_1 U_o = 0\,,\qquad c_{N+1} = k_{N+1} = 0 \qquad (9)$$

and h_n is the height of the n-th story, m_n the mass of the n-th floor, U_n the horizontal translation of the n-th story caused by the free field earthquake displacement U_g, and u and v are the interaction displacements of the mass points of the foundation model.

5. Steady State Response

To examine the influence of the foundation parameters on the dynamic response of the interaction systems, five, ten and fifteen-story buildings are analyzed for both harmonic and transient excitations. These are single bay shear structures with the flexural stiffnesses taken in accordance with Housner and Brady [11] but reduced for unit length normal to the direction of vibration. The buildings have a bay width of twenty feet, equal story heights of twelve feet, floor unit weight of 100 psf and the values of α_o are 1.5, 2 and 2.5 for the five, ten and fifteen-story buildings respectively. The interfloor damping coefficient c_n is taken as one percent of critical damping. In addition, the foundation medium has a unit weight of 110 pcf while Poisson's ratio and the shear wave velocity are the parameters of this study.

The differential equations of motion are solved for the harmonic excitation $U_g = Qe^{i\omega t}$, where Q is the amplitude. The ratio θ, plotted versus the shear wave velocity V_s in Fig. 9, is the maximum response U^* of the interaction system divided by the corresponding maximum flexural response $\bar{U}$ of the same building resting on a rigid foundation, i.e., $V_s = \infty$. The latter case is obtained by solving the N equations given by (8c) with $U_o = \Psi = 0$.

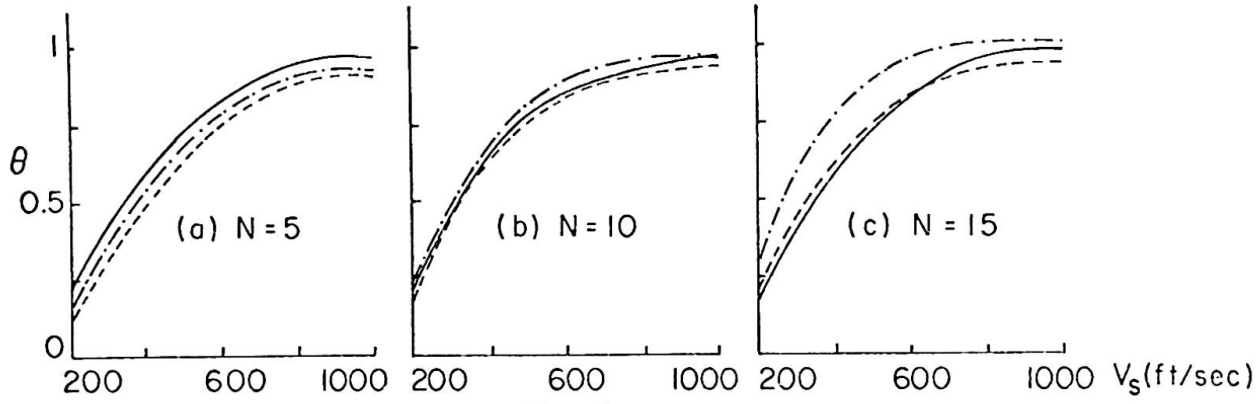

Fig. 9

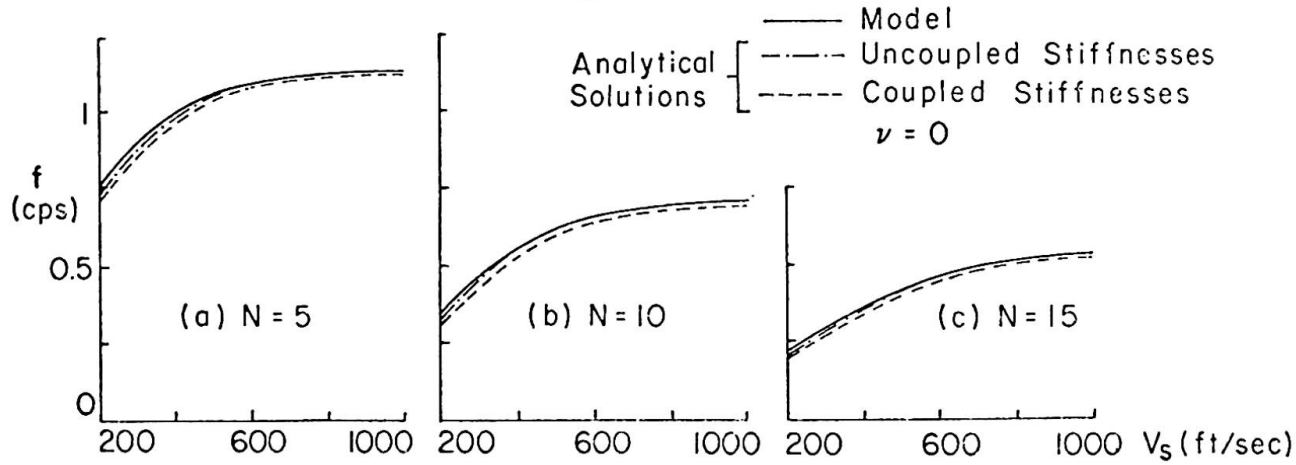

Fig. 10

Also shown in Fig. 9 are the corresponding analytical results using the stiffnesses presented by Karasudhi, Keer and Lee [10]. In their study of the harmonic rocking and horizontal vibrations of an infinitely long rectangular rigid body on an elastic half space, both uncoupled and coupled motions are considered. It was found, that while the uncoupled stiffnesses are in fairly good agreement with the diagonal elements of the stiffness matrix for the coupled vibration, the effect of the off-diagonal elements is significant. In Fig. 9 the analytical solution using the coupled stiffnesses shows consistent agreement with the results obtained from the model, while the uncoupled stiffnesses yield results which diverge from the other two solutions. Figure 10 shows the variation of the fundamental frequency f with the shear wave velocity given by the model as well as the analytical solution.

As the foundation medium becomes more flexibile, i.e., as V_S decreases, the values of θ and f decrease monotonically as shown in Figs. 9,10. For the three cases studied it is noted that foundation media with a shear wave velocity of 1000 ft/sec closely approximate the rigid foundation, and that the interaction effect is significant only for lower values.

It is evident from Figs. 9,10 that the proposed model is phenomenologically satisfactory for use in the study of the dynamic response of soil-structure interaction systems.

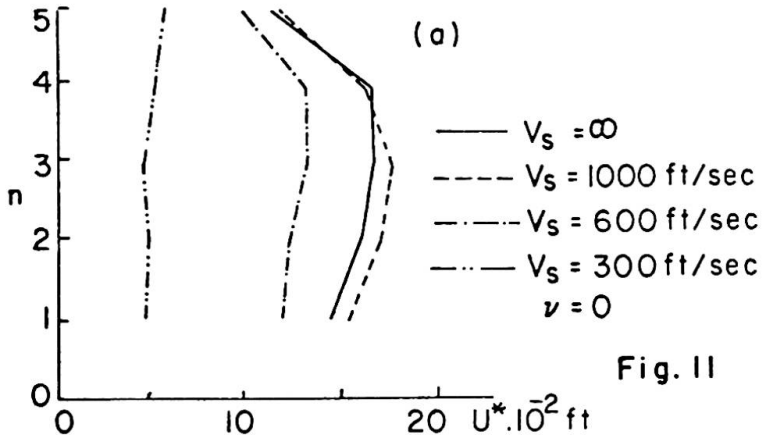

Fig. 11

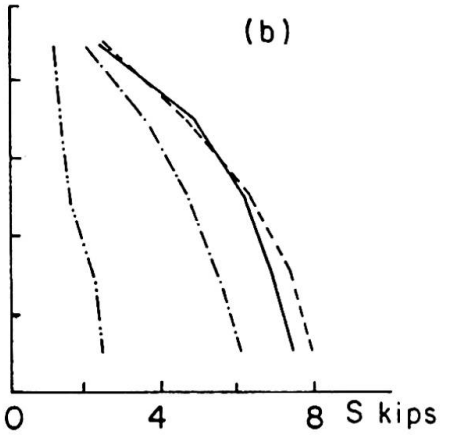

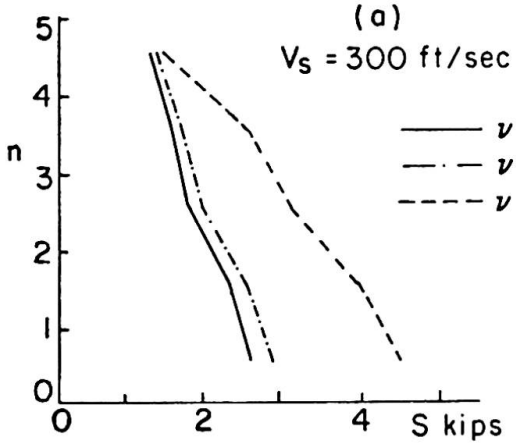

Fig. 12

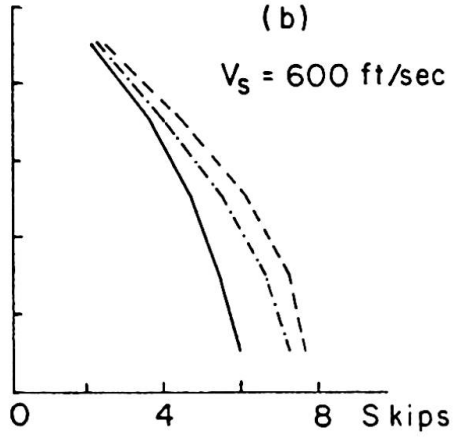

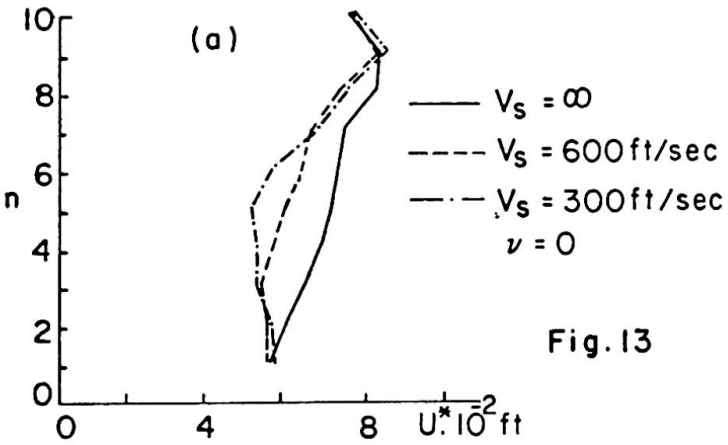

Fig. 13

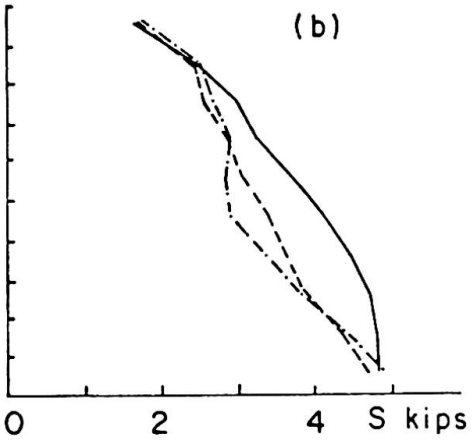

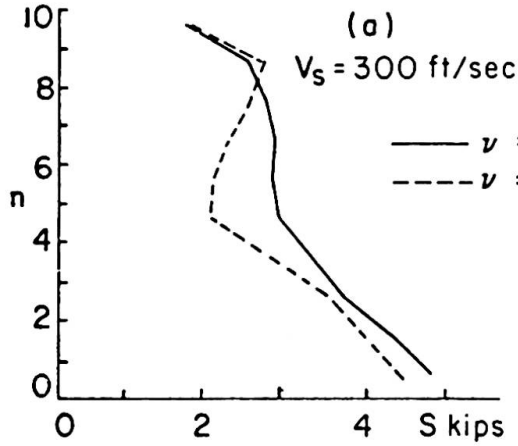

Fig. 14

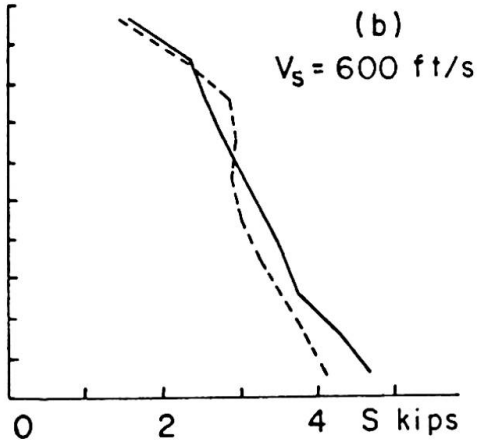

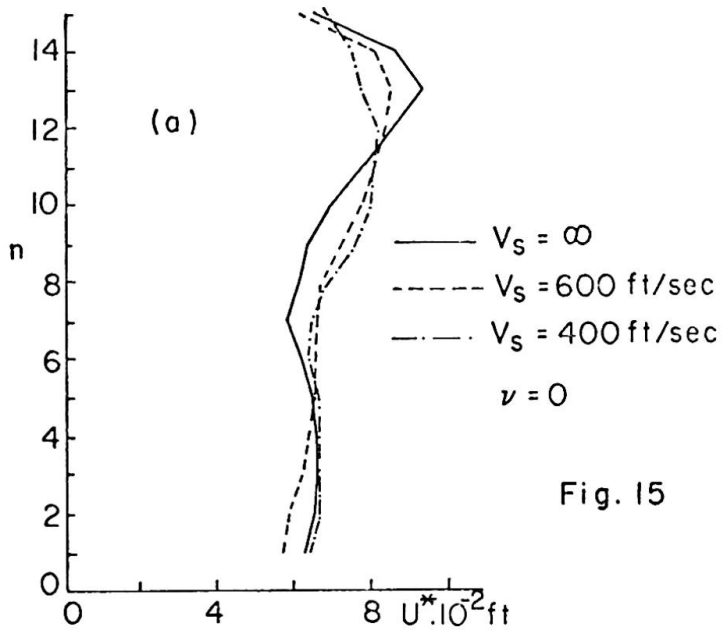

Fig. 15

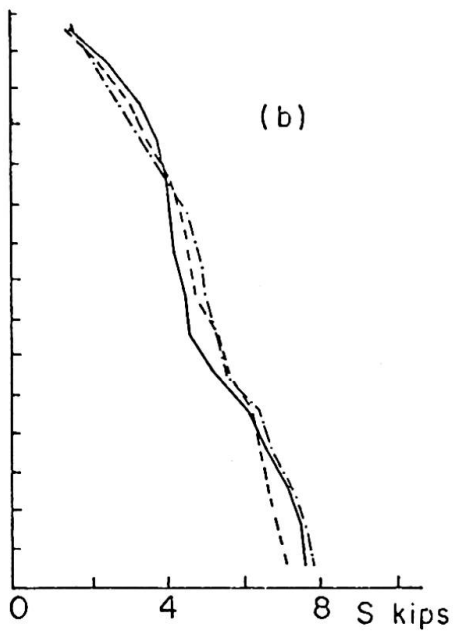

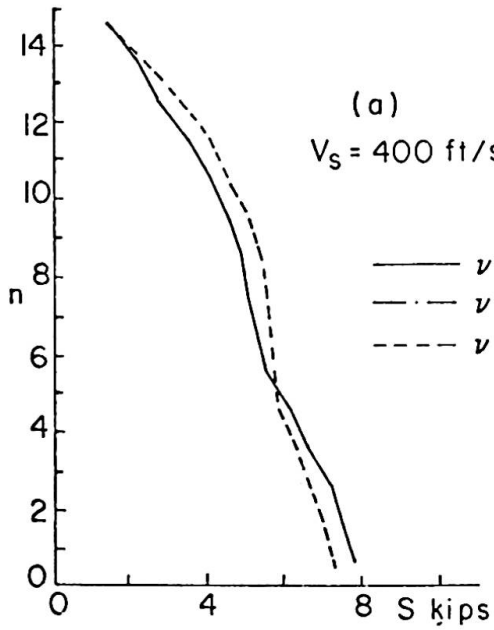

Fig. 16

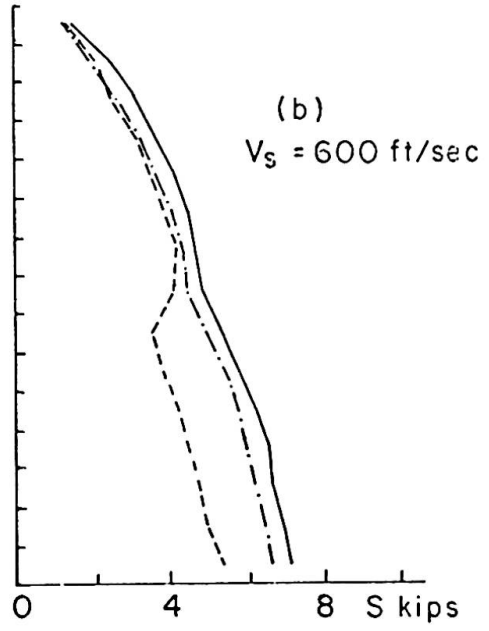

6. Transient Response

The accelerogram for the N-S component of El Centro, California, earthquake of May 18, 1940 is used for the following investigation. The system of differential equations of motion is solved using the step-by-step numerical integration procedure suggested by Wilson and Clough [12].

Figures 11 to 16 show the effect of the foundation properties on the maximum flexural response U* and story shears S when the three interaction systems are subjected to the above mentioned earthquake excitation in the ranges $300 \leq V_s \leq 1000$ ft/sec and $0 \leq \nu \leq 0.5$. The corresponding results obtained for rigid foundations are also shown for comparison.

Figure 11 shows the response of the five-story building for $\nu = 0$. When $V_s = 1000$ ft/sec the base shear is about 6% higher than the rigid case and then decreases with decreasing shear wave velocity. Unlike the ten and fifteen-story buildings, shown in Figs. 14,16, the five-story shears increase steadily

with increasing values of Poisson's ratio as shown in Fig. 12. The high story shears are characteristic of the response of this building to the particular earthquake excitation. This type of interrelationship has been observed and discussed by many investigators [2,13]. It should be noted that the first four natural periods of the five-story building on rigid foundation coincide with as many peaks in the velocity spectrum curve for the earthquake. This fact is the major contribution to the large flexural displacements and high story shears.

The response of the ten-story building in Fig. 13 shows a general reduction in story shears with decreasing shear wave velocity and even further reduction in the lower floors (Fig. 14) as Poisson's ratio is increased from zero to 0.5. However, this pattern of behavior is not observed in the case of the fifteen-story building (Fig. 15) which shows a decrease in story shears in the lower floors for V_s = 600 ft/sec, compared with the rigid case, an increase in the middle floors and again a decrease in the upper floors. On the other hand, as the shear wave velocity decreases to 400 ft/sec, an increase in story shears is observed in the lower floors and a decrease in the upper floors. The effect of increasing Poisson's ratio for V_s = 600 ft/sec results in continued decrease in the story shears (Fig. 16) while for V_s = 400 ft/sec the decrease is only in the lower floors followed by an increase in the upper stories.

7. Conclusions

A mathematically consistent lumped-parameter model of finite size to represent the elastic half plane for the study of initial and boundary-value problems is presented. The proposed model is used to investigate the effects of the flexibility of the foundation medium on the seismic response of long multi-story buildings. Damping elements are introduced along the boundaries of the model to dissipate the energy and reduce wave reflection. The model can be extended to the treatment of anisotropic and/or inelastic foundation media by incorporating the appropriate constitutive equations in the stress points.

It has been shown that the influence of the flexibility of the foundation on the seismic response of multi-story buildings is significant. The physical properties that affect the foundation stiffness and damping characteristics are the shear wave velocity and Poisson's ratio.

For steady state excitations, the flexibility of the foundation results in continued reduction in the flexural displacements, story shears and frequencies compared to the values obtained by rigid foundation. Extending these conclusions to the transient response is unjustifiable since the results for the latter show no general pattern of behavior with the variation of the foundation properties for the cases studied. The results clearly demonstrate that the effect of the flexibility of the foundation on the transient response of multi-story buildings depends not only on the characteristics and nature of the earthquake excitation, but also on the physical properties of the building as well as the foundation medium. This conclusion is in agreement with previous studies [8]. The shear wave velocity has the effect of changing the natural periods of the interaction system and thereby altering the energy input to the building indicated by the ordinates of the spectral velocity curve of the earthquake excitation.

8. Acknowledgements

The research upon which this paper is based was supported in part by the National Science Foundation under Grant No. GK-1910 to Northwestern University.

9. References

1. L. E. Goodman, E. Rosenblueth and N. M. Newmark, "Aseismic Design of Elastic Structures Founded on Firm Ground," Proc. ASCE, Vol. 79, No. 349, Nov. 1953.

2. R. W. Clough, "Dynamic Effects of Earthquakes," Trans. ASCE, Vol. 126, Part 2, 1961, pp. 847-876.

3. K. Suyehiro, "Engineering Seismology, Notes on American Lectures," Proc. ASCE, Vol. 58, No. 4, Part 2, May 1932.

4. R. Tanabashi and H. Ishizaki, "Earthquake Damages and Elastic Properties of the Ground," Bulletin Disaster Prevention Research Inst., Kyoto Univ., No. 4, May 1953.

5. R. G. Merritt and G. W. Housner, "Effect of Foundation Compliance on Earthquake Stresses in Multistory Buildings," Bulletin of the Seismological Society of America, Vol. 44, No. 4, Oct. 1954, pp. 551-569.

6. D. L. Lycan and N. M. Newmark, "Effect of Structure and Foundation Interaction," Proc. ASCE, Journal Eng. Mech. Div., Vol. 87, No. EM5, Oct. 1961, pp. 1-31.

7. R. A. Parmelee, "Building-Foundation Interaction Effects," Proc. ASCE, Journal Eng. Mech. Div., Vol. 93, No. EM2, April 1967, pp. 131-152.

8. R. A. Parmelee, D. S. Perelman and S. L. Lee, "Seismic Response of Multiple-Story Structures on Flexible Foundations," submitted for publication.

9. A. H.-S. Ang and G. N. Harper, "Analysis of Contained Plastic Flow in Plane Solids," Proc. ASCE, Journal Eng. Mech. Div., Vol. 90, No. EM5, Oct. 1964, pp. 397-418.

10. P. Karasudhi, L. M. Keer and S. L. Lee, "Vibratory Motion of a Body on an Elastic Half Plane," submitted for publication.

11. G. W. Housner and A. G. Brady, "Natural Periods of Vibration of Buildings," Proc. ASCE, Journal Eng. Mech. Div., Vol. 89, No. EM4, Aug. 1963, pp. 31-65.

12. E. L. Wilson and R. W. Clough, "Dynamic Response by Step-by-Step Matrix Analysis," Symposium on the Use of Computers in Civil Engineering, Paper No. 45, Lisbon, Portugal, Oct. 1962.

13. G. W. Housner, "Behavior of Structures During Earthquakes," Proc. ASCE, Vol. 85, No. EM4, Oct. 1959, pp. 109-129.

SUMMARY

Summary

A mathematically consistent lumped-parameter model of finite size to simulate the elastic half space for investigating the effects of the flexibility of the foundation on the seismic response of long multi-story buildings is presented. Appropriate damping elements are introduced at the boundaries to dissipate energy and reduce wave deflection. The proposed model yields phenomenologically satisfactory results as evidenced by a comparison with the results obtained by analytical solutions for the steady state response of several soil-structure interaction systems.

A parametric study of the transient response of soil-structure systems shows that the foundation flexibility modifies the response of the structure in comparison with rigid foundation and that the effects depend on the physical properties of the structure and the foundation medium, as well as the characteristics of the earthquake excitation.

RÉSUMÉ

Cette contribution présente un modèle de grandeur finie, mathématiquement valable, avec paramètres adéquats, simulant le demi-espace élastique. Ce modèle permet l'étude de la flexibilité des fondations sous des secousses sismiques sur des constructions longues à beaucoup d'étages. Des amortisseurs appropriés ont été utilisés sur les bords pour dissiper l'énergie et pour réduire la déflection des ondes. Le modèle proposé donne des résultats phénoménologiquement satisfaisants, comme le démontre la comparaison avec les calculs analytiques sur plusieurs systèmes.

Une étude paramétrique montre que la réaction de la construction dépend de la flexibilité des fondations, et que les effets dépendent des propriétés physiques de la structure et des fondations aussi bien que des caractéristiques de l'excitation sismique.

ZUSAMMENFASSUNG

Ein mathematisch verträgliches Modell endlicher Grösse mit "Umfassungs"-Parameter zur Nachahmung des elastischen Halbraums für Untersuchungen der Fundamentsteifigkeit unter Erdbeben wird für lange mehrstöckige Bauten angegeben. Es sind an den Rändern Dämpfungselemente eingeführt worden, um die Energie zu verbrauchen sowie die Wellenausschläge zu vermindern. Das vorgeschlagene Modell ergibt phänomenologisch befriedigende Ergebnisse im Vergleich mit denjenigen der analytischen Lösung.

Eine Parameter-Studie der Uebergangsbestimmung der Bodenstrukturen zeitigt, dass die Fundamentsteifigkeit die Bestimmung der Struktur im Vergleich mit steifen Fundamenten verändert, und dass die Wirkung von den physikalischen Verhältnissen der Struktur, des Fundamentes und sowohl als auch von der Erdbebencharakteristik abhängt.

Leere Seite
Blank page
Page vide

VI

Problem of Prediction of Wind Forces on Engineering Structures and Application to Practice

Problèmes de l'estimation des charges de vent sur une construction et application à la pratique

Probleme der Voraussagung von Windkräften auf Bauwerke und die Anwendung in der Praxis

A.B.O. SOBOYEJO
Faculty of Engineering
University of Lagos
Lagos, Nigeria

INTRODUCTION

Principles of maximum entropy is used to develop minimally biased probability distribution functions for maximum value of the horizontal components of wind velocities. An attempt is made to throw some fresh ideas on the formulation of a sound statistical model for the evaluation of wind velocities and wind pressures on engineering structures.

Since wind velocities vary with time and space, it is shown that wind force on a structure is not static in nature, and as such cannot be obtained from instantaneous wind velocity by a simple formula of a static wind force. An attempt is made to obtain a design wind force, only by changing numerical values of gust factors referring to size, and structural characteristics.

In order to obtain the gust factors for determining the wind loading on various structures, the space correlation of velocity fluctuations is considered in addition to power spectrum. Moreover, the essential procedures used in arriving at the gust factors are outlined. This evaluation is not intended to be rigorous, however, it does describe the practical procedures and the essential assumptions and approximations that can be used to simplify the results into usable form.

2. PRINCIPLE OF MAXIMUM ENTROPY AND ITS APPLICATION IN THE DEVELOPMENT OF STATISTICAL MODELS FOR WIND VELOCITIES AND WIND PRESSURES

The static wind pressure can be taken to be

$$\bar{p}(z) = \frac{1}{2}\rho \bar{U}^2 C_p(z) \qquad (2.1)$$

where $\bar{p}(z)$ is the mean pressure at a point z above the ground, $\bar{U}$ is the mean velocity at the level at the top of the structure in the place where the structure will serve, ρ is the density of the air, and $C_p(z)$ is the pressure co-efficient of point z . Of course in design, the maximum wind velocity should be used in place of the mean wind velocity in order to obtain the maximum wind pressure from equation (2.1).

The maximum wind velocity for a given place should be obtained by statistical means from a long record of annual maximum wind velocities. For a given averaging time of the annual maximum wind velocity record for any place, it is possible to use the principle of maximum entropy for the estimation of the instantaneous maximum wind velocity and hence the evaluation of the maximum wind pressure. The uncertainty in the value of the maximum wind velocity at any given height can be evaluated by the specification of its entropy, which can be expressed mathematically (1) by

$$H = -K \sum_i \bar{g}_i(U) \ln \bar{g}_i(U) \qquad (2.2)$$

where H is the entropy or uncertainty in the value of maximum wind velocity, K is an arbitrary constant, $\bar{g}_i(U)$ is the probability density function of the maximum wind velocity U for the ith possible outcome of the maximum value of the wind velocity. Equation (2.2) gives a measure of the uncertainty or ignorance of the true state of the maximum value of the wind velocity. Maximizing equation (2.2) leads to the condition of maximum uncertainty, from which can be derived the minimally biased probability density function for the maximum wind velocity. The form of the minimally biased probability density function, can be shown to be given (2, 3, 4, 5) by expression (2.3) for any given prior estimates of the mean $\bar{U}$ and the standard deriviation σ_μ of the maximum value of the wind velocity.

$$\tilde{g}(U) = \exp(-a_0 - a_1 U - a_2 U^2) \qquad (2.3)$$

In equation (2.3); a_0, a_1, and a_2 are Lagrangian multipliers. Furthermore, it can be shown that, (4,5)

$$a_0 = \frac{a_1^2}{4a_2} - \frac{1}{2}\ln a_2 + \ln\left[1 - \mathrm{erf}\left(\frac{a_1}{2\sqrt{a_2}}\right)\right] + \ln\frac{\sqrt{\pi}}{2\Delta U} \qquad (2.4)$$

$$\bar{U}a_1 = -2X^2 + Z \qquad (2.5)$$

$$\left(\frac{\sigma_\mu}{\bar{U}}\right)^2 = \frac{2X^2 + 2X^2 Z - Z^2}{4X^4 - 4X^2 Z + Z^2} \qquad (2.6)$$

where $Z = \frac{2}{\sqrt{\pi}} \frac{X \exp(-X^2)}{(1 - \mathrm{erf}(X))}$ (2.7)

and $X = \frac{a_1}{2\sqrt{a_2}}$ (2.8)

Thus, using the results of equations (2.4 to 2.9), and Figures 1 and 2, the values of the Lagrangian multipliers a_0, a_1 and a_2 can be determined in terms of $\bar{U}$ and σ_μ ; and then the minimally biased probability distribution function for the maximum wind velocity can be evaluated from equation (2.3). The results given by this approach are satisfactory enough for the normal range of wind velocities which are of interest in civil engineering applications. It has been found that actual data (5) are well-fitted by this type of distribution. The great advantage of this type of analysis is that all the recorded extreme values are used and that the best available estimate can be obtained of the speed which is likely to be exceeded on the average only once in any specified number of years.

Furthermore, it should be realised that wind speeds are affected by such factors as variations in height, averaging times and topographical effects. Some of the well-known results, concerning the effects of these factors, on the maximum velocity distribution which are of interest in civil engineering applications, can be directly applied, in conjunction with the results obtained in this paper.

3. DYNAMIC CONSIDERATIONS IN STRUCTURAL DESIGN AGAINST WING

In equation (2.1) for mean wind pressure, it can be assumed that both $\bar{U}$ and $C_p(z)$ are affected by the roughness of the surface of the ground, and in fact several expressions have been developed to show the relationships between the variations of $\bar{U}$ and $C_p(z)$, and other essential parameters such as height above the ground, gradient velocity, and the ground roughness coefficient.

In design, the gust pressure factor is intended to take account of the superimposed dynamic effects of gusts. The gust factor is used in conjunction with the mean load, so that the total design wind load should satisfy the condition,

$$p(z)_{max} \geq G\bar{p}(z) \qquad (3.1)$$

The value of $(p(z)\ max)$ is chosen such that it corresponds to the value of maximum design wind velocity, by the help of equation (2.1).

In equation (3.1), G the gust factor can be expressed as,

$$G = 1 + gr\sqrt{(B+R)} \qquad (3.2)$$

where g is the peak factor which depends on the fundamental frequency of vibration of the structure and time over which the mean velocity is averaged (see Figure 3); r is the roughness factor which depends on the location of the structure and the height of the structure above the ground (see Figure 4); B is the excitation by background turbulence which depends only on the height of structure above ground (see Figure 5); and R is the excitation by turbulence resonant with structure. The quantity R can be expressed as

$$R = \frac{sF}{\beta} \qquad (3.3)$$

where F is the gust energy ratio (see Figure 6); S is the size reduction factors which depends on the breadth b and the height h of the structure, and other important parameters (see Figure 7); and β is the critical damping ratio of the structure, this critical damping ratio, β, comprises contributions to damping from both mechanical and aerodynamic factors.

Other essential factors which sould be taken into account in design are the problems arising from unsymmetrical loading, vortex excitation, and aeroelastic instability. Moreover, wind tunnel testing and meteorological tests at the site should be conducted, in order to take necessary cognizance of aeroelastic model testing in the wind tunnel and of making meteorological measurements at the site in all instances in which dynamic factors are likely to be significant.

4. THE VARIATION OF GUST FACTOR

The wind velocity $U(z,t)$ in a place at a given height z and time t, can be divided into two parts, namely the mean velocity $\bar{U}(z)$ and the fluctuating velocity $\mu(z,t)$ as follows:

$$U(z,t) = \bar{U}(z) + \mu(z,t) \qquad (4.1)$$

The mean square of the fluctuating velocity can be expressed in terms of its power spectral density, F(n), which is a function of the frequency n,

$$\bar{\mu}^2(z,t) = 2\int_{\frac{1}{2}T}^{\infty} F(n)\,dn \qquad (4.2)$$

Equation (4.1) shows that since the wind velocity is a varying quantity, the value of the actual wind pressure on the structure will also vary, and as such the value of the gust factor G can also be shown to vary.

Some of the important factors which can contribute to this variation include the effects of analysis time, averaging time, length of the structure, mechanical characteristics of the structure and the variation of the turbulent energy of the wind with frequency which can be described conveniently by the power spectral density F(n).

The rate of decrease of the gust factor G with the length of the structure, can be obtained by referring to differences of phase in velocity fluctuations between two points which are apart by more than the scale of mean eddies in the wind. In other words, it suffices to show statistically that the air flow with maximum instantaneous velocity will not act on the whole length of the structure. For the purpose of mathematical formulation, space correlation between two points must be used in addition to spectral density, F(n).

For a long structure, wind load will be greatest in the wind direction perpendicular to the axis of the structure. The space correlation $\Pi(x)$ is obtained simply from the velocity fluctuations $\mu(x_o,t)$ and $\mu(x_o+x, t)$, at two points separated horizontally by a distance x in the perpendicular direction to the wind, as follows:

$$\Pi(x) = \overline{\mu(x_o,t) \cdot \mu(x_o+x,t)} \qquad (4.3)$$

As shown in (4.3), the space correlation is only a function of distance between two points, and can be shown to be:

$$\Pi_1(x) = \bar{\mu}^2(x_o) \exp\left[-\frac{x}{L}\left(1-\frac{x}{2L}\right)\right] \qquad (4.4)$$

where L is the lateral scale of turbulence. When the turbulence is isotropic, space correlation along mean wind becomes,

$$\Pi_2(x) = \bar{\mu}^2(x_o) \exp\left(-\frac{x}{L}\right) \qquad (4.5)$$

The space correlation can now be expressed as a function of the frequency n,

$$\Pi(x) = 2\int_0^\infty |S(x,n)|\, dn \qquad (4.6)$$

where $|S(x,n)|$ is the absolute value of the cross spectral density. In homogeneous wind field, the spectral densities at two horizontal points x_o and (x_o+x) are the same; and the correlation coefficient of fluctuating velocity of frequency n between two points separated by a distance x can be defined as follows,

$$R(x,n) = |S(x,n)| / F(n) \qquad (4.7)$$

Finally, for this case, equation (4.3) and (4.6) can be expressed as:

$$\Pi(x) = 2\int_0^\infty F(n)R(x,n)dn \qquad (4.8)$$

It is now possible to use the above results to develop necessary maximum velocity which is likely to be exceeded on the average only once in any specified number of years: and also to compute the necessary gust factor G for any long structure, (see Figure 8) for typical results. Also the use of the size reduction factor S in equation (3.3), (see Figure 7), has also taken the effect of the size of the structure into account, in the practical evaluation of the gust factor G for various structures.

5. CONCLUSION

The problem of estimating maximum design wind forces and pressures on structure can be divided into the assessments of,(a) the maximum design wind velocity,(b) the shape and pressure coefficients which are incorporated in the parameter (11), Cp (z), and (c) the final evaluation of gust factors and wind pressures.

A considerable degree of uncertainty exists in the estimates of both the design wind speeds, the coefficients and other essential parameters of this problem. A method of obtaining the design wind speed is described, which is based on the application of maximum entropy technique; and an attempt is made to obtain the design wind force of various structures from the formula of static wind force, only by changing numerical values of gust factors, refereing to size and structural characteristics. Codes of practice are often used for relevant information on factors which are essential in this problem. However, for many structures the design demands more detailed and specific wind-loading data than are given in codes. The conditions under which wind-tunnel tests to obtain more specific data are carried out required careful consideration. Properties of the local natural wind, such as shear and turbulence, the Reynolds number of the flow, and the influence of local topographical factors, grouping of buildings, etc., may have to be reproduced in the wind tunnel to ensure full confidence in the accuracy of the data.

Wind effects are important considerations for the design of safe and economic structures, but their estimation remains subject to considerable uncertainties. These uncertainties will become better understood as improvements in the experimental facilities and wind tunnel techniques develop, and also as more meteorological data effect improvements in the

experimental facilities and wind tunnel techniques develop, and also as more meteorological data effect improvents in the statistical evaluation and reliability of the long range prediction of maximum wind speeds and pressures; and in our knowledge of the turbulence and shear characteristics of the wind.

REFERENCES

1. Shannon. C.E.: "A Mathematical Theory of Communications" Bell System Technical Journal, July and October 1948

2. Jaynes E.T: "Probability Theory in Science and Engineering" McGraw Hill, New York 1951.

3. Tribus. M: "Use of the Maximum Entropy Estimate in the Estimation of Reliability" Information and Decision Processes edited by Machol and Gray

4. Shah. H.C: "Reliability of Aircraft Structures Under Random Repeated Loading" Aeronautical Structures Laboratory, Report N156 - 45588, Navy Air Engineering Centre, Philadelphia, Pennylvania, U.S.A.

5. Soboyejo A.B.O. Unpublished notes and reports of work on Wind Loadings on Structures, with special reference to Nigeria in particular, and West Africa in general. Faculty of Engineering, University of Lagos, Lagos, Nigeria.

6. Merchant D.H: "A Stochastic Model of Wind Gusts" Department of Civil Engineering, Stanford University, Stanford, California, U.S.A. Technical Report No. 4B, November 1964.

7. Shellard H.C: "Wind Records and their Application to Structural Design" Symposium on Natural Draught Cooling Towers-Ferrybridge and After, Institution of Civil Engineers, June 1967

8. Davenport A.G: "The specirum of Horizontal Gustiness Near the Ground in High Winds" Quarterly Journal of the Royal Meteorological Society, London, Vol.87, April 1961, pp. 194 - 211

9. Borges F.J: "Dynamic Loads (In particular Wind and Earthquake Loads)" Preliminary Publication, 8th Congress of the International Association for Bridge and Structural Engineering, New York, Sept. 1968.

10. Thom. H.C.S: "Toward a Universal Climatological Extreme Wind Distribution" Proc. Intl. Seminar on Wind Effects on Buildings. National Research Council, Ottawa, 1967

11. Scruton. C. "The Problem of Estimating Wind Loading on Structures with Special Reference to Cooling Towers" Symposium on Natural Draught Cooling Towers - Ferrybridge and After, Institution of Civil Engineers, June 1967.

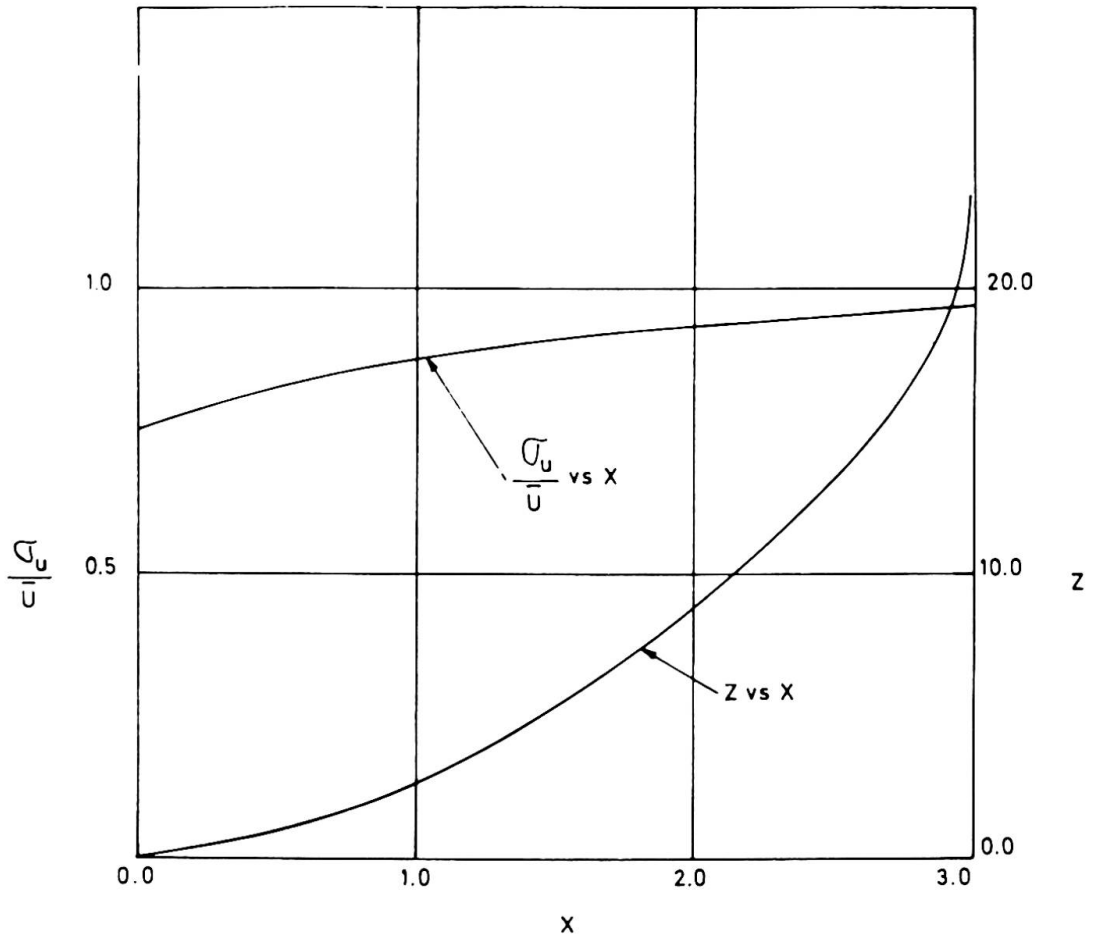

Fig. 1

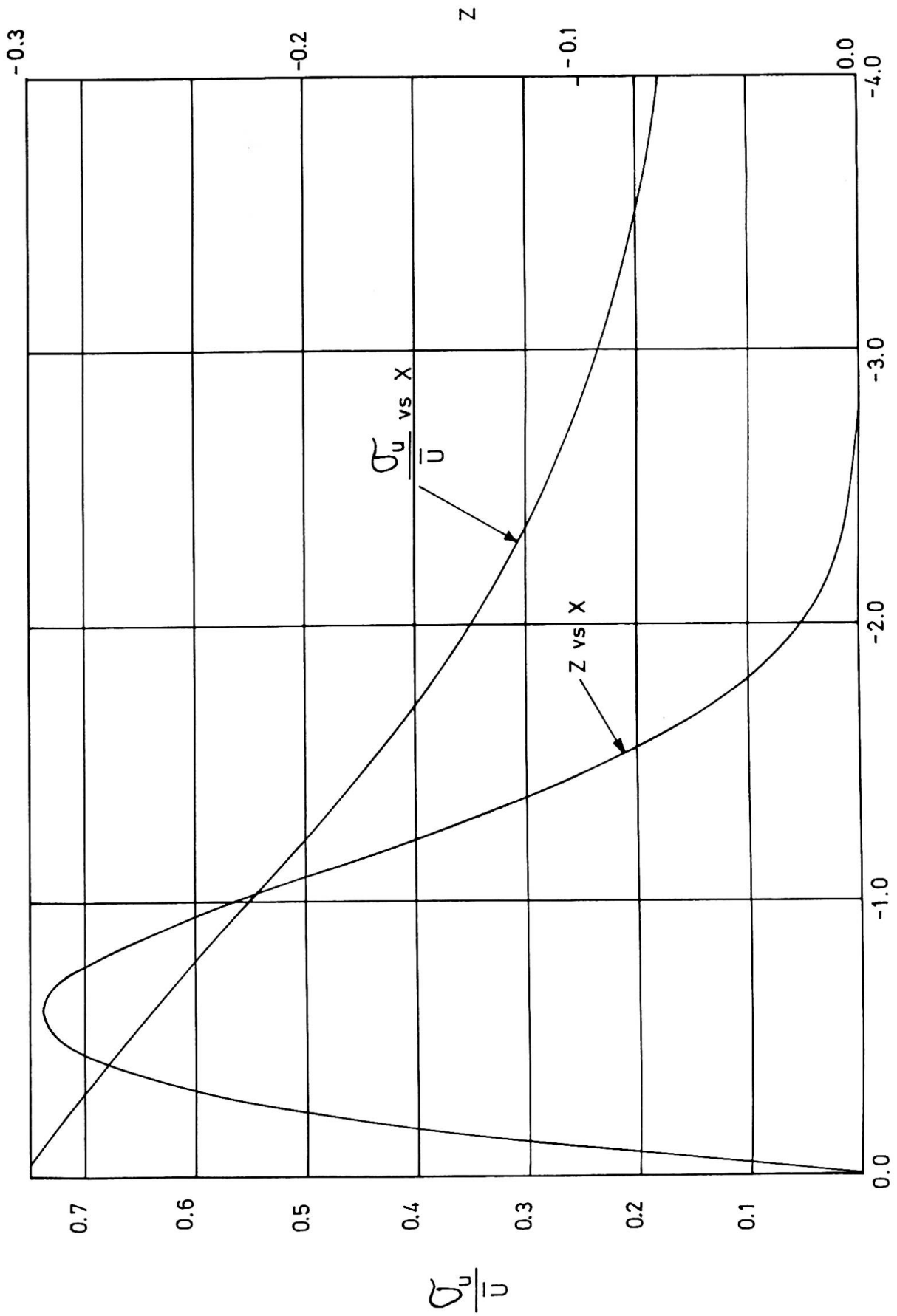
Z
-0.3
-0.2
-0.1
0.0
-4.0
-3.0
-2.0
-1.0
0.0
$\sigma_u/\bar{u}$ vs X
Z vs X
0.7
0.6
0.5
0.4
0.3
0.2
0.1
$\sigma_u/\bar{u}$

Fig. 2

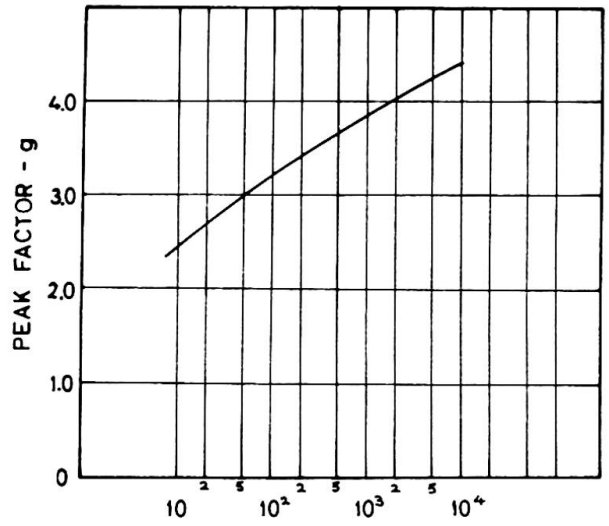

n_o = FUNDAMENTAL FREQUENCY OF VIBRATION

T = TIME OVER WHICH MEAN VELOCITY IS AVERAGED

Fig. 3: Peak Factor

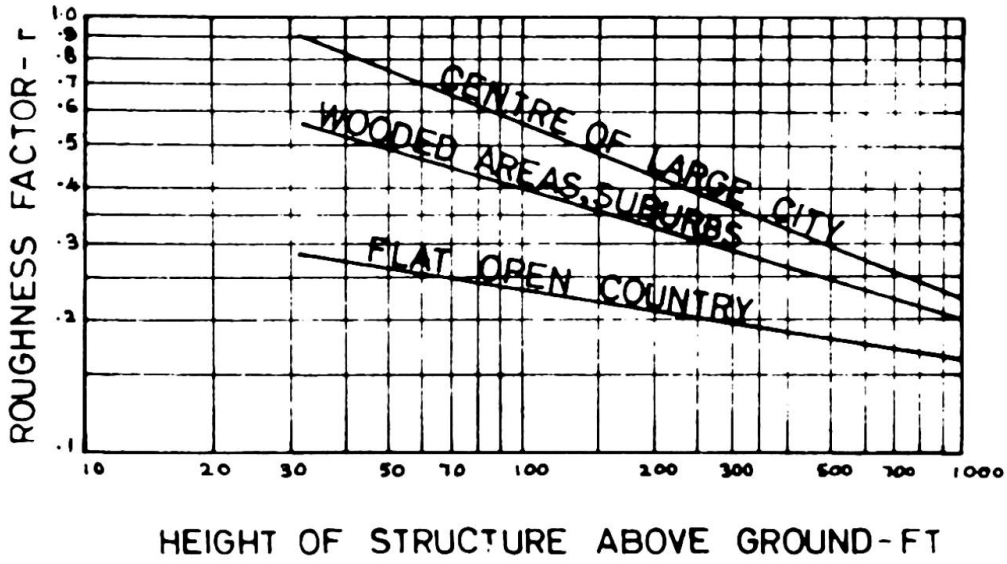

Fig. 4: Roughness Factor

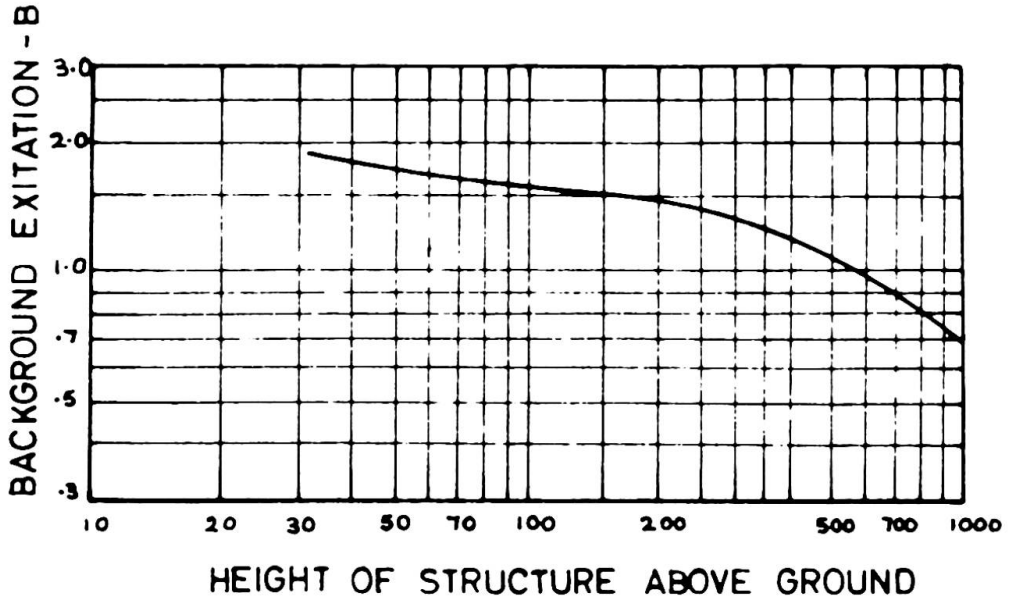

Fig. 5: Exitation Caused by Background Turbulence

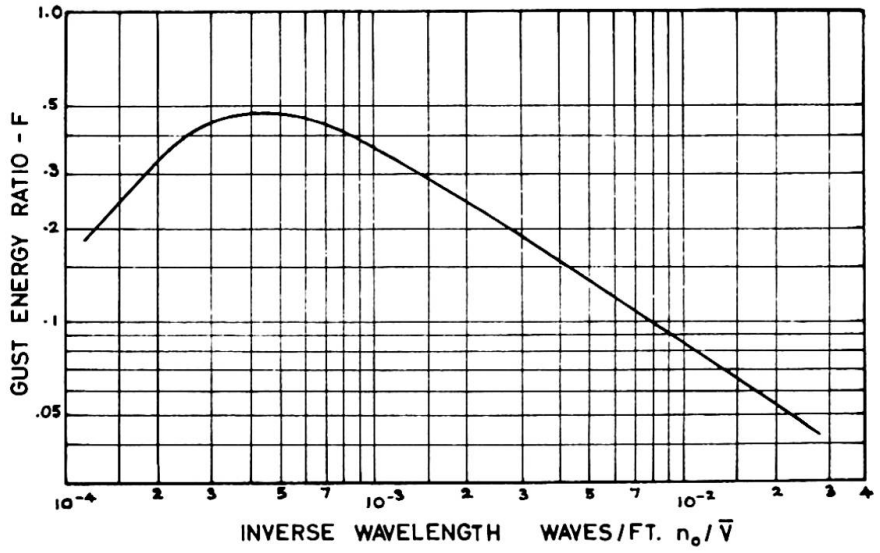

Fig. 6: Gust Energy Ratio

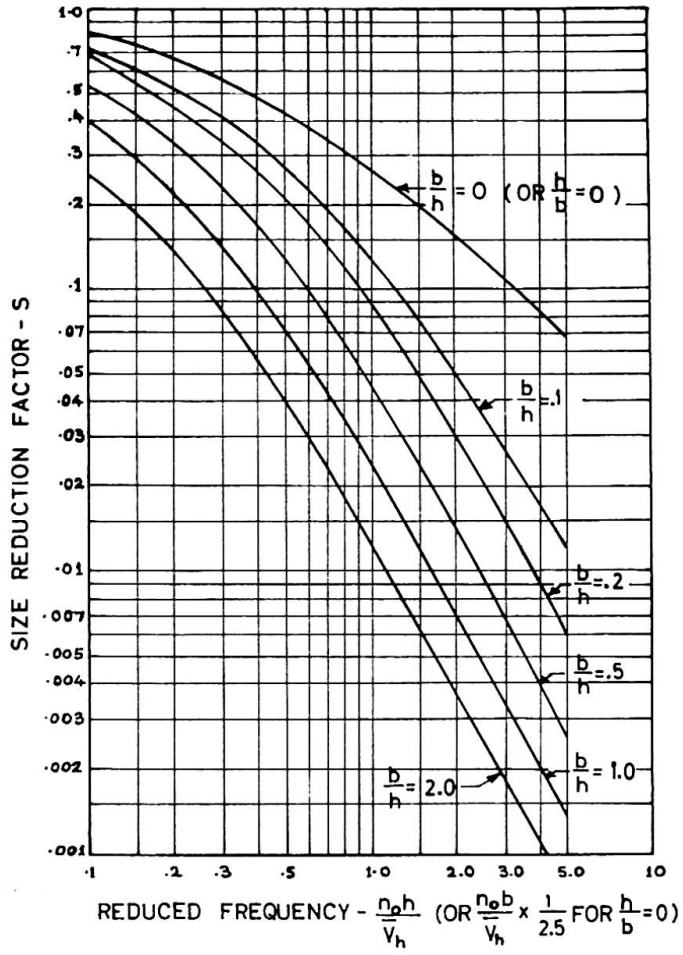

Fig. 7: Size Reduction Factor

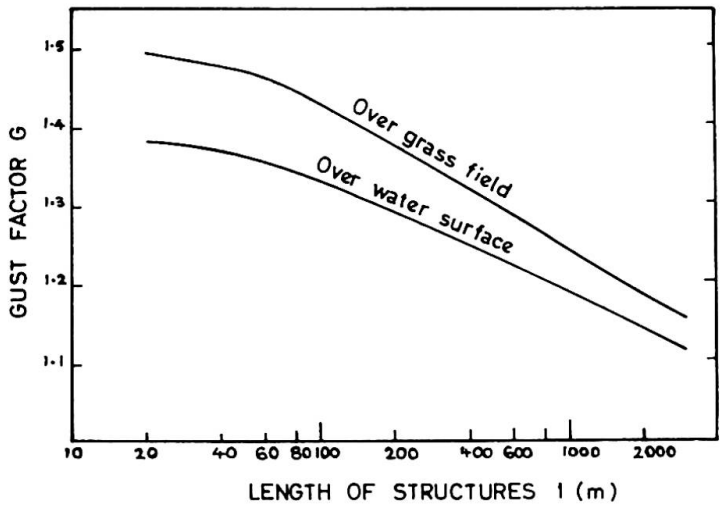

Fig. 8: Variation of Gust Factor of Long Structures with Length of Structures

SUMMARY

Minimally biased probability distribution functions for maximum value of the horizontal components of wind velocities and pressures, acting on engineering structures, are developed using maximum entropy concepts. In order to evolve a meaningful design wind force, it is found important to consider the dynamics of the problem, by considering among other factors, relevant changes in the numerical values of the gust factors referring to size, structural characteristics, and the space correlations of velocity fluctuations in addition to power spectrum.

RÉSUMÉ

A l'aide de conceptions d'entropie maximale on a développé des fonctions de répartition de la probabilité les moins vagues possibles pour les valeurs maximales des composantes horizontales de la vitesse et de la pression du vent. Pour trouver une force utile au dimensionnement, il est important de considérer le côté dynamique du problème, en tenant compte entre autres des changements importants du facteur de rafales, dépendant des dimensions et des caractéristiques de la structure, ainsi que des relations dans l'espace des fluctuations de vitesse en addition aux variations de puissance.

ZUSAMMENFASSUNG

Mit Hilfe Maximal-Entropie-Prinzipien werden Verteilungsfunktionen kleinster Schiefe für den grössten Wert der waagrechten Windgeschwindigkeits- und Winddruckkomponente auf Bauten hergeleitet. Um eine sinnvolle Kraft für die Bemessung zu bestimmen, muss die dynamische Wirkung unbedingt berücksichtigt werden, indem unter anderem die erheblichen Aenderungen des Böenfaktors in Funktion der Abmessungen und der baulichen Charakteristiken der Konstruktion sowie die räumlichen Zusammenhänge der Geschwindigkeits- und Kraftvariationen in Betracht gezogen werden.

Leere Seite
Blank page
Page vide

VI

Response of Structures Subjected to Sonic Booms

Influence des détonations supersoniques sur les constructions

Wirkung des Überschallknalls auf Bauwerke

GEORGE HERRMANN
Professor of Civil Engineering
Northwestern University
Evanston, Illinois

DUSAN KRAJCINOVIC
Solid Mechanics Research
Ingersoll-Rand Research Center
Princeton, New Jersey

1. Introduction

The advent of supersonic commercial air-transport operations brings with it a host of new and different problems, such as the transient pressure generated by the sonic boom that is associated with the shock waves stemming from the aircraft. The response problem will involve not only people, but also structures on the ground, and thus transient response of buildings and other structures to the supersonic shock has to be studied.

As measurements of the history of the far-field atmospheric pressure (signature) induced by a sonic boom indicate, the loading on a structure consists of a sudden overpressure followed immediately by a sharp underpressure. The total duration of this applied disturbance has been measured to be of the order of a fraction of a second. Because of the shape of this signature and the relatively short duration time, the authors are proposing to represent the applied load as a dipole in time. A dipole has been defined and used extensively as a generalized derivative of a Dirac delta function only if the independent variable is a spatial coordinate. Even though some work has already been carried out on the effects of the sonic boom on structures, the proposed representation of the loading as a dipole in time (called here bipulse) has the advantage that the structural response may be treated conveniently as a homogeneous initial value problem.

In Section 2 the proposed representation of the sonic boom loading is discussed, while the response of some simple structures is analyzed in Section 3.

A more extensive treatment of the response of structures to sonic booms, including problems of continuous structures, will be presented by the authors in a later study.

2. The Sonic Boom Loading

A large number of measurements of the pressure on the ground generated by sonic booms has been recorded and published in the last few years [1]. The

measured diagram showing the variation of the pressure with respect to time (the

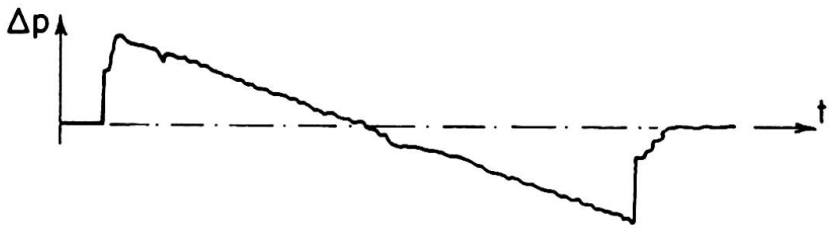

Fig. 1. Pressure signature due to the sonic boom
$\Delta p = 0$ corresponds to atmospheric pressure.

signature), Fig. 1, may be closely approximated by two triangles of identical area, Fig. 2.

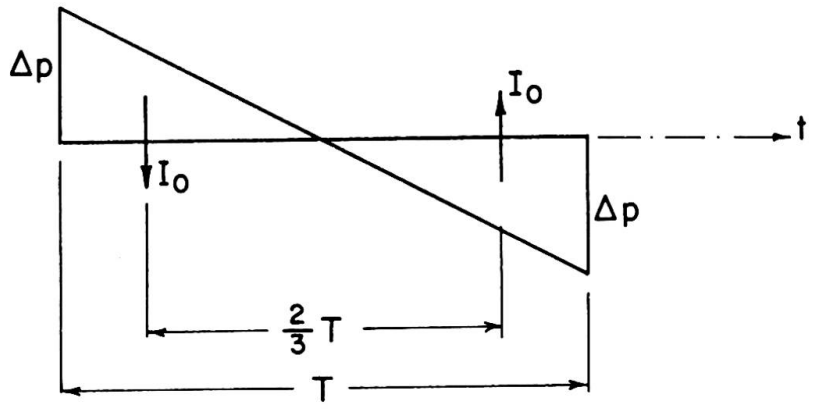

Fig. 2. Idealized pressure signature due to the sonic boom.

The two most significant parameters for the structural engineer are the peak overpressure Δp and the time duration T.

According to the measurements reported in Ref. [1], the duration T is 0.04 sec for the sonic boom generated by the present-day fighters, 0.1 sec for the largest present-day operational aircrafts, and is expected to be 0.4 sec for the supersonic transport (SST). It has been established also that Δp is not considerably different for the three cases mentioned.

In analyzing a structure subjected to sonic boom loading, it is necessary to represent the pressure signature in a mathematically convenient manner. For loads which have a large intensity and short duration (impulsive loads) it is a standard procedure to make use of the Dirac delta function defined by

$$\delta(t-\tau) = \begin{cases} 0 & t \neq \tau \\ \infty & t = \tau \end{cases}$$

$$\int_{-\infty}^{\infty} \delta(t-\tau)dt = 1 .$$

It can be shown readily that such impulsive loading may be regarded as the difference between two step loads of the same intensity P(x) applied immediately one after another, i.e.,

$$\lim_{\substack{P(x)\Delta t \\ \Delta t \to 0}} \frac{H(t-\tau) - H(t-\tau+\Delta t)}{\Delta t} = I(x)\delta(t-\tau), \tag{1}$$

where $H(t-\tau)$ is the Heaviside step function defined by

$$H(t-\tau) = \begin{cases} 0 & t < \tau \\ 1 & t > \tau \end{cases}$$

and

$$I(x) = \lim_{\substack{\Delta t \to 0 \\ P(x) \to \infty}} [P(x)\Delta t]. \tag{2}$$

It occurred to the authors that the sonic boom signature may be conveniently represented by two impulsive loads, opposite in sign, and acting in rapid succession one after another. This implies mathematically that the signature may be idealized by a time derivative of a Dirac delta function, i.e.,

$$\lim_{I(x)\Delta t} \frac{\delta(t-\tau) - \delta(t-\tau+\Delta t)}{\Delta t} = - B(x)\dot{\delta}(t-\tau), \tag{3}$$

where $\dot{\delta}(t-\tau)$ is a dipole of positive unit moment applied at $t = \tau$ on the time axis and is defined by

$$- \dot{\delta}(t-\tau) = \lim_{\Delta t \to 0} \frac{\delta(t-\tau+\Delta t) - \delta(t-\tau)}{\Delta t} = \frac{d\delta(t-\tau)}{dt}.$$

The function B(x), having the dimension of the force multiplied by the square of the time unit, is defined as

$$B(x) = \lim_{\substack{\Delta t \to 0 \\ I(x) \to \infty}} [I(x)\Delta t]. \tag{4}$$

Spatial derivatives of the Dirac delta function have been used extensively in various branches of physics and engineering (e.g., acoustics) under the name dipole of doublet. To distinguish these from the time derivative defined by Eq. (3), we propose to use the term "bipulse" for the latter.

Based on these definitions, let us now calculate the bipulse idealizing a sonic boom signature. The impulse I(x), see Fig. 2, is

$$I(x) = \frac{\Delta p(x)T}{6},$$

while the bipulse is the "moment" of the two impulses, i.e.,

$$B(x) = \frac{2}{3} TI(x) = \frac{1}{9} \Delta p(x)T^2.$$

3. Response of a Lumped-Parameter Structure

In this Section we wish to calculate the response of a simple system subjected to a sonic boom loading and compare the results with the responses to other types of dynamic loads, such as step load and an impulse. The structure shall be considered to possess only a single mass m and a single stiffness k. The differential equation of such a system with one degree of freedom is, in terms of a displacement w,

$$\frac{d^2w}{dt^2} + \omega^2 w = \frac{F(t)}{m} , \tag{5}$$

where

$$\omega^2 = \frac{k}{m}$$

is the natural frequency of free vibrations, t is the time, and F(t) is the applied load. The static displacement w_{st} due to the static force $F(t) = F_o$ is

$$w_{st} = \frac{F_o}{k} = \frac{F_o}{m\omega^2} . \tag{6}$$

The general solution to Eq. (5), as combined from the transient and steady-state part, reads

$$w(t) = w(0)\cos\omega t + \dot{w}(0)\,\frac{\sin\omega t}{\omega} + \frac{1}{\omega}\int_0^t \frac{F(t)}{m}\,\sin\omega(t-\tau)dt, \tag{7}$$

where w(0) and $\dot{w}(0)$ are the initial displacement and the initial velocity, respectively. We will confine our attention to the solution of an initial value problem with

$$w(0) = \dot{w}(0) = 0.$$

It is well known that the response to a step load results in a maximum displacement

$$w_{max} = 2w_{st}$$

such that the so-called displacement amplification factor $A \equiv |w_{dyn\ max}|/|w_{st}|$ is in this case

$$A_H = 2. \tag{8}$$

Next we calculate the response to a single impulse applied at time t = 0. The forcing term in Eq. (5) now reads

$$\frac{F(t)}{m} = \frac{I_o}{m}\,\delta(t) \tag{9}$$

resulting in a displacement

$$w_I = \frac{I_o}{m\omega} \sin\omega t = \frac{I_o \omega}{F_o} w_{st} \sin\omega t. \tag{10}$$

The amplification factor is now a function of the structural parameters and reads

$$A_I = \frac{I_o \omega}{F_o} . \tag{11}$$

Finally, for the bipulse loading, the forcing term in Eq. (5) is

$$\frac{F(t)}{m} = - \frac{B_o}{m} \dot{\delta}(t) \tag{12}$$

such that the displacement is

$$w_B = \frac{B_o}{m} \cos\omega t = \frac{B_o \omega^2}{F_o} w_{st} \cos\omega t \tag{13}$$

and the displacement amplification factor is

$$A_B = \frac{B_o \omega^2}{m} , \tag{14}$$

which again depends on the properties of the structure.

It is useful, now, to define the ratio μ between the maximum displacement due to the bipulse and due to the impulse, i.e.,

$$\mu = \frac{|w_{B\ max}|}{|w_{I\ max}|} = \frac{B_o \omega}{I_o} . \tag{18}$$

Since $$B_o = \frac{2}{3} T I_o$$

μ can also be written as

$$\mu = \frac{2}{3} T \omega . \tag{19}$$

The limiting value ω^* of the natural frequency of the free vibrations of the system, above which the bipulse induces larger displacements than the impulse is, according to Eq. (19), obtained for $\mu = 1$. Using the values of T for the three different aircrafts mentioned in Section 2, we obtain

$$\omega^* = \begin{cases} \frac{3}{2(0.04)} = 37.5 \text{ sec}^{-1} & \text{(fighters)} \\ \frac{3}{2(0.1)} = 15 \text{ sec}^{-1} & \text{(present-day aircrafts)} \\ \frac{3}{2(0.4)} = 3.75 \text{ sec}^{-1} & \text{(SST)} \end{cases} \tag{20}$$

It is obvious from the numerical values given above that the representation of the sonic boom by a simple impulse, as this is sometimes assumed, may lead to

results which greatly underestimate the structural response.

As an illustration let us consider a cantilevered beam of length ℓ and mass per unit of length m. If only the lowest mode is assumed to contribute to the response, the corresponding natural frequency of free vibrations is known to be

$$\omega^2 = 3\,\frac{20\,EI}{9\,m\ell^4}\,,$$

where EI is the flexural rigidity. If ω^* is taken as 15 sec^{-1} (largest present-day aircrafts), then for

$$\frac{EI}{m\ell^4} > 33.7\ sec^{-2}$$

the response to a bipulse is larger than that to an impulse.

Note that for $\mu = 1$ the duration of the bipulse is almost 1/4 of the natural vibration period. This means that the proposed idealization leads to an overestimation of displacements. Consequently $\mu = 1$ may be regarded only as a lower bound under which sonic boom results in smaller displacements than predicted by an impulsive load.

4. Conclusions

Having proposed that the effect of the sonic boom on a simple structure may be represented as a dipole in time ("bipulse"), the authors show that this idealization leads to convenient mathematical analysis. The commonly used displacement amplification factor as a measure of the severity of dynamic response is introduced. It is shown that the amplification factor depends on the free vibration frequency of the structure and that, consequently, some structures undergo larger displacements due to the bipulse load than due to other types of dynamic loads (such as impact load). The procedure is exemplified by a simple discrete system.

In a later paper the authors intend to treat the problem in greater detail, proving that it reduces to an initial value problem and extending it to continuous systems.

5. Acknowledgment

The authors are very grateful to Professor C. Dyrbye of the Technical University of Denmark for a most constructive discussion of this work. They also wish to acknowledge the support of the Air Force Office of Scientific Research under grant AF-AFOSR-100-67.

Reference

1. "Proceedings of the Sonic Boom Symposium," J. Acoust. Soc. Am. 39, No. 5, Part 2, S1-S80 (1966).

SUMMARY

It is suggested in this paper that the loading on structures induced by the sonic boom generated by supersonic aircraft can be represented by a dipole in time. The term "bipulse" is introduced for this type of transient loading. It is shown that simple structures subjected to such bipulse loading may be conveniently analyzed and the response readily compared with that due to other types of dynamic effects such as, for example, step loading and impulsive loading.

RÉSUMÉ

La rédaction suggère de représenter la charge appliquée à une construction due à une détonation supersonique par un dipôle du temps. On introduit le terme "bipulse" pour désigner ce type de charge variable. Cette charge "bipulse" peut être facilement analysée et son effet comparé à celui d'autres types d'effets dynamiques comme charge progressive ou charge impulsive, dans le cas de structures simples.

ZUSAMMENFASSUNG

In diesem Beitrag wird vorgeschlagen, dass die aus Ueberschallknall der Ueberschallflugzeuge entstandene Belastung durch ein Dipol der Zeit dargestellt werden kann. Der Ausdruck "Bipuls" ist für diese Art veränderlicher Belastung eingeführt worden. Es wird gezeigt, dass einfache Bauwerke unter solcher Bipulslast bequem gelöst werden können, und dass die Antwort leicht fällt verglichen mit jenen, die anderen dynamischen Wirkungen unterworfen sind, zum Beispiel Stufenlast und impulsiver Last.

Leere Seite
Blank page
Page vide

Untersuchungen über den Erregungscharakter winderregter Querschwingungen kreiszylindrischer Stäbe im unterkritischen Reynolds-Bereich

Investigations in the Subcritical Reynolds Range on the Nature of Wind-Induced Lateral Vibrations of Circular-Cylindrical Tubes

Recherches dans le domaine sous-critique de Reynolds sur la nature des vibrations latérales, provoquées par le vent dans un tuyau circulaire-cylindrique

W. HOYER
Prof.Dipl.-Ing.

G. HÖLZEL
Dr.-Ing.

Technische Universität Dresden
Lehrstuhl für Technische Mechanik und Baudynamik

1. Einleitung

Turbulenter Wind kann elastische Stäbe zu Schwingungen in Windrichtung erregen (Borges [1]). Bei gleichmäßigem Wind und besonders bei relativ niedrigen Geschwindigkeiten werden oft starke Schwingungen beobachtet, die senkrecht zur Windrichtung erfolgen. Schäden infolge derartiger Querschwingungen sind bisher von dünnwandigen, schlanken Stahlkonstruktionen mit geringer Eigendämpfung und kreisförmigem Querschnitt bekannt, z.B. von Stahlschornsteinen, stählernen Fernsehtürmen und Stahlrohrkonstruktionen.

Für beliebige Querschnittsformen kommt eine Grenzschichtablösung mit Wirbelbildung und für aerodynamisch instabile Querschnitte zusätzlich eine Selbsterregung als Querschwingungsursache in Frage. Der Kreisquerschnitt ist als aerodynamisch indifferent aufzufassen, so daß er nur durch Wirbelablösung erregt werden kann.

Im unterkritischen Reynolds-Bereich $Re < Re_{kr} \approx 3{,}5 \cdot 10^5$ beobachtet man für $Re > 10^2$ im Nachlauf hinter einem umströmten Zylinder eine regelmäßige, alternierende Wirbelschleppe (Kármánsche Wirbelstraße) mit einer konstanten dimensionslosen Wirbelfrequenz $S \approx 0{,}17 \ldots 0{,}20$ (Bild 1).

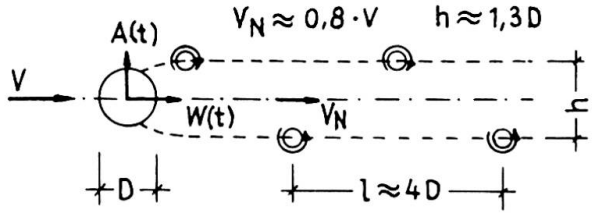

Bild 1: Kármánsche Wirbelstraße

Reynoldsche Ähnlichkeitszahl

$$Re = \frac{V \cdot D}{\nu} \qquad (1)$$

$\nu = 1{,}45 \cdot 10^{-5}$ m²/s für Luft bei 15° C und 760 mmHg

Strouhal-Zahl

$$S = S(Re) = \frac{f \cdot D}{V} \qquad (2)$$

f - Wirbelablösefrequenz

Auf Grund dieser periodischen Wirbelanordnung wird bisher allgemein für die Quertriebserregung eine harmonische Kraft mit diskreter Frequenz angenommen (z.B. Novák [6]).

Auftrieb (Quertrieb) $A(t) = c_A(t).q.D$ (3)

$$q = \frac{1}{2} \varrho . V^2 \quad \text{- Staudruck}$$

Quertriebsbeiwert $c_A(t) = c_A . \sin(2\pi . \frac{S.V}{D} t)$ (4)

Der von Drescher [2] am starren Zylinder im Wasserkanal gemessene Verlauf der Quertriebskräfte weist zwar eine etwa konstante Periode auf, die Amplituden zeigen aber größere Schwankungen. Weaver [8] spricht von einer "sinusförmigen" Kraftfunktion mit zufälliger Amplitude und erfaßt die Amplitudenschwankungen durch Angabe der Wurzel aus dem statistischen Amplitudenquadratmittel $\overline{c_A} = \sqrt{c_A^2}$; die in Gleichung (4) formulierte Erregerart behält er aber bei.

Im überkritischen Strömungsbereich $Re > Re_{kr}$ beobachtet man einen regellosen Nachlauf ohne dominierende Wirbelfrequenz. Fung [3] faßt die Erregung als stationären stochastischen Prozeß auf und gibt Spektraldichten an. Damit können die winderregten Querschwingungen im überkritischen Bereich erklärt werden, die keinen Resonanzcharakter aufweisen und in der Eigenfrequenz der Konstruktion erfolgen.

Für Bauwerke mit großem Durchmesser (z.B. Schornsteine) ist im allgemeinen der überkritische Re-Bereich maßgebend, für Bauteile mit kleinem Durchmesser (z.B. Stahlrohrstäbe von Fachwerkkonstruktionen) der unterkritische Re-Bereich.

2. Widersprüche im unterkritischen Re-Bereich

Für die zu beobachtenden Amplitudenschwankungen fehlt eine exakte Erklärung. Die analytische Darstellung einer harmonischen Kraftfunktion mit regelloser Amplitude ist mathematisch nicht einwandfrei. Die im Windkanal gemessenen Schwingungsbeanspruchungen zeigen ein resonanzartiges Maximum (Bild 2), wenn die Wirbelfrequenz f mit einer Eigenfrequenz n_k des Stabes übereinstimmt. Außerhalb dieser kritischen Geschwindigkeit treten aber wesentlich größere Amplituden auf, als sie sich theoretisch mit obiger Annahme (4) ergeben müßten. Die Schwingungsfrequenz müßte linear mit der Windgeschwindigkeit ansteigen, beobachtet wird aber vorwiegend besonders bei kleiner Eigendämpfung die Stabeigenfrequenz. Bei kleinen Anblasgeschwindigkeiten $V \approx 0{,}5 . V_{kr}$ kann man besonders bei größerer Dämpfung ein Gemisch aus der Eigenfrequenz und der zu V gehörigen Kármánschen Wirbelfrequenz f feststellen, ebenso im Bereich nahe der kritischen Geschwindigkeit, wo sich dieses Gemisch als Schwebung äußert.

Die bisher übliche Deutung, daß die Wirbelablösung auch außerhalb der Resonanzstelle vom schwingenden Stab gesteuert werde und deshalb stets die Eigenfrequenz beobachtet werde, kann für sehr kleine Auslenkungen bzw. für Verhältnisse der Schwinggeschwindigkeit zur Windgeschwindigkeit von weniger als 0,1 % (z.B. für $V \approx 1{,}5 . V_{kr}$) nicht als zutreffend angesehen werden und ist

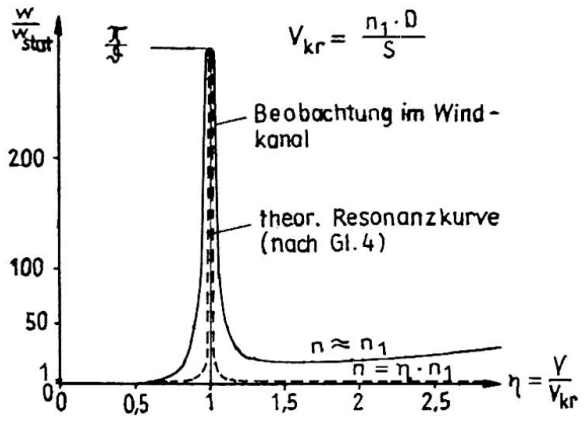

Bild 2: Schwingungsverhalten für $\vartheta \approx 0{,}01$

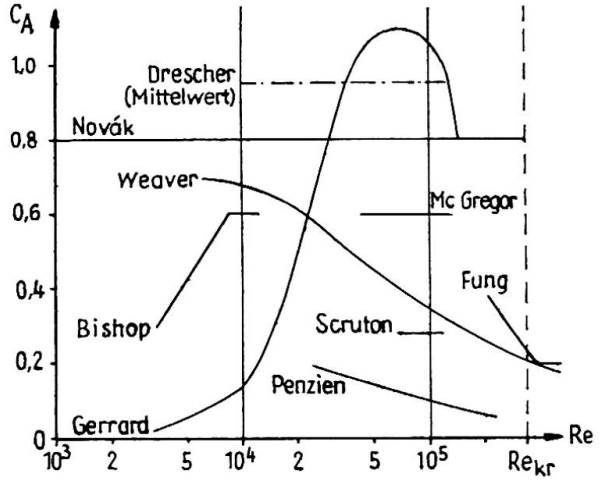

Bild 3: Quertriebsbeiwerte c_A (Quellenangaben in [5])

inzwischen experimentell widerlegt. Bei Versuchen im Windkanal der Technischen Universität Dresden wurde festgestellt, daß die Wirbelfrequenz im Nachlauf hinter einem in der Eigenfrequenz schwingenden Schornsteinmodell linear mit der Anblasgeschwindigkeit ansteigt. Diese Messung bestätigt die im Abschnitt 3 vorgelegte Hypothese.

Versuche mit gelenkig gelagerten Stahlrohren zeigten Resonanz bis zur 4. Eigenfrequenz. Das Auftreten dieser höheren Eigenformen setzt voraus, daß in Stablängsrichtung veränderliche Quertriebskomponenten wirken. Nach der bisherigen Annahme der mit der Wirbelablösung verbundenen Kraftwirkungen ist diese Erscheinung unter Berücksichtigung des Helmholtzschen Wirbelsatzes nicht erklärbar.

Die von verschiedenen Autoren angegebenen Quertriebsbeiwerte c_A für Kreiszylinder (im Bild 3 sind einige wichtige Werte dargestellt) schwanken außerordentlich stark und sind als Grundlage für eine Bemessung sehr unbefriedigend.

Gerrard [4] hat an einem starren Kreiszylinder eine Frequenzanalyse des Oberflächendruckes, allerdings nur für einen einzigen Punkt des Querschnitts, durchgeführt und entgegen der Erwartung ein Spektrum statt einer diskreten Frequenz messen können.

Die angeführten Widersprüche und Unklarheiten führen zu dem Schluß, daß die bisher angenommene harmonische Erregung trotz der periodischen Wirbelstraße nicht dem tatsächlichen Erregungscharakter entspricht.

3. Hypothese einer schmalbandigen spektralen Erregung

Direkte Messungen der Quertriebskräfte am schwingenden Zylinder sind nicht bekannt. Es muß aus den aus der Literatur bekannten Tatsachen und aus den eigenen im Niedergeschwindigkeits-Windkanal der Technischen Universität Dresden durchgeführten Versuchen auf die Erregungsart geschlossen werden.

Alle bekannten Erscheinungen sind nur erklärbar, wenn für die Quertriebskraft A(t) bzw. den Quertriebsbeiwert $c_A(t)$ nach Gl. (3) eine stationäre Zufallsfunktion mit einem schmalbandigen Spektrum angenommen wird. Mit Hilfe der Enveloppenmethode der mathematischen Statistik (siehe z.B. Sweschnikow[7]) läßt sich nachweisen, daß ein derartiger stochastischer Prozeß mit einem Spektrum $\Delta S/S_{kr} = \Delta\omega/\omega_{kr} \ll 1$ (Bild 4b) als Realisierung eine sinus-ähnliche Kurve mit etwa konstanter Periode und langsam veränderlicher Amplitude ergibt. Die Frequenz entspricht dabei der mittleren Bandfrequenz ω_{kr}. Die Amplituden sind nur als statistische Wahrscheinlichkeitswerte darstellbar. Der von Drescher gemessene Quertriebsverlauf stimmt mit einer solchen Realisierung überein.

Die Strömungsvorgänge am Kreiszylinder und die dabei auftretenden Kraftwirkungen können etwa folgendermaßen gedeutet werden: Der Nachlauf in einer gewissen Entfernung hinter dem umströmten Querschnitt ist zwar entsprechend dem Kármánschen Stabilitätsnachweis periodisch, am Körper selbst sind aber Störungen möglich, die rasch abklingen. Die Kraftwirkungen am umströmten Körper könnten also zunächst regellos sein, vom Nachlauf wird rückwirkend ein gewisser Rhythmus aufgezwungen, so daß sich ein schmalbandiges Spektrum ergibt, dessen Realisierung eine Periode entsprechend der Nachlauffrequenz aufweist.

Die Quertriebserregung wird als stationärer stochastischer Prozeß aufgefaßt. Die statistischen Mittelwerte für den Kreiszylinder lauten

$$\overline{c_A(t)} = \lim_{T\to\infty} \frac{1}{T}\int_{-T/2}^{T/2} c_A(t)\,dt = 0 \qquad \overline{c_A^2(t)} = \lim_{T\to\infty} \frac{1}{T}\int_{-T/2}^{T/2} c_A^2(t)\,dt = \text{const.} \quad (5)$$

Für die Erregung wird eine Frequenzanalyse mit Hilfe des Leistungsspektrenverfahrens (Power-Spectral-Method) durchgeführt, die zu einer Spektraldichte ϕ_A in Abhängigkeit von der dimensionslosen Frequenz S führt. S entspricht formal der Strouhal-Zahl nach Gl. (2). Um das Einführen zweier Parameter zu vermeiden, wird $\phi_A(S)$ nicht wie bei Fung [3] normalisiert, sondern die Spektraldichte wird so definiert, daß der Inhalt des Spektrums gleich dem quadratischen Quertriebsmittelwert ist. Eine ausführliche Darstellung der folgenden Entwicklungen ist in [5] zu finden.

$$\overline{c_A^2(t)} = \int_{S=0}^{\infty} \phi_A(S)\,dS \qquad S = \frac{\omega \cdot D}{2\pi \cdot V} \quad (6)$$

Wenn Realisierungen $c_A(t)$ bekannt wären, könnte $\phi_A(S)$ aus der Korrelationsfunktion $R_A(\tau)$ ermittelt werden.

Die Schwingungsgleichung eines quererregten Stabes lautet:

$$(E.J.w'')''+2\mu.\omega_b.\dot{w}+\mu.\ddot{w} = A(x,t) \quad (7)$$

$$w' = \frac{\partial w(x,t)}{\partial x} \qquad \dot{w} = \frac{\partial w(x,t)}{\partial t}$$

μ – Massenbelegung

E.J – Biegesteifigkeit

Durch Entwicklung der Schwingungsauslenkung $w(x,t)$ nach Eigenformen $w_k(x)$

$$w(x,t) = \sum_{k=1}^{\infty} q_k(t) \cdot w_k(x) \tag{8}$$

erhält man ein System verallgemeinerter Schwingungsgleichungen. Für die k-te Eigenform gilt

$$\ddot{q}_k(t) + \frac{\vartheta_k}{\pi}\omega_k \cdot \dot{q}_k(t) + \omega_k^2 \cdot q_k(t) = \frac{Q_k(t)}{M_k} \tag{9}$$

ω – k-te Eigenkreisfrequenz

$\vartheta_k = \omega_b \cdot \frac{2\pi}{\omega_k}$ – logar. Dekrement der Dämpfung

$Q_k(t) = \int A(x,t) \cdot w_k(x)dx \qquad M_k = \int \mu(x) \cdot w_k^2(x)dx$

Die Verteilung der Luftkraft $A(x)$ bzw. ihres Beiwertes $c_A(x)$ ist auch in Stablängsrichtung x als statistischer Prozeß aufzufassen. Da die Korrelationsfunktion

$$R_A(\Delta x) = \overline{c_A(x) \cdot c_A(x+\Delta x)} \tag{10}$$

noch unbekannt ist, wird vorläufig diese Verteilung determiniert durch Entwicklung nach den Eigenformen erfaßt

$$c_A(x,t) = \sum_{k=1}^{\infty} c_{Ak}(t) \cdot \frac{\mu(x) \cdot w_k(x)}{|\mu \cdot w_k|_{max}} \tag{11}$$

Das Spektrum der Systemauslenkung in der k-ten Eigenform erhält man über die Betrachtung der Belastung als regellose Impulsfolge und über die Korrelationsfunktion der Auslenkung zu

$$\Phi_{wk}(\omega) = \frac{S \cdot q^2 \cdot D^2}{\omega \cdot \omega_k^4 \cdot (\mu \cdot w_k)^2_{max}} \cdot \varkappa_k^2(\omega) \cdot \Phi_{Ak}(S) \qquad \eta_k = \frac{\omega}{\omega_k} = \frac{S}{S_k} \tag{12}$$

$$\varkappa_k^2(\omega) = \frac{1}{(1-\eta_k^2)^2 + \frac{\vartheta_k^2}{\pi^2} \cdot \eta_k^2} \text{ – Frequenzübertragung}$$

Der quadratische Mittelwert der generalisierten Auslenkung ergibt sich damit als Inhalt des Spektrums

$$\overline{q_k^2(t)} = \int_{\omega=0}^{\infty} \Phi_{wk}(\omega) \cdot d\omega = \frac{q^2 \cdot D^2}{\omega_k^4 \cdot (\mu \cdot w_k)^2_{max}} \cdot \int_{S=0}^{\infty} \frac{\Phi_{Ak}(S) \cdot dS}{(1-\eta_k^2)^2 + \frac{\vartheta_k^2}{\pi^2} \cdot \eta_k^2} \tag{13}$$

Da $\Phi_A(S)$ abhängig von Re ist, erscheint eine technische Näherungslösung des Integrals der Gl. (13) zweckmäßiger für die praktische Anwendung als eine "strenge" Lösung für eine angenommene Vergleichskurve. Die Frequenzübertragungsfunktion $\varkappa_k^2(\omega)$ nach Gl. (12) kann als sehr schmalbandiger Filter aufgefaßt werden, der im wesentlichen nur die der Eigenfrequenz n_k entsprechende Erregungsintensität $\Phi_{Ak}(S_k) = \Phi_A(S_k)$ passieren läßt. Da die Querschwingungen nur bei schwach gedämpften Systemen interessieren, für die $\vartheta \lesssim 0{,}05$ angenommen werden kann, ist der Fehler der Näherungslösung mit der Annahme $\Phi_A(S) \approx$ const ("weißes Rauschen") klein gegenüber anderen Unsicherheiten (z.B. Dämpfung, Turbulenz, Meßfehler für ermittelte Spektraldichten ua.). Für $\vartheta = 0{,}05$ beträgt der Fehler für die Amplitude ca. 15 %, er nimmt

etwa linear mit der Dämpfung ab.

Mit dem Amplitudenwert $\overline{w_0^2} = 2 \cdot \overline{w^2(t)}$ gilt für die k-te Eigenform an der Stelle x der maximalen Auslenkung

$$\sqrt{{}^{k}w_{0,\max}^{2}} \approx \frac{q \cdot D \cdot \sqrt{S_k} \cdot \sqrt{\Phi_A(S_k)}}{4\pi \cdot \mu \cdot n_k^2 \cdot \sqrt{\vartheta_k}} \qquad S_k = \frac{n_k \cdot D}{V} \tag{14}$$

Zum Vergleich dazu gilt nach der herkömmlichen Auffassung im Resonanzfall

$${}^{k}w_{\max}^{\mathrm{Res}} = \frac{q \cdot D \cdot C_{Ak}}{4\pi\mu \cdot n_k^2 \cdot \vartheta_k} \tag{15}$$

Wenn für $V \neq V_{kr}$ die Lösung der Gl. (13) vollständiger erfaßt werden soll, kann nach Bild 4 geschrieben werden

$$\sqrt{{}^{k}w_{\max}^{2}(t)} \approx \frac{q \cdot D}{4\pi\mu \cdot n_k^2}\left[\sqrt{\frac{S_k \cdot \Phi_A(S_k)}{2 \cdot \vartheta_k} + \frac{\Phi_A(S_{kr}) \cdot \Delta S}{\pi^2 (1-\eta_{kF}^2)^2}}\right] \tag{16}$$

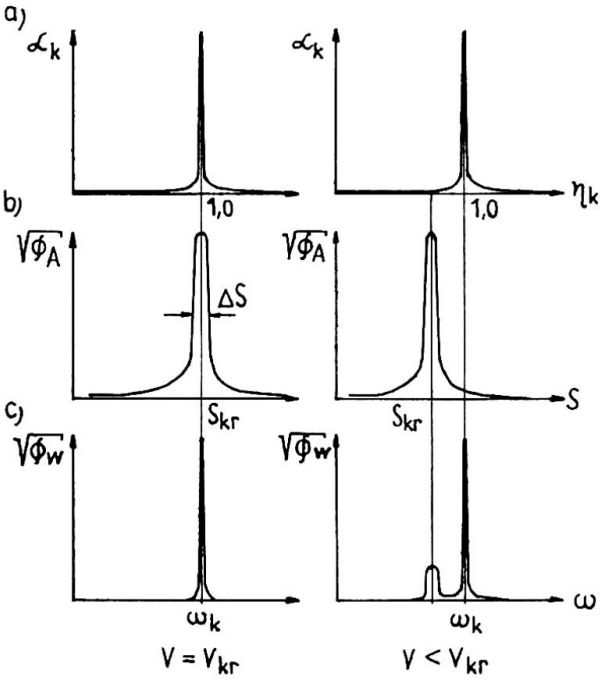

Mit der hier vorgelegten Hypothese einer schmalbandigen statistischen Erregung können alle bisher bekannten Widersprüche gelöst werden. Im Bild 4 ist für zwei Fälle angedeutet, welche Formen das Spektrum der Systemreaktion annehmen kann. Daraus sind das Vorherrschen der Eigenfrequenz, das Auftreten von Schwebungen und der Kármánschen Frequenz besonders bei größeren Dämpfungen ersichtbar.

Bild 4: Zusammenhang zwischen Frequenzübertragsfunktion (a), Erregerspektrum (b) und Spektrum der Systemauslenkung (c) nach Gl. (12)

4. Ergebnisse der durchgeführten Versuche

Im Windkanal wurde das Schwingungsverhalten an gelenkig gelagerten Stahlrohren von 32...108 mm Durchmesser und 1,5 m bzw. 2,5 m Länge und an einseitig aufgehängten Stahl- bzw. Holzzylindern von 89 mm bzw. 200 mm Durchmesser gemessen (siehe [5]). Die Düse hatte einen Durchmesser von 2,0 bzw. 3,0 m. Die Kanalturbulenz in der offenen Meßstrecke betrug ohne Berücksichtigung einer gewissen Pulsation des gesamten Geschwindigkeitsfeldes 0,1...0,2 %.

Der gesamte Verlauf der registrierten Querschwingungen konnte nicht durch einen Beiwert nach Gl. (4) dargestellt werden. Aus den Meßwerten einer Vielzahl von Versuchen wurden Spektraldichten nach Gl. (14) ermittelt. Für alle Versuche mit gleichartig gelagerten Stäben ergaben sich im durchfahrenen unterkritischen Bereich gleiche Kurven für die Spektraldichten. Nur die maximalen Ordinaten (für die kritische Frequenz S_{kr}) erwiesen sich als Re-abhängig. Um die Versuchsergebnisse auf Stäbe normaler Schlankheit im natürlichen Wind übertragen zu können, wurden bei den Versuchen keine Endscheiben verwendet. Dadurch zeigte der Verlauf der Spektraldichten für beide Modelltypen Unterschiede. Für die gelenkig gelagerten Stahlrohrmodelle ist die Umströmung im Stabmittelbereich maßgebend für die Schwingungserregung, während bei den auf der einen Seite federnd und auf der anderen Seite gelenkig gelagerten Zylindern die Strömungsverhältnisse am beweglichen freien Ende bestimmend sind, wobei sich infolge eines Belüftungseffektes qualitative Unterschiede ergeben.

Bei den gelenkig gelagerten Stäben nahm die kritische Frequenz (S_{kr} = 0,17...0,20) mit steigender relativer Amplitude w/D ab. Diese Beobachtung entspricht dem Steinmanschen Verstärkungseffekt, der als Wirbelstraßenverbreiterung gedeutet wird. Der Wert nach Steinman

$$\nu = 1+1{,}54 \cdot w/D \qquad \text{(siehe z.B. Weaver [8])} \qquad (17)$$

wurde bestätigt. Dagegen lag die kritische Frequenz bei den Zylindermodellen konstant bei $S_{kr} \approx 0{,}145$. Bemerkenswert ist das Auftreten eines zweiten Maximums bei letzteren Modellen für $S < 0{,}05$. In einigen Fällen mußten die Versuche wegen zu großer Beanspruchungen (Schwingungen in der Grundfrequenz bei einem Mehrfachen der ersten kritischen Geschwindigkeit) abgebrochen werden.

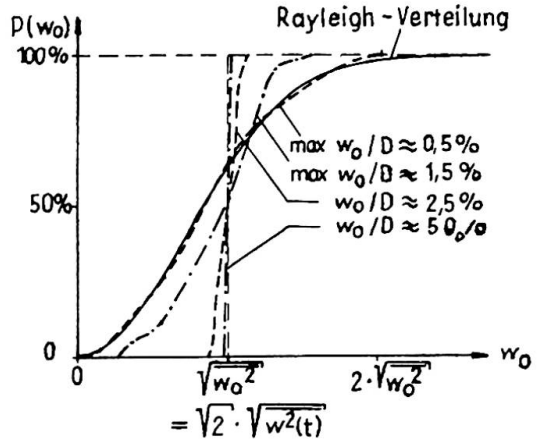

Bild 5: Gemessene Wahrscheinlichkeitsverteilung der Amplituden

Die Wahrscheinlichkeitsverteilung der Erregung ist nicht bekannt. Wird eine Gaußsche Normalverteilung oder eine der Normalverteilung nahekommende Verteilung angenommen, dann müßte die Systemreaktion eine Normalverteilung aufweisen (Sweschnikow [7]), bzw. wenn nur die Amplituden betrachtet werden, müßte sich eine Rayleigh-Verteilung (Bild 5) ergeben. Für kleine relative Amplituden w/D < 0,5 %, die durch künstliche Zusatzdämpfung erzielt wurden, stimmt die gemessene statistische Verteilung mit diesem theoretischen Wert etwa überein. Bei größeren relativen Amplituden, wie sie für v_{kr} bei kleinen Dämpfungswerten stets auftreten, konnte eine zunehmende Amplitudenstabilisierung (Bild 5) beobachtet werden, so daß statt des Wahrscheinlichkeitswertes $\sqrt{w_0^2}$ der determinierte

Wert w_o geschrieben werden kann. Diese Erscheinung kann als Selbststeuerung oder Rückkopplung gedeutet werden. Eine mathematische Darstellung dieser Kopplung der Erregerkraft mit der Systemreaktion kann nicht gegeben werden.

5. Berechnungswerte

Von den gelenkig gelagerten Modellen wird auf Stäbe, die an beiden Enden gehalten sind (eingesapnnt oder gelenkig), extrapoliert und von den einseitig federnd aufgehängten Zylindern auf Stäbe mit einem freien Ende (Kragstäbe).

5.1. Querschwingungen von Stäben, die an beiden Enden gehalten sind.

Die aus den Versuchswerten ermittelten Kurven $\phi_A(S)$ wurden auf eine gemeinsame kritische Frequenz $S^*_{kr} = 0{,}19$ bezogen (Bild 7). Diese Strouhalzahl S^* gilt für den "starren" Stab ($w = 0$). Die kritische Frequenz und die kritische Geschwindigkeit ändern sich beim schwingenden Stab um den Verstärkungsfaktor ν nach Gl. (17) auf die Werte

$$S_{kr} = \frac{1}{\nu} \cdot S^*_{kr} \qquad V_{k,kr} = \nu \cdot V^*_{k,kr} = \nu \cdot \frac{n_k \cdot D}{0{,}19} \tag{18}$$

Für die praktische Bemessung interessiert meist nur die Beanspruchung im "Resonanzfall" (für die kritische Geschwindigkeit). Die Spektraldichte wird für die zugehörige Reynoldsche Zahl aus Bild 7 entnommen. Zunächst ermittelt man die Schwingungsauslenkung w^*. Die tatsächliche Auslenkung in der k-ten Eigenform an der Stelle x der maximalen Amplitude erhält man durch Multiplikation mit dem Verstärkungsfaktor nach Bild 6.

$$\frac{{}^{k}w^*_{o,max}}{D} \approx \frac{q^* \cdot \sqrt{S_k^*} \cdot \sqrt{\phi_A(S_k^*)}}{4\pi\mu \cdot n_k^2 \cdot \sqrt{\vartheta}} \qquad {}^{k}w_{o,max} = \sqrt{\nu^3} \cdot \frac{{}^{k}w^*_{o,max}}{D} \cdot D \tag{19}$$

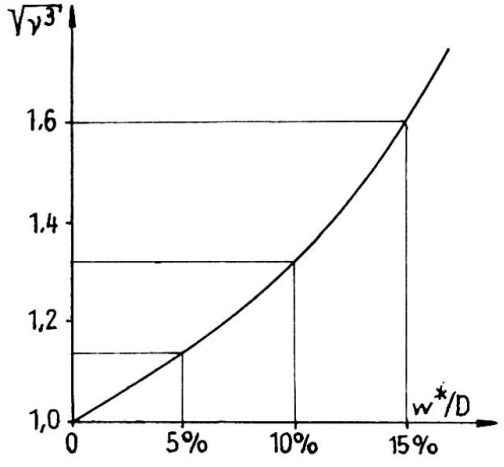

Bild 6: Verstärkungsfaktor

Handelt es sich um ein schwingendes System mit einem winderregten Stab, kann die Schwingungsamplitude durch Multiplikation mit dem Faktor M^A_k / M_k ermittelt werden. M^A_k ist die generalisierte Masse des erregten Stabes nach Gl. (9), M_k die generalisierte Masse aller schwingenden Stäbe in der k-ten Eigenform.

5.2. Querschwingungen von Kragstäben

Für Stäbe mit einem frei umströmten Ende gilt als kritische Strouhalzahl $S_{kr} \approx 0{,}145$. Die kritische Geschwindigkeit beträgt in der ersten Eigenform

$$V_{1,kr} = \frac{n_1 \cdot D}{0{,}145} \tag{20}$$

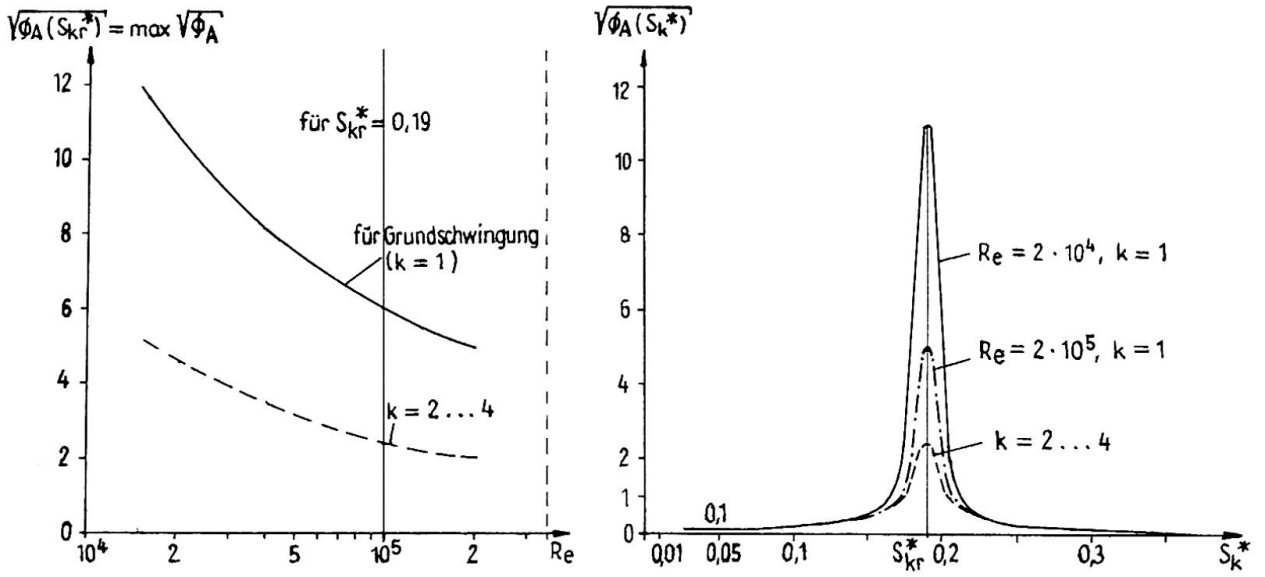

Bild 7: Spektraldichten glatter kreiszylindrischer Stäbe mit unverschieblichen Stabenden im unterkrit. Re-Bereich

Entsprechend den Messungen wird $\nu = 1$ gesetzt. Die Schwingungsauslenkung beträgt in der ersten Eigenform (Meßwerte für höhere Eigenformen liegen nicht vor)

$$ {}^1w_{0,max} \approx \frac{q \cdot D \cdot \sqrt{S_1} \cdot \sqrt{\Phi_A(S_1)}}{4\pi\mu \cdot n_1^2 \cdot \sqrt{\vartheta}} \qquad S_1 = \frac{n_1 \cdot D}{V} \qquad (21) $$

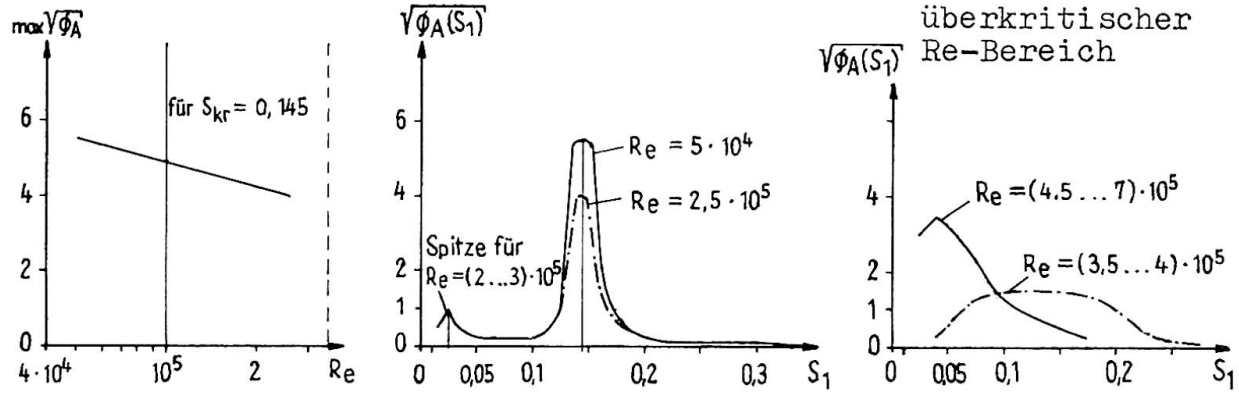

Bild 8: Spektraldichten glatter kreiszylindrischer Kragstäbe

Die hier gemessenen Werte im überkritischen Bereich sind für $S \lesssim 0{,}1$ etwa 5-fach größer als die Angaben nach Fung [3], die allerdings nicht für Kragstäbe gelten. Ein Vergleich mit den Beobachtungswerten an den Stahlrohrpendelstützen der Bogenbrücke bei Žďákov in der ČSSR zeigt, daß wesentlich größere Amplituden auftreten können als nach Fung für gleiche Geschwindigkeiten zu erwarten wären.

6. Übertragungsmöglichkeit auf Bauteile im natürlichen Wind

An einzelnen Stahlrohr-Fachwerkstäben einer Kurzwellenrichtantenne wurden bei ganz bestimmten, eng begrenzten Windge-

schwindigkeiten relative Doppelamplituden von 10...15 % beobachtet. An einigen Stabanschlüssen mit breitgedrückten Rohrenden sind dabei Risse infolge Dauerbruch aufgetreten. Die beobachteten Auslenkungen stimmen mit den hier angegebenen Berechnungswerten unter Zugrundelegung an der Antenne gemessener Dämpfungswerte überein. Dagegen ergäben sich mit der Annahme nach Gl. (4) im Resonanzfall für $c_A = 0{,}8$ (z.B. Novák [6]) etwa 2,5-fach größere Beanspruchungen. Da die Spannungen in einem Rohrstab für die kritische Geschwindigkeit etwa linear mit dem Verhältnis D/t (t - Wandstärke) sowohl nach Gl. (14) als auch nach der herkömmlichen Annahme Gl. (15) anwachsen, ist es unter Berücksichtigung des angegebenen Beiwertes $c_A \approx 0{,}8$ kaum möglich, Konstruktionen aus sehr dünnwandigen Rohren auszuführen. Aus Gründen der Wirtschaftlichkeit ist es deshalb unbedingt erforderlich, die bisherige Annahme durch eine Darstellung, die die tatsächlichen Verhältnisse besser zu erfassen versucht, zu ersetzen.

Bei dünnwandigen Stäben kleiner Schlankheit (steife Stäbe), bei denen die Resonanzgeschwindigkeit im Bereich der maximalen Windgeschwindigkeit liegt, könnten theoretisch sowohl nach der bisherigen als auch nach der hier vorgeschlagenen Annahme Beanspruchungen auftreten, die die Fließgrenze normalen Baustahls überschreiten. Beobachtet wurden aber unseres Wissens bei großen Windgeschwindigkeiten keine gefährlichen Querschwingungen, da diese im unterkritischen Re-Bereich nach Bild 2 nur in einem sehr engen Geschwindigkeitsbereich auftreten. Mit großen Windgeschwindigkeiten ist im allgemeinen eine sehr starke Turbulenz bzw. Böigkeit verbunden, so daß sich große Schwingungsamplituden in Querrichtung nicht ausbilden können. Um diesen Erfahrungswerten im natürlichen Wind nahezukommen, wird vorläufig mangels besserer Kenntnisse vorgeschlagen, von einer bestimmten Geschwindigkeit ab (z.B. für $V > 15$ m/s) die errechneten Querschwingungsbeanspruchungen abzumindern.

Eine Voraussage der zu erwartenden Dämpfungswerte für eine bestimmte Konstruktion ist bisher nicht möglich. Für die hier in Frage kommenden Bauteile wurden an verschiedenen geschweißten, dünnwandigen Stahlkonstruktionen stets sehr niedrige Dämpfungswerte ermittelt. An Stahlrohrstäben einer Fachwerkkonstruktion, an Stahlrohrpendelstützen einer Bogenbrücke und an frei hängenden Stahlrohr-Pipe-Lines hat man logarithmische Dekremente der Dämpfung in der Größe

$$\vartheta \approx 0{,}007...0{,}03 \qquad (22)$$

gemessen. Für die Bemessung von Stahlkonstruktionen wird ein Wert in dieser Größenordnung empfohlen.

7. Offene Probleme

Um für die Übertragbarkeit auf den natürlichen Wind bessere Kriterien als oben angegeben zu finden, ist es erforderlich, die Spektraldichten in Abhängigkeit von der Turbulenz zu bestimmen, d.h. die Turbulenz im Kanal muß planmäßig variiert werden können. Im natürlichen Wind sind Turbulenzmessungen in einem solchen Umfang erforderlich, daß für jeden Ort und jede Höhe Wahrscheinlichkeitswerte für die zu erwartende Windturbulenz angegeben werden können.

Am Stab sind weiterhin Messungen der Korrelation der Quertriebskräfte in Stablängsrichtung nach Gl. (10) erforderlich, d.h. in zwei benachbarten Querschnitten sind im variablen Abstand Δx synchrone Oberflächendruckmessungen erforderlich.

Im natürlichen Wind ist besonders für die Anwendung auf hohe Bauwerke wie Maste und Türme die räumliche Korrelation der Windgeschwindigkeiten zu messen. Die Werte, die im Windkanal für kleine Stäbe und mit einer konstanten Geschwindigkeit über die ganze Stablänge gemessen wurden, würden für sehr hohe bzw. lange Bauteile zu ungünstige Beanspruchungen liefern.

Die Untersuchungen sind auch auf nicht kreisförmige Querschnittsformen zu erweitern. Es bedarf noch umfangreicher Arbeiten, bis das Problem des Schwingungsverhaltens von Stäben im natürlichen Wind als abgeschlossen betrachtet werden kann.

Literatur

[1] Borges, J.F.: Dynamische Belastungen (Wind und Erdbeben) Vorbericht zum 8. Kongreß der IVBH, Zürich 1967

[2] Drescher, H.: Messungen der auf querangeströmte Zylinder ausgeübten zeitlich veränderlichen Drücke Zeitschrift für Flugwissenschaft 1956

[3] Fung, Y.C.: Fluctuating lift and drag acting on a cylinder in a flow at supercritical Reynolds number Journal of the Aerospace Sciences, vol. 27 (1960)

[4] Gerrard, J.H.: An experimental investigation of the oscillating lift and drag of a circular cylinder shedding turbulent vortices Journal of Fluid Mechanics, vol. 11 (1961)

[5] Hölzel, G.: Ein Beitrag zum Problem winderregter Querschwingungen kreiszylindrischer Stäbe im unterkritischen Reynolds-Bereich Dissertation Technische Universität Dresden 1968

[6] Novák, M.: The wind-induced lateral vibration of circular guyed masts IASS-Symposium on tower-shaped steel and reinforced concrete structures Preliminary report - Bratislava 1966

[7] Sweschnikow, A.A.: Untersuchungsmethoden der Theorie der Zufallsfunktionen mit praktischen Anwendungen. Teubner-Verlag, Leipzig 1965

[8] Weaver, W.: Wind-induced vibrations in antenna members Proc. ASCE, vol. 87 (1961), No. EM 1

ZUSAMMENFASSUNG

Es wird nachgewiesen, daß die bisher übliche Annahme einer harmonischen Quertriebskraft im unterkritischen Reynolds-Bereich im Widerspruch zu dem zu beobachtenden Schwingungsverhalten steht. Gestützt auf Windkanalversuche werden die resonanzartigen Querschwingungen aus dem Wirken einer stochastischen Quertriebskraft mit einem schmalbandigen Spektrum erklärt. Berechnungswerte werden angegeben.

SUMMARY

The conventional hypothesis of a harmonic lateral force in the subcritical Reynolds range has now been proved to be contradictory to the observed behaviour of vibrations. Based on tests in wind tunnels, the resonancelike transverse vibrations are explained as results of the action of a random lateral force with a small-band spectrum. Calculation values are given.

RÉSUMÉ

L'hypothèse conventionelle d'une force transversale harmonique dans le domaine sous-critique de Reynolds s'est trouvée être contradictoire au comportement des vibrations observées. Suivant les essais dans le tunnel aérodynamique, les vibrations transversales, ressemblant aux résonances, sont interprétées comme l'action d'une force transversale stochastique au spectre d'une bande étroite. Valeurs pour le calcul sont donnée.

VI

On the Damping of Vibrations

Amortissement des vibrations

Über die Dämpfung von Schwingungen

LIVIO NORZI
Italy

It is well known that classical elasticity offers to the structural engineer many valuable results and some powerful general methods to calculate the characteristic frequencies of his buildings.

But we have to remember that, from the dynamic viewpoint, a world of perfect elasticity would be very unstable and brittle (with materials of finite strength) whilst, fortunately in practice, many resonant frequencies are not at all dangerous, thanks to damping.

Our knowledge on this subject is not as wide as it should be to answer, at least with a practically sufficient approximation, to questions like the following:

what is the maximum alternating stress that a given structure can endure in a definite interval of time?

is it possible to build with materials of higher static strength without losing something as to the capability to withstand dynamic actions?

since the damping coefficients increase with stress, to

what extent does abundancy of dimensions really improve dynamic safety?

With a view to bring some contribution towards the solution of such problems, or of many others that naturally arise from them, we started in February 1967 a program of systematic research on the damping of vibrations in the frequency range 1 ÷ 100 hz which is of interest not only for civil engineering (1 ÷ 10 hz) but also for the design of machines (10 ÷ 100 hz).

This program is carried out at the Building Science Institute of Turin Polytechnic School, with the support of the Italian National Council for Research (C.N.R.).

Without any claim to have reached final conclusions, I wish to point out some results, both theoretical and experimental, that appear to be promising or that deserve at least a deeper analysis.

1) Deduction of the Equations of Small quasi-Elastic Oscillations and Discussion on the Relationship between Relaxation Time and Frequency for Beams in Bending.

From a thermodynamic view point, the simplest hypothesis that can be made about the dissipation of energy for unit time and unit volume is the following:

$$\frac{dW}{dt} = g_1 \cdot (\text{rate of change of elastomechanical energy})^2 + g_2 \cdot (\text{local gradient of velocity})^2 \qquad (1)$$

without any "a priori" assumption concerning g_1, g_2 (but, of course, for irreversibility $g_1 > 0$, $g_2 \geq 0$)

It is fundamental to observe: first, the logical simmetry connecting elastic after-work (caused by the variation of elastomechanical energy with respect to time) and internal friction (caused by the variation of kinetic energy in space); se-

cond, that to evaluate the local density of energy and its rate of change we have to take into account the static stresses pre-existing to vibratory motion.

If we apply hypothesis (1) to bending of a uniform beam, neglecting shear and rotatory inertia and denoting with

f the elastic deplacement

M_o the pre-existing bending moment,

the principle of conservation of energy expresses the stationary property of the form:

$$\int_o^L [EJ \left(\frac{\partial^2 f}{\partial x^2}\right)^2 + \rho A \left(\frac{\partial f}{\partial t}\right)^2 + \int_o^t g_1 M_o^2 \left(\frac{\partial^3 f}{\partial x^2 \partial t}\right)^2 dt + \int_o^t g_2 \rho A \left(\frac{\partial^2 f}{\partial x \partial t}\right)^2 dt] dx \tag{2}$$

By transformation into a double integral we get a normal problem of the calculus of variations, and if we put:

$g_1 M_o^2 / \rho A = 2a \qquad EJ/\rho A = b^2 \qquad g_2 = 2c$

the indefinite equation may be written (in the case of constant coefficients):

$$2a \frac{\partial^5 f}{\partial x^4 \partial t} + b^2 \frac{\partial^4 f}{\partial x^4} - 2c \frac{\partial^3 f}{\partial x^2 \partial t} + \frac{\partial^2 f}{\partial t^2} = 0 \tag{3}$$

For a simply supported beam, of length L, under its own weight only, it is easy to deduce from (3) the relaxation time in the form:

$$\theta = \frac{A}{g_1 M_o^2 \nu^2 + g_2 \frac{B}{L^2}} \tag{4}$$

or, since $M_o \equiv L^2 \equiv 1/\nu$

$$\theta = \frac{1}{\alpha + \beta \nu} \tag{5}$$

where A,B α,β are constants.

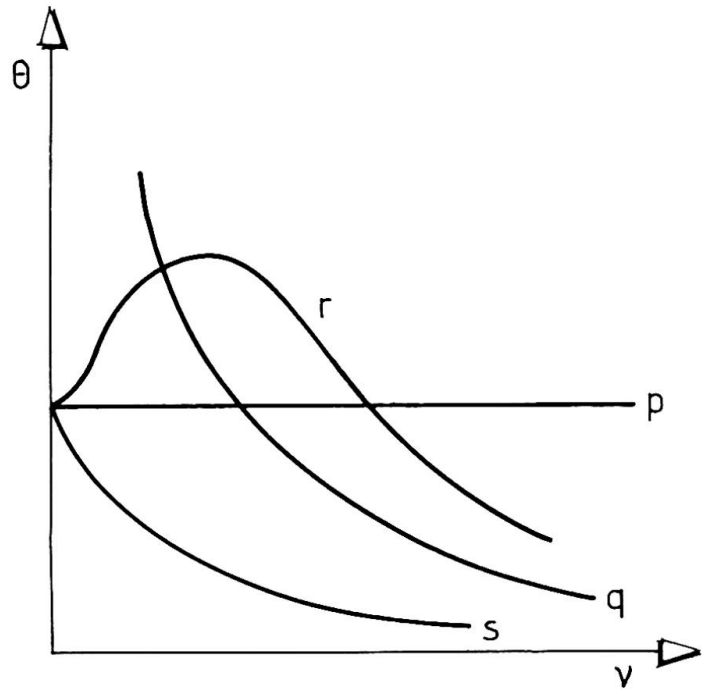

fig.1

In fig. 1 a comparison is made between different theories about the relationship $\theta=\theta(\nu)$:

Neglecting internal friction ($g_2 = 0$) and the influence of pre-existing stresses ($g_1 M_o^2 = \text{const}$) we have the curve q that would mean disaster as to antiseismic strength because by $\theta\nu^2 = \text{const}$ damping would be too low for low frequencies.

If we put $g_2 = 0$, $g_1 = \text{const}$ we get the line p (in agreement, e.g. with POZZO's observations on concrete (')).

By assuming $g_1 = \text{const}$, $g_2 = \text{const}$, we find the hyperbola s that eliminates the paradox of undamped low frequencies.

However a real curve may look like r (see fig. 2 from BO and LEPORATI's experiments on Burback tracks (')) and this fact can be explained by considering

2) The Influence of Microstructure

As it is reasonable to suppose that energy be dissi-

pated mainly through weak grains, large enough to have a chance of undergoing plastic deformation, we are interested in knowing the minimum grain size D_0 that may be "activated" in this sense and the fraction F(D) of mass constituted by grains of size D or more (F(0) = 1, F(∞) = 0)

D_0 may be given by a formula as $\sigma^2 D_0 = const$ or the like, decreases with stress and increases with frequency, whereas the contrary occurs for $F(D_0)$.

Consequently in (4) g_1, g_2 that increase with $F(D_0)$ will decrease with ν and in (5), with $\frac{d\alpha}{d\nu} < 0, \frac{d\beta}{d\nu} < 0$, it will be possible to have a maximum for θ (ν).

So we come to think that damping depends chiefly on stress, especially at low frequencies when the controlling factor is the number of cycles.

In fig. 2 we see the results of experiments on small oscillations of uniform beams with the same cross section vibrating at the same frequency under different end conditions (''). The amplitude of oscillation A was between 1/25th and 1/50th of the static deflection.

Plotting the relaxation time $\theta = -\frac{1}{2} A/(\frac{dA}{dt})$ against frequency seems to demonstrate that the assumption of seismic coefficients depending only on frequency (as prescribed by several regulations) is an over-simplification too far from reality.

To study the combined effect of stress, frequency and grain-size we have performed many more experiments using I beams HE 100 B UNI (5397-64) on

3) The Damping of Large Oscillations

During each experiment the variation of θ with A, σ has been quite evident.

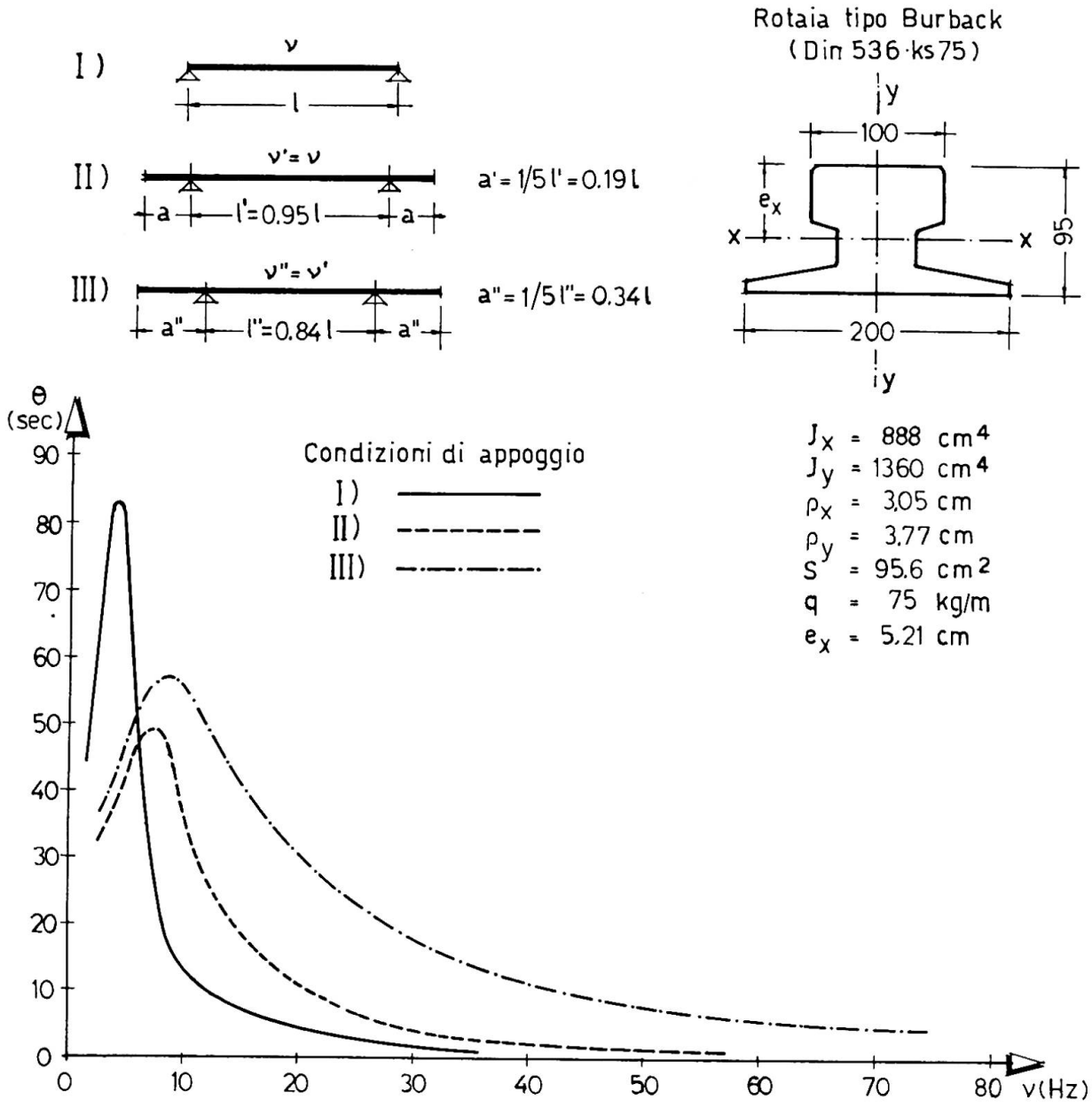
I)
ν
l
II)
ν'= ν
a'= 1/5 l'= 0.19 l
a
l'=0.95 l
a
III)
ν''= ν'
a''= 1/5 l''= 0.34 l
a''
l''=0.84 l
a''
Rotaia tipo Burback
(Din 536-ks75)
y
100
e_x
x
x
95
200
y
J_x = 888 cm⁴
J_y = 1360 cm⁴
ρ_x = 3.05 cm
ρ_y = 3.77 cm
S = 95.6 cm²
q = 75 kg/m
e_x = 5.21 cm
θ (sec)
Condizioni di appoggio
I)
II)
III)
90
80
70
60
50
40
30
20
10
0
0
10
20
30
40
50
60
70
80
ν(Hz)

fig. 2

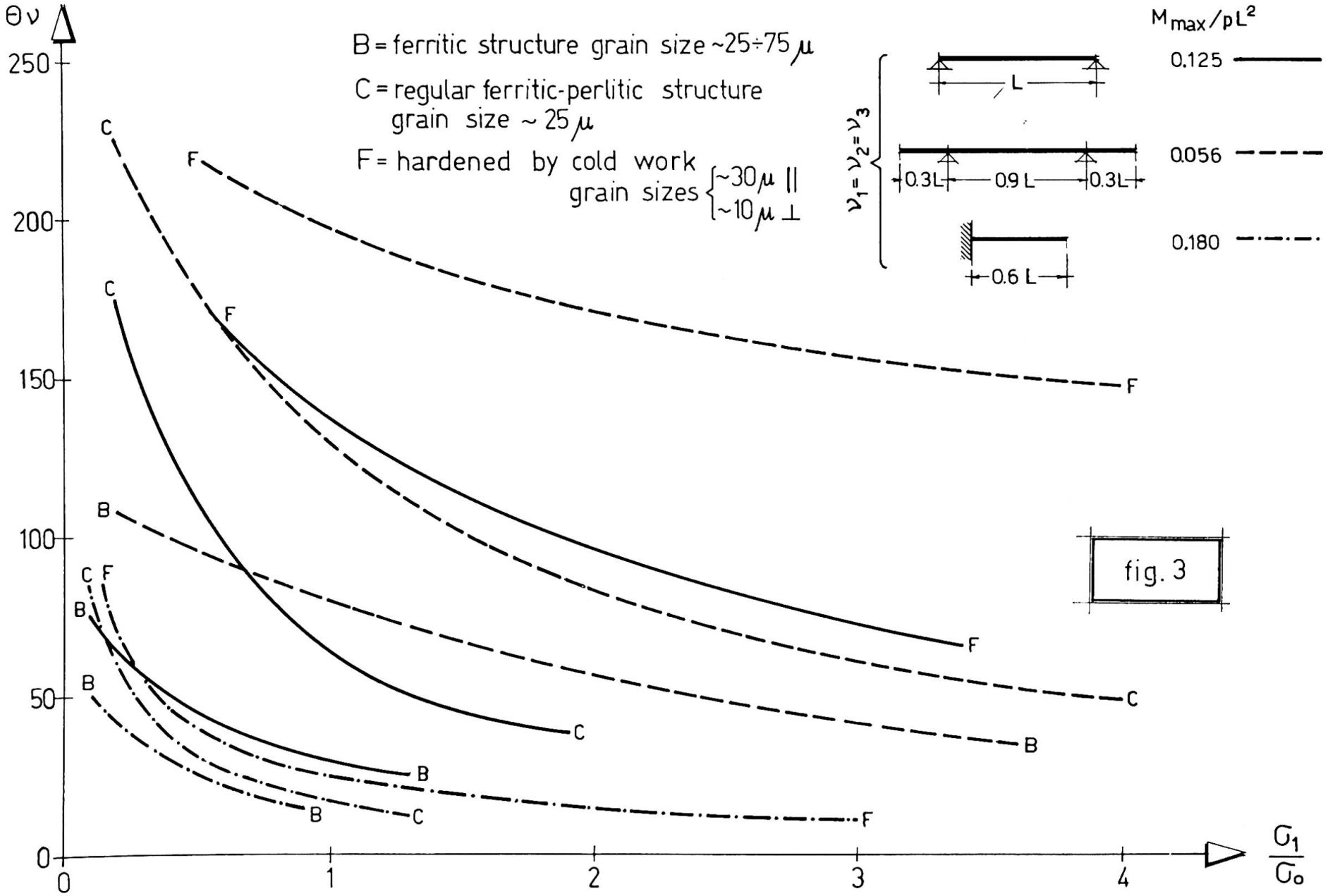
Θν
250
200
150
100
50
0
0
1
2
3
4
σ1/σ0
B = ferritic structure grain size ~25÷75 μ
C = regular ferritic-perlitic structure grain size ~ 25 μ
F = hardened by cold work grain sizes ~30 μ ||, ~10 μ ⊥
Mmax/pL²
0.125
0.056
0.180
ν1 = ν2 = ν3
L
0.3L
0.9 L
0.3L
0.6 L
C
F
B

fig. 3

The results appear in fig. 3 where two dimensionless parameters have been introduced: $\theta\,\nu$ (a number of cycles) and

$$\frac{\sigma_1}{\sigma_0} = \frac{\text{dynamic amplitude of stress oscillation}}{\text{pre-existing static stress}}$$

$$(\sigma = \sigma_0 + \sigma_1 \sin 2\pi\nu\, t)$$

Here again three different geometrical conditions corresponding to nearly equal frequencies have been considered. The maximum bending moments are roughly as 1:2:3.

A micrography of every specimen has been kindly prepared and analyzed by prof. BURDESE.

We observe that

a) a hyperbolic law fits well enough with the experimental curves

$$\theta\,\nu = \frac{1}{A + B\,(\sigma_1/\sigma_0)} \qquad (6)$$

So far we are in agreement with (1): the rate of dissipation of energy is proportional to $\sigma_1 . \sigma_0 / \theta$ and must be equalized to the terms of the second member that necessarily comprehend a velocity factor $\sigma_1 \nu$ multiplied by a function of σ_0, σ_1 which, to a first approximation, can be expressed as $A\sigma_0 + B\sigma_1$

b) the constants of hyperbolae depend on material and end conditions:

for a given material, the structures under heavier stress damp out vibrations more rapidly; for a given geometry of structure damping is quicker in materials with coarse and larger grains.

Normalized damping tests may be useful in quality control.

Finally I wish to draw attention to the influence of dissimetry in the excitation of vibrations and emphasize the reasons that cause large variations of the damping coefficients in the general problem.

Let us consider

4) The Characteristic Equation

$$b^2 \xi^4 + 2 (a \xi^2 - c) \xi^2 z + z^2 = 0 \qquad (7)$$

connecting the exponents of the elementary solution $\exp (\xi x + z t)$ of eq. (3)

If we put:

$$\xi = u + i v = r e^{i\varphi} = \frac{1}{R} e^{-i\varphi}$$

$$z = - \chi + i \omega$$

and consider (7) as an equation of the 2nd degree in z ,we get, with the assumption, surely acceptable for steel, of dissipation so modest as to influence frequency but little:

$$z = \xi^2 (c - a \xi^2 \pm ib)$$

Writing:

$$c \pm ib = \gamma e^{i\epsilon} \qquad a = \lambda \gamma$$

and using the inversion to represent long waves at increasing distances from the origin, we obtain:

$$- \chi = \frac{\gamma}{R^2} [\cos (2 \varphi + \epsilon) - \frac{\lambda}{R^2} \cos 4 \varphi]$$

$$\omega = \frac{\gamma}{R^2} [\sin (2 \varphi + \epsilon) - \frac{\lambda}{R^2} \sin 4 \varphi] \qquad (8)$$

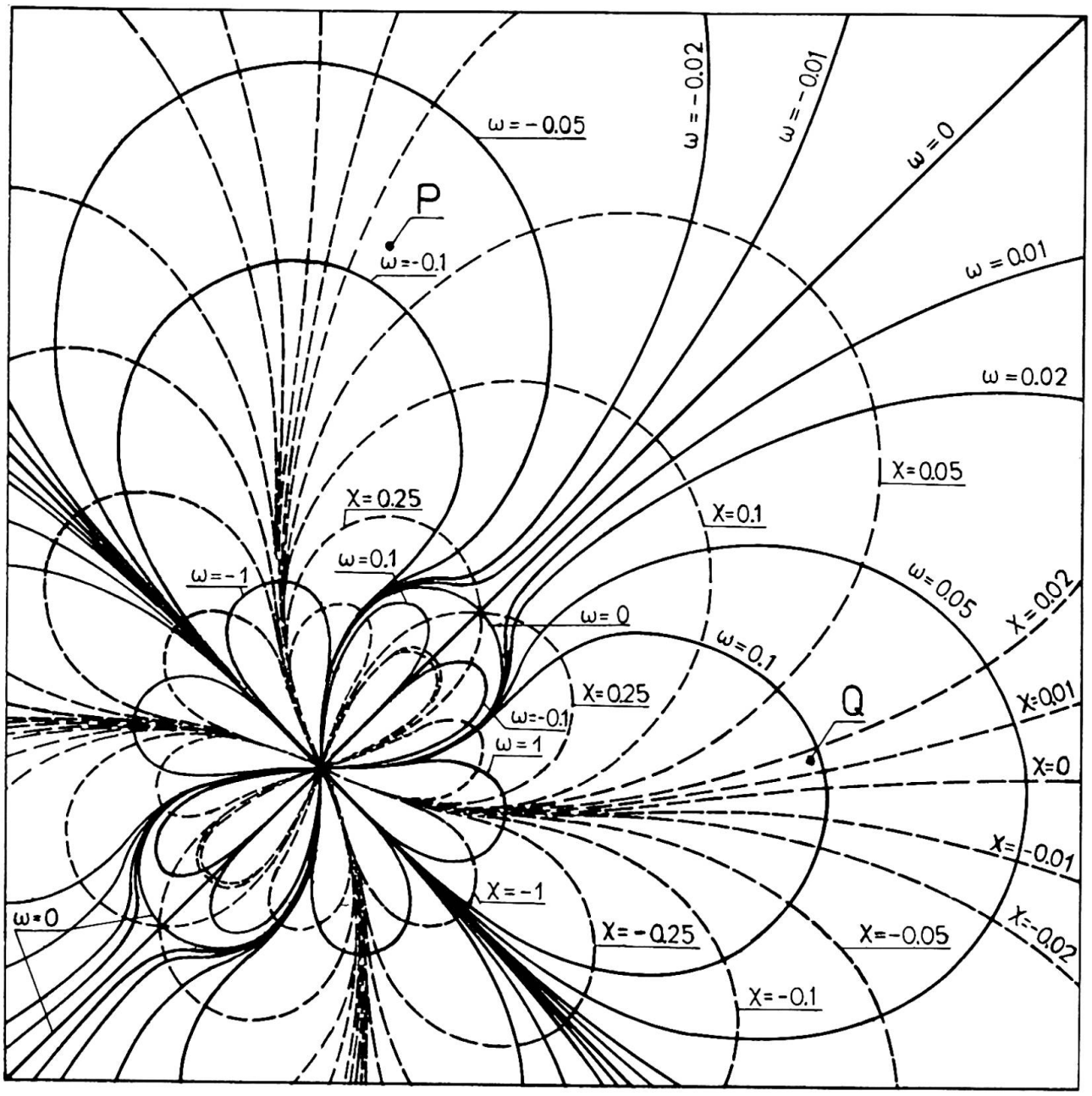

fig.4

In fig. 4 the curves of constant damping χ and their orthogonal trajectories of constant pulsation ω are traced in the particular case $\gamma = \lambda = 1, \varepsilon = \pi/2$

So, in Gauss' plane, we have an immediate representation of the correspondence between the dissimetrical attenuation of waves in space and time respectively.

It may be seen at once that near points like P, repre-

senting long slightly unsimmetrical waves, the same value of χ corresponds to very different frequencies; whilst near Q a minor change in the wave form causes different damping for equal frequencies.

fig.5

The almost undistorted permanence of complicated wave forms, like the one of Fig. 5 observed (") during more than 5 minutes of free oscillations of a Burback track, may be perhaps better understood through these considerations rather than by associating definite damping coefficients to simple harmonics.

REFERENCES:

(') POZZO - Le forze smorzanti nella dinamica dei ponti
Indagine e risultati sperimentali.
Rivista "Il Cemento" - Lug. Ag. 1961

(") BO e LEPORATI - Misure sperimentali di azioni dissipative in travi inflesse.
Ist. Sc. Costr. Politecnico di
Torino, Sett. 1967.

SUMMARY

Elastic systems with the same frequency may have different relaxation times. Materials under heavy stresses and coarse-grained materials damp out vibrations more quickly and so show a greater reserve of dynamical strength. In propagation phaenomena the damping factor may be very sensitive to comparatively small changes in the shape of waves.

RÉSUMÉ

Des systèmes élastiques de la même fréquence peuvent avoir des temps d'amortissement très différents. Les matériaux plus sollicités et ceux à gros grains amortissent les vibrations plus rapidement et montrent ainsi une plus grande réserve de résistance dynamique. Dans les phénomènes de propagation le facteur d'amortissement peut être très sensible à des modifications relativement petites de la forme des ondes.

ZUSAMMENFASSUNG

Elastische Systeme mit gleicher Frequenz können sehr verschiedene Relaxationszeiten zeigen.
Stark belastete sowie grobkörnige Materialien dämpfen die Schwingungen schneller und zeigen eine grössere dynamische Widerstandsreserve. In Verbreitungsphänomena kann der Dämpfungsfaktor sehr empfindlich auf relativ geringe Veränderungen der Wellenform sein.

VI

The Treatment of Damping Coefficient on the Dynamic Problem

Sur le coëfficient d'amortissement dans les problèmes dynamiques

Die Behandlung des Dämpfungskoeffizienten bei dynamischen Problemen

Y. OHCHI
College of Technology
Hosei University
Tokyo, Japan

INTRODUCTION

Recently the use of digital computer having become very popular, a number of papers dealing with the response analysis of complex structures is published. Very few of them set apart, however, they do not give detailed explanations about damping force. The writer having also developed a program for response analysis of framed structures, computed the responses of various types of them, and is in every time troubled by how the damping coefficients are selected. As response displacements depend largely upon them, even it is possible that we insist on the propriety of the certain damping coefficients obtained inversely from the required response displacements.

Damping force is a force that suppresses vibrations and comes from various origins. Though it is quite natural that efforts to catch the causes dominating the damping forces and to include them in the equation, such a frontal attack would not be so expected under existing circumstances. In case of complex structures, it is also very hard to determine the ratios to the critical damping coefficient, as in a one-mass-system, because of its complexity.

Then the writer, referring to the results of vibrational experiments about one-mass-system, and noticing that damping constant is of three terms (first inversely proportional, second unrelated and third proportional, to the frequency), has tried to extend the idea to multi-mass-system. There are such four forces, further saying, as inertia force ($M\ddot{x}$), damping force ($C\dot{x}$), restoring force (Kx) and external force ($-M\ddot{x}_e$ in case of earthquakes) which determine a vibration, the theme of this paper is then the second force. Restoring force is determined from the static relation between external force and deformations of the structure. This subject is dealt with in other papers of which one is published by the writer[1)2)]. In this paper is shown in another form extended thereafter. It is inevitable to encounter what type of seismic waves is selected, but such problem should belong to the field of seismology. Finally, as for inertia force, it is usual to concentrate the mass to some points, but as actually the mass is distributed along structural members, this effect must be introduced. The discussion about this problem is left for another chance.

ONE-MASS-SYSTEM

The kinetic equation of one-mass-system is

$$Kx = -M(\ddot{x} + \ddot{x}_e) - C\dot{x}$$

Dividing by M and replacing

$$P = \sqrt{\frac{K}{M}}, \quad h = \frac{C}{C_{cr}}, \quad C_{cr} = 2\sqrt{K \cdot M}$$

Eq.(1) is reduced to

$$\ddot{\chi} + 2h p\dot{\chi} + p^2\chi = -\ddot{\chi}_e \tag{3}$$

in which p is circular natural frequency and h is called damping constant, the ratio of actual damping coefficient(C) to critical value of that (C_{cr}). The relation between damping constant(h) and logarithmic decrement (Δ) is

$$\Delta = \frac{2\pi h}{\sqrt{1-h^2}} = 2\pi h$$

The solution of Eq.(3) is

$$\chi = P^{-1} S_v(t) \tag{4}$$

$$S_v(t) = -\int_0^t \frac{\ddot{\chi}_e}{\sqrt{1-h^2}} e^{-p(t-\lambda)} \cdot \sin P\sqrt{1-h^2}(t-\lambda)\, d\lambda$$

Substituting in Eq.(4) actual seismic waves, and calculating maximum values of $S_v(t)$ for various values of p, we can get a response velocity spectrum by plotting $S_v(t)$ against p. To average the values of $S_v(t)$ for a number of cases of actually occurred earthquakes makes so-called average response velocity spectrum ($\overline{S_v}$) proposed by Hausner.

After our simple experiment, h is constant or proportional to p (see Fig. 1, 2). Making a reference[3], h is in inverse proportion with p. Then, we shall be able to put

$$h = h_0 P^{-1} + h_1 + h_2 P \tag{5}$$

Substituting this in Eq.(3) and using Eq.(2), Eq.(1) becomes

$$M\ddot{x} + (2h_0 M + 2h_1\sqrt{KM} + 2h_2 K)\dot{\chi} + K\chi = -M\ddot{x}_e \tag{6}$$

Damping coefficient is then expressed in such a form as

$$C = 2h_0 M + 2h_1\sqrt{KM} + 2h_2 K \tag{7}$$

Using Eq.(5) as damping constant under such condition that h_0 and h_2 have constant values, average response velocity spectrum of Hausner is calculated as shown in Figs. 3(a),(b).

MULTI-MASS-SYSTEM (MODAL ANALYSIS)

The kinetic equation of a multi-mass-system is, by using matrices, expressed as follows.

$$\mathbb{K}\boldsymbol{x} = -\mathbb{M}(\ddot{\boldsymbol{\chi}} + \mathbb{F}\ddot{x}_e) - \mathbb{C}\dot{\boldsymbol{\chi}} \tag{8}$$

Now, introducing a linear equation

$$(\mathbb{M}\lambda^2 - \mathbb{K})\,\boldsymbol{\chi} = 0$$

let v_i be the root other than zero, and P_i^2 be the value of λ^2 (the number is as much as the rank of the matrices), that is to say, the eigenvector and eigenvalue. If $\mathbb{V}$ denotes the matrix arranging v_i in a column, and $\mathbb{P}^2$ the matrix arranging P_i^2 diagonally, the relation between them is

$$\mathbb{V}^T \mathbb{K}\,\mathbb{V} = \mathbb{V}^T \mathbb{M}\,\mathbb{V}\,\mathbb{P}^2 \tag{9}$$

Each element of $\mathbb{P}$ is circular natural frequency, and each column of $\mathbb{V}$ shows proper mode of vibration. Further, changing the independent variables χ_i of Eq.(8) to q by the relation

$$\mathcal{X} = \mathbb{V}\mathbf{q} \tag{10}$$

and multiplying $\mathbb{V}^T$ from the left side, Eq.(11) is obtained.

$$\mathbb{V}^T\mathbb{M}\mathbb{V}\ddot{\mathbf{q}} + \mathbb{V}^T\mathbb{C}\mathbb{V}\dot{\mathbf{q}} + \mathbb{V}^T\mathbb{M}\mathbb{V}\,\mathbb{P}^2\mathbf{q} = -\mathbb{V}^T\mathbb{M}\mathbb{F}\ddot{x}_e \tag{11}$$

Because the critical damping coefficient matrix of the kinetic equation (8) for a multi-mass-system is $2\mathbb{M}\mathbb{V}\mathbb{P}\mathbb{V}^{-1}$ (see APPENDIX I), defining, on an analogy of Eq.(7), the damping coefficient matrix of multi-mass-system as

$$\mathbb{C} = 2h_0\mathbb{M} + 2h_1\mathbb{M}\mathbb{V}\mathbb{P}\mathbb{V}^{-1} + 2h_2\mathbb{K} \tag{12}$$

and modifying the second term of Eq.(11) and considering Eq.(9), we find

$$\mathbb{V}^T\mathbb{C}\mathbb{V} = 2h_0\mathbb{V}^T\mathbb{M}\mathbb{V} + 2h_1\mathbb{V}^T\mathbb{M}\mathbb{V}\mathbb{P} + 2h_2\mathbb{V}^T\mathbb{M}\mathbb{V}\mathbb{P}^2$$

Eq.(11) is therefore transformed into

$$\ddot{\mathbf{q}} + 2(h_0\mathbb{P}^{-1} + h_1\mathbb{U} + h_2\mathbb{P})\mathbb{P}\dot{\mathbf{q}} + \mathbb{P}^2\mathbf{q} = -(\mathbb{V}^T\mathbb{M}\mathbb{V})^{-1}\mathbb{V}^T\mathbb{M}\mathbb{F}\ddot{x}_e \tag{13}$$

When $\mathbb{P}^{-1}\mathbb{S}v_i(t)$ is the solution of Eq.(3) in which Eq.(5) and circular natural frequency P_i of multi-mass-system are substituted, $\mathbb{S}v_i(t)$ being the matrix of diagonal arrangement of $Sv_i(t)$, the solution of Eq.(13) is

$$\mathbf{q} = \mathbb{P}^{-1}\mathbb{S}v(t)(\mathbb{V}^T\mathbb{M}\mathbb{V})^{-1}\mathbb{V}^T\mathbb{M}\mathbb{F}$$

and the relative displacement is obtained by substituting in Eq.(10), as follows:

$$\mathcal{X} = \mathbb{V}\mathbb{P}^{-1}\mathbb{S}v(t)(\mathbb{V}^T\mathbb{M}\mathbb{V})^{-1}\mathbb{V}^T\mathbb{M}\mathbb{F} \tag{14}$$

Sectional forces would be then calculated from the displacement method of statics.

MULTI-MASS-SYSTEM (DIRECT METHOD)

Damping coefficient of Eq.(8) being substituted by equation (12), and replacing

$$\dot{\mathcal{X}} = \mathcal{Y}\,,\ \dot{\mathcal{Y}} = -\mathbb{F}\ddot{x}_e - (\mathbb{C}\mathcal{Y} + \mathbb{K}\mathcal{X}) \tag{15}$$

Eq.(8) would be solved by the numerical integral method[2] such as the Runge-Kutta-Gill or Milne's Method, under the initial condition, $\mathcal{X} = \mathcal{Y} = 0$ at $t=0$. As described at the head, there are so few papers dealing with damping force that the writer has proposed the equation (12). But, when using direct method, the second term of equation (12) seems troublesome. So it would be better to compute Eq.(15) after normalizing the eigenvector by using the relation

$$\mathbb{V}^T\mathbb{M}\mathbb{V} = \mathbb{E}$$

into the form

$$\mathbb{C} = 2h_0\mathbb{M} + 2h_1\mathbb{M}\mathbb{V}\mathbb{P}\mathbb{V}^T\mathbb{M} + 2h_2\mathbb{K} \tag{16}$$

or letting include the influence of the second term to the first and the third term

$$\mathbb{C} = 2h_0'\mathbb{M} + 2h_2'\mathbb{K} \tag{16'}$$

STIFFNESS MATRIX

For calculation of the responses of multi-mass-system using Eq.(14) or (15), it is necessary to make up mass matrix ($\mathbb{M}$) and stiffness matrix ($\mathbb{K}$) in addition to damping coefficient matrix ($\mathbb{C}$). If the mass is concentrated to the structural nodes, mass matrix is to be diagonal matrix, but actually the mass is distributed. Though the writer is researching to take into consideration the influence of distribution, but it is not yet the time to publish.

Stiffness matrix is obtained from the static relation between loads ($\mathbb{P}$) and displacements ($\mathbb{X}$)

$$\mathbb{K}\mathbb{X} = \mathbb{P} \tag{17}$$

Many studies in this field being published, their results should be used. The writer has also published a method[1)2)]. Afterwards the writer modified to be able to use for a member with one hinged end. Here is a simple explanation.

The linear equation by which the framed structure is solved statically is written as follows

$$\mathbb{D}\mathbb{k}\mathbb{D}^T\mathbb{X} = \mathbb{P} - \mathbb{A}\mathbb{C}^T\mathbb{F}_{fa} - \mathbb{B}\mathbb{C}^T\mathbb{F}_{fb} \tag{18}$$

$\mathbb{D}\mathbb{k}\mathbb{D}^T$ is stiffness matrix, $\mathbb{X}$ is displacement vector and the first term of the right side is force vector composed of external forces acting on the nodes. The second and third terms of the right side are vectors composed of external forces acting on the intermediate members connecting the nodes, $\mathbb{F}_{fa}$ and $\mathbb{F}_{fb}$ are end reactions of fixed beam (or modified end reactions when hinged), $\mathbb{C}^T$ is transformation matrix of coordinates (local to global), and, $\mathbb{A}$ and $\mathbb{B}$ are also transformation matrices from sectional forces at the member's end to nodal forces. The contents of $\mathbb{D}$, $\mathbb{k}$ are shown in APPENDIX II.

Solving Eq.(18) with performing an operation to the supports, sectional forces of the both ends $\mathbb{F}_a$ and $\mathbb{F}_b$ would be obtained.

$$\mathbb{F}_a = \mathbb{T}_a\mathbb{k}\mathbb{D}^T\mathbb{X} + \mathbb{F}_{fa}, \quad \mathbb{F}_b = \mathbb{T}_b\mathbb{k}\mathbb{D}^T\mathbb{X} + \mathbb{F}_{fb} \tag{19}$$

The operation to the supports is, for example, to sweep out the corresponding row and column of the stiffness matrix, if the node i is fixed in one direction, and/or to add a spring constant to the corresponding diagonal element of the stiffness matrix, if the node j is supported elastically in one direction.

NUMERICAL EXAMPLE

The suspension bridge shown in Fig.(4) is modelled and shows in Fig.(5). By substituted various values of h_0 , h_1 , h_2 into equation (12), the numerical calculations are carried out. If the suspension bridge and the seismic wave acting at the both tower bases are symmetric, the response of displacements and/or member forces of the center span are reduced to extremely small. In order that we increased the masses of the right tower ten per cent more than that of the left for this numerical example.

Results of the calculations are tabulated in the table 1. The figures in this table are obtained from eq.(14) using a seismic wave of the reduced El Centro NS component (the maximum acceleration is 200 gals). Here we also calculated the response of displacements using other types of above seismic waves, but we can not show the results in this paper because of space limitations.

ACKNOWLDGEMENTS

This paper is a part of the research entrusted by Tetsudō Kensetsu Kōdan (the Railway Construction Corporation). The writer wishes to express his appreciation to the member of the Corporation. He also wishes to acknowledge the members of Itō Chū Electronic Computer Service Co., Ltd. who took a part for numerical computation, and to the members of the Research Section of Dai-Nippon Consultants Co., Ltd. for their aid in the arrangement of this paper.

REFERENCES

1. Ohchi, Y., "Matrix Solution of Framed Structures" Transactions of the Japan Society of Civil Engineers, No.87 (1962) or Quarterly Report of the Railway Technical Research Institute Vol.3, No.4 (1962).
2. Ohchi, Y., "Response Analysis of Framed Structures" Proc. of 3rd World Conference of Earthquake Engineering (1965).
3. Itō, H., and Katayama, T., "Vibrational Damping of Bridge Structure", Trans. of the Japan Society of Civil Engineers, No.117 (1965).

APPENDIX I CRITICAL DAMPING COEFFICIENT MATRIX

Supposing $q = \mathbb{Q}e^{-\omega t}$ in the expression (11), let the right side equals zero, it becomes

$$(\mathbb{V}^T \mathbb{M} \mathbb{V} \omega^2 - \mathbb{V}^T \mathbb{C} \mathbb{V} \omega + \mathbb{V}^T \mathbb{M} \mathbb{V} \mathbb{P}^2) \mathbb{Q} e^{-\omega t} = 0 \qquad (a)$$

The above equation represents the system of free vibration accompanying with damping, if ω is real, the system does not vibrate. In order that ω be of a value at the border between being real and imaginary, that is to say ω be identical roots, the next expression should stand.

$$\mathbb{V}^T \mathbb{C}_{cr} \mathbb{V} = 2 \mathbb{V}^T \mathbb{M} \mathbb{V} \mathbb{P} \qquad (b)$$

This would be confirmed by substituting (b) into the expression (a), which makes

$$\mathbb{V}^T \mathbb{M} \mathbb{V} (\mathbb{F} \omega^2 - 2 \mathbb{P} \omega + \mathbb{P}^2) \mathbb{Q} e^{-\omega t} = 0$$

or $$\mathbb{V}^T \mathbb{M} \mathbb{V} (\mathbb{F} \omega - \mathbb{P})^2 \mathbb{Q} e^{-\omega t} = 0$$

From the expression (b), $\mathbb{C}_{cr}$ is obtained.

$$\mathbb{C}_{cr} = 2 \mathbb{M} \mathbb{V} \mathbb{P} \mathbb{V}^{-1} \qquad (c)$$

APPENDIX II EXPLANATION OF Eqs. (18) AND (19)

If the structure is constructed in the xy plane of the global co-ordinate xyz, the elements of matrices which are included in eqs.(18) and (19) are as follows.

(1) For plane framed structure (Loads and deflections are restricted to the inside of the xy plane)

$$\mathbb{D} = \begin{bmatrix} \delta\ X\ L^{-1} & \delta\ Y\ L^{-1} & 0 \\ \delta\ Y\ L^{-1} & \delta\ X\ L^{-1} & 0 \\ 0 & \frac{1}{2}\mu\ L & \frac{1}{2}\delta\ L \end{bmatrix} \qquad \mathbb{k} = \begin{bmatrix} a & 0 & 0 \\ 0 & b & 0 \\ 0 & 0 & c \end{bmatrix}$$

$$\mathbb{T}a = \begin{bmatrix} U & 0 & 0 \\ 0 & U & 0 \\ 0 & \frac{1}{2}\varepsilon a(2U-\varepsilon b)L & \frac{1}{2}L \end{bmatrix} \qquad \mathbb{T}b = \begin{bmatrix} -U & 0 & 0 \\ 0 & -U & 0 \\ 0 & \frac{1}{2}\varepsilon b(2U-\varepsilon a)L & \frac{1}{2}L \end{bmatrix}$$

$$\mathbb{x} = \begin{bmatrix} x \\ y \\ \Theta_z \end{bmatrix} \qquad \mathbb{P} = \begin{bmatrix} P_x \\ P_y \\ m_z \end{bmatrix} \qquad \mathbb{F}a = \begin{bmatrix} Nua \\ Sva \\ Mwa \end{bmatrix} \qquad \mathbb{F}b = \begin{bmatrix} Nub \\ Svb \\ Mwb \end{bmatrix}$$

(2) For grid-type structure (Loads and deflections point to the outside of the xy plane)

$$\mathbb{D} = \begin{bmatrix} \delta X L^{-1} & -\mu Y L^{-1} & -\delta Y L^{-1} \\ \delta Y L^{-1} & \mu X L^{-1} & \delta X L^{-1} \\ 0 & -(\varepsilon a + \varepsilon b)L^{-1} & 0 \end{bmatrix} \qquad \mathbb{k} = \begin{bmatrix} d & 0 & 0 \\ 0 & e & 0 \\ 0 & 0 & f \end{bmatrix}$$

$$\mathbb{T}a = \begin{bmatrix} U & 0 & 0 \\ 0 & \varepsilon a & U \\ 0 & -(Ea + Eb)L^{-1} & 0 \end{bmatrix} \qquad \mathbb{T}b = \begin{bmatrix} -U & 0 & 0 \\ 0 & \varepsilon b & -U \\ 0 & -(Ea + Eb)L^{-1} & 0 \end{bmatrix}$$

$$\mathbb{x} = \begin{bmatrix} \Theta x \\ \Theta y \\ z \end{bmatrix} \qquad \mathbb{P} = \begin{bmatrix} mx \\ my \\ P_z \end{bmatrix} \qquad \mathbb{F}a = \begin{bmatrix} Tua \\ Mva \\ Swa \end{bmatrix} \qquad \mathbb{F}b = \begin{bmatrix} Tub \\ Mvb \\ Swb \end{bmatrix}$$

Where

$$a = EAL^{-1} \quad b = 3(\varepsilon a + \varepsilon b)^2\{U + (\varepsilon a + \varepsilon b)^2\,\Omega\}^{-1} EIwL^{-1} \quad c = 4\varepsilon a\,\varepsilon b\,EIw\,L^{-3}$$

$$d = GJL^{-1} \quad e = 3(\varepsilon a + \varepsilon b - \varepsilon a\,\varepsilon b)\{U + (\varepsilon a + \varepsilon b)^2\,\Omega\}^{-1} EIuL^{-1} \quad f = \varepsilon a\,\varepsilon b\,EIvL^{-1}$$

$$\delta = \alpha - \beta$$

$$\mu = \begin{cases} \alpha\,\varepsilon a\,(2U - \varepsilon b) + \beta\,\varepsilon b\,(2U - \varepsilon a) & \text{for plane framed S.} \\ \alpha\,\varepsilon a + \beta\,Eb & \text{for grid-type S.} \end{cases}$$

$$\Omega = \begin{cases} 3\kappa E I_w (GAL^2)^{-1} & \text{for plane framed S.} \\ 3\kappa E I_v (GAL^2)^{-1} & \text{for grid-type S.} \end{cases}$$

U = unit matrix

E, G, κ = diagonal matrices, the (i, i) element in diagonal matrix shows the Young's modulus, the shear modulus and the shear coefficient of member i.

A, I_v, I_w, J, L, X, Y = diagonal matrices in which the (i, i) element represent the cross sectional area, the moment of inertia of the section around the local v, w axis, the tortional moment of inertia of the section, the length and the projection of the length on the global , axis respectively.

α, β = matrices indicating with which member is connected at member's node. For example, $\alpha_{ij} = 1$ or $\beta_{ij} = 1$, it shows that the end a or b of member j is connected with the node i; otherwise $\alpha_{ij} = 0$ or $\beta_{ij} = 0$.

ε_a , ε_b = diagonal matrices, in which the (i, i) element equal zero, if a hinge is located at the end a or b of member i; otherwise equals 1.

x , y , z $(\theta x, \theta y, \theta z)$ = column vectors, the ith element shows the deflection (deflection angle) of node i.

N_{ua} , S_{va} , S_{wa} (T_{ua}, M_{va}, M_{wa}) = column vectors, the ith element shows the U , V , W component of the sectional forces (moments) at the end a of member i.

APPENDIX III NOTATION

C, $\mathbb{C}$ = damping coefficient and damping coefficient matrix

C_{cr}, $\mathbb{C}_{cr}$ = critical damping coefficient and critical damping coefficient matrix

Δ = logalithmic decrement

$\mathbb{F}$ = This vector represents the difference of absolute and relative displacement vector dividing by $\ddot{x}_{ei}$; while the displacement is the same direction as seismic acceleration, the values of elements in this vector are 1, otherwise equal zero.

h = damping constant (C/C_{cr})

h_0, h_1, h_2 = constants defining h (see Eq.(7) or (12))

K, $\mathbb{K}$ = spring constant and stiffness matrix

M, $\mathbb{M}$ = mass and mass matrix

P, $\mathbb{P}$ = circular natural frequency and circular natural frequency matrix

$\bar{S}_v$ = average response velocity spectrum

$S_v(t)$, $\mathbf{S}_v(t)$ = see Eqs.(4) and (14)

, $\mathbb{U}$ = unit matrix

w_i , $\mathbb{W}$ = mode vector and mode matrix

x , $\mathbb{X}$ = relative displacement and relative displacement vector

$\ddot{x}_e$ = seismic acceleration

$\mathbb{A}$, $\mathbb{B}$, $\mathbb{C}^T$, $\mathbb{D}$, $\mathbb{F}_a$, $\mathbb{F}_b$, $\mathbb{F}_{fa}$, $\mathbb{F}_{fb}$, $\mathbb{R}$, $\mathbb{P}$, $\mathbb{T}_a$, $\mathbb{T}_b$ = see APPENDIX II

FIG. 1

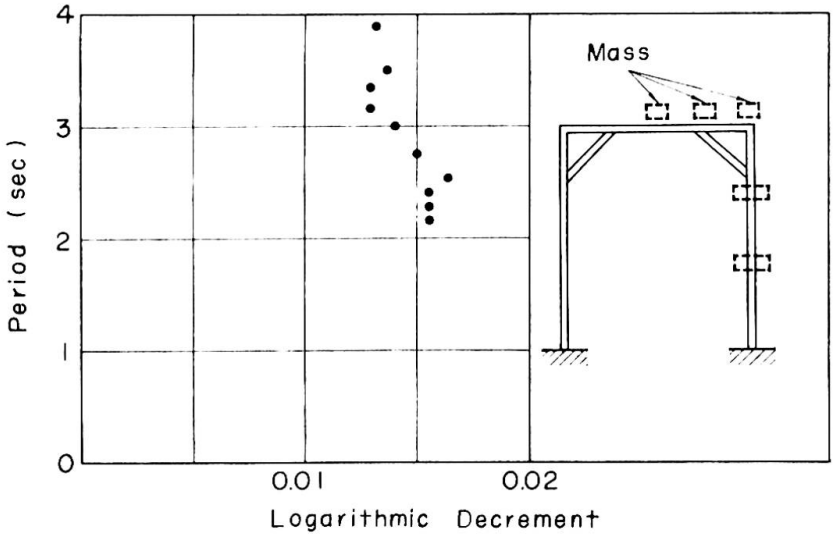

FIG. 2

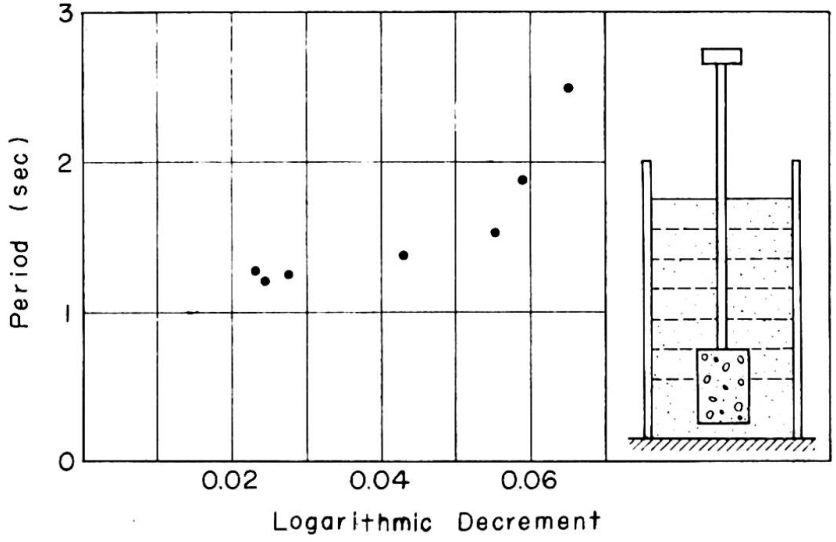

FIG. 3 (a)

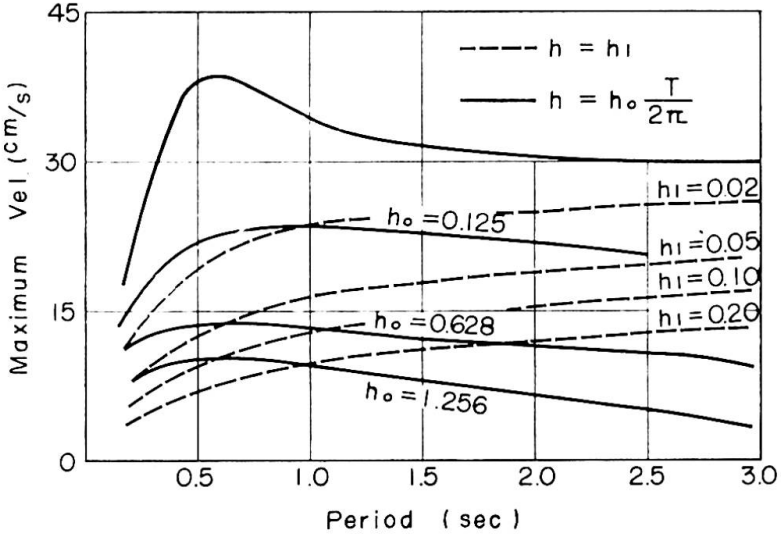

FIG. 3 (b)

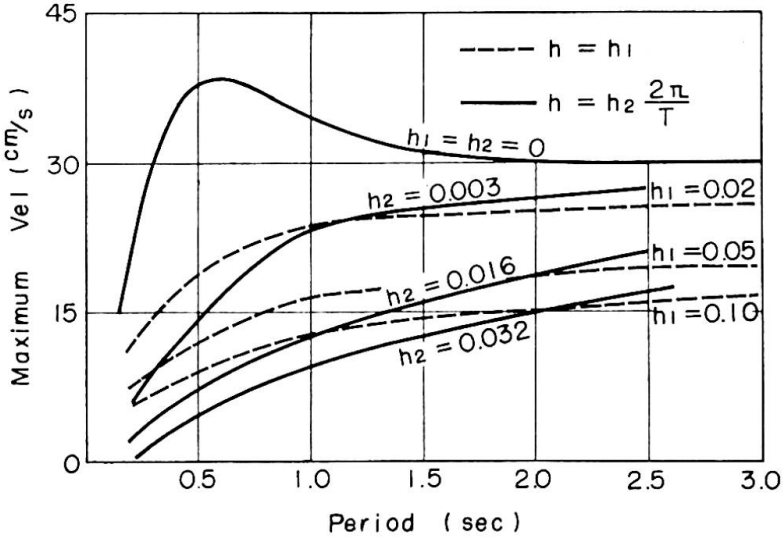

FIG. 4

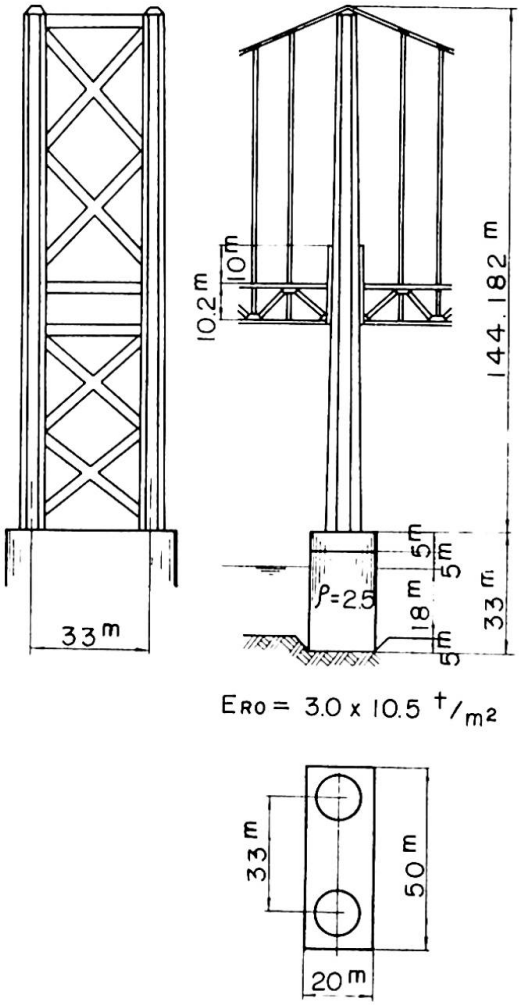
33 m
10.2 m
10 m
144.182 m
5 m
5 m
18 m
5 m
33 m
ρ=2.5
ERO = 3.0 x 10.5 t/m²
33 m
50 m
20 m

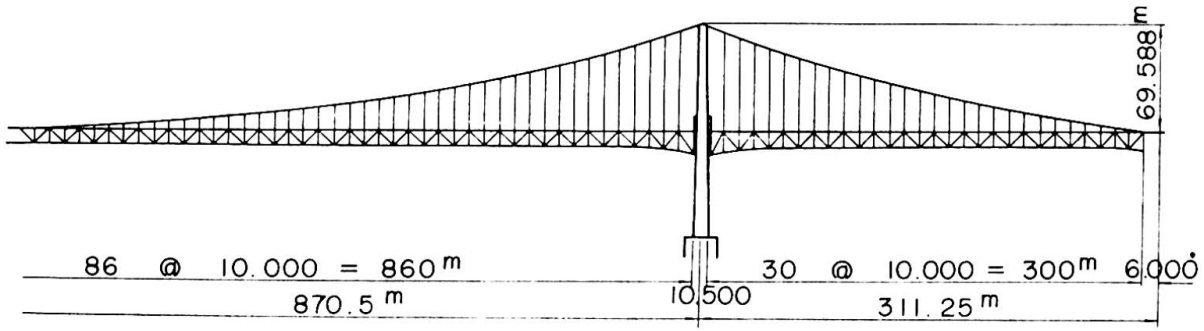
69.588 m
86 @ 10.000 = 860 m
870.5 m
10.500
30 @ 10.000 = 300 m
311.25 m
6.000

FIG. 5

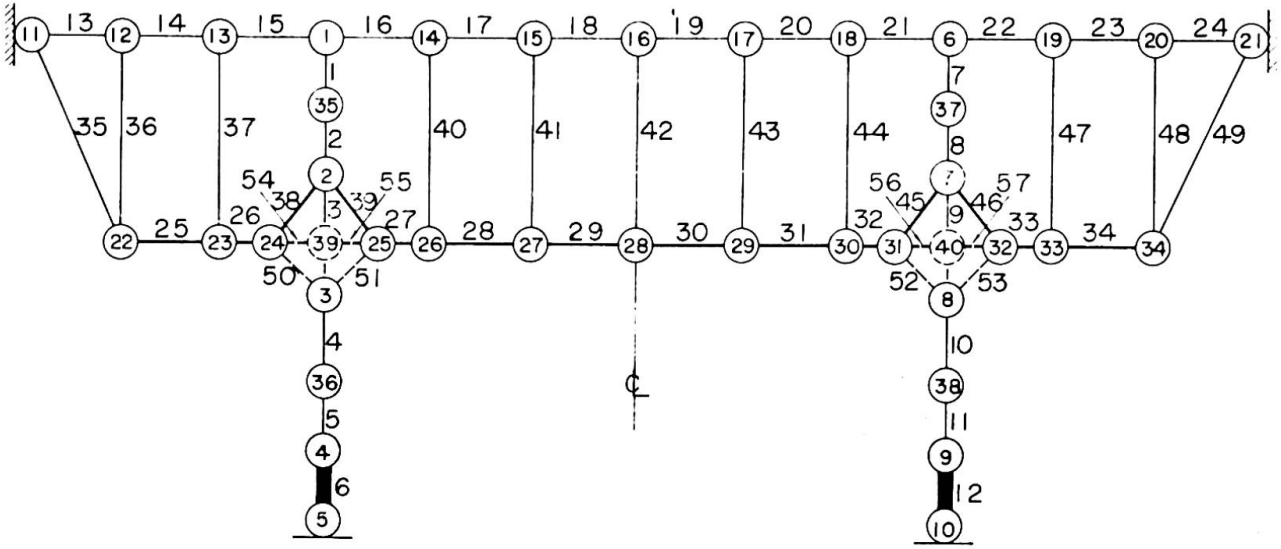
11 13 12 14 13 15 1 16 14 17 15 18 16 19 17 20 18 21 6 22 19 23 20 24 21
35 36 37 40 41 42 43 44 47 48 49
22 25 23 24 39 25 26 28 27 29 28 30 29 31 30 31 40 32 33 34
54 38 39 55 56 45 46 57
50 51 52 53
1 2 3 4 5 6 7 8 9 10 11 12
35 36 37 38

Table 1

damping Const.	h_0	—	0.628	—	0.314
	h_1	0.100	—	—	—
	h_2	—	—	0.0159	0.008
NORMAL FORCE (t)					
side cable	13	1 070	1 090	1 030	1 050
	14	1 080	1 100	1 040	1 060
	15	1 100	1 120	1 060	1 080
center cable	16	57.6	70.3	56.8	55.7
	17	56.5	69.3	55.7	54.6
	18	55.7	68.0	55.0	53.9
side hanger	35	201	228	174	187
	36	88.7	95.4	85.6	86.7
	37	55.6	57.1	52.5	53.7
	38	42.9	487	372	400
center hanger	39	44.4	54.4	41.4	40.4
	40	2.96	4.06	2.88	2.80
	41	5.50	6.67	5.46	5.30
	42	4.69	5.77	4.61	4.50
BENDING MOMENT (t, m)					
tower	1	21 400	21 000	22 700	21 200
	2	24 700	23 500	26 000	24 200
	3	16 600	16 400	17 100	16 600
	4	12 500	12 300	12 800	11 000
	5	40 400	41 600	39 100	39 800
	6	522 000	522 000	524 000	522 000
stiff girder	26	1 150	844	1 250	987
	28	151	154	162	152
	29	79.8	58.7	96.1	62.7
	30	88.6	28.5	122	42.7

damping Const.	h_0	—	0.628	—	0.314
	h_1	0.100	—	—	—
	h_2	—	—	0.0159	0.008
SHEARING FORCE (t)					
tower	1	575	566	611	570
	2	126	136	125	116
	3	549	588	523	544
	4	870	878	854	863
	5	1 030	1 020	1 050	1 030
	6	14 800	14 800	14 800	14 800
DISPLACEMET (cm)					
left tower	1	16.9	3.84	19.0	4.88
	35	16.2	14.8	17.4	13.6
	2	16.6	16.2	16.8	14.7
	3	14.0	13.7	14.2	12.3
	37	8.37	13.5	8.44	7.24
	4	3.35	3.38	3.29	2.88
	5	—	—	—	—
side span	22	132	23.8	154	39.1
	23	47.4	8.61	54.8	14.0
	24	41.5	11.2	46.8	15.4
center span	25	3.31	3.30	3.42	3.26
	26	1.67	1.87	1.58	1.77
	27	2.60	0.66	3.05	0.51
	28	3.39	0.55	4.04	0.93
	29	3.15	1.32	3.61	1.56
	30	2.68	2.22	2.70	2.29
	31	3.42	3.32	3.50	3.34

SUMMARY 1191

From our simple experiments about this field, we propose the equation (12) or (16') for the damping coefficient matrix of the multi-mass-system. Results obtained from usual method were compared with some series of our numerical calculations, we find that h_0 in eq.(12) is more important and influential than that of h_2 on conforming the result obtained from usual method. We consider that some questions still exist in adapting damping coefficient matrix to be used in usual method.

In order to obtain more adequate value of $h_0 \sim h_2$, we conclude that more field test or more detail of experiment for determining the damping coefficient matrix is necessary.

RÉSUMÉ

De nos expériences dans ce domaine nous arrivons à proposer l'équation (12) ou (16') pour la matrice de coëfficient d'amortissement du système à masses multiples. Les résultats reçus par la méthode habituelle ont été comparés avec quelques séries de nos calculs numériques. Nous trouvons le facteur ho dans l'équation (12) plus grand et influent que h2, en adaptant le résultat obtenu par la méthode habituelle. Nous pensons que tous les problèmes ne sont pas résolus dans l'adaptation de la matrice du coëfficient d'amortissement à la méthode de calcul normale.

Nous concluons qu'il est nécessaire de faire plus de tests sur nature ou de détailler d'avantage les expériences pour obtenir des valeurs ho ~ h2 plus adéquates à la détermination de la matrice de coëfficient d'amortissement.

ZUSAMMENFASSUNG

Aufgrund unserer einfachen Versuche auf diesem Gebiet empfehlen wir die Gleichung (12) oder (16') für die Dämpfungskoeffizienten-Matrix des Viel-Massen-Systems. Ergebnisse der üblichen Verfahren sind mit einigen Sätzen unserer numerischen Berechnung verglichen worden, und wir finden, dass ho in Gleichung (12) wichtiger und einflussreicher denn h2 bei Anpassung an die Ergebnisse der üblichen Verfahren ist. Wir berücksichtigen, dass einige Fragen bei der Anwendung der Dämpfungskoeffizienten-Matrix im üblichen Verfahren noch offen bleiben.

Um mehr hinreichende Werte ho ~ h2 zu erhalten, folgern wir, dass mehr Felduntersuchungen oder mehr Prüfungsdetails zur Bestimmung der Dämpfungskoeffizienten-Matrix notwendig sind.

Leere Seite
Blank page
Page vide

Application of Modern Design Techniques to Practical Wind Problems

Application des techniques de projection modernes aux problèmes pratiques posés par le vent

Anwendung der modernen Entwurfstechniken auf praktische Windprobleme

E.M. LEWIS R.A. WALLER
W.S. Atkins and Partners
Epsom, Surrey
Great Britain

Introduction

It is clear that the days when wind was considered as a static phenomenon have gone. Gone also in many cases is the simplicity of the quasi-static load case which has normally been assumed as applicable to wind loadings.

The equivalent static load concept is adhered to very strongly. It is clearly valid to express answers as an equivalent static load but it can, if we are not careful, tend to cover up gross inadequacies in the method of calculation and in the assumptions that have been made.

This contribution to the prepared discussion describes attempts to apply the latest concepts and techniques of analysis to dynamic wind loading conditions.

Two major dynamic effects will be considered. There is the problem of aerodynamic instability caused by the formation of regular patterns of vortices in the lee of certain shaped structures requiring the techniques of dynamic analysis of complex structures. There is the problem of gusting as it relates to the more flexible structures involving in addition the techniques of random vibration analysis.

Gusting

Buffeting in a gusty wind occurs largely at random. The random velocity fluctuations are, however, contained within an overall spectrum which defines the amount of wind energy available (on an average) at various frequencies (Prelim. Publication 8th Congress IABSE).

All structures have modes in which they naturally vibrate, the sway modes of vibration being particularly important in the context of wind gusting as they can interact with the wind and accentuate the dynamic effect.

The work done by Davenport (Davenport 1961) was aimed at producing simplifications of the basic techniques of random vibration allowing the engineer to take gusting into consideration. The following is the expression for the effective force which is applied to a structure taking into account its dynamic response.

The effective force = hourly wind pressure x gustiness of wind x structural response x a factor

This last factor is a statistical measure which defines the peak response in which we are interested; e.g. Davenport suggests taking the average of the peak responses which occur within periods of an hour. This factor varies little with the characteristics of the structure. The mean hourly wind pressure and the gustiness of the wind are clearly also independent of the properties of the structures concerned.

The simplest case to consider is that of the lightly damped structures where the response is largely governed by movements which take place at the natural frequency of the structure (fortunately many practical structures respond in this way). In this case Davenport shows that the response is proportional to $\sqrt{\frac{n\ Sn}{\delta}}$ where Sn is the spectral density of the gusting at the natural frequency n of the structure and δ the logarithmic decrement.

It happens that the reduced spectral density in the frequency range from 0.1 Hz upwards is closely given by an algebraic polynomial. Davenport suggests $\frac{x^2}{(1+x^2)}^{4/3}$ and Harris (Harris 1968) suggests $\frac{x}{(2+x^2)}^{5/6}$ where x in each case is given by $1200\ \frac{n}{V}$ where V is the wind velocity in metres/sec. Where x is significantly greater than 1 as it is when n is greater than 0.1, both these polynomials reduce to $x^{-2/3}$.

Hence the effective force is proportional to:

$$n^{-1/3}\quad \delta^{-1/2}.$$

Clearly, therefore, the lower frequency structures are more susceptible to wind gusting as the effective force is greater.

A further effect exists in that the lower frequency gusts tend to be more highly correlated over larger areas than the higher frequency gusts. Conversely, the higher the gust frequency the smaller the effective area over which the gust pressure is applied. There comes a point at which the gusts are so small in relation to the structural size that they do not have a significant effect. Davenport suggests that once the gust frequency exceeds the ratio of the maximum wind velocity to a typical dimension of the building, then the effect of gusting can be ignored.

We will now consider a few examples of buildings which have been designed and constructed where gusting was of sufficient importance to influence their design.

A Building on Springs

A block of flats (Albany Court) was erected in 1966 over the underground railway in London (Figure 1). The building was supported on a number of laminated rubber springs to isolate it from the vibrations generated by the railway. This is probably the first complete building to be isolated in this way from low frequency ground-borne vibrations (Waller 1966).

FIGURE 1

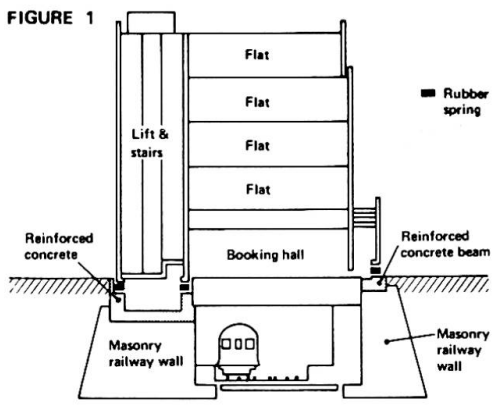

Clearly the introduction of springs for this purpose significantly alters the natural frequencies of the building. In this case the vertical frequency of the system was designed to be 7 Hz. It is a characteristic of the laminated rubber spring that its horizontal stiffness is two orders less than its vertical stiffness so that in the first instance the

designed horizontal frequency of the spring system was about 0.5 Hz. This frequency was sufficiently low for there to be a significant possibility that the building would respond to gusting especially as this frequency is in the range at which eddies would be shed from nearby buildings. It would clearly be unsatisfactory if in eliminating the ground-borne vibrations the building were made significantly sensitive to the wind.

At the low frequencies involved the human sensitivity to vibration can be represented as proportional to acceleration. No rigorous estimate could be made of the likely magnitude of the acceleration induced by wind. It was judged however that there might be a problem at 0.5 Hz as an effective dynamic pressure of 1 lb./ft.^{2} was equivalent to an acceleration of 0.001g for this particular building, a level at which a significant number of people can perceive low frequency vibration.

Now acceleration is proportional to (amplitude)x(frequency)^2 and amplitude is proportional to (effective force)/stiffness. Stiffness in this case is proportional to (mass)x(frequency)^2. Thus acceleration is proportional to:

$$n^{-1/3} \quad \delta^{-1/2} \quad m^{-1}$$

if m is the effective mass of the building.

To reduce this acceleration there are therefore three possibilities: we can increase mass, damping, or natural frequency. In this particular case it was decided that the simplest and cheapest course was to increase the natural frequency. It was found possible to increase the horizontal natural frequency to 2.5 Hz without significantly reducing the attenuation of the ground-borne vibrations.

The building in this case could be considered substantially as a rigid body on a number of springs and the analysis was fairly straightforward. There was little coupling between the various modes although clearly in the vertical planes the horizontal natural frequencies and the frequencies in sway or rock (6 Hz in this case) are coupled together to some extent. Indeed it is this coupling which limits the extent to which the so-called horizontal natural frequency of the spring system can be raised.

Raising the lowest natural frequency to 2.5 Hz eliminated the possibility of interaction with eddies from nearby buildings and kept the effective 'natural' wind energy likely to interact to a minimum.

The effectiveness of the measure can only be judged by experience. Two years have elapsed without significant vibrations being reported.

In the case of the taller and more flexible buildings the flexibility of the structure itself must be taken into account in the analysis. It will often arise that the horizontal frequencies cannot be raised enough to avoid significant gust action. With the taller structures which have natural frequencies in sway of the order of 0.5 Hz it will be impossible to avoid the problem of gust action by increasing the natural frequencies. Here it will be useful to consider the addition of damping into the foundation.

Water Tower

The type of water tower that will be described was the subject of an extensive development programme. The programme was aimed at producing a new form of water tower which would combine the economics of the cheaper form of towers with the appearance of the more expensive. The form of water container finally chosen can be described as an inverted parachute with the fabric made of nylon reinforced rubber and the cables of high tensile steel. These cables are fixed to a stiff annulus which is mounted at the top of the tower leg (Figure 2).

It is well known that the natural frequency of water contained in a tank is low and it was possible that the tower might respond to gusting and to vortex excitation. One twentieth scale wind tunnel tests were commissioned at the National Physical Laboratory (Smith 1964) and indicated that vortex excited instability was unlikely. Unfortunately it is not yet possible to simulate gusting conditions in a wind tunnel and recourse to calculation was necessary in this respect.

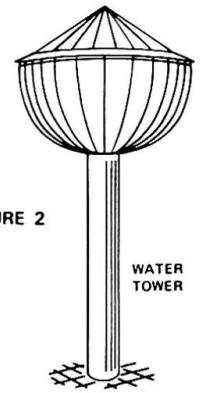

FIGURE 2

The natural frequencies for the tower were difficult to calculate. The mode of particular importance can perhaps be best described as the 'sloshing' mode. Formulae do exist for the 'sloshing' of water within rigid containers (Housner 1963), but the nature of the present container was such that no previous solution could be found that was applicable and it was decided that scale models would be a better method of establishing the natural frequencies than a theoretical exercise. The other mode of vibration of relevance is the vibration of the stalk itself with the water playing little part. It is easy to show that this frequency is much higher than the 'sloshing' frequency of the water in the tank. From the scale model used in the wind tunnel tests the natural frequencies were measured with various amounts of water in the tank and the lowest natural frequency occurred with the full tank. Further it was found that the system was essentially linear.

% Capacity	Natural frequency Hz
5	3.78
40	0.82
100	0.81

The ability to scale models for this purpose is of considerable advantage. Analysis demonstrated that the system could be considered, for scaling purposes, as a compound pendulum for which natural frequency is proportional to (linear scale)$^{-\frac{1}{2}}$. Pressure is proportional to (linear scale) and force is proportional to (linear scale)^3 when velocity is proportional to (linear scale)$^{\frac{1}{2}}$. The model was made to represent as closely as possible the full scale situation; there remained many uncertainties; however the logarithmic decrement of 0.025 measured in still air conditions was taken to represent a full scale tank. The effect of wind was to increase this damping slightly. It was also considered that the likely effect of foundation damping, joints in the structure, etc. would be to increase it again and that this figure would be on the safe side.

One other significant factor had to be established in relation to the behaviour of the tank before its full scale behaviour could be predicted. Not all the wind force is modified by the dynamic behaviour of the tank. A proportion of it is effectively applied directly to the top of the tank and stalk which is more rigid. The remaining part of the wind force can be considered as acting upon the flexible portion of the tank and therefore modified by the tank's dynamic characteristics. The distribution of the wind force was measured by displacing the tank in a steady wind stream until it was completely stationary. When the displacing wind force was suddenly removed the tank and water were set into a state

TABLE

Steady Wind Overturning Moment

Mean hourly wind speed = 27 m s^{-1}

Equivalent model speed = $27\sqrt{\frac{1}{20}}$

= 6 m s^{-1}

Model overturning moment = 0.7 kg m from test (Smith 1964)

Full scale overturning moment = 0.7×20^4 kg m

Full scale mean hourly overturning moment = 110,000 kg m

Additional Moment Due to Gusting

Additional moment = (mean hourly moment)x(gustiness)x(response)x(factor)
(Davenport 1961)

(i) Mean hourly moment as above.

(ii) Gustiness.

Gustiness = $2.45\sqrt{K}\ (\frac{z}{10})^{-\alpha}$ = 0.145 for an open site

When K = surface drag = 0.005
α = power law exponent = 0.16
z = height of centre of pressure = 30m

(iii) Response.

The additional moment due to gusting can be divided into two components, one third being modified by the dynamic response and two thirds acting on a 'rigid' structure.

$$\text{Response} = 2\sqrt{\frac{\text{velocity spectrum area}}{\text{response spectrum area}}}$$

Unmodified response = 2

$$\text{Modified response} = 2\sqrt{\frac{0.82}{\delta}\ \frac{nSn}{K\,V_{10}^2}} = 10.6$$ (ignoring aerodynamic magnification)

for $\frac{n}{v}$ = .008 m^{-1}

δ = .025

(iv) Factor.

Factor for unmodified component = 4.1
Factor for modified component = 3.8

Total Overturning Moment

= mean hourly moment x $(1 + \frac{2}{3} \times 0.145 \times 2 \times 4.1 + \frac{1}{3} \times 0.145 \times 10.6 \times 3.8)$

= 110,000 x (1 + 0.8 + 1.9)kg m

= 400,000 kg m*

* Using Davenport 1967 Total overturning moment = 360,000 kg m.

of motion. The motion took place in various modes simultaneously but predominantly in the two modes associated with the 'sloshing' of the tank and contents and the sway of the stalk. The motion of the stalk decayed quite rapidly but the 'sloshing' of the water continued for some time afterwards. By monitoring the motion of the tank by sensing the displacement of the stalk and extrapolating the behaviour of the water back to zero time, it was possible to show (Figure 3) that the wind load was distributed approximately two-thirds on to the stalk and one-third on to the flexible tank and water. It is this third of the force which is potentially magnified by the dynamic response of the water and the tank.

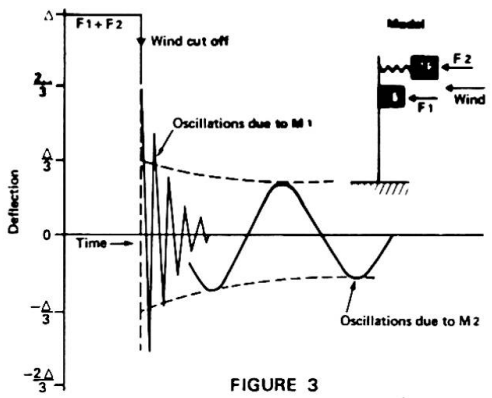

FIGURE 3

It is instructive perhaps now to consider the wind loads on a typical full scale tower. Taking a capacity of 500 cubic metres of water the diameter the tank would be about 12.2 m. The calculations appropriate to such a tower are scheduled in the facing table. The wind speed and surface roughness coefficients used have been estimated for an exposed site.

The total calculated wind loads are roughly double those which would have been assumed, taking an averaging period of 1 minute as suggested by British Standard Code of Practice CP3, Chapter V, or 70 percent greater than the loads on a rigid structure taking account of gust loading.

Drax Chimney

When completed this will probably be the world's largest multi-flue chimney. It will have a height of 260m and will have a constant outside diameter of 26m. The outer shell is made of reinforced concrete whose thickness varies from 1.5m at the base to .37m at the top; the three flues are also of reinforced concrete and they are elliptical in section, having major and minor axes of 13.7m and 9.2m respectively.

A circular cross-section was chosen for the chimney because it is this shape which has the lowest level of vortex excitation. Nonetheless there is still considerable doubt as to the behaviour of tall flexible cylindrical structures, and it was necessary to carry out a number of studies and analyses of the potential behaviour, both under gusting conditions and under potential vortex excitation. As the flues are in 22m lengths and are carried on expansion bearings (Figure 4) in order to prevent thermal effects from inducing unacceptable stresses in the concrete shell, the dynamic behaviour of the chimney as a whole is extremely complex. Too complex in fact to contemplate a wind tunnel model. A computational model was therefore built up and one element of it is shown in Figure 5.

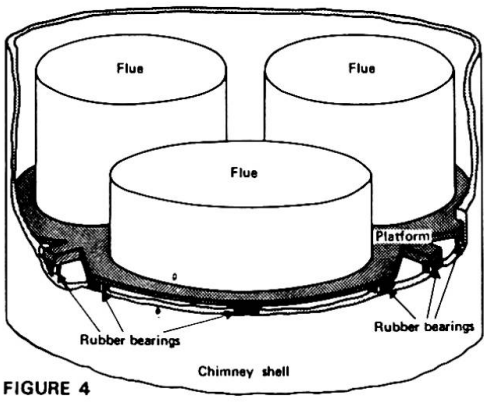

FIGURE 4

The flues are represented as a mass with rotational inertia supported on the bearings which had a finite stiffness in the horizontal direction but which have been regarded as infinitely stiff in the vertical (as above, the vertical stiffness is 100 times

the horizontal). The shell is broken up into an equal number of elements (i.e. 11) to correspond with the flue sections and here again rotational inertia has been allowed for. Hysteretic damping has been included both in the bearings and in the shell. The complete system therefore has been represented by twenty-two masses with associated spring and damping systems.

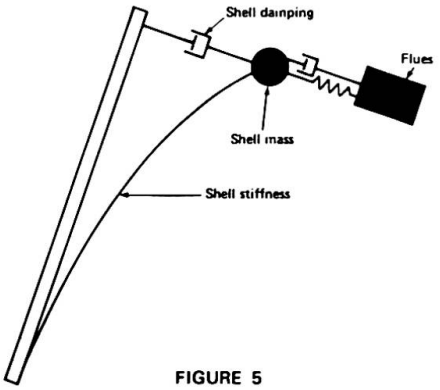

FIGURE 5

Unit sinusoidal forces were applied in turn to each mass element of the shell and the response of the whole system calculated. The computer programme centres round the 88 square matrix which was condensed to a diagonal matrix rather than inverted. The total effect is obtained by summing the effects of the loads on each shell element. This is done for various frequencies, and the interval between the frequencies was chosen depending on the sensitivity of the response of the chimney to frequency.

The first calculations were for a chimney with normal laminated rubber expansion bearings supporting the flues (Figure 6). For comparison, the case without expansion bearings was calculated and is represented by a curve labelled monolithic. It can be seen that the behaviour of the two systems is entirely different. It was a relatively simple step from knowing the response characteristics of the chimney to calculate its behaviour under gust conditions. This was done by integrating the response spectrum obtained using these frequency characteristics, and the net result showed that the chimney with flexible expansion bearings had in fact a dynamic response of only about half that of the monolithic chimney. This was based on the assumption that the damping in the shell structure, i.e. the quadrature component due to damping, was 2 per cent of that due to stiffness. The bearing damping was taken as 12 per cent. In either case the significance of gusting was small in relation to the total load, and particularly so when account was taken of the probable lack of correlation of wind pressure over the height of the chimney. It was estimated that a gust lasting for at least 15 seconds was required in order to envelope the chimney, and this compared with the period for the structure of between 1 and 2 seconds. Clearly there is unlikely to be much dynamic response under these conditions.

FIGURE 6

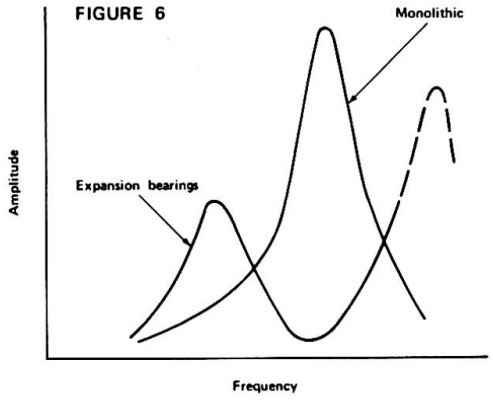

Vortex excitation

The second type of dynamic problem discussed in this contribution is that of vortex excitation. Indeed it is this vortex excitation which is the main problem with structures like the Drax chimney. The difficulty is that little data exists on the behaviour of structures of this size. It is also virtually impossible to carry out model tests in a wind tunnel because of the very high Reynold's number (approximately 10^8) which prevents the correct scaling of the dynamic effects. What data there is suggests that the cross-wind lift coefficient can have any value from 0.7 down to 0.1, and indeed recent papers at an International Symposium (Wootton 1968) suggested that the force coefficient might be even less. Whilst it is difficult therefore to calculate in advance the magnitude of the loads and movements of the chimney, the computer model enabled comparisons to be

made between the various possibilities. The previous Figure indicating the response of the chimney to unit forces (as a function of frequency) is now modified to take account of the variation of wind force with velocity (a function of frequency via a Strouhal number of 0.27). Figure 7 then represents the non-dimensionalised response of the chimney to winds of varying velocity. It was clear that the use of the expansion bearings had significantly modified the behaviour of the chimney compared to the monolithic case. Further, the vibration amplitudes were reduced. This suggested that if the properties of the expansion bearings were chosen with the dynamic behaviour in mind then the overall maximum amplitude of the chimney could be further reduced. This was done by decreasing the shear stiffness of the bearings until the amplitude at the top of the chimney was less than one tenth of that in monolithic case. There are two peaks in the amplitude curve. The first is at relatively low wind speed where the frequency of vortex shedding corresponds with the natural frequency of vibration in the horizontal mode of the flue segments. The magnitude of their response is limited by the damping in the bearings. At higher wind velocities and frequencies the shell itself is playing the major part in the mode of vibration, and its amplitude increases as the wind speed approaches that corresponding to its natural frequency giving a second amplitude peak. However, the maximum wind speed likely to occur is somewhat lower than that necessary to produce a resonant condition here.

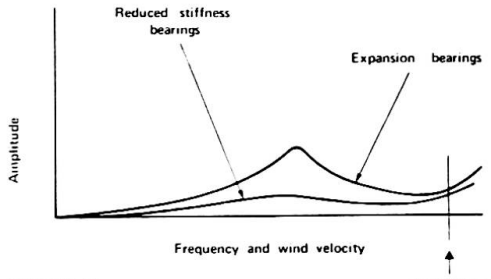

FIGURE 7

It is worth commenting that there are three basic ways of reducing vibration amplitudes due to vortex excitation in a structure. Firstly there is changing the natural frequency to avoid resonance; secondly increasing the damping to keep the amplitude to a reasonable level; and thirdly the prevention of the formation of the vortices by changing the shape of the chimney. In this case the cheapest solution involved changing the natural frequency and damping simultaneously to give a better performance. The possibility of eliminating the vortices at source was also considered and in parallel with the above computations a test programme was commissioned on behalf of the Central Electricity Generating Board (Walshe & Bearman 1967). Several methods of preventing the formation of vortices were considered, including the use of helical strakes and a perforated shroud. The tests demonstrated that the helical strakes produced a marked increase in the overturning moment due to wind whilst the perforated shroud did not. Although the effectiveness aerodynamically of the shroud was not as great as that of the strakes it was considered in the event of a chimney being subject to vortex excited oscillations that the shroud represented a more reasonable repair scheme. It reduced the vortex excitation quite significantly but did not introduce an increase in the wind drag load.

The behaviour of the Drax chimney will be monitored during construction so that the calculations can be compared with actuality, when in the unlikely event of the effects being underestimated the chimney can be modified accordingly.

Whilst the main theme of this paper has been the use of the more advanced techniques of analysis one lesson which could be drawn from the examples quoted is the need to monitor the non-standard structure during its erection and immediate post-erection period to determine the likelihood or otherwise of untoward behaviour.

It is also clear from this paper that whilst modern techniques are being used the amount of data available and the quality of the data are poor. This has been the subject

of another paper by one of the authors (Waller 1968) in which the general conclusion was that more of the research efforts should be directed towards the full scale interaction of the wind and structures so that the more sophisticated design techniques can be utilised with confidence.

Notation

α	wind power law exponent.
δ	logarithmic decrement.
g	acceleration due to gravity
K	surface drag coefficient.
m	effective mass.
n	natural frequency.
V	mean hourly wind speed.
x	$1200\frac{n}{v}$.
z	height above ground.
$\frac{n\,Sn}{K\,V_{10}^2}$	reduced gust velocity spectrum.

REFERENCES

Preliminary Publication of 8th Congress IABSE.

British Standard Code of Practice. CP3 - Chapter V Loading, 1952.

Davenport, A. G. The Response of Slender Line-like Structures to a Gusty Wind. Proceedings of the Institution of Civil Engineers, November, 1962.

Davenport, A. G. The Application of Statistical Concepts to the Wind Loading of Structures. Proceedings of the Institution of Civil Engineers, August 1961.

Davenport, A. G. Gust Loading Factors. Journal of the Structural Division Proceedings of the American Society of Civil Engineers, Vol. 93, No. ST3, June 1967.

Harris, R. I. Measurements of wind structure at heights up to 598 ft. above ground level. Symposium on Wind Effects on Buildings and Structures, Loughborough, 1968.

Housner, G. W. The Dynamic Behaviour of Water Tanks. Bulletin of the Seismological Society of America, February, 1963.

Smith, I. P. An Investigation of the Aeroelastic Stability of a Water Tower. N.P.L. Aero Report, 1104, 1964.

Waller, R. A. Building on Springs. Nature, August 10th, 1966.

Waller, R. A., Dukes, T. P., and Dalley, E. J. A Comparison Between the Quality of the Techniques and the Data Available to the Environmental Engineer with Regard to Wind Loading. Symposium on Wind Effects on Buildings and Structures, Loughborough, 1968.

Walshe, D. E. and Bearman, P. W. The Aerodynamic Investigation for the Proposed 850 ft. high Chimney Stack for the Drax Power Station. N.P.L. Aero Report 1227, April 1967.

Wootton, L. R. The Oscillations of Model Circular Stacks due to Vortex Shedding at Reynolds Numbers in the Range 10^5 to 3 x 10^6. Symposium on Wind Effects on Buildings and Structures, Loughborough, 1968.

SUMMARY

Several structures are described which are novel in that dynamic wind excitation was a significant design parameter. Gust excited vibration is considered in terms of occupant comfort in a block of flats and the structural integrity of a water tower. The reduction of vortex excited vibration of a 260 m chimney is described. The quality of wind data is poor and consequently the need to monitor the behaviour of such structures during and following erection is emphasised.

RÉSUMÉ

On parle de plusieurs structures qui sont nouvelles en ce sens que l'excitation dynamique par le vent a été un paramètre important de leur dessin. Les vibrations causées par des coups de vent sont considérées en relation au confort des locataires d'un immeuble et à l'intègrité structurelle d'un château d'eau. On décrit la diminution des vibrations causées par tourbillons d'une cheminée de 260 m de hauteur. Les data donnés pour le vent ne sont pas très sûrs et on souligne donc la nécessité de surveiller le comportement de telles structures pendant et après l'érection.

ZUSAMMENFASSUNG

Verschiedene Strukturen werden beschrieben, welche insofern neu sind, als die dynamische Erregung durch Wind ein massgebender Konstruktionsparameter war. Durch Windstösse verursachte Schwingungen werden mit Hinblick auf den Komfort der Bewohner eines Wohnblocks und auf die strukturelle Integrität eines Wasserturms bewertet. Ferner wird das Nachlassen der durch Wirbel verursachten Schwingungen an einem 260 m hohen Schornstein beschrieben. Die auf Wind bezüglichen Daten sind nicht sehr zuverlässig, und es wird daher auf die Notwendigkeit hingewiesen, das Verhalten solcher Strukturen während des Aufbaus und danach zu überwachen.

Dynamic Effects on Precast Bridge Structures

Effets dynamiques sur des ponts en préfabriqué

Der dynamische Einfluß auf vorfabrizierte Brückenteile

VLADIMIR KOLOUŠEK
Prof.Ing.Dr., Dr.Sc.
Praha

In recent times, prestressed structures assembled of precast concrete elements are used also for railway bridges. There is not much experience about their dynamic properties and therefore research first theoretical and then experimental on actual bridges had to be undertaken.

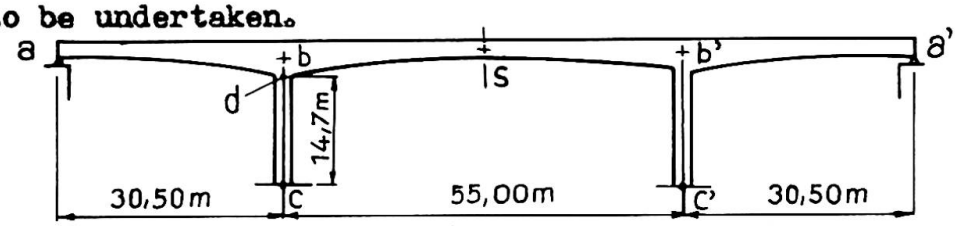

Fig. 1.

The statical system of the structure which we have used in the investigation is a three span rigid frame.(Fig.1) The cross-section in the middle of the central span is in fig.2. The elements of the superstructure which were manufactured in a central precasting plant were transported on a trailer, lifted, rectified and prestressed.

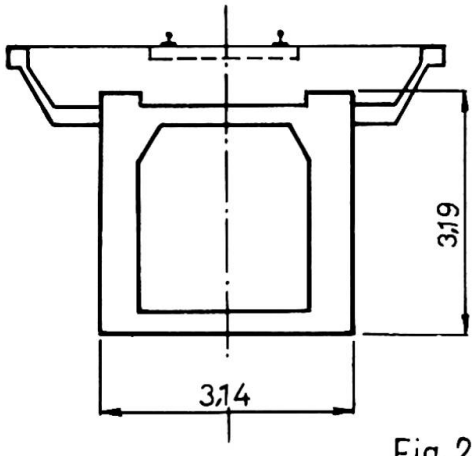

Fig. 2

The object of the research was to find theoretically the dynamic characteristics of the system i.e. the natural frequencies and modes,

and to determine the forced vibrations produced by the load crossing the bridge. The results were then compared with the results of measurement on an actual structure.

The theoretical investigation.

The horizontal beams of the frame structure are of box-shaped cross-section with variable mass and moment of inertia. The theoretical analysis of such a system can be executed by various methods of different accuracy and laboriousness. The differential equation for the vertical motion in this case becomes

$$\mu(x)\,\frac{\partial^2 v(x,t)}{\partial t^2} + E\,\frac{\partial}{\partial x^2}\left[I(x)\,\frac{\partial^2 v(x,t)}{\partial x^2}\right] = 0 \qquad (1)$$

where the notation is as follows

$\mu(x)$ ..... is the variably distributed mass

x ..... is the abscissa of the point in question if the origin is at the left end of each span

$v(x,t)$ ..... is the vertical deflection of the point x at the time t

$I(x)$ ..... the variable moment of inertia

E .....modulus of elasticity

Solution of the equation (1) can be found in the explicit form for special cases only. The major part of solutions [2] start from the work by Kirchhoff[1] who investigated the vibrations of a conical cantilever. They are available e.g. for the beams with the distribution of $\mu(x)$ and $I(x)$ as follows

$$I(x) = I_b \left(\frac{x}{L}\right)^{n+2} \qquad (2)$$

$$\mu(x) = \mu_b \left(\frac{x}{L}\right)^{n} \qquad (3)$$

where μ_b and I_b are the mass and moment of inertia on the right end of the beam and L is the distance of the right end from the conveniently chosen origin (fig.3). There are only four arbitrary constants in expressions(2) and (3) and it is evident that not any distribution of $\mu(x)$ and $I(x)$ can be expressed. Consequently, for an actual structure this laborious solution represents, as a rule, an

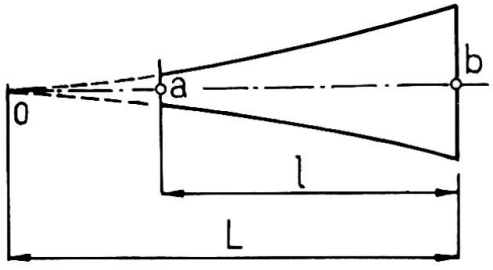

Fig. 3.

1) Kirchhoff G.: Vorlesungen über mat. Physik. Mechanik. Leipzig 1876

2 Коренев Б.Г.: Некоторые задачи теории упругости. Москва 1960.

approximation only.

Equally, some aproximative methods such as those of Rayleigh, Stodola, Ritz or Galerkin can be used, but if an adequate accuracy of calculus is to be attained, all these methods end in tedious computations.

Therefore, the author of this contribution has used his own procedure which enables us to determine the dynamical characteristics in a relatively simple way and with arbitrary required accuracy. This method, which can be called the simplified slope--deflection method, starts from the following considerations. Let us consider a beam which vibrates harmonically, and mark on it some points (fig.4). Between the points the deformed axis of the bar creates a curve, whose shape is determined not only by the position of the points a, b, c .... and their rotations, but also by the inertial forces which act on the distributed mass of the vibrating bar between these points. Let us imagine now the same beam which, however, does not vibrate but is statically deformed by some forces and moments acting in the points a, b, c ... so that the displacements and rotations of these points are the same as in the first case. It is evident that the deformed axis of the bar between the marked points will now be different, owing to the absence of the inertial forces (see the dotted line in fig.4). The difference between both shapes will decrease with decreasing both of the frequency of vibrations and the distance of the points a, b, c ..... .

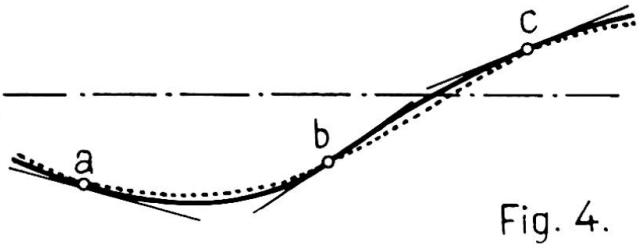

Fig. 4.

Using the slope-deflection method, we divide the system by joints into singular bars. The displacements of joints can be determined by means of slope-deflection equations which are obtained from conditions of equilibrium of end forces and moments of all bars connected in singular joints. In our case, the joints are in the points a, b, s, b', a' and the bars a-b, b-c, b-s, s-b', b'-c', b'-a'.

The first task is the determination of moments and forces acting on the bar ends if they displace or rotate with an amplitude equal to unity. In fig.5 the bar a-b is represented in the case that the end b rotates harmonically.The amplitudes of end moments

are[3]

$$M_{ab}(\xi_b=1)=M_{ab\ stat}(\xi_b=1)-\omega^2\int\mu(x)\,v_1(x)\,v_2x\,dx$$
$$M_{ba}(\xi_b=1)=M_{ba\ stat}(\xi_b=1)-\omega^2\int\mu(x)\,v_1^2(x)\,dx \qquad (4)$$

where ω is the angular frequency and $M_{ab\ stat}(\xi_b=1)$ is the end moment in the point b if this point is statically deformed with $\xi_b=1$. If the first natural frequency of the system is to be determined, the dynamical curves $v_1(x)$, $v_2(x)$ can be substituted by the statical ones $\bar{v}_1(x)$, $\bar{v}_2(x)$. The curves $\bar{v}_1(x)$, $\bar{v}_2(x)$ (statical influence lines) determined for the bar a-b of the system represented in fig. 1, are in fig. 6,

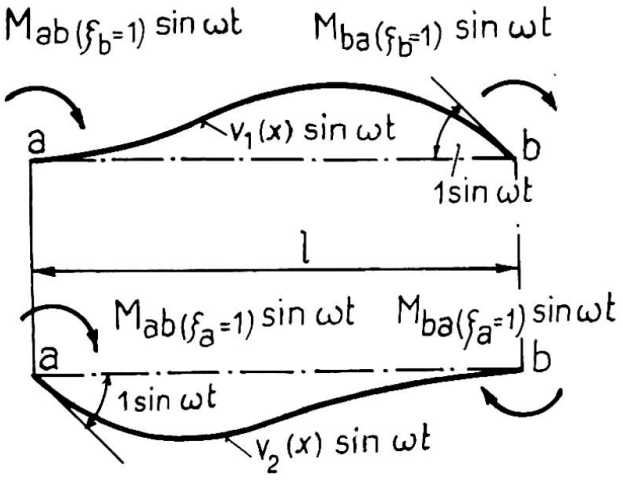

Fig. 5.

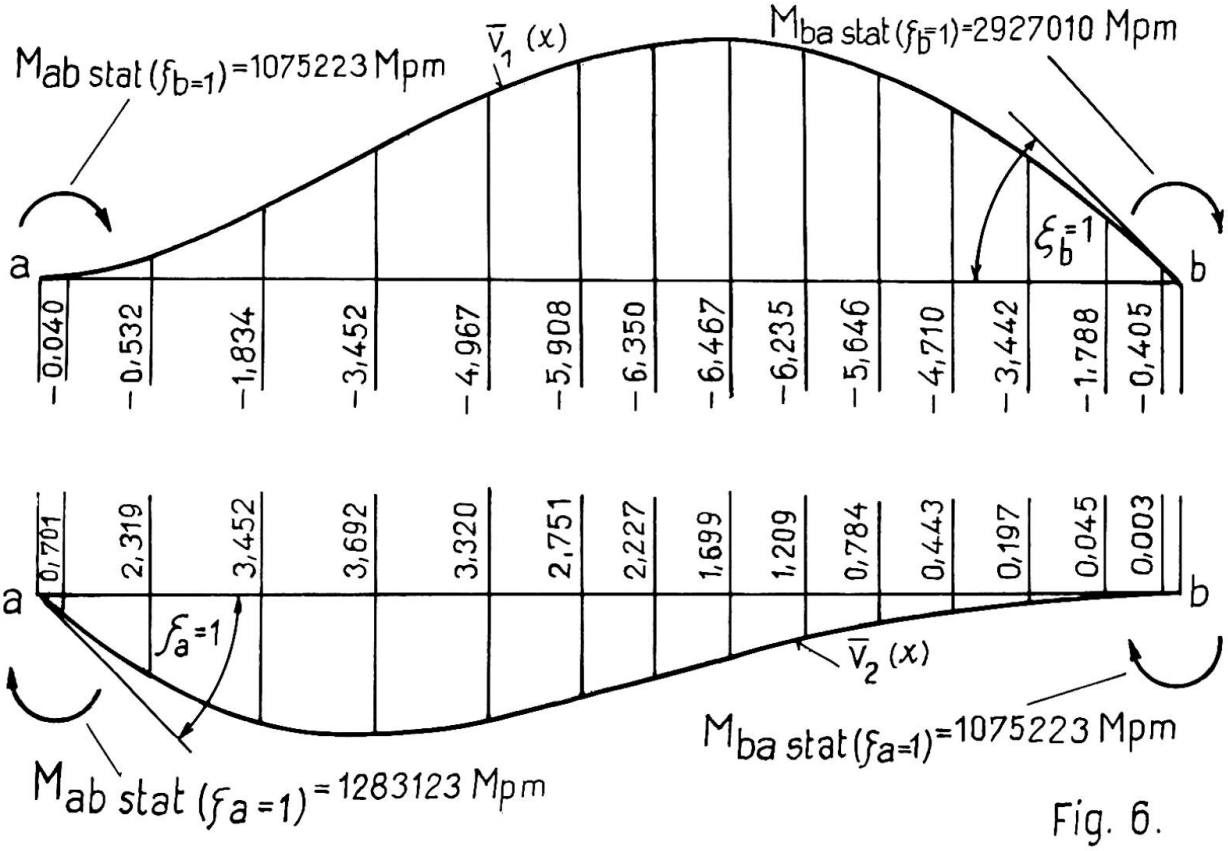

Fig. 6.

3) Koloušek V.: Vibrations of Systems with Curved Members. Publications IABSE.VXXIII. Zurich 1963.P.219-232

Where also the end moments are indicated supposing E =3850 000 Mp/m^2. The integral in (4) can be evaluated with sufficient accuracy by numerical summation of finite differences dividing the bar into strips. Then it is

$$M_{ab}(\xi_b=1) = M_{ab\ stat}(\xi_b=1) - \omega^2 \sum_i m_i \bar{v}_{1i} \bar{v}_{2i} \qquad (5)$$

where m_i denotes the mass of the strip i and $\bar{v}_{1i}$, $\bar{v}_{2i}$ the vertical displacements in the centre of gravity of the strip i. Another proceeding can be applied for the determination of the end-moments of piers which are of constant cross-section. The pier and the horizontal beams penetrate in the upper part of the pier d-b (fig.7) and the rigidity of the pier increases in this part substantially. It can be assumed that the moment of inertia is infinitely large there. The low end was assumed to be fixed rigidly, which holds only when the foundation reposes on solid rock. The end moment acting on the upper end can be expressed by frequency functions F (λ) which have been developed by the author [4)5)]. It is

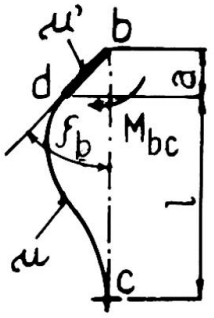

Fig. 7.

$$M_{bc}(\xi_b=1) = \frac{EI}{\ell}\left[F_2(\lambda) - \frac{2a}{\ell} F_4(\lambda) + \frac{a^2}{\ell^2} F_6(\lambda)\right] - \frac{1}{3}\mu' a^3 \omega^2 \qquad (6)$$

The last term in exp. (6) expresses the moment of inertial forces of the rigid part d-b of the length a and μ' is its mass per unit of length. It was assumed

$$I = 2{,}286\ m^4$$
$$\mu = \mu' = 17{,}31 t/m\ (=1{,}76\ Mps^2\ m^{-2})$$
$$\lambda = \sqrt{\omega}\, \ell \sqrt[4]{\frac{\mu}{EI}} = 0{,}3354$$
$$E = 2850\ 000\ Mp/m^2$$

Further it can be assummed for small values of λ

$$F_2(\lambda) \doteq 4 - \frac{1}{105}\lambda^4 \qquad F_4(\lambda) \doteq -6 + \frac{11}{210}\lambda^4 \qquad F_6(\lambda) \doteq 12 - \frac{13}{35}\lambda^4$$

Substituting into eq.(6) we obtain

$$M_{bc}(\xi_b=1) = 2143961 - 301{,}15\ \omega^2$$

The values of end moments and forces of all bars which were determined according to exp. (5) or (6) are given in Table I.

4) Koloušek V.: Baudynamik der Durchlaufträger und Rahmen. Fachbuchverlag, Leipzig 1953

5) Koloušek V.: Calcul des efforts dynamiques dans les ossatures rigides. Dunod, Paris 1959

Table 1.

	$\xi_a = 1$	$\xi_b = 1$	$\xi_s = 1$	$v_s = 1$
M_{ab}	$1283123-286{,}20\omega^2$	$1075223+412{,}80\omega^2$		
M_{ba}	$1075223+412{,}80\omega^2$	$2927010-1124{,}46\omega^2$		
M_{bs}		$3421740-819{,}45\omega^2$		$-168850-57{,}35\omega^2$
M_{bc}		$2143961-301{,}15\omega^2$	$1221640+301{,}02\omega^2$	
$\sum$	$1075223+412{,}80\omega^2$	$8492711-2245{,}06\omega^2$	$1221640+301{,}02\omega^2$	$-168850-57{,}35\omega^2$
M_{sb}		$1221640+301{,}02\omega^2$	$1462100-207{,}56\omega^2$	
Y_{sb}		$-168850-57{,}35\omega^2$		$9701{,}97-15{,}111\omega^2$

Free symmetrical vibrations. The first natural mode is represented in fig. 8. The slope-deflection equations are

$$\begin{aligned} M_{ab} &= 0 \\ M_{ba} + M_{bs} + M_{bc} &= 0 \\ Y_{sb} &= 0 \end{aligned} \qquad (7)$$

where

$$\begin{aligned} M_{ab} &= M_{ab(\xi_a=1)} \cdot \xi_a + M_{ab(\xi_b=1)} \cdot \xi_b \\ M_{ba} &= M_{ba(\xi_a=1)} \cdot \xi_a + M_{ba(\xi_b=1)} \cdot \xi_b \\ M_{bs} &= M_{bs(\xi_b=1)} \cdot \xi_b + M_{bs(v_s=1)} \cdot v_s \\ M_{bc} &= M_{bc(\xi_b=1)} \cdot \xi_b \\ Y_{sb} &= Y_{sb(\xi_b=1)} \cdot \xi_b + Y_{sb(v_s=1)} \cdot v_s \end{aligned} \qquad (8)$$

ξ_a and ξ_b denote the amplitudes of rotation in joints a and b respectively, v_s is the amplitude of vertical displacement in the joint s, and Y_{sb} is the amplitude of end force.

After substituting numerical values into (8) and (7) we obtain the equations of the Table II. Setting the determinant of the equations equal to zero, we obtain

$$\omega^6 - 16\,078\omega^4 + 36\,175075\omega^2 - 9353\,402\,000 = 0$$

and thereof

$$\omega_{(1)} = 17{,}235\ s^{-1}, \quad \omega_{(2)} = 48{,}4\ s^{-1}, \quad \omega_{(3)} = 116\ s^{-1}$$

The last two values are of an informative character only. The first natural mode is given by ξ_a, ξ_b and v_s; one of them can be chosen and two other calculated from the equations of Table II.

Table II.

ζ_a	ζ_b	v_s
$1283123 - 286{,}20\omega^2$	$1075223 + 412{,}80\omega^2$	$= 0$
$1075223 + 412{,}18\omega^2$	$8492711 - 2245{,}06\omega^2$	$-168850 - 57{,}35\omega^2 = 0$
	$-168850 - 57{,}35\omega^2$	$9701{,}97 - 15{,}111\omega^2 = 0$

Supposing that $v_s = 1_m$, we have

$$\zeta_a = -0{,}02003 \qquad \zeta_b = 0{,}02804$$

The deformations of singular bars can then be obtained using the statical curves of deformations which for the bar a-b are in fig. 6. The first mode of the system is shown in fig. 8.

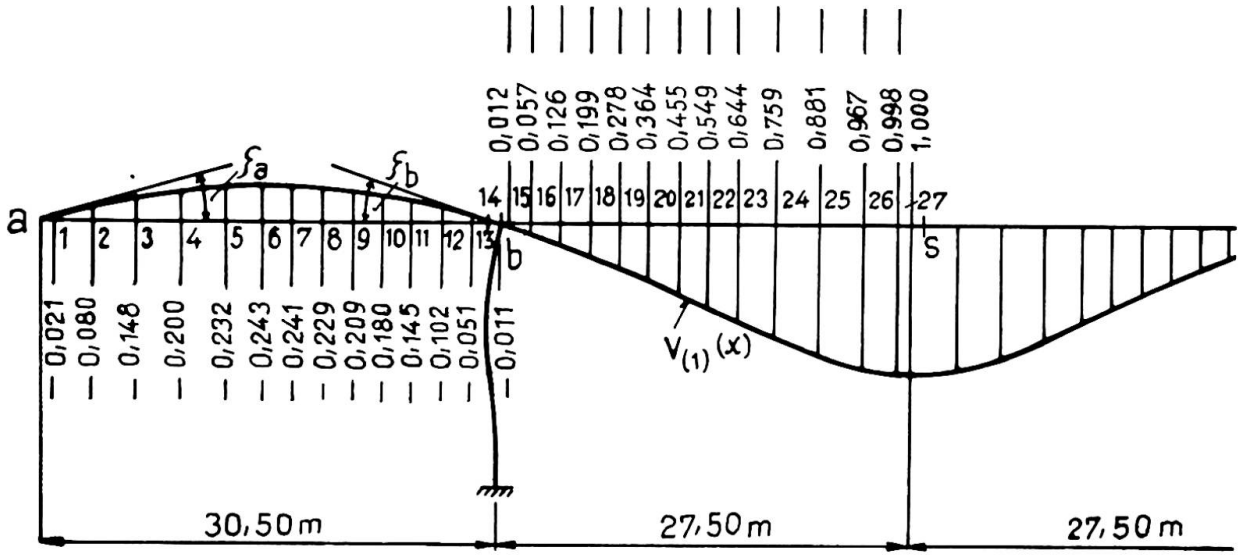

Fig. 8.

Forced vibrations. The forced vibrations of the structure are produced by the movement of vehicles crossing the bridge. The computation was executed for the case of a two cylinder locomotive of the weight G = 97 t moving at a constant speed, the driving wheels of which produce the centrifugal force $P=0{,}3\ N^2$ (in Mp, if N denotes the number of revolutions per second) with angular velocity $\Omega = 2\pi N$. The problem can be solved by expanding the vibrations into a series of natural modes by the same method which was described in detail in previous works of the author [5)6)7)].

6) Koloušek V.: Schwingungen der Brücken aus Stahl und Stahlbeton. Abhandlungen IVBH. B. XVI. Zürich 1956. S. 301-332.

7) Koloušek V.: Vibrations of Bridges with Continuous Main Girders. Publications IABSE. V. XIX. Zürich 1959. P. 111-132.

The critical speed by which N is equal to the first natural frequency is

$$c = \bar{n}_{(1)} \pi D$$

where $\bar{n}_{(1)} = \frac{\bar{\omega}_{(1)}}{2\pi}$ is the first natural frequency of the loaded bridge and D is the diameter of the driving wheels. It will be assumed that the alternating forces of axles act only when moving along the central span. The time variation of the deflection in the middle of the central span produced by the alternating force is given by the formula (45) in the paper [6] p.326

$$v\left(\frac{\ell}{2}, t\right) = \frac{A v_{(1)}(\ell/2) P \sin \bar{\omega}_{(1)} t}{2 \bar{\omega}_{(1)} (\omega^2 + \omega_b^2)} \left[(\cos \omega t - e^{-\omega_b t}) - \omega_b \sin \omega t\right] \quad (9)$$

where $\omega = \frac{\pi c}{\ell}$ and ω_b is a damping coefficient. A is given by

$$A = \frac{B_1}{\Sigma \int_0^\ell \mu(x)\, v^2_{(1)}(x)\, dx} \quad (10)$$

where $v_{(1)}(x)$ denotes the first natural mode and the summation Σ is to be extended over all the spans of the system. B_1 is the coefficient of the first term in the Fourier series

$$v_{(1)}(x) = B_1 \sin \frac{\pi x}{\ell} + B_3 \sin \frac{3\pi x}{\ell} + \ldots$$

The angular frequency $\bar{\omega}_{(1)}$ of the bridge loaded by a locomotive is lower than of an unloaded one. If the centre of gravity of the locomotive is in x = d, it can be calculated according to [7] p.123

$$\bar{\omega}_{(1)} = \omega_{(1)} \sqrt{\frac{\mu}{\bar{\mu}}} \quad (11)$$

where

$$\bar{\mu} = \mu \left(1 + \frac{m_L v^2_{(1)}(d)}{\Sigma \int_0^\ell \mu v^2_{(1)}(x)\, dx}\right) \quad (12)$$

and m_L is the mass of the locomotive. In our case it is (see fig. 8) in the central span

$$v_{(1)}(x) = 0{,}8766 \sin \frac{\pi x}{\ell} - 0{,}0452 \sin \frac{3\pi x}{\ell} \quad (13)$$

so that

$$B_1 = 0{,}8766$$

We obtain further by numerical integration (see fig.8)

$$\Sigma \int_0^\ell \mu v^2_{(1)}(x)\, dx = 42{,}103 \text{ Mp s}^2 \text{ m}^{-1}$$

In accordance with preceding experience, we can assume that $d = \frac{\ell}{3}$. Then $v_{(1)}(d) = 0{,}75$ and

$$\frac{\bar{\mu}}{\mu} = 1 + \frac{97}{9{,}81} \cdot \frac{0{,}75^2}{42{,}103} = 1{,}132$$

Further, it is $\bar{\omega}_{(1)} = \omega_{(1)} \sqrt{\frac{1}{1,132}} = 17,235.0,940 = 16,198\ s^{-1}$

$$\bar{n}_{(1)} = \frac{\bar{\omega}_{(1)}}{2\pi} = 2,578\ Hz$$

$$A = \frac{0,8766}{1,132.42,103} = 0,01873\ Mp^{-1}s^{-2}m$$

$$P = 0,3.2,578^2 = 1,994\ Mp$$

With D = 1,26 m it is

$$c = 2,578.\pi\,.\,1,26 = 10,21\ m/s = 36,75\ km\ p\,.\,h$$

$$\omega = \frac{\pi.10,21}{55} = 0,583\ s^{-1}$$

We can put

$$\omega t = \frac{\pi a}{\ell}$$

where a = ct is the distance of the load of the beginning of the central span. Then we have

$$\bar{\omega}_{(1)}\, t = \frac{\bar{\omega}_{(1)}}{\omega} \frac{\pi a}{\ell} = 27,8\, \frac{\pi a}{\ell}$$

$$\omega_b\, t = \frac{\omega_b}{\omega} \frac{\pi a}{\ell} = 0,025253\ a$$

The logarithmic decrement was appreciated in the value $\delta = 0,1$ so that $\omega_b = \delta \bar{n}_{(1)} = 0,258\ s^{-1}$. Substituting into (10) we obtain

$$v(\ell/2,t) = \frac{0,01873.1,994 \cos \frac{27,8\pi a}{\ell}}{2.16,198(0,583^2 + 0,258^2)} \left[0,583\left(\cos \frac{\pi a}{\ell} - e^{-0,02525a}\right) - 0,258 \sin \frac{\pi a}{\ell}\right] \qquad (14)$$

The curve (14) is shown in fig.9a. According to our supposition that the resonance exists only when the locomotive passes the central span, we can determine the amplitudes A(t) of the curve $v(\ell/2,t)$ in the span b' - a', from the formula

$$A(t) = C\, e^{-\omega_b t}$$

where C denotes the amplitude of vibrations when the locomotive has left the central span. In fig. 9b the curve of fig.9a is superposed above the curve of statical deflection produced by the weight of the locomotive moving along the bridge. This curve represents the theoretical curve of dynamic deflection in the centre of the bridge. The dynamic augmentation of the static deflection is 20 % .

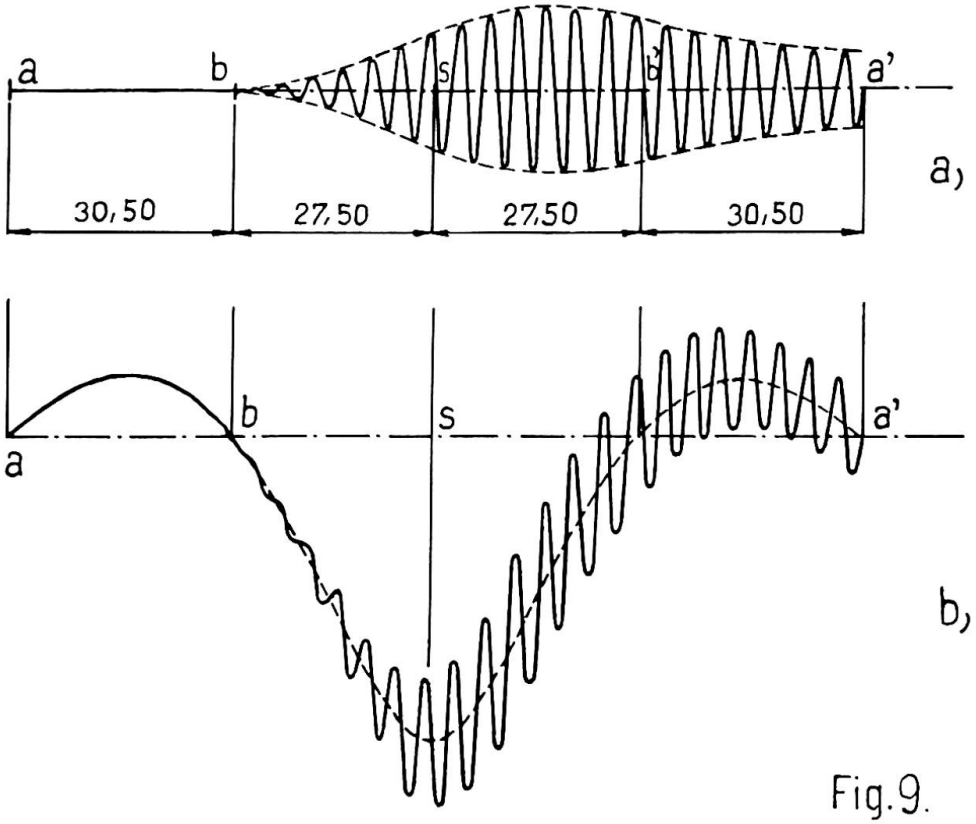

Fig.9.

Results of load-tests.

First of all, the bridge was tested by statical loads. The measured deflections attained only 70 % of theoretical values. The real rigidity was consequenty 1,42 times larger than the assumed one. The attained value E of concrete was larger than was supposed in the analysis and the moment of inertia was elevated by the monolithic execution of sidewalks. The natural frequency increases proportionally to the $\sqrt{EI}$. It can be expected that the actual first natural frequency and the critical speed will be $\sqrt{1,42}=1,19$ multiple of the theoretical value

$$c = 1,19.36,75 \doteq 44 \text{ km p.h}$$

A 97 ton two cylinder locomotive was used for the tests. The deflection in the middle of the central span was measured by means of a Stoppani deflection meter. At the same time the stresses in the lower part of the middle span girder were registered by means of strain-gauges and Brüell-Kjaer registration apparatus. The diagrams recorded at the speed of 44 km p.h. are shown in figs. 10 and 11. The first of them should be compared with the theoretical diagram of fig. 9. It is evident that the measured dynamic effects

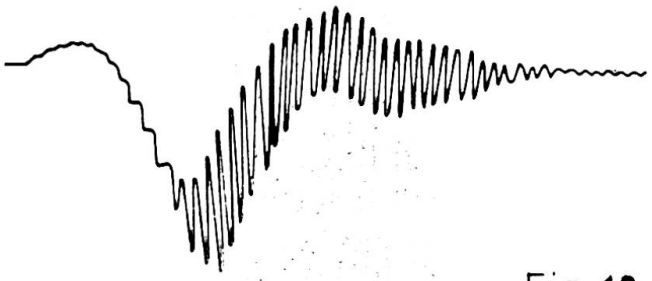

Fig. 10.

are larger than the calculated ones. Themeasured dynamic augmentation attains about 35 % of the statical deflection compared with the 20 % calculated. The difference is mainly the result of the higher rigidity of the actual structure. The centrifugal force P

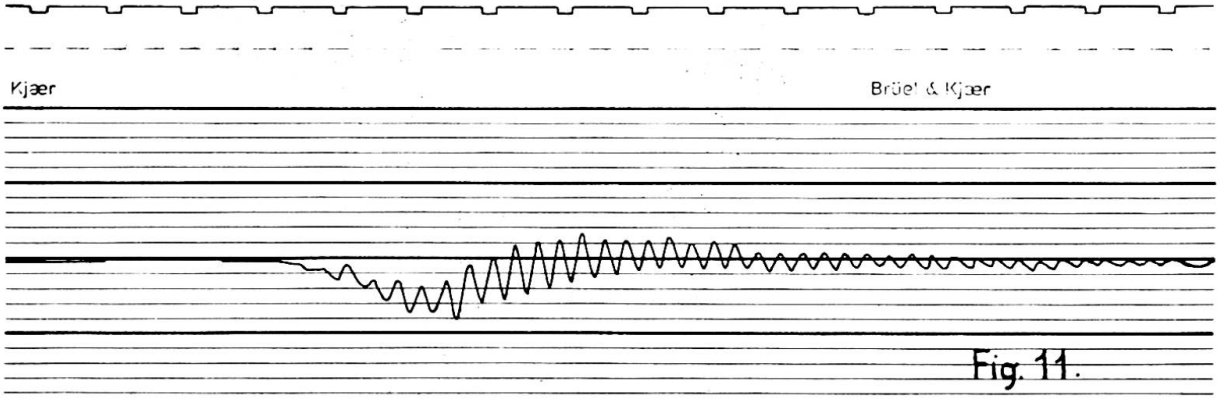

Fig. 11.

increases with the second power of the critical speed so that actually P will be 1,42 times larger than as calculated. In the same proportion, the dynamical augmentation of the deflection will increase and will theoretically attain the value of 28 %. The remaining difference between 28 % and 35 % is to be attributed to the inaccuracy of measurement, of presuppositions e.g. the value of damping and that of unbalanced masses of driving wheels and partly also to the inaccuracy of the theoretical analysis which neglects the movement of the masses along the bridge, etc.

Bibliography .

1) Kirchhoff G.: Vorlesungen über matematische Physik. Mechanik. Leipzig 1876

2) Korenev B.G.: Some problems of the theory of elasticity. Moscow 1960

3) Kolousek V.: Vibrations of Systems with Curved Members. Publications IABSE. V. XXIII. Zurich 1963 . P. 219-232

4) Kolousek V.: Baudynamik der Durchlaufträger und Rahmen. Fachbuchverlag, Leipzig 1953

5) Koloušek V.: Calcul des efforts dynamiques dans les ossatures rigides. Dunod, Paris 1959

6) Koloušek V.: Schwingungen der Brücken aus Stahl und Stahlbeton. Abhandlungen IVBH. B. XVI, Zürich 1956. S 301-332

7) Koloušek V.: Vibrations of Bridges with Continuous Main Girders. Publications IABSE. V. XIX. Zürich 1959. P.111-132

SUMMARY

In the paper the dynamic effects of moving load on a railway bridge of prestressed concrete are discussed. The results of theoretical investigation are compared with the values obtained by the dynamic tests on the actual structure. The results are qualitatively in good accordance but the measured amplitudes of vibrations are somewhat larger than theoretically assumed.

RÉSUMÉ

Les effects dynamiques des charges mobiles sur les ponts rails en béton précontrainte sont analysés dans la contribution. Les valeurs de la solution théorique sont comparées avec les résultas experimentaux obténus sur la construction actuelle. Les amplitudes des vibrations mésurées surpassent un peu ceux de l'analyse théorique.

ZUSAMMENFASSUNG

In der Arbeit sind die dynamischen Einflüsse der beweglichen Belastung auf die Eisenbahnbrücken aus vorgespannten Beton untersucht. Die Ergebnisse der theoretischen Untersuchung sind mit den experimentellen Werten verglichen, die bei dynamischen Messungen auf einer fertigen Brücke erhalten wurden. Beide Ergebnisse stimmen qualitativ gut überein, die gemessenen Amplituden sind jedoch ein wenig höher als die theoretisch gerechneten Werte.

Structural Dynamic Considerations in Horizontally Curved Bridges

Quelques considérations sur le comportement dynamique de ponts en courbe

Dynamische Betrachtungen an waagrechtgekrümmten Brücken

SIDNEY SHORE
Professor of Civil Engineering
University of Pennsylvania
Philadelphia, Pennsylvania, USA

1. INTRODUCTION

As the engineer is turning his attention more and more from aerospace to "geospace" and his environment, a more sophisticated understanding of the response of earthbound structures subjected to natural and other forces assumes greater importance. In particular with the development of high speed transportation systems, for example in the United States, Japan, and France, it is essential to consider the dynamic loads caused by the present and future vehicles, and the dynamic response of bridge or elevated structures.

A number of analytical studies have been reported in the past fifteen years of the dynamic response of bridges on straight alignments subjected to simulated highway or railway loading. However, little or nothing of substance has been reported for horizontally curved bridges, and as is seen from the results presented herein, this increasingly used geometry gives rise to substantially higher dynamic amplification factors for displacements and stress resultants (shear, flexural and torsional moments).

This contribution discusses some analytical results obtained for either a concentrated force or a simulated vehicle traversing a horizontally curved bridge at constant velocity. The significance of this type of study assumes greater importance when it is realized that in the next ten years the world will witness new and more efficient and probably automated transportation systems in which vehicle speeds will approach 500 miles per hour.

2. CURRENT SPECIFICATIONS

In the United States and in many foreign countries the American Railway Engineering Association Specifications [1] are used to determine the dynamic effects of all types of moving trains by a Cooper's E-72 loading. In applying the AREA Specifications to obtain dynamic effects, an impact factor, expressed as a percentage of the static live load, is calculated on the basis of only one independent variable, a characteristic length L in feet, which in general is taken as the loaded length of the member being examined. For example, for the direct vertical impact of moving trains for beam spans, stringers, girders, ...:

$$\text{Impact Percentage} = \begin{cases} 60 - \dfrac{L^2}{500} & L < 100 \text{ ft.} \\ \dfrac{1800}{L+40} + 10 & L \geq 100 \text{ ft.} \end{cases} \qquad (1a)$$

and for truss spans

$$\text{Impact Percentage} = \frac{4000}{L+25} + 15 \qquad (1b)$$

A simple calculation shows that the greatest impact percentage can never exceed 40% of the static live load.

The standard live loading for highway bridges in the United States is the HS 20 - 44 representing a highway truck-trailer of 72,000 pounds, or alternately a uniformly distributed lane loading of 640 pounds per linear foot of lane with either a concentrated force of 18000 pound (for moment) or 26000 pounds (for shear). Again, the dynamic effects are accounted for by utilizing only one independent variable L, which represents the length in feet of the portion of the bridge span that is loaded to produce the maximum stress in the member being investigated. The AASHO formula is:

$$\text{Impact Factor} = \frac{50}{L+25} \leq 0.30 \qquad (2)$$

It must be noted that neigher of these specifications consider other important parameters such as the velocity of the vehicle, the uneveness of the deck of the bridge, the initial conditions of the vehicle upon entering the span (pitching motion for example), or the geometry of the span, that is, a straight alignment, a vertical curve, or a horizontal curve.

3. STRAIGHT BRIDGES

Comprehensive analytical studies of the dynamic behavior of simple and multi-span bridges on a straight alignment have been reported in the literature [e.g. 3,4,5]. Some of the parameters considered in these studies involve: the speed of the vehicle; the ratio of the total weight of the vehicle to the total weight of the bridge; the ratio of the natural frequency of the j^{th} axle to the fundamental frequency of the bridge; rotatory inertia of the vehicle in pitching motion; axle spacing; shape of the roadway profile; initial condition of the vehicle (vertical and angular displacements) upon entering the span; initial condition of the bridge (dynamic deflection and velocity) when the vehicle enters the span. When these parameters are varied through the ranges of values that describe the vehicle-bridge system of todays dynamic increments as high as 1.0 are obtained; however, for the more basic parameters ratios involving vehicle velocity, weights of vehicle and bridge, and natural frequencies of vehicle and span, the maximum dynamic increments are of the order of magnitude of 0.30. The term "dynamic increment" is defined as the difference between the dynamic value of a function (e.g. deflection, shear, moment) at a specified section and the value of the function for the same force or load statically applied at the same specified section, this difference being divided by the absolute maximum static value of the function at the specified section.

Thus, it can be concluded that even though all the parameters upon which the dynamic response of a bridge depend are not included in the AREA and AASHO Specifications, the impact values specified by these organizations appear feasible and reasonable for current design procedures.

4. HORIZONTALLY CURVED BRIDGES

As horizontally curved bridges (many times approximated by a series of short straight segments) were being utilized more frequently in highway design, the University of Pennsylvania initiated, a few years ago, a study to determine the dynamic response characteristics of such structures. The major objective of this study was to ascertain the dynamic increments for realistic bridge-vehicle systems and thus determine whether the specifications in current use were adequate.

A simply supported, single span, horizontally curved bridge was chosen (see Figure 1) and two types of input were used: (1) A single force traversing the bridge along its centerline at constant velocity, and (2) A rigid mass (sprung mass) connected by a linear spring and a viscous damper to a rigid mass (unsprung mass) which was always in contact with the bridge deck, traversing the bridge along its centerline at constant velocity. See Figure 2. The parameters considered and their corresponding ranges were:

1. Central Angle, θ_1
   $0.125 \text{ radian} \leq \theta_1 \leq 1.0 \text{ radian}$
2. Radius of Horizontal Curvature, r
   $200 \text{ ft.} \leq r \leq 800 \text{ ft.}$
3. Rigidity Ratio of the Bridge Cross-section, A

$$A = \frac{\text{torsional rigidity + warping rigidity function}}{\text{Flexural rigidity}}$$

$$0.05 \leq A \leq 1.00$$

4. Speed Parameter, α_v

$$\alpha_x = \frac{\text{(velocity of vehicle) (fundamental period of equivalent straight bridge*)}}{2\text{(length of equivalent traight bridge*)}}$$

$$0.06 \leq \alpha_v \leq 0.18 \quad (20 \text{ mph} \leq v \leq 60 \text{mph})$$

5. Weight Ratio, R_v

$$R_v = \frac{\text{total weight of vehicle}}{\text{weight of bridge}}$$

$$0.08 \leq R_v \leq 1.00$$

6. Frequency Ratio, ϕ_v

$$\phi_v = \frac{\text{natural frequency of vehicle}}{\text{natural frequency of equivalent straight bridge*}}$$

*The equivalent straight bridge is defined as having the same length as the curved bridge.

The displacement equations of motion representing this system were coupled, non homogeneous partial differential equations which were solved by techniques described previously in detail by Tan and Shore [6,7] . The major conclusions drawn from this study of horizontally curved bridges were: (1) The dynamic increments (as defined in Section 3) for deflections and stress resultants for the moving constant force were generally higher by at least 10% than for an equivalent straight beam; (2) The dynamic increments for the moving vehicle for deflections and stress resultants were significantly higher than for an equivalent straight beam; (3) When the frequency ratio and the weight ratio are 0.30 or less the response of the bridge due to the constant force can be used; (4) For a rigidity ratio greater than 0.5 and a central angle less than 0.50 radians, the curved bridge response can be predicted by an equivalent straight bridge; (5) Preliminary results indicate that the dynamic increments for vertical deflection, w, rotation, β , and stress resultants are essentially the same for a given set of parameters. Two typical response curves for curved bridges are shown in Figures 3 and 4. In these Figures the following notation is used:

DIWSB = dynamic increment for vertical deflection of an equivalent straight bridge of length L_c ; DIWCB = dynamic increment for vertical deflection of the horizontally curved bridge.

On the basis of the results obtained in this study of the response of horizontally curved bridge the following recommendations appear in order:

(1) An appraisal of the current specified impact and dynamic factors to determine whether other variables should be incorporated in addition to only a characteristic length.

(2) Since for curved bridges the dynamic increment is extremely sensitive to the rigidity ratio parameter, attention should be given to methods for accurately calculating the torsional, warping, and flexural rigidities of complex bridge structures. It appears necessary and feasible that work on analytical methods by finite element techniques verified by model tests should be initiated for predicting these rigidity ratios.

(3) Dynamic response tests on laboratory models of curved beams appears advisable. These models should simulate as closely as possible the mathematical model used in References 6 and 7, to verify the analytical results.

(4) Field tests of actual curved bridge structures subjected to dynamic loads should be initiated to correlate both the analytical results and model tests.

(5) Further analytical work should be initiated for curved bridges to include other effects such as superelevation which introduces an initial twist in the bridge, vehicle speeds up to possibly 500 mph, longitudinal forces due to braking, accelerations, and

(5) Continued:

decelerations at these high speeds, as well as the other parameters listed in Section 3 which were reported for straight bridges, but which were not included in the study reported in References 6 and 7.

REFERENCES

1. AREA - Specifications for Steel Railway Bridges, Chicago, 1965.
2. AASHO - Standard Specifications for Highway Bridges, Washington, D. C., 1965.
3. Hillerborg, A., "Dynamic Influences of Smoothly Running Loads on Simply Supported Girders". Institute of Structural Engineering and Bridge Building of the Royal Institute of Technology, Stockholm, 1951.
4. Biggs, J. M., Suer, H. S., and Louw, J. M., "Vibration of Simple-Span Highway Bridges", Transactions ASCE 124: 291 (1959).
5. Huang, T. and Veletsos, A. S., "Dynamic Response of Three-Span Continuous Highway Bridges", Civil Engineering Studies, Structural Research Series No 190, University of Illinois, 1960.
6. Tan, C. P. and Shore, S., "Dynamic Response of a Horizontally Curved Bridge", Journal of the Structural Division, Proceedings of the ASCE, March, 1968, pp 761 - 781.
7. Tan, C. P. and Shore, S., "Response of a Horizontally Curved Bridge to a Moving Load", Journal of the Structural Division, Proceedings of the ASCE. Publication pending.

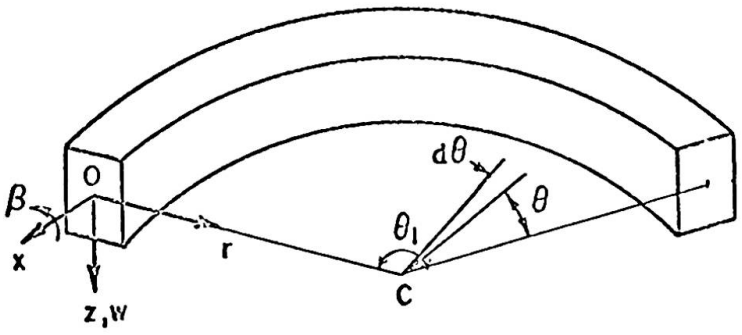

FIG. 1. CURVED BEAM GEOMETRY

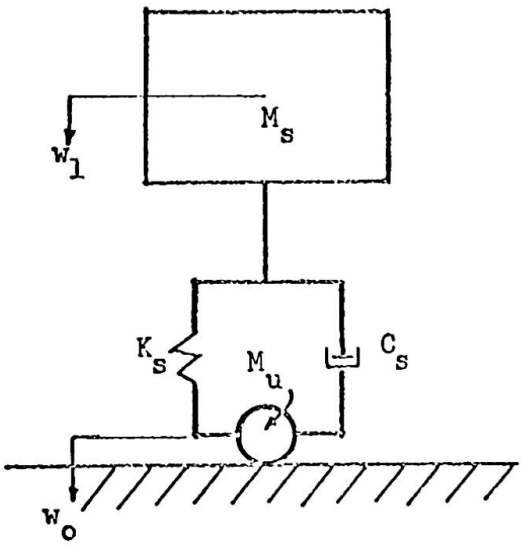

FIG. 2. IDEALIZED VEHICLE

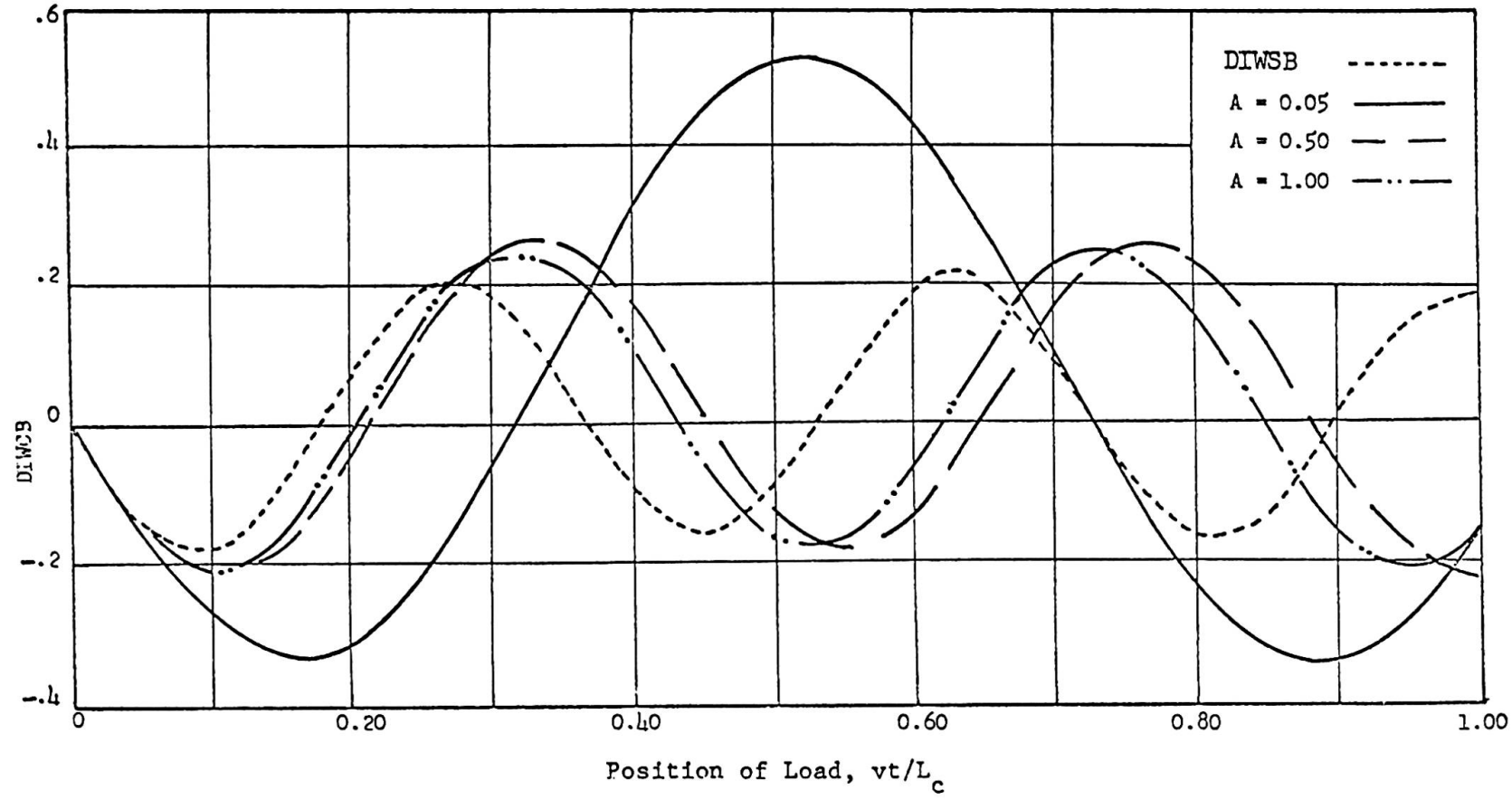

FIG. 3. EFFECT OF RIGIDITY RATIO ON DYNAMIC INCREMENT FOR DEFLECTION AT MIDSPAN CONSTANT MOVING FORCE, $L_c = r = 200'$, $\alpha_v = 0.18$

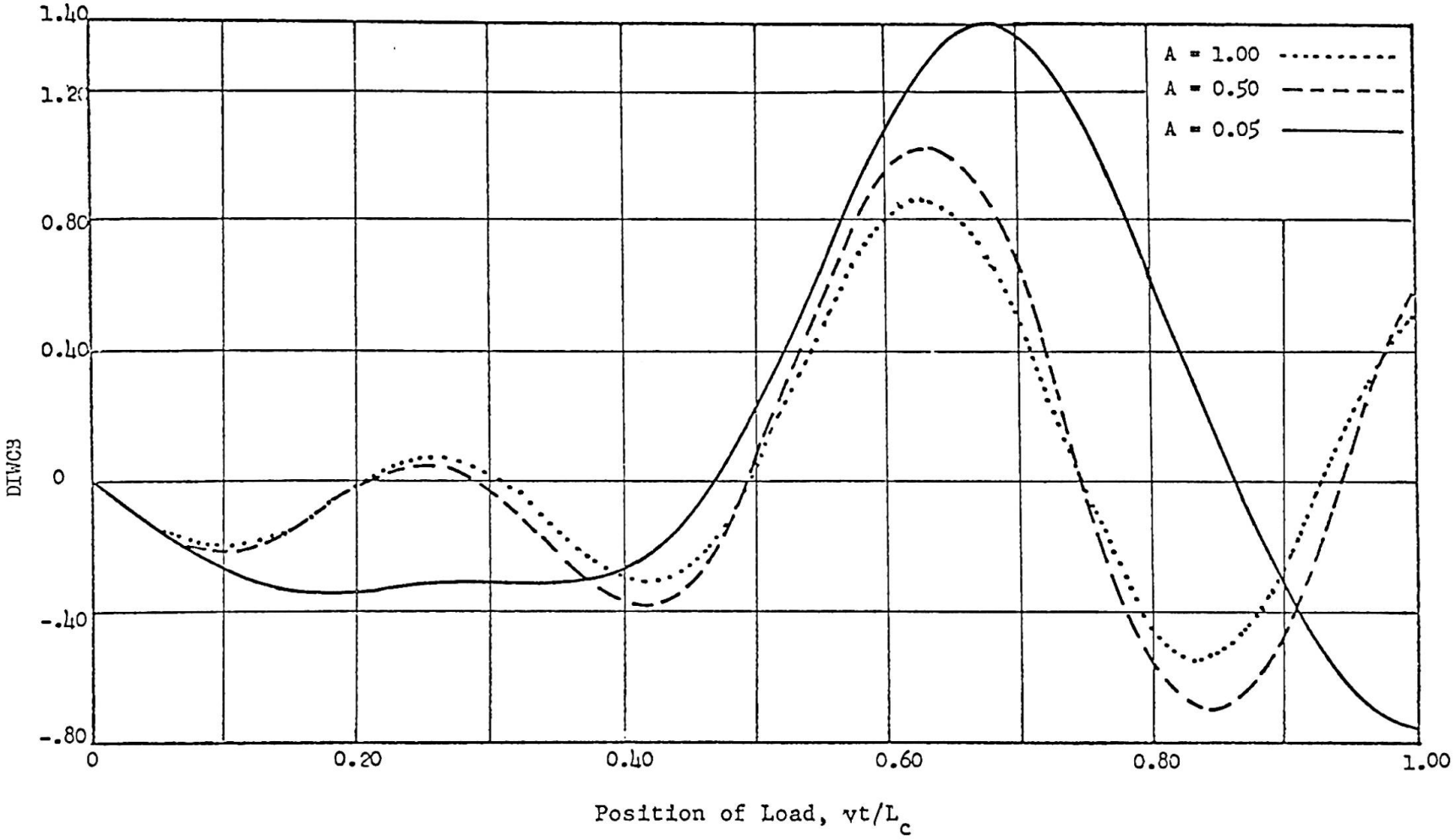

FIG. 4. EFFECT OF RIGIDITY RATIO ON DYNAMIC INCREMENT FOR DEFLECTION AT MIDSPAN SMOOTHLY MOVING VEHICLE, $L_c = r = 200'$, $\alpha_v = 0.18$, $R_v = 0.50$, $\varphi_v = 0.50$

SUMMARY

Many studies have been reported in the past fifteen years concerning the dynamic response of bridges on straight alignments subjected to simulated highway loading. However, little has been reported for horizontally curved bridges and this rather common alignment on highway and railway systems gives rise to substantially higher dynamic amplification factors for displacements and stress resultants. Such a study has been made for a simulated highway vehicle traversing a curved bridge considering such parameters as radius of curvature, flexural to torsional rigidity ratio, velocity of the vehicle, and vehicle mass to bridge mass ratio. Some overall results will be reported and recommendations made in light of current specifications.

RÉSUMÉ

De nombreuses études ont été faites ces dernières 15 années sur le comportement dynamique de ponts droits soumis à une charge d'autoroute simulée. Cependant, on a presque totalement négligé les ponts en courbe, beaucoup employés pour routes et chemins de fers. Pourtant, on a ici des facteurs d'amplification dynamique considérablement plus grands pour les déplacements et pour des tensions résultantes. Une telle étude a été faite pour un véhicule de route simulé traversant un pont courbe, considérant des paramètres tels rayon de courbure, rapport des rigidités à la flexion et à la torsion, vitesse du véhicule, et rapport des masses du véhicule et du pont. Quelques résultats universels et des recommandations concernant les exécutions courantes seront publiés.

ZUSAMMENFASSUNG

Viele Untersuchungen sind in den letzten fünfzehn Jahren betreffend das dynamische Verhalten von geradlinigen Brücken unter Verkehrslast angestellt worden. Wie auch immer, wenig ist über waagrechtgekrümmte Brücken gesagt worden; diese weniger gebräuchliche Ausführung der Strassen- und Eisenbahnbrücken zeitigt erheblich höhere Schwingungsamplituden für die Verschiebungen und Spannungen. Eine solche Untersuchung wurde für ein simuliertes Fahrzeug bei folgenden Parametern angestellt: Halbmesser, Drillsteifigkeit, Geschwindigkeit des Fahrzeugs sowie Ausmass desselben im Verhältnis zu dem der Brücke. Einige Gesamtspannungen und Empfehlungen aus gebräuchlichen Ausführungen sind aufgeführt.

VI

Non-Stationary Vibrations of Bridges Under Random Moving Load

Vibrations non-stationnaires de ponts sous une charge en mouvement arbitraire

Nichtstationäre Brückenschwingungen unter zufälliger, beweglicher Last

LADISLAV FRÝBA
Doc. Ing.Dr.Sc.
Head Research Scientist
Research Institute of Transport
Prague, Czechoslovakia

1. Introduction

It has been assumed up to this time that the traffic loading of bridges, i.e. the static and dynamic component of the service load, is a well known function of the space and time coordinate (a deterministic process), see [1], [2]. This paper deals with the essentially opposite case supposing that the traffic loading of bridges is a random process. This new conception is in better accordance with observations because the true traffic loading is influenced by the random composition of the traffic flow, by the random initial conditions when the vehicles enter the bridge, by the irregularities of unevenness of the road surface etc.

In general the static and dynamic deflection of bridges is described by the linear differential equation

$$L[v(x,t)] = p(x,t) \tag{1}$$

where $v(x,t)$ denotes the deflection and $p(x,t)$ the load. The random variation of $p(x,t)$ is assumed not only with respect to the time coordinate t but also to the position coordinate x and in addition the load $p(x,t)$ is regarded as a nonstationary Gaussian random process of non-Markov type.

L represents a linear differential operator of the type

$$L = L_o + \mu \frac{\partial^2}{\partial t^2} + 2\mu\omega_b \frac{\partial}{\partial t} \tag{2}$$

where L_o is a self-adjoint linear operator in the space coordinate x, μ - mass per unit length and ω_b - circular frequency of viscous damping.

2. Probability Analysis

2.1. Normal - Mode Analysis. Elastic systems described by Eqs. (1) and (2) are with advantage solved by means of the normal-mode analysis

$$v(x,t) = \sum_{j=1}^{\infty} v_{(j)}(x)\, q_{(j)}(t) \tag{3}$$

$$p(x,t) = \sum_{j=1}^{\infty} \mu\, v_{(j)}(x)\, Q_{(j)}(t) \tag{4}$$

where $v_{(j)}(x)$ are the normal modes of vibration that are obtained with regard to the boundary conditions from the equation

$$L_o\left[v_{(j)}(x)\right] = \mu\, \omega^2_{(j)} v_{(j)}(x) \quad , \tag{5}$$

$\omega_{(j)}$ is the natural circular frequency of the system,

$$Q_{(j)}(t) = \frac{1}{V_{(j)}} \int_o^{\ell} p(x,t)\, v_{(j)}(x)\, dx \tag{6}$$

is the generalized force,

$$V_{(j)} = \int_o^{\ell} \mu\, v^2_{(j)}(x)\, dx \quad , \quad \int_o^{\ell} \mu\, v_{(j)}(x) v_{(k)}(x)\, dx = 0 \text{ for } j \neq k \tag{7}$$

and $q_{(j)}(t)$ is the generalized deflection that is obtained with regard to the initial conditions from the equation

$$\ddot{q}_{(j)}(t) + 2\,\omega_b\, \dot{q}_{(j)}(t) + \omega^2_{(j)}\, q_{(j)}(t) = Q_{(j)}(t) \tag{8}$$

The solution of Eq.(8) with zero initial conditions is

$$q_{(j)}(t) = \int_o^t h_{(j)}(t-\tau) Q_{(j)}(\tau)\, d\tau = \int_{-\infty}^{\infty} h_{(j)}(\tau) Q_{(j)}(t-\tau)\, d\tau \tag{9}$$

where $h_{(j)}(t)$ denotes the impulsive function

$$h_{(j)}(t) = \begin{cases} \dfrac{1}{\omega'_{(j)}}\, e^{-\omega_b t} \sin \omega'_{(j)} t & \text{for } t \geq 0 \\ 0 & \text{for } t < 0 \end{cases} \tag{10}$$

and $\omega'^2_{(j)} = \omega^2_{(j)} - \omega^2_b$. The limits of integration in (9) may be extended to ∞ and $-\infty$, respectively, because $Q_{(j)}(t-\tau) = 0$ for $\tau > t$ and $h_{(j)}(\tau) = 0$ for $\tau < 0$, respectively.

The functions $h_{(j)}(t)$ and $v_{(j)}(x)$ are deterministic while

$q_{(j)}(t)$, $Q_{(j)}(t)$, $v(x,t)$ and $p(x,t)$ are random ones.

2.2. Correlation Analysis. The probability analysis recquires to know the statistic characterisitcs of the input

$$p(x,t) = E\left[p(x,t)\right] + \overset{\circ}{p}(x,t) \tag{11}$$

$$K_{pp}(x_1,x_2,t_1,t_2) = E\left[\overset{\circ}{p}(x_1,t_1)\,\overset{\circ}{p}(x_2,t_2)\right] \tag{12}$$

where E represents the mean value linear operator, $\overset{\circ}{p}(x,t)$ - the centred value of the load and $K_{pp}(x_1,x_2,t_1,t_2)$ - the covariance of the nonstationary function $p(x,t)$.

As follows from the definition of the covariance (12) the covariance of the generalized deflection may be evaluated from (9)

$$K_{q_{(j)}q_{(k)}}(t_1,t_2) = \int_{-\infty}^{\infty}\int_{-\infty}^{\infty} h_{(j)}(\tau_1)h_{(k)}(\tau_2)K_{Q_{(j)}Q_{(k)}}(t_1-\tau_1,t_2-\tau_2)\,.$$
$$\cdot\, d\tau_1\, d\tau_2\,, \tag{13}$$

the covariance of the deflection from (3)

$$K_{vv}(x_1,x_2,t_1,t_2) = \sum_{j=1}^{\infty}\sum_{k=1}^{\infty} v_{(j)}(x_1)v_{(k)}(x_2)K_{q_{(j)}q_{(k)}}(t_1,t_2) \tag{14}$$

and the covariance of the load from (4)

$$K_{pp}(x_1,x_2,t_1,t_2) = \sum_{j=1}^{\infty}\sum_{k=1}^{\infty} \mu^2 v_{(j)}(x_1)v_{(k)}(x_2)K_{Q_{(j)}Q_{(k)}}(t_1,t_2) \tag{15}$$

In Eqs. (13) and (15) the covariance of the generalized force is calculated from (6)

$$K_{Q_{(j)}Q_{(k)}}(t_1,t_2) = \frac{1}{V_{(j)}V_{(k)}}\int_{0}^{\ell}\int_{0}^{\ell} v_{(j)}(x_1)v_{(k)}(x_2)K_{pp}(x_1,x_2,t_1,t_2)\,.$$
$$\cdot\, dx_1\, dx_2 \tag{16}$$

2.3. Spectral Density Analysis. The spectral density of a nonstationary function is defined in [3] and for the generalized deflection the Wiener-Khinchine relations between the spectral density and the covariance are as follows

$$S_{q_{(j)}\,q_{(k)}}(\omega_1,\omega_2) = \frac{1}{4\pi^2}\int_{-\infty}^{\infty}\int_{-\infty}^{\infty} K_{q_{(j)}\,q_{(k)}}(t_1,t_2)e^{-i(\omega_2 t_2-\omega_1 t_1)}\,dt_1 dt_2 \tag{17}$$

$$K_{q_{(j)}q_{(k)}}(t_1,t_2) = \int_{-\infty}^{\infty}\int_{-\infty}^{\infty} S_{q_{(j)}q_{(k)}}(\omega_1,\omega_2)e^{i(\omega_2 t_2-\omega_1 t_1)}\,d\omega_1\, d\omega_2 \tag{18}$$

For the spectral density analysis it is also convenient to introduce the transfer function

$$H_{(j)}(\omega) = \int_{-\infty}^{\infty} h_{(j)}(t)\, e^{-i\omega t}\, dt = \frac{1}{\omega_{(j)}^2 - \omega^2 + 2i\omega_b\omega} \tag{19}$$

as a Fourier integral transformation of $h_{(j)}(t)$ given by (10).

Then the spectral density of the generalized deflection may be evaluated as a function of the spectral density of the generalized force, see [4]:

$$S_{q_{(j)}q_{(k)}}(\omega_1,\omega_2) = \bar{H}_{(j)}(\omega_1)\, H_{(k)}(\omega_2)\, S_{Q_{(j)}Q_{(k)}}(\omega_1,\omega_2) \tag{20}$$

where $\bar{H}_{(j)}(\omega)$ is a complex conjugate function of $H_{(j)}(\omega)$.

Here we used the spectral density $S_{Q_{(j)}Q_{(k)}}(\omega_1,\omega_2)$ of the generalized force defined similarly as in (17); this can be adapted with regard to the Eq. (16)

$$S_{Q_{(j)}Q_{(k)}}(\omega_1,\omega_2) = \frac{1}{4\pi^2}\int_{-\infty}^{\infty}\int_{-\infty}^{\infty} K_{Q_{(j)}Q_{(k)}}(t_1,t_2)\, e^{-i(\omega_2 t_2 - \omega_1 t_1)}\, dt_1 dt_2 =$$

$$= \frac{1}{V_{(j)}V_{(k)}}\int_0^{\ell}\int_0^{\ell} v_{(j)}(x_1)\, v_{(k)}(x_2)\, S_{pp}(x_1,x_2,\omega_1,\omega_2)\, dx_1 dx_2 \tag{21}$$

$$K_{Q_{(j)}Q_{(k)}}(t_1,t_2) = \int_{-\infty}^{\infty}\int_{-\infty}^{\infty} S_{Q_{(j)}Q_{(k)}}(\omega_1,\omega_2)\, e^{i(\omega_2 t_2 - \omega_1 t_1)}\, d\omega_1 d\omega_2 \tag{22}$$

The spectral density of the deflection is then with respect to (14)

$$S_{vv}(x_1,x_2,\omega_1,\omega_2) = \sum_{j=1}^{\infty}\sum_{k=1}^{\infty} v_{(j)}(x_1)\, v_{(k)}(x_2)\, S_{q_{(j)}q_{(k)}}(\omega_1,\omega_2) \tag{23}$$

from which the covariance of the deflection can be calculated similarly as in (18) and (14).

3. Random Moving Load

3.1. Random Moving Force. As an example we shall solve a simple beam of span ℓ loaded ba a massless force $P(t) = P + \mathring{P}(t)$ with constant mean value $E\left[P(t)\right] = P$ which is moving with constant velocity c along the beam. The analogous deterministic case was solved in

[2] and [4] and it represents the mean value of the present solution $E[v(x,t)]$, so that we will now investigate the stochastic case only.

The load per unit length and its mean and centred values are in our case

$$p(x,t) = \delta(x-ct)P(t) \,, \quad E[p(x,t)] = \delta(x-ct)P \,, \quad \overset{o}{p}(x,t) = \delta(x-ct)\overset{o}{P}(t) \tag{24}$$

where $\delta(x)$ represents the Dirac-delta function. The covariance of the load can be calculated from (12)

$$K_{pp}(x_1,x_2,t_1,t_2) = \delta(x_1-ct_1)\,\delta(x_2-ct_2)\,K_{PP}(t_1,t_2) \tag{25}$$

where $K_{PP}(t_1,t_2)$ is the known covariance of the load $P(t)$. We substitute (25) into (16) and then, with regard to the well known properties of the Dirac function, we obtain the covariance of the generalized force

$$K_{Q_{(j)}Q_{(k)}}(t_1,t_2) = \frac{1}{V_{(j)}V_{(k)}}\, v_{(j)}(ct_1)v_{(k)}(ct_2)K_{PP}(t_1,t_2) \tag{26}$$

Using (26) the covariances of the deflection can be calculated from (13) and (14).

As an example let us assume the covariance of the force $P(t)$ in the form

$$K_{PP}(t_1,t_2) = K_{PP}(t_2-t_1) = 2\pi S_P\,\delta(t_2-t_1) \tag{27}$$

where S_P is the constant spectral density (white noise). Then we obtain from the Eq. (13)

$$K_{q_{(j)}q_{(k)}}(t_1,t_2) = \frac{1}{V_{(j)}V_{(k)}} \int_{-\infty}^{\infty}\int_{-\infty}^{\infty} h_{(j)}(\tau_1)h_{(k)}(\tau_2)v_{(j)}[c(t_1-\tau_1)] \cdot v_{(k)}[c(t_2-\tau_2)]\,K_{PP}(t_1-\tau_1,t_2-\tau_2)\,d\tau_1\,d\tau_2 =$$

$$= \frac{2\pi S_P}{V_{(j)}V_{(k)}} \int_{-\infty}^{\infty} h_{(j)}(\tau_1)h_{(k)}(\tau_1+t_2-t_1)v_{(j)}[c(t_1-\tau_1)] \cdot v_{(k)}[c(t_1-\tau_1)]\,d\tau_1 \tag{28}$$

If for simplification we neglect the cross-correlation of the generalized deflection, i.e. $K_{q_{(j)}q_{(k)}}(t_1,t_2) = 0$ for $j \neq k$, the variance of the deflection can be received from (14) :

$$\sigma_v^2(x,t) = K_{vv}(x,x,t,t) = \sum_{j=1}^{\infty} v_{(j)}^2(x) K_{q_{(j)}q_{(j)}}(t,t) =$$

$$= \sum_{j=1}^{\infty} \frac{2\pi S_P}{V_{(j)}^2} v_{(j)}^2(x) \int_{-\infty}^{\infty} h_{(j)}^2(\tau_1)\, v_{(j)}^2[c(t-\tau_1)]\, d\tau_1 \qquad (29)$$

The following expressions hold true for a simple beam of span ℓ and of bending stiffness EJ, see [4]

$$v_{(j)}(x) = \sin\frac{j\pi x}{\ell}, \quad V_{(j)} = \frac{\mu\ell}{2}, \quad \omega_{(j)}^2 = \frac{j^4\pi^4}{\ell^4}\frac{EJ}{\mu} \qquad (30)$$

Substituting (30) and (10) into (29) we obtain (note that the limits of integration may be changed as $h_{(j)}(\tau_1) = 0$ for $\tau_1 < 0$ and $v_{(j)}[c(t-\tau_1)] = 0$ for $\tau_1 > t$) :

$$\sigma_v^2(x,t) = \sum_{j=1}^{\infty} \frac{8\pi S_P}{\mu^2\ell^2\omega_{(j)}'^2} \sin^2\frac{j\pi x}{\ell} \int_0^t \left[e^{-\omega_b\tau_1} \sin\omega_{(j)}'\tau_1 \sin\frac{j\pi c}{\ell}(t-\tau_1)\right]^2 d\tau_1 =$$

$$= \sum_{j=1}^{\infty} \frac{8\pi S_P}{\mu\ell\omega_{(j)}'^2} \sin^2\frac{j\pi x}{\ell} \frac{1}{16}\left\{ \frac{\omega_{(j)}'+j\pi c/\ell}{(\omega_{(j)}'+j\pi c/\ell)^2+\omega_b^2}\left[\sin 2j\pi ct/\ell + e^{-2\omega_b t}\cdot\right.\right.$$

$$\left. \cdot \sin 2\omega_{(j)}' t + \frac{\omega_b}{\omega_{(j)}'+j\pi c/\ell}(\cos 2j\pi ct/\ell - e^{-2\omega_b t}\cos 2\omega_{(j)}' t)\right] +$$

$$+ \frac{\omega_{(j)}'-j\pi c/\ell}{(\omega_{(j)}'-j\pi c/\ell)^2+\omega_b^2}\left[-\sin 2j\pi ct/\ell + e^{-2\omega_b t}\sin 2\omega_{(j)}' t + \frac{\omega_b}{\omega_{(j)}'-j\pi c/\ell}\cdot\right.$$

$$\left.\cdot(\cos 2j\pi ct/\ell - e^{-2\omega_b t}\cos 2\omega_{(j)}' t)\right] - \frac{2\omega_b}{j^2\pi^2c^2/\ell^2+\omega_b^2}\left(\frac{j\pi c/\ell}{\omega_b}\sin 2j\pi ct/\ell + \right.$$

$$\left. + \cos 2j\pi ct/\ell - e^{-2\omega_b t}\right) - \frac{2\omega_b}{\omega_{(j)}^2}\left[1 - e^{-2\omega_b t}(\cos 2\omega_{(j)}' t - \frac{\omega_{(j)}'}{\omega_b}\cdot\right.$$

$$\left.\left.\cdot\sin 2\omega_{(j)}' t)\right] + \frac{2}{\omega_b}(1 - e^{-2\omega_b t})\right\} \qquad (31)$$

As the variance of the deflection is a function of the time the resulting vibration of the beam appears as a nonstationary process although we have taken into account the movement of a stationary random force.

For subcritical velocities ($c < c_{cr}$) the greatest static and

dynamic effects of a moving force appear approximately in the moment when the force crosses the beam centre. Therefore the coefficient of variance, defined as $C_v(x,t) = \sigma_v(x,t)/E[v(x,t)]$, is to be calculated for $x = \ell/2$ and $t = T/2 = \ell/(2c)$. It represents then the relative dynamic increment of the deflection effected by the random moving force and it takes the following form (from (31) for j=1 approximately, see [4]) :

$$C_v(\ell/2, T/2) = C_p \cdot C_{vP} \tag{32}$$

Here C_p is an analogous coefficient of variance of the force P(t) and C_{vP} is represented graphically in Fig. 1 as a function of the parameters α and β where α is a velocity parameter and β a damping parameter, respectively :

$$\alpha = c/c_{cr} \quad ; \quad c_{cr} = (\pi/\ell)(EJ/\mu)^{1/2} \tag{33}$$

$$\beta = \omega_b / \omega_{(1)} \tag{34}$$

The same results can be obtained using the spectral density analysis from the section 2.3. In this case the load (24) must be taken for a function of the time only, see [4].

3.2. Random Moving Distributed Load. As a next example we shall solve a simple beam loaded by an infinitely long random strip which is moving with constant velocity c along the beam. The analogous deterministic case was solved in [4] where not only the movement of the continous load p (measured per unit length) but also the effects of its inertia mass $\mu_p = p/g$ were taken into account.

The load is assumed to have the following form

$$p(x,t) = p(x-ct)\, r(t) \tag{35}$$

The first of the components p(x-ct) is a random variable in the moving coordinate system $\xi = x-ct$ while the second r(t) is a random function of time. The mean values of these two functions are assumed to be constant

$$E[p(\xi)] = p \quad , \quad E[r(t)] = 1$$

so that the load (35) may be written as

$$p(x,t) = p + \overset{o}{p}(x,t) = [p + \overset{o}{p}(\xi)] \cdot [1 + \overset{o}{r}(t)] \tag{36}$$

where $\overset{o}{p}(x,t) = \overset{o}{p}(\xi) + p\overset{o}{r}(t) + \overset{o}{p}(\xi)\overset{o}{r}(t)$. Then with respect to (12) the covariance of the load is

$$K_{pp}(x_1,x_2,t_1,t_2) = K_{pp}(\xi_1,\xi_2) + p\, K_{pr}(\xi_2,t_1) + K_{ppr}(\xi_1,\xi_2,t_1) +$$

$$+ pK_{pr}(\xi_1,t_2) + p^2K_{rr}(t_1,t_2) + p\,K_{prr}(\xi_1,t_1,t_2) + K_{ppr}(\xi_1,\xi_2,t_2) +$$

$$+ p\,K_{prr}(\xi_2,t_1,t_2) + K_{pprr}(\xi_1,\xi_2,t_1,t_2) \tag{37}$$

where $\xi_i = x_i - ct_i$, $i = 1, 2$. Let us assume approximately that the functions $p(\xi)$ and $r(t)$ have no cross-correlation of the second up to the fourth order; then (37) reduces to

$$K_{pp}(x_1,x_2,t_1,t_2) = K_{pp}(\xi_1,\xi_2) + p^2\,K_{rr}(t_1,t_2) \tag{38}$$

where $K_{pp}(\xi_1,\xi_2)$ is the covariance of the load function in the moving coordinate system ξ and $K_{rr}(t_1,t_2)$ is the covariance in the time coordinate.

As an example let us assume the covariances of these functions in the following form

$$K_{pp}(\xi_1,\xi_2) = 2\pi S_p\,\delta(\xi_2-\xi_1)\,, \quad K_{rr}(t_1,t_2) = 2\pi S_r\,\delta(t_2-t_1) \tag{39}$$

where S_p and S_r are the constant spectral densities (wide-band spectra). Putting (38) and (39) into (13) the covariance of the generalized deflection may be evaluated; hence

$$K_{q_{(j)}\,q_{(k)}}(t_1,t_2) = \frac{1}{V_{(j)}V_{(k)}} \int_{-\infty}^{\infty}\int_{-\infty}^{\infty}\int_{0}^{\ell}\int_{0}^{\ell} h_{(j)}(\tau_1)h_{(k)}(\tau_2)v_{(j)}(x_1)v_{(k)}(x_2)\,\cdot \tag{40}$$

$$\cdot\left\{2\pi S_p\,\delta[x_2-x_1-c(t_2-\tau_2-t_1+\tau_1)] + 2\pi S_r p^2\,\delta(t_2-t_1-\tau_2+\tau_1)\right\} dx_1\,dx_2\,d\tau_1\,d\tau_2$$

The limits of integration with respect to time τ are considered from 0 to ∞ in accordance with (10) and because the movement of the load has an infinitely long duration.

Neglecting the cross-correlation $K_{q_{(j)}q_{(k)}}(t_1,t_2) = 0$ for $j \neq k$ the variance may be calculated from (40) and (14) :

$$\sigma_v^2(x,t) = K_{vv}(x,x,t,t) = \sum_{j=1}^{\infty} v_{(j)}^2(x)\,K_{q_{(j)}q_{(j)}}(t,t) =$$

$$= \sum_{j=1}^{\infty} \frac{4\pi S_p c}{\mu^2\,\ell^2(1+\varkappa)^2\,\bar\omega_{(j)}^2\bar\omega'_{(j)}\bar\omega_b D} \sin^2\frac{j\pi x}{\ell}\left\{\frac{\bar\omega_{(j)}^2\bar\omega'_{(j)}\bar\omega_b\ell}{c} + \frac{j^2\pi^2c^2/\ell^2}{D}\left\{\bar\omega'_{(j)}\left[D + \right.\right.\right.$$

$$\left.\left.\left. + 4\,\bar\omega_b^2(\bar\omega_b^2 - 3\,\bar\omega_{(j)}^2 + j^2\pi^2c^2/\ell^2)\right](1 - e^{-\bar\omega_b\ell/c}\cos\bar\omega'_{(j)}\ell/c.\cos j\pi) -\right.\right.$$

$$- \bar{\omega}_b\left[D + 4\bar{\omega}'^2_{(j)}(\bar{\omega}'^2_{(j)} - 3\bar{\omega}_b^2 - j^2\pi^2c^2/\ell^2)\right] e^{-\bar{\omega}_b \ell/c} \sin \bar{\omega}'_{(j)}\ell/c.\cos j\pi\Big\}+$$

$$+ \sum_{j=1}^{\infty} \frac{4S_r p^2(1 - \cos j\pi)}{\mu^2 j^2\pi \bar{\omega}^2_{(j)} \bar{\omega}_b^{(1+\varkappa)^2}} \sin^2 \frac{j\pi x}{\ell} \qquad (41)$$

where $\bar{\omega}^2_{(j)} = \omega^2_{(j)}(1 - \alpha^2\varkappa/j^2)/(1 + \varkappa)$, $\bar{\omega}'^2_{(j)} = \bar{\omega}^2_{(j)} - \bar{\omega}_b^2$

$$\bar{\omega}_b = \omega_b/(1 + \varkappa) , \quad D = (\bar{\omega}^2_{(j)} - j^2\pi^2c^2/\ell^2)^2 + 4j^4\bar{\omega}_b^2\pi^2c^2/\ell^2$$

$$\varkappa = \mu_p/\mu \qquad (42)$$

The result (41) does not depend on time so that the vibration of the beam is a random process stationary in time. The coefficient of variance for the centre of the beam can be approximately brought to the following form, see [4]

$$C_v(\ell/2,t) = \sigma_v(\ell/2,t)/E\left[v(\ell/2,t)\right] = C_p\, C_{vp} + C_r \cdot C_{vr} \qquad (43)$$

where C_p and C_r are the analogous coefficients of variance of functions $p(\xi)$ and $r(t)$ respectively and the expressions C_{vp} and C_{vr} are represented in Figs. 2 and 3 as functions of α, β and mass parameter $\varkappa$, see (33), (34) and (42).

4. Application of the Theory and Experimental Results

The theory presented above can be applied to bridge structures assuming that their moving load is a random function. The solution is shown for two typical cases which concern (a) short span bridges and (b) long span bridges.

(a) The load of short span bridges or short longitudinal beams is idealized by a concentrated force of random time variation moving along a beam. Structures of this type are usually loaded by one axle of the vehicle only.

(b) The load of long span bridges is idealized by an infinitely long random strip (35). The first component of this load $p(\xi)$ expresses the random distribution of the static load in the bridge span direction while the second component $r(t)$ interprets the true dynamic effect of the load. The large span bridges are usually loaded by a series of axles resulting either from continous highway

traffic or from a railway train whose length is supposed to be much longer than the span of the bridge.

In reality the traffic loading is - generally speaking - an unknown random process. Therefore a solution was given also for the problem inverse to that given in the present paper, see [5]. The probability analysis [5] starts with the known statistic characteristics of the response v(x,t) giving the input characteristics for p(x,t) as a result. The statistic characteristics of any particular bridge (i.e. the beam deflections or stresses in some points) can be measured without difficulties under service conditions and on this basis the load characteristics can be evaluated.

As an example the Fig. 4 shows a covariance function measured on a railway bridge.

References

[1] V. Koloušek: Schwingungen der Brücken aus Stahl und Stahlbeton. Mémoires de l'A.I.P.C., vol. 16, Zürich, 1956, pp.301-332

[2] L. Frýba: Les efforts dynamiques dans les ponts-rails métalliques. Bull.mens.Assoc.intern.Congrès Chem.fer, 40 (1963), Nr.5, pp. 367-403

[3] S.H. Crandall (editor): Random Vibration. Vol.2. Cambridges, Mass., 1963, The M.I.T. Press

[4] L. Frýba: Vibration of Solids and Structures Under Moving Load. Manuscript of a book

[5] L. Frýba: The Inverse Problem in Stochastic Processes. Zeitschrift für angewandte Mathematik und Mechanik, in press

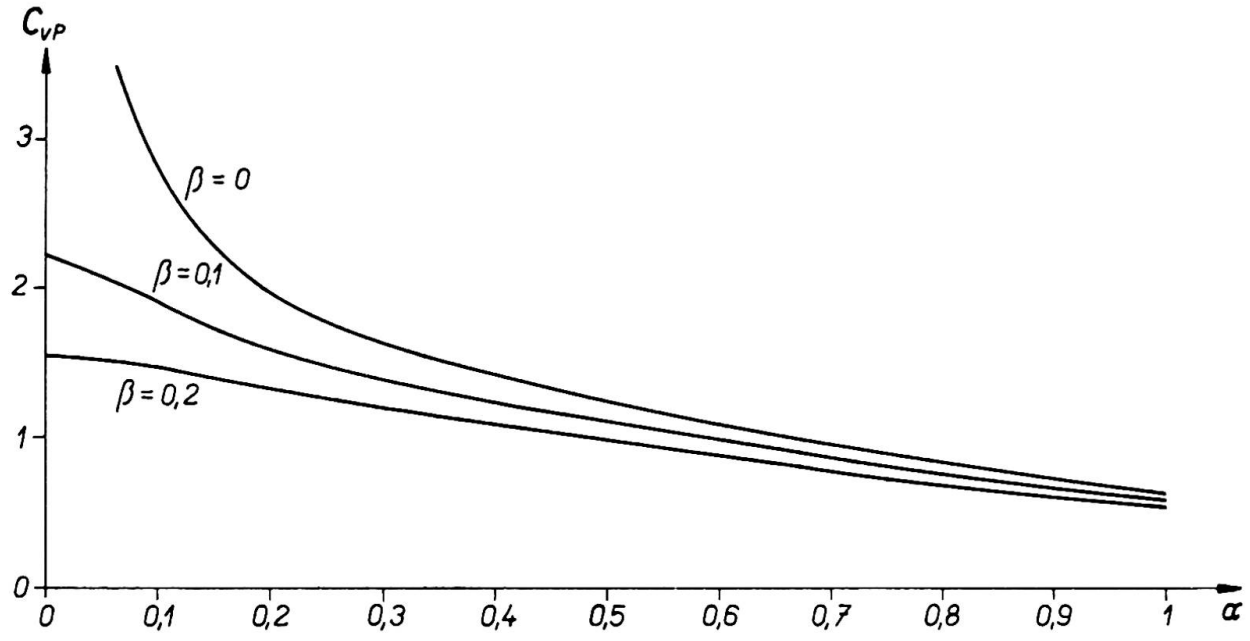

Fig.1. The coefficient C_{VP} as a function of the velocity parameter α and damping parameter β

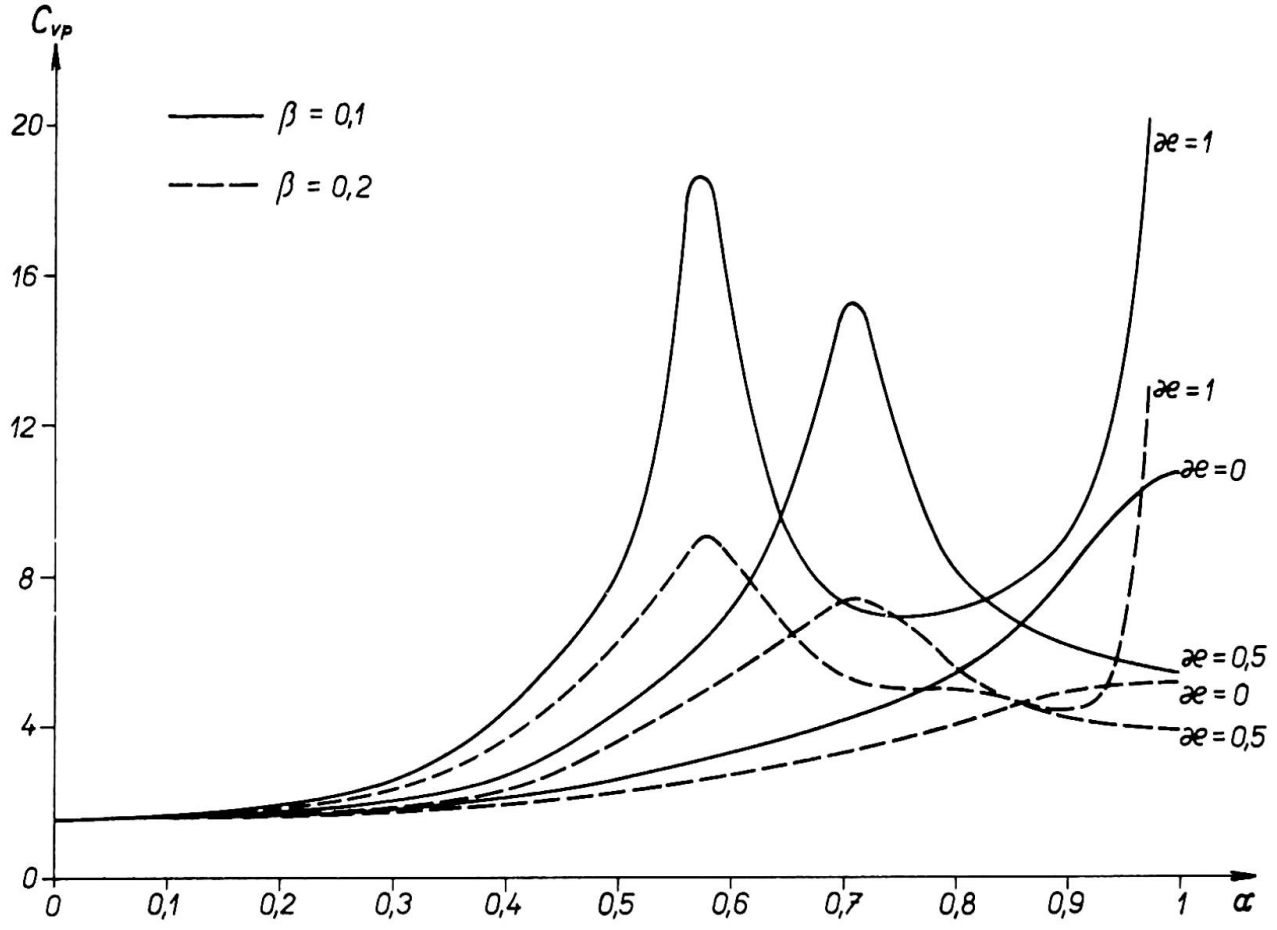

Fig.2. The coefficient C_{VP} as a function of the velocity parameter α, damping parameter β and mass parameter $\mathfrak{ae}$

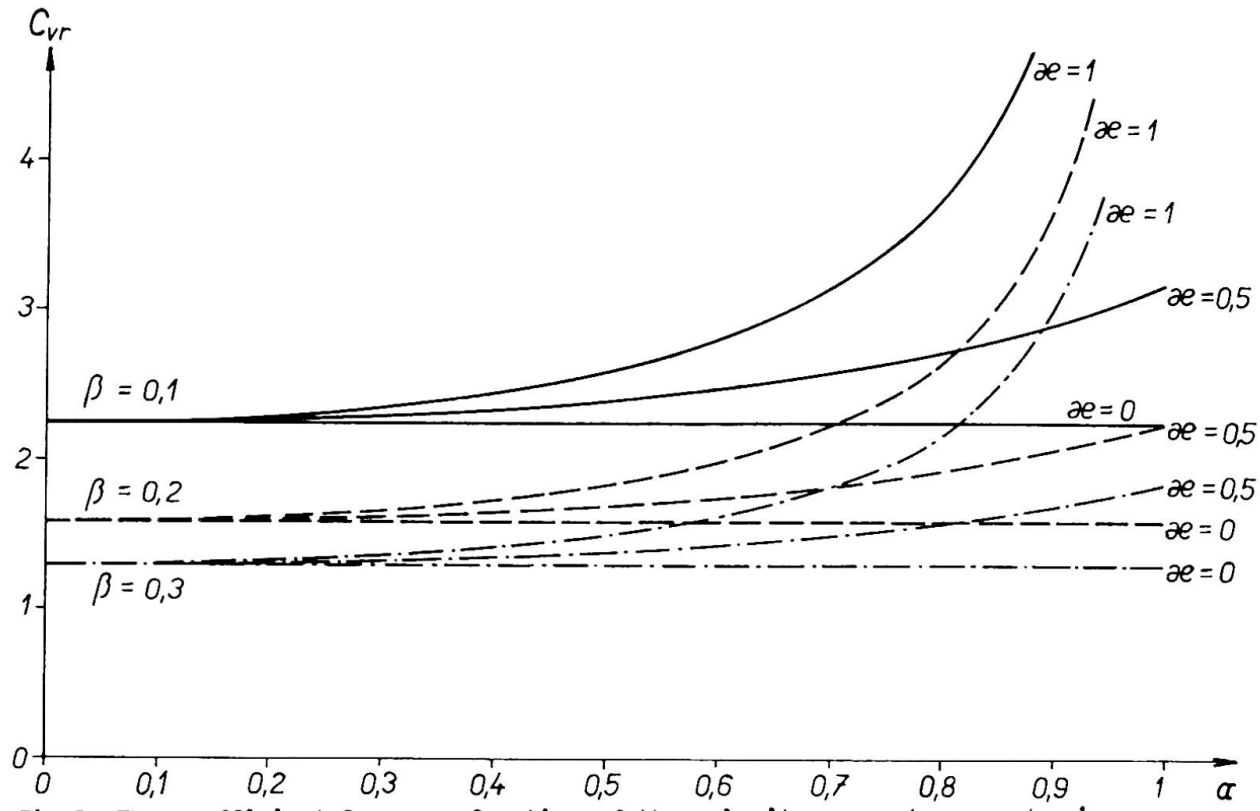

Fig.3. The coefficient C_{vr} as a function of the velocity parameter α, damping parameter β and mass parameter $\mathfrak{ae}$

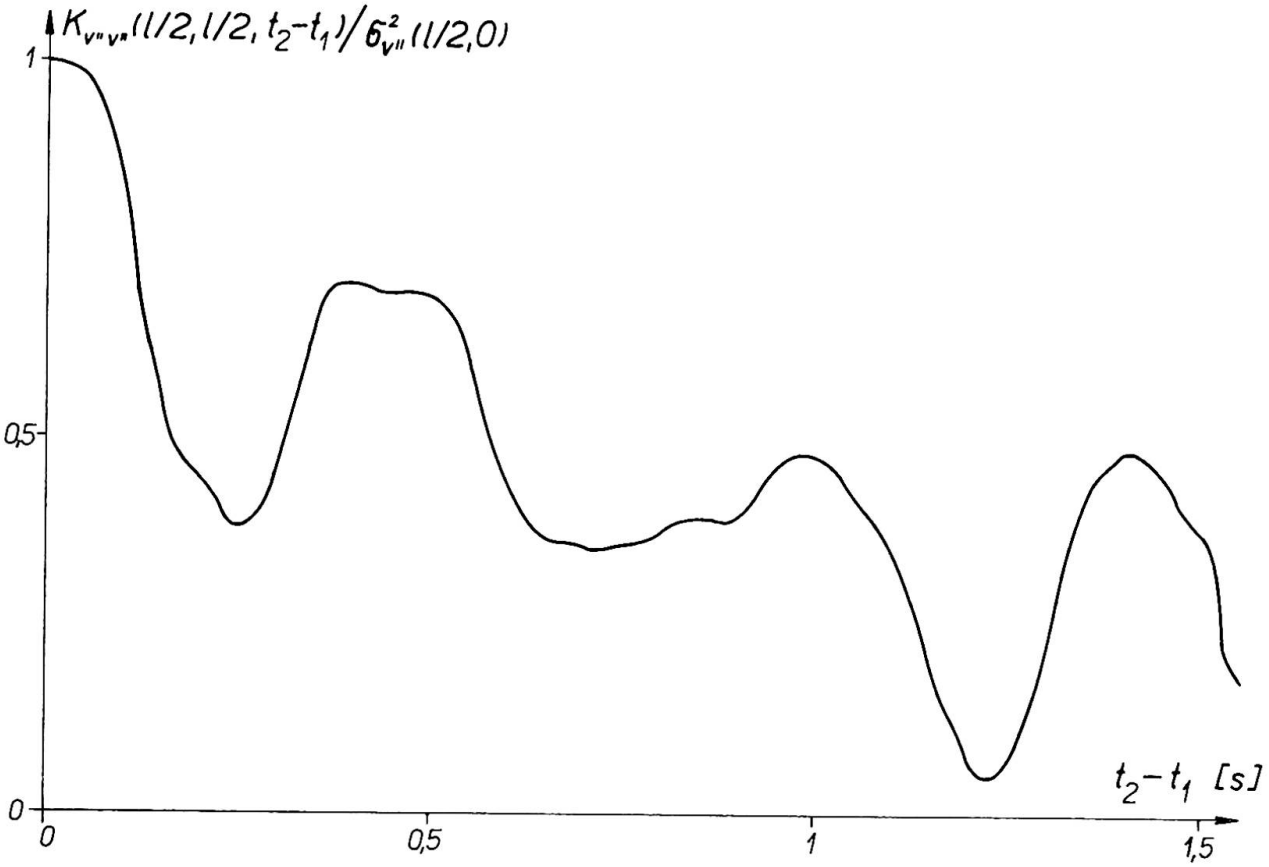

Fig.4. The experimental covariance measured from the stresses in the longitudinal beam on a steel-railway bridge

SUMMARY

The traffic loading of bridges is considered as a nonstationary random process. Starting from the statistic characteristics of the load the theory supplies information as to the statistic characteristics of the deflections or stresses in a bridge , i.e. the mean value, the covariance, the spectral density, the variance or the coefficient of variance.

The solution is shown for two typical cases which concern small and large span bridges.In the former case the load is idealized by a concentrated force of random time variation moving with constant velocity along a simply supported beam. The random effects of this load are decreasing with increasing velocity and damping (Fig. 1).

In the latter case the load is idealized by an infinitely long random strip which is moving again with constant velocity along a simple beam. This type of load induces in the beam a stationary random vibration the amplitudes of which are increasing with decreasing damping and for velocities approaching the critical speed which depends also on the mass of the traffic load (Figs. 2 and 3).

RÉSUMÉ

Le traffic sur un pont est considéré comme une charge stochastique non-stationnaire. En partant des caractéristiques statistiques de cette charge, la théorie donne des informations concernant les caractéristiques statistiques des déformations ou des tensions dans un pont, c-à-d. la valeur moyenne, la covariance, la densité spectrale, la variance ou le coëfficient de variance.

Deux cas typiques ont été traités pour un pont court, resp. long. Dans le premier cas, la charge est idéalisée par une force concentrée, variable arbitrairement avec le temps et voyageant avec une vitesse constante le long d'une poutre simple. L'effet arbitraire de cette charge décroît avec vitesse et amortissement croissant (fig. 1).

Dans le deuxième cas, la charge est idéalisée par une charge répartie stochastique infiniment longue voyageant sur la poutre simple avec une vitesse constante. Cette charge provoque une vibration stationnaire arbitraire, dont les amplitudes croissent inversément avec l'amortissement et augmentent avec des vitesses approchant la vitesse critique, qui dépend également de la masse de la charge de traffic (voir fig. 2 et 3).

ZUSAMMENFASSUNG

Die Verkehrslast von Brücken wird als nichtstationärer, zufälliger Vorgang aufgefasst. Ausgehend von den statistischen Charakteristiken der Last liefert die Theorie Auskunft über die statistischen Charakteristiken der Verformungen oder Spannungen einer Brücke, die da sind der Hauptwert, die Kovarianz, die Verteilungsdichte, die Varianz oder der Koeffizient der Varianz.

Die Lösung wird an zwei ausgeprägten Beispielen mit einer kurzen und einer langen Brücke gezeigt. Im ersterwähnten Fall ist die Belastung durch eine Einzellast idealisiert, die sich bei zufälliger Zeitvariation mit konstanter Geschwindigkeit entlang des einfachen Balkens bewegt. Die zufällige Wirkung dieser Last ist verschwindend bei wachsender Geschwindigkeit und Dämpfung (Fig. 1).

Im letzteren Fall ist die Belastung durch einen unendlich langen Streifen idealisiert worden, der sich wiederum mit konstanter Geschwindigkeit bewegt. Dies bewirkt im Balken eine stationäre, zufällige Schwingung, deren Amplitude mit abnehmender Dämpfung und mit Geschwindigkeiten, die sich der kritischen nähern, welche von der Lastmasse abhängt, wächst.

VI

The Wind-Induced Vibrations of Large Cylindrical Structures

Vibrations dues au vent dans de grands ouvrages de forme cylindrique

Windschwingungen langer Zylinderbauwerke

MILOS NOVAK
Visiting Associate Professor, Faculty of Engineering Science,
The University of Western Ontario, London, Ontario, Canada; on
leave of absence from the Czechoslovak Academy of Sciences, Prague

The difficulties caused by the wind-induced lateral vibrations have increased with modern high cylindrical structures and columns of large bridges. The nature of the excitation and the aerodynamic damping of lateral vibrations are discussed in this paper.

1. Introduction

In recent years, wind-induced lateral vibrations excited by the fluctuating lift forces have occurred with some large cylindrical structures in many countries. These dangerous vibrations are usually excited at low and medium wind velocities and have their predominant components in a plane perpendicular to that of the wind. The lateral vibrations have caused serious trouble in many cases, as described, for example, in papers [6,8,12,16,17, 20]. An illustration of a difficulty of this kind is the lateral vibration of the high cylindrical columns of a 330 m span arch bridge [9,12]. The vibration which was much stronger than in the case described by Kunert [6] produced in the columns additional dynamic stresses of up to roughly 780 kg/cm^2 that of course highly compromised their desirable bearing capacity. A similar problem recently arose with the cylindrical hangers of a large arch bridge in Canada. So it appears that the possibility of lateral vibration must be taken into account not only with masts and towers, but with all structures containing slender cylindrical members and thus, also with some steel arch bridges.

In general practice, the problem is not usually faced until the structure is finished and the cure is difficult. The prediction of the lateral vibration already in the design stage is therefore of major importance.

2. The Nature of Lateral Vibration Excitation

A considerable number of experiments have been carried out with the aim of elucidating the nature of lateral oscillations.

Understanding the problem has already had quite an interesting history. For many years, the lateral vibration was considered to be a response of the structure to fluctuating lift forces which accompany the regular eddy shedding creating the well-known pattern in the wake, usually called Karman street. This explanation leads to the solution of the response in terms of deterministic vibrations which results in very simple formulae even for rather complicated structures [8]. This approach seems justified, especially in the subcritical range; however, already the earlier measurements in the wake have shown that even in this range the vortex pattern is not perfectly periodic, with the only exception of extremely low Reynolds numbers (see Roshko [14]). Thus the lift is composed of periodic and random parts and the response should be solved in terms of random vibration. This approach shows the strong dependence of the intensity of vibration on the ratio of the random and periodic parts of the lift [9].

Later studies of cylinder behaviour in the supercritical range led to the conclusion that the lift is chaotic (see Fung [4]) and the statistical approach, based on Fung's power spectrum of lift, became very favourable for the whole supercritical range. Nevertheless, this calculation sometimes leads to considerably small amplitudes with large structures [9].

Finally, investigations in the region of very high Reynolds numbers proved a reappearance of harmonic component of the lift or narrow band lift in this domain, sometimes called the transcritical range. The papers by Roshko [15] and by Cincotta, Jones and Walker [2] represent very important contributions in this respect.

To provide further information about the fluctuating forces acting on the cylinder, pressure measurements on the surface of the body are useful [5]. Fig. 1 represents an example of such measurements carried out by the author and O. Fisher on a cylinder with a diameter of 31 cm at Reynolds number R = 265000 and Strouhal number S = 0.194. The upper trace is the motion of the cylinder, the lower traces show the surface pressures measured at two points situated 2.35 diameters apart in a plane perpendicular to the direction of the air flow. (The sensitivity of the two pressure pick-ups Disa Pu2a was different, as indicated). These measurements were made at a wind velocity, which was lower than that at the resonance (below the resonance). It can be seen that the pressures are approximately in phase with the motion. In the region of resonance, there was a distinct phase shift $\pi/2$ between the pressures and the vibration. Above the resonance, the periodicity was not so well pronounced as in the former cases. However, whenever the periodicity could be recognized, the phase shift between pressure and motion approached π. These observations of phase conditions

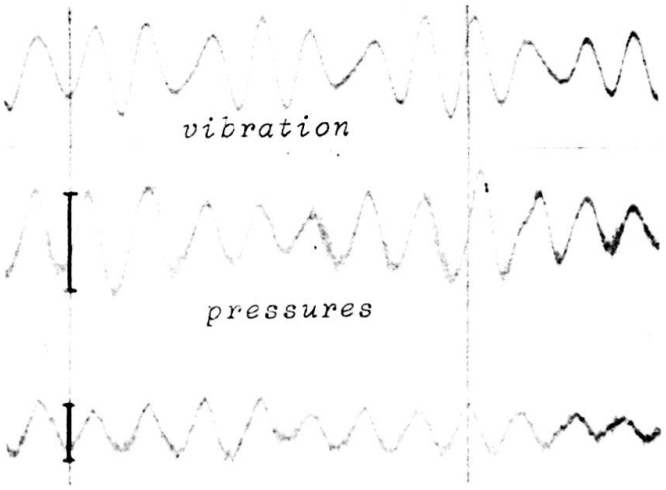

Fig. 1. Surface Pressures on a Circular Cylinder

between the fluctuating lift force and the response of the cylinder evidently agree with phase conditions of mechanical systems excited by an external force. Therefore, the outlined pressure measurements support the assumption that the lateral vibration may be considered as excited oscillations.

This conclusion is important because some authors tend to explain the lateral vibration of circular cylinders as oscillations induced by negative aerodynamic damping. This explanation does not seem justified for the following reasons:

1. The existence of fluctuating lift forces has been proven many times, even with steady cylinders performing no motion.

2. The mentioned phase shift $\pi/2$ at resonance (out of phase force) is typical for excited oscillations.

3. The negative aerodynamic damping, as usually understood, represents forces which are induced by the motion of a body, the cross-section of which is aerodynamically unstable. The square cross-section represents the well-known example of this kind. However, the instability clearly defined with the square cross-section cannot be defined in the same way with the circular cross-section. Furthermore, the self-excited vibration of bodies with unstable cross-section significantly differs from circular cylinder oscillations. The main feature of self-excited oscillations is the monotonous increase in steady amplitudes with wind velocity above a certain value. An example of wind-induced oscillations of this kind is given by Fig. 2. This figure represents the universal galloping response of square cylinders having different normal modes under the action of wind with constant and variable mean speed [11].

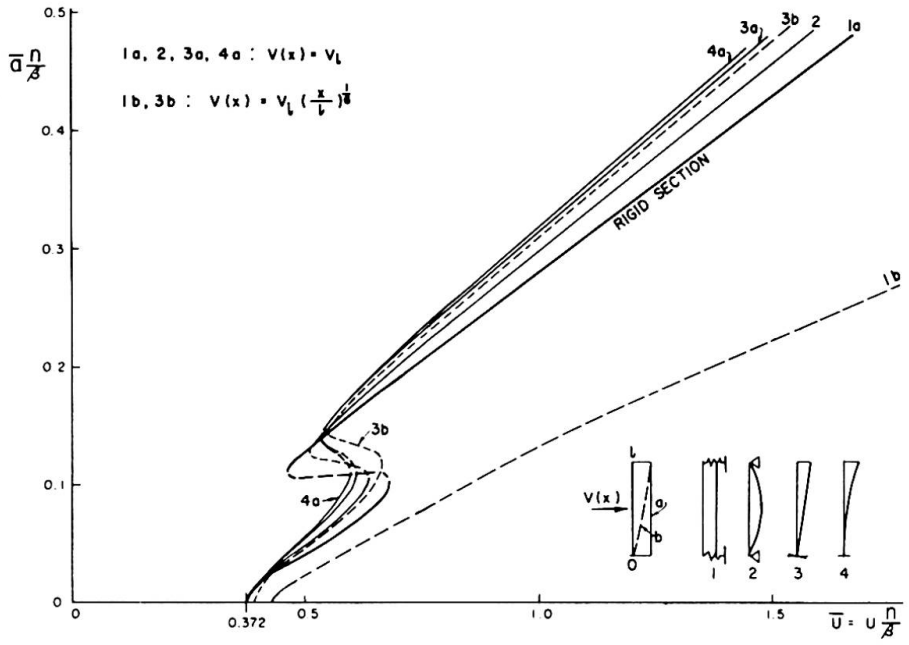

Fig. 2. Universal Galloping Response of Square Cylinders Having Different Normal Modes

$\bar{a} = \frac{a}{h}$ - reduced amplitude of displacement

h - length of side of the prism

$U = \frac{V}{\omega h}$ - reduced air velocity

V - air velocity

ω - natural circular frequency

$n = \frac{\rho h^2}{4\mu}$ - mass parameter

μ - mass per unit of length

ρ - air density

β - reduced damping coefficient (log. decrement/2π)

This representation holds generally for all bodies with different mass, damping and normal modes but with square cross-section [11]. In other cases of negative aerodynamic damping, the character of the response as a function of wind velocity is similar; however, this character is principally different from that of circular cylinder vibration. Laberal response of circular cylinders always implies either a more or less well pronounced resonance peak alike as curve *a* in Fig. 3, or a continuous progressive increase in amplitudes, as diagrammatically shown by curve *b* in the same figure. According to the previous, the latter case is typical for the supercritical range with the purely random lift.

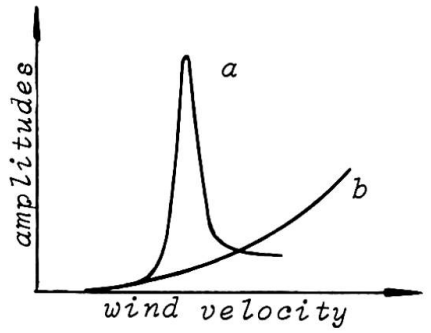

Fig. 3. General Character of Lateral Vibration

For all these reasons, the assumption that the lateral vibrations of circular cylinders can be calculated as excited (forced) oscillations seems to be well founded. The problem, of course, is to know the lift forces as functions of all main factors which govern the phenomenon. For a reliable prediction, the lift forces should be defined by their power spectra and cross-spectra as functions of Reynolds number, intensity and scale of the turbulence and dimensionless amplitude of vibration.

Despite the large amount of experimental work which has been carried out, a full description of lift forces is not available. The research of ground wind effects in relation to launch vehicles has recently provided some very interesting information concerning the range of very high Reynolds numbers inaccessible in standard wind tunnels. Especially the work of Cincotta, Jones and Walker [2] must be referred to here because the range of very high Reynolds numbers is particularly important for large structures. As for the nature of lift forces, these authors came to the following conclusions concerning different ranges of Reynolds numbers:

In Reynolds Number Range:	The Nature of Lift is:
1.4 to 3.5 million	Wide band random
3.5 to 6 million	Narrow band random
6 to 18.2 million	Random plus periodic

The Strouhal number determined from the autocorrelation functions increases with the increase in Reynolds number from 0.15 to 0.3, but the value 0.3 remains constant throughout the random plus periodic range.

So far, the previous measurements by Fung [4] and Roshko [14] agree with these results.

However, the measurements by Schmidt [18] in the range of Reynolds numbers up to 5 million led to another result. His power spectrum for lift force at R = 5 million has no well-pronounced peak. Contradictions of this kind occurred with other measurements too. It seems likely that these contradictions have their reason in differences in surface roughness of the body and the intensity and scale of the turbulence of the flow.

2.1 The effect of turbulence

The extent to which the behaviour of bluff bodies in wind can depend on turbulence is demonstrated by Fig. 4. The sharp peak caused by vortices in smooth flow completely disappeared due to turbulence and the character of response is quite different in both cases.

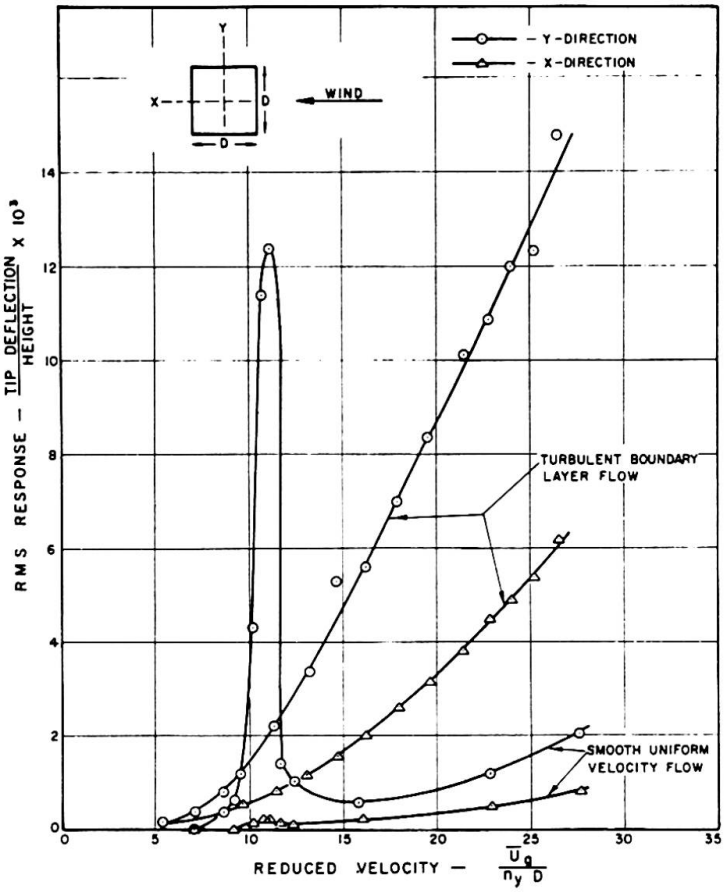

Fig. 4. Response of a Square Cantilevered Prism in Turbulent and Smooth Flow. (Measured in the Boundary Layer Wind Tunnel Laboratory of The University of Western Ontario by P. Rosati)

The turbulence and the surface roughness thus highly affect the nature of aerodynamic forces acting on the cylinder. These factors therefore also affect the value of the critical Reynolds number which divides the subcritical range from the supercritical one. Some information of this kind is provided by Simon [19]. Uncertainty in the estimation of the critical Reynolds number is sometimes very unpleasant.

For example, the columns of the large arch bridge mentioned in the introduction performed the strongest vibration at R = 551000. It was not quite clear in which regime the columns vibrated at this R. This made the decision of how to suppress the vibration difficult. Vibrations were decreased by filling the columns with granulated gravel. The efficiency of such a method depends on the regime of the flow round the body as discussed in paper [12]. This explains why this approach to the cure of vibration may fail in some cases, as was experienced with a Canadian bridge, whereas the same cure may be successful in other very similar cases [6,9,12].

This example indicates that the elucidation of the effect of atmospheric turbulence on the lift nature is really desirable.

2.2 Dependence of lift on the motion

The influence of the motion on the lift forces is a further important factor. To study it experimentally two approaches can be used: the motion is controlled by an exciter, or by changing the structural damping. The former way has been used more often.

In the range of random plus periodic lift at very high Reynolds numbers (6-18.2 million), Cincotta and associates [2] found a very strong increase in the lift with the amplitude at the coincidence of the frequency of excitation with the frequency determined by the

pertinent Strouhal number. (This resonance case is of major importance). Assume that with small vibration amplitude v (with structures usually $v/D < 0.1$, even in very serious cases) this increase can be expressed by a linear law

$$\frac{C_L}{C_{L_s}} = 1 + k\frac{v}{D}$$

Here C_L is the lift coefficient at vibration with the amplitude v, C_{L_s} the lift coefficient of a stationary cylinder, k a constant and D the diameter. Then a coefficient $k = 47.0$ can be derived from data contained in paper [2], which means a considerable increase in lift with the amplitude.

In subcritical range, a much lower increase was found by Bishop and Hassan [1]. From their data a coefficient of $k = 2.25$ can be calculated for R = 6000 and small dimensionless amplitudes.

Finally, in supercritical range, characterized by random lift, Fung [4] did not find any remarkable increase in lift with the amplitude of motion. (See also [10]).

All these authors applied external excitation of the vibration. There is also a possibility of controlling the amplitude of the vibration without any interference with the mechanism of the excitation by changing only the intensity of damping. Plotting the resonance amplitudes against structural damping can provide some information about the character of excitation; however, even this involves complications. If the dependence of resonance amplitudes on the inverse value of the structural damping is linear (Fig. 5 curve *a*) the excitation may be supposed harmonic and independent of the amplitude. If this dependence has character, as curve *b* in Fig. 5, the reason for this may be the random nature of the fluctuating lift or the presence of positive aerodynamic damping. The latter factor is discussed in the next paragraph.

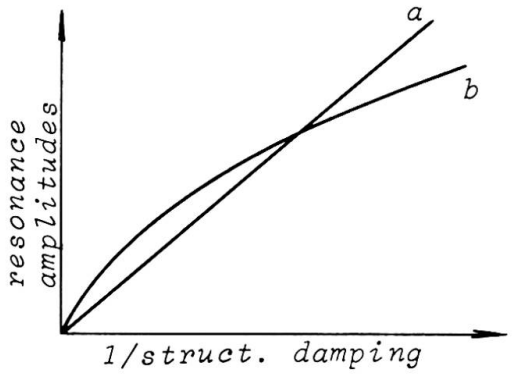

Fig. 5. Dependence of Resonance Amplitudes on Inverse Value of Structural Damping

2.3 Positive aerodynamic damping

Severe lateral vibrations usually occur with structures having extremely low structural (system) damping. In such cases the resistance of the air flow to the motion of the structure can result in a positive aerodynamic damping which is comparable with the structural damping. The intensity of the aerodynamic damping can be estimated as follows.

Assume a cylinder under two dimensional flow conditions moving with the velocity $\dot{v}$ perpendicularly to the direction of the wind blowing with the velocity V (Fig. 6), which is the situation with lateral vibration. Then the resultant relative wind with the velocity V_{rel} acts on the body under the angle of incidence α.

Neglecting the mass effect, the drag force on a unit of length has a component in the direction of the motion

$$F_y = \frac{1}{2}\rho C_D D V_{rel}^2 \sin\alpha \tag{1}$$

Here ρ is the air density and C_D the drag coefficient; with small angles α $\sin\alpha = \tan\alpha = \dot{v}/V$ and $V_{rel} \doteq V$.

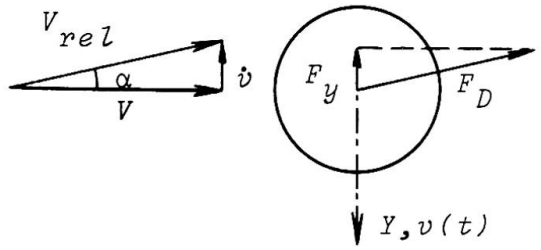

Fig. 6. Vibrating Cylinder in the Flow

The mean wind speed increases with the height of the structure which may be taken into account by putting

$$V(x) = Vw(x) \tag{2}$$

Now V means the wind speed at a reference point x_r and $w(x)$ a function describing the mean wind increase, so that $w(x_r) = 1$. Then the air resistance which acts on a differencial unit of length of a structure at position x is

$$f(\dot{v})dx = \frac{1}{2}\rho C_D D V w(x)\dot{v}dx \tag{3}$$

Under the assumption that this holds even during vibration (quasi-steady approach) this resistance of the wind to the lateral vibration evidently has a nature of viscous damping.

The exciting aerodynamic forces are small during the lateral vibration. Therefore steady lateral vibration cannot differ too much from the normal mode of free vibration $v_n(x)$ and may be expressed as

$$v(x,t) = a v_n(x)\cos\omega_n t \tag{4}$$

where a is the amplitude at the reference point x_r, and ω_n the circular frequency of the n-th mode. The mode $v_n(x)$ is chosen in such a scale that $v_n(x_r) = 1$.

The work done during a period T of steady vibration by aerodynamic damping forces (3) on the whole structure is

$$W = \int_o^l \int_o^T f(\dot{v})dx dv(t) \tag{5}$$

After substitution from (3) and (4)

$$W = \int_o^l \int_o^T \frac{1}{2}\rho C_D D V w(x) a^2 \omega_n^2 v_n^2(x) \sin^2\omega_n t dx dt \tag{6}$$

and after integration with respect to t

$$W = \frac{1}{2}\pi\rho C_D D V a^2 \omega_n \int_o^l w(x) v_n^2(x) dx \tag{7}$$

The maximum potential energy calculated as maximum kinetic energy for the deflection (4) is

$$L = \int_o^l \frac{1}{2}\mu(x)\dot{v}^2 dx = \frac{1}{2}a^2\omega_n^2 \int_o^l \mu(x) v_n^2(x) dx \tag{8}$$

where $\mu(x)$ is the mass of the structure per unit of length.

Logarithmic decrement of damping can be defined as $\delta = \frac{W}{2L}$. This yields for log. decrement of aerodynamic damping with lateral vibration in variable mean wind

$$\delta_a = \frac{\pi\rho C_D D V \int_o^l w(x) v_n^2(x) dx}{2\omega_n \int_o^l \mu(x) v_n^2(x) dx} \tag{9}$$

Here the Strouhal number may be introduced.

$$S = \frac{\omega_n D}{2\pi V} \tag{10}$$

With constant mass $\mu(x) = \mu$ and constant mean wind speed $w(x) = 1$ the log. decrement of aerodynamic damping is simply

$$\delta_a = \frac{\pi \rho C_D D}{2\omega_n \mu} V = \frac{\rho}{4} \frac{C_D}{S} \frac{D^2}{\mu} \tag{11}$$

In variable mean wind but with constant mass, the log. decrement of aerodynamic damping

$$\delta_a' = \delta_a c \tag{12}$$

where the constant

$$c = \frac{\int_o^l w(x) v_n^2(x)\,dx}{\int_o^l v_n^2(x)\,dx} \tag{13}$$

expresses the decrease in aerodynamic damping due to variable mean wind velocity. This is calculated for some simple normal modes in Table 1.

l, x, 0; $w(x)$, $v_n(x)$						
Mode $v_n(x)=$	1		x/l		x^2/l^2	
Wind incr. $w(x)=$	$(x/l)^{\frac{1}{6}}$	$(x/l)^{\frac{1}{3}}$	$(x/l)^{\frac{1}{6}}$	$(x/l)^{\frac{1}{3}}$	$(x/l)^{\frac{1}{6}}$	$(x/l)^{\frac{1}{3}}$
Constants c	$\frac{6}{7}$	$\frac{3}{4}$	$\frac{18}{19}$	$\frac{9}{10}$	$\frac{30}{31}$	$\frac{15}{16}$

Table 1. Decrease in Aerodynamic Damping c Due To Variable Mean Wind Velocity

The wind increase $w(x)$ is taken here, as recommended by Davenport [3]. The exponent 1/6 corresponds to conditions in open country, 1/3 to centres of large cities. The top $x=l$ is considered the reference point. In other cases, the reduction c can be calculated from (13) or estimated according to Table 1, because its value is not too sensitive to the exact form of the normal mode and very little to changes in the wind profile with cantilevered structures.

The existence of the positive aerodynamic damping has been recognized and experimentally proven. From the point of view of structures, Scruton [16] and Davenport (e.g. [3]) pay a great deal of attention to this damping. Davenport experimentally studied it in detail and presented its general discussion [3]. However, the aerodynamic damping has found little application with lateral vibration of cylindrical structures, where it should be considered at least in two directions: when estimating the effect of changes in damping, and when evaluating the experiments.

The practical importance of the first application is evident from the numerical value of the aerodynamic damping.

The expression (11) provides constant damping for resonance vibration in regions in which C_D and S may be considered constant. In subcritical range with $S = 0.2$, $C_D = 1.2$ and $\rho \doteq 1/8\ kg\ m^{-4}s^2$

$$\delta_a = \frac{3}{16}\frac{D^2}{\mu} \tag{14}$$

In transcritical range for $S = 0.3$, $C_D = 0.54$ (see [2])

$$\delta_a = \frac{0.9}{16}\frac{D^2}{\mu} \tag{15}$$

In supercritical range the damping must be calculated with respect to the wind velocity.

The columns of the mentioned arch bridge have $D = 1\ m$, $\mu = 29.9\ kg\ m^{-2}s^2$ and the aerodynamic damping (14) is $\delta_a \doteq 0.0063$. The log. decrement of structural damping was of the same order, namely $\delta_s \doteq 0.0078$. Thus the total damping $\delta_a + \delta_s$ should be introduced into calculations. On the other hand, the increase in δ_a by application of strakes (spoilers) due to the increase in C_D (see [10]) contributes to the total damping and thus to the effectiveness of such advices.

As for the evaluation of vibration experiments, this task is complicated by the simultaneous presence of three factors: the aerodynamic damping, the randomness of lift (even when dominant frequency is well pronounced), and the dependence of excitation on the amplitude of motion. Neglecting the aerodynamic damping can therefore affect the result concerning the two latter factors.

3. Structural Damping

The structural damping represents a further factor, the estimation of which is always uncertain. It is very small with modern structures, often $\delta_s < 0.01$, which is the main reason for the frequent occurance of strong lateral vibration, especially with all welded structures. Finding suitable devices to provide a considerable increase in structural damping would, therefore, be the most important contribution to the practical part of the problem. (Reed and Duncan's [13] hanging chains represent an example of this kind.) Some effective coating or other means without any additional construction would be desirable.

References

[1] Bishop, R.E.D., Hassan, A.Y.: The Lift and Drag Forces on a Circular Cylinder Oscillating in a Flowing Fluid. Proc. Royal Soc. of London, Ser. A., Vol. 277, 1964, pp.51-75.

[2] Cincotta, J.J., Jones, G.W., Walker, R.W.: Experimental Investigation of Wind Induced Oscillation Effects on Cylinders in Two-dimensional Flow at High Reynolds Numbers. Mtg. on ground wind load problems in relation to launch vehicles. Compilation of papers presented at the NASA Langley Research Center, June 7-8, 1966, pp.20.1-20.35.

[3] Davenport,A.G.: The Treatment of Wind Loading on Tall Buildings. Proc. of the Symp. on Tall Buildings, Southampton, April 1966, pp.3-44.

[4] Fung, Y.C.: Fluctuating Lift and Drag Action on a Cylinder in a Flow at Supercritical Reynolds Numbers. Jour. of the Aerospace Sciences, Vol. 27, Nov. 1960, No. 11, pp.801-814.

[5] Ferguson, N., Parkinson, G.V.: Surface and Wake Flow Phenomena of the Vortex-Excited Oscillation of a Circular Cylinder. Trans. ASME Jour. of Eng. for Industry, Paper No. 67-Vibr-31, pp.1-8.

[6] Kunert, K.: Vibration of Slender Columns in Steady Air Flow (in German). Bauing 1962, pp.168-173.

[7] Nakagawa, K.: An Experimental Study of Aerodynamic Devices for Reducing Wind-Induced Oscillatory Tendencies of Stacks. Bul. of Univ. of Osaka Prefecture, Ser. A, Vol. 13, No. 2, 1964, pp.1-18.

[8] Novak, M.: The Wind-Induced Lateral Vibration of Circular Guyed Masts. Prelim. report, IASS "Symposium on Tower-Shaped Steel and Reinforced Concrete Structures", Bratislava 1966, p.34.

[9] Novak, M.: A Statistical Solution of the Lateral Vibrations of Cylindrical Structures in Air Flow. Acta Technica CSAV, 1967, Academia, Prague, pp.375-405.

[10] Novak, M.: On Problems of Wind-Induced Lateral Vibrations of Cylindrical Structures. Internatl. Research Seminar: Wind Effects on Bldgs. & Structures, Ottawa, Sept. 1967.

[11] Novak, M.: Aeroelastic Galloping of Rigid and Elastic Bodies. Research Report BLWT-3-68, The University of Western Ontario, Faculty of Engineering Science, London, Canada, March 1968.

[12] Novak, M.: The Wind-Excited Lateral Oscillation in Columns of a Large Arch Bridge (in German). Stahlbau (to be published).

[13] Reed, W.H. III, Duncan, R.L.: Dampers to Suppress Wind-Induced Oscillations of Tall Flexible Structures. Presented at 10th Midwestern Mechanics Conf., Fort Collins, Colorado, Aug. 21-23, 1967.

[14] Roshko, A.: On the Development of Turbulent Wakes from a Vortex Street, N.A.C.A., T.N. 2913, 1953.

[15] Roshko, A.: Experiments on the Flow past a Circular Cylinder at Very High Reynolds Numbers; Jour. of Fluid Mech., Vol. 10, 1961, pp.345-356.

[16] Scruton, C.: On the Wind-Excited Oscillations of Stacks, Towers and Masts. Proc. of the Conf. "Wind Effects on Buildings and Structures", Teddington 1963, pp.798-832.

[17] Scruton, C.: Effects of Wind on Stacks, Towers and Masts. IASS Symp. on Tower-Shaped Steel and Reinforced Concrete Structures, Bratislava, 1966, p.25.

[18] Schmidt, L.V.: Fluctuating Force Measurements upon a Circular Cylinder at Reynolds Numbers up to 5×10^6. The same publication as [2], pp.19.1-19.17.

[19] Simon, W.E.: Predictions and Implications of the Flow Field Parameter Analysis of the Wind Induced Oscillation Problem. The same publication as [2], pp.13.1-13.31.

[20] Vickery, B.J., Watkins, R.D.: Flow-Induced Vibrations of Cylindrical Structures. Hydraulics and Fluid Mechanics, Proc. of the First Australasian Conference, 1962; Pergamon Press 1964, pp.213-241.

SUMMARY

Despite the increasing understanding of the lateral vibration of cylindrical structures, the preciseness of a quantitative calculation necessary for a reliable prediction is limited. For prediction of dynamic behaviour of large structures in wind, experimental investigation on models in wind tunnels is therefore most recommendable.

RÉSUMÉ

Malgré les connaissances croissantes sur les vibrations latérales des structures cylindriques, la précision requise pour une prévision valable n'est guère obtenue par un calcul quantitatif. C'est pourquoi on ne peut assez recommander des essais expérimentaux sur modèles réduits dans le tunnel aérodynamique quand il s'agit de prévoir le comportement dynamique d'une grande structure soumise au vent.

ZUSAMMENFASSUNG

Trotz des wachsenden Verständnisses seitlicher Schwingungen zylindrischer Bauwerke ist die Genauigkeit für eine quantitative Rechnung, notwendig zu einer wirklichen Voraussage, beschränkt. Deshalb ist für die Voraussage über das dynamische Verhalten langer, windausgesetzter Bauwerke die experimentelle Untersuchung im Windkanal am Modell das wohl empfehlenswerteste.

Leere Seite
Blank page
Page vide

VI

Dynamic Wind Response of Guyed Masts

Mâts haubannés dans le vent turbulent

Abgespannte Maste unter dem Einfluß von turbulentem Wind

MICHAEL SHEARS C.A. FELIPPA R.W. CLOUGH J. PENZIEN
University of California, Berkeley

1. INTRODUCTION

Engineering interest in the analysis of guyed masts was stimulated by the introduction of radio transmission, and one of the earliest contributions, by Walmsley (1) in 1924, was concerned with the static loads applied to stay-ropes used to support wireless masts. Problems associated with the dynamic behavior of cables have received much attention in classical texts for well over a century. The motion of inextensible loose chains and the small oscillations of tight elastic strings have been discussed extensively by Routh (2) in 1860, and Rohrs (3) in 1851. Probably the earliest detailed method for the static and dynamic analysis of guyed masts under the action of wind forces, however, was due to Kolousek (4) in 1947. In more recent years, due largely to the increased heights and importance of telecommunications masts, there has been considerable interest in this field of study, with notable contributions by Cohen (5), Dean (6) and Davenport (7).

In the past, the static analysis of guyed masts has usually been accomplished by treating the shaft as a continuous beam-column resting on non-linear, elastic supports using solution techniques based on modified slope-deflection equations. Generally, the solution methods employed and the description of the system have been rather cumbersome and not entirely suited to the analysis of the fully integrated guyed mast system. For this reason, various approximations have been made in both the guy cable representation and in the manner of application of the steady wind forces, the result being the evolution of a number of similar methods of analysis differing only in the number, or degree of approximations to the real system.

The dynamic analysis of guyed masts has received very limited attention to date, and those methods proposed are often quite unsuitable for any detailed investigation of the dynamic responses to fluctuating wind excitations. An exception was the report by Hartmann and Davenport (8) in 1966, which described the spectral response analysis of a tall, guyed mast utilizing a single degree of freedom, discrete parameter model to represent the cables. Even in this case, however, the effect of the wind on the cables was neglected in the analysis.

The purpose of this paper is to report on detailed computer studies made using a suitable discretized model to investigate the response characteristics

of guyed masts under the action of turbulent wind influences (9). The model representing the system is fully integrated geometrically and structurally, and may be used to study both the static and dynamic behavior of the system. Estimates of the dynamic responses of a tall, guyed mast are evaluated deterministically using actual wind velocity data, and non-deterministically using the theory of random vibrations and incorporating available wind velocity spectra. A comparison between the deterministic and non-deterministic responses, and a discussion of the relative merits of the two procedures are also presented.

2. THE CABLE MODEL

2.1 Finite Element Discretization

The real cable is represented by an assembly of one-dimensional cable elements (CE) interconnected at nodal points located on the initial cable profile, utilizing a lumped mass idealization for the dynamic analysis.

The stiffness properties of the CE are derived in a local cartesian system $(\bar{x},\bar{y},\bar{z})$ where $\bar{x}$ is the chord axis and $\bar{y}$ is in the plane of the element. Three degrees of freedom are defined at each node: the two displacements $\bar{u}$ and $\bar{v}$ in the $\bar{x}$ and $\bar{y}$ directions, respectively, and the rotation $\bar{\varphi}$ about $\bar{z}$. The CE stiffness matrix includes the conventional axial stiffness and the geometric stiffness, which accounts for the effect of the cable tension T. The secant CE axial stiffness (along the $\bar{x}$ axis), which results from the assumption that the CE profile is a shallow parabola, is given by (5)

$$k_A = \frac{\Delta T}{\Delta c} = \frac{1}{c}\left[\frac{1}{EA} + \frac{W_n^2}{24}\,\frac{(2T+\Delta T)}{(T+\Delta T)^2\,T^2}\right]^{-1} \qquad (2\text{-}1)$$

where c is the chord length of the element, W_n is the total applied load normal to the chord, E is the elastic modulus and A the cross-sectional area of the cable material. Since ΔT and Δc are not known a priori, the tangent axial stiffness

$$k_A = \frac{dT}{dc} = \frac{1}{c}\left[\frac{1}{EA} + \frac{W_n^2}{12T^3}\right]^{-1} \qquad (2\text{-}2)$$

is used for each linearized step of the iterative static solution (Section 3.3). The (6 x 6) CE stiffness matrix is completed with the geometric stiffness, which is obtained by assuming a cubic $\bar{v}(\bar{x})$ variation defined in terms of the nodal values of $\bar{v}$ and $\bar{\varphi}$.

2.2 Cable Frequency Studies

In order to test the convergence properties of the finite element idealization as the number of elements is increased, the lowest natural frequencies of a single cable were computed and compared with the results obtained from a series solution for an assumed overall parabolic profile. Before presenting the numerical examples, the parabolic cable solution is outlined for clarification.

Parabolic Cable Series Solution: The undamped equation of motion of an end-fixed, inclined parabolic cable under a uniform dead load per unit of chord length w, (Fig. 1), vibrating about the parabolic equilibrium position y(x) is given by

$$\frac{w}{g}\,\ddot{v} = T\,\frac{d^2v}{dx^2} + dT\,\frac{d^2y}{dx^2} \qquad (2\text{-}3)$$

By expressing v(x,t) as a Fourier sine series

$$v(x,t) = \sum_{n=1}^{\infty} Y_n(t)\,\sin\frac{n\pi x}{c} \qquad (2\text{-}4)$$

and taking account of orthogonality, Eq. (2-3) may be reduced to two infinite systems of ordinary differential equations representing the symmetric and antisymmetric modes (8,9) of vibration.

For the symmetric modes (n odd)

$$\ddot{Y}_n + \bar{\omega}_n^2 \left(1 + \frac{\zeta}{n^4}\right) Y_n + \bar{\omega}_n^2 \zeta \sum_{\substack{s=1,3\ldots \\ s\neq n}}^{\infty} \frac{1}{n^3 s} Y_s = 0 \qquad (2\text{-}5)$$

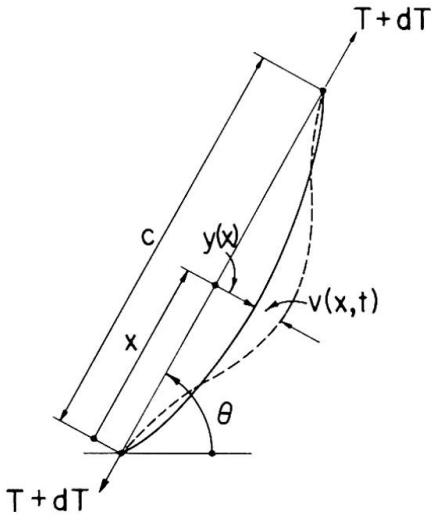

FIG. 1

where $\bar{\omega}_n = n\pi\sqrt{(Tq/w\,c^2)}$ is the n-th taut string frequency and

$$\zeta = \frac{8\,A\,E\,w^2\,c^2}{\pi^4\,T^3}\cos^2\theta \qquad (2\text{-}6)$$

is a dimensionless constant providing the cross coupling between the symmetric modes and hereafter termed the "cable parameter". The symmetric mode natural frequencies ω_n can be computed from (2-5) using standard eigenvalue techniques. For a relatively taut cable, the cross coupling becomes negligible and ω_n approaches $\bar{\omega}_n$, whereas for a slack cable considerable coupling develops, especially between the first (n = 1) and second (n = 3) symmetric modes.

For the antisymmetric modes (n even), the frequency equation is identical to that of a taut string ($\zeta = 0$) and $\omega_n = \bar{\omega}_n$ (n = 2,4....).

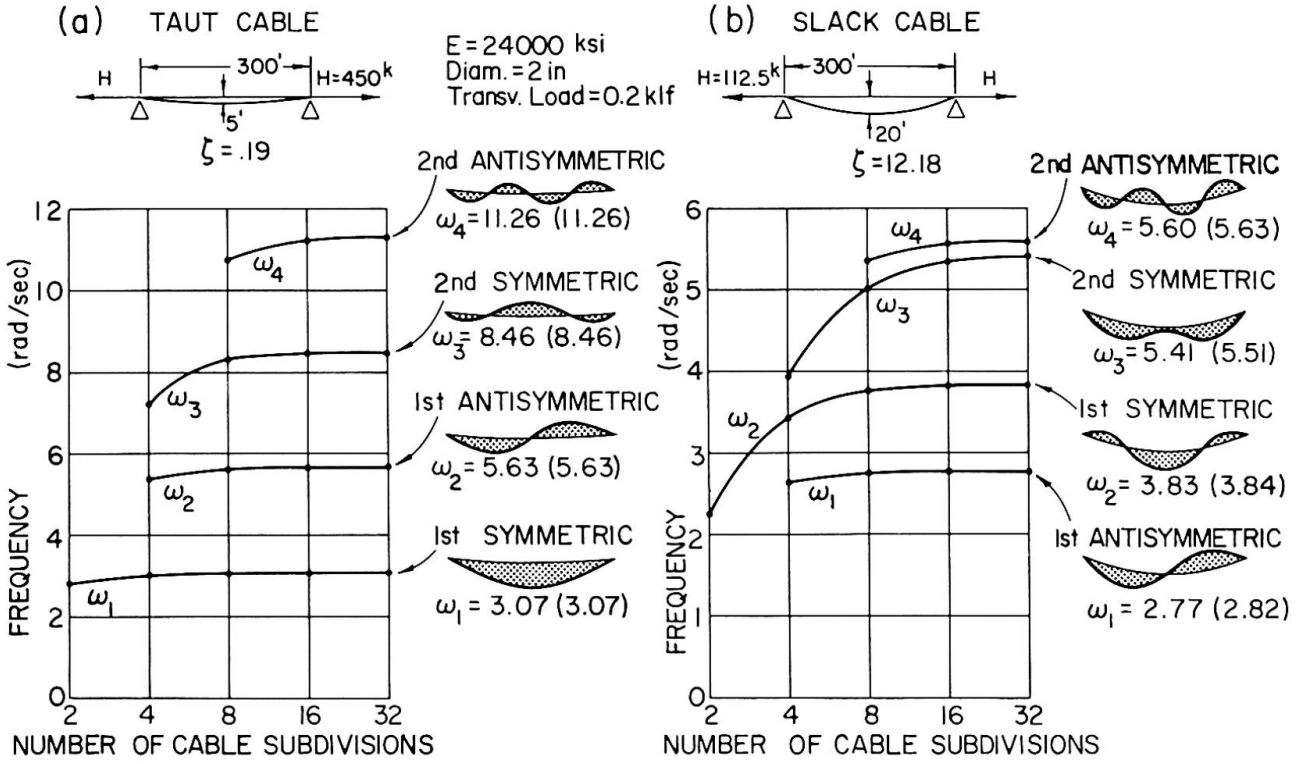

FIG. 2 CABLE MODEL FREQUENCY CONVERGENCE STUDY

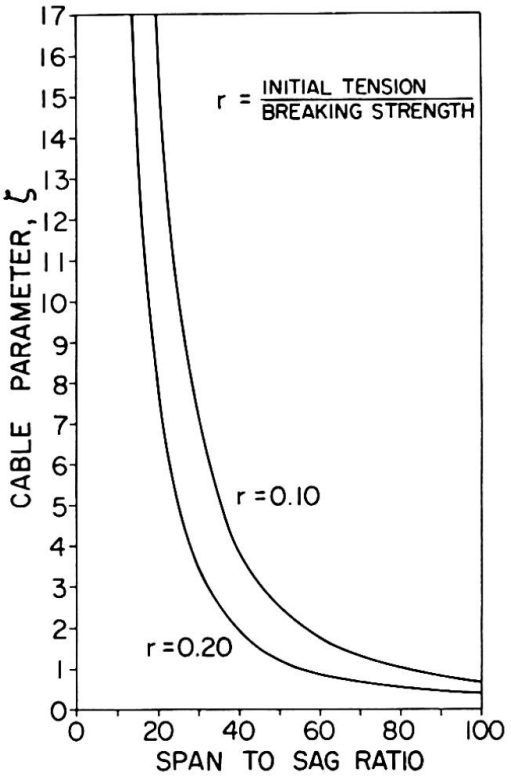

FIG. 3

Comparison of Results: A 300 ft. horizontal cable under $w = 200$ plf was selected for the comparison. Two midspan sags were assumed: 5 ft. for the taut case ($\zeta = 0.19$) and 20 ft. for the slack case ($\zeta = 12.16$). Fig. 2 presents the results of the finite element frequency analysis for various subdivisions. The convergence is very fast in the case of the taut cable, and slower for the slack cable. The frequencies obtained for the parabolic cable are indicated in parentheses.

Other Guy Cable Characteristics: To further ensure that the cable model adequately represents the properties of guy cables, a numerical investigation of the fundamental frequencies was performed for a series of cables with chord lengths varying between 250 and 1000 ft. and initial tension levels between 10-20% of the breaking strength. The range of cables investigated was intended to include most of the cables likely to be used in the construction of guyed masts. A curve illustrating the relationship between the cable parameter ζ and the chord length to normal sag ratio is given in Fig. 3, which clearly shows that most practical guy cables lie within a closely bounded region. It was also found that for a given initial tension all cables considered fell on the same curve, indicating that the cable parameter is a direct measure of the tautness irrespective of the cable dimensions. The frequencies calculated using a six-element cable model were found to agree with the analytic solutions obtained from (2-4) to within 5%, see Fig. 4, indicating that the commonly assumed parabolic cable profile is satisfactory for most guy cables.

3. THE GUYED MAST MODEL

3.1 Finite Element Discretization

In order to complete the finite element idealization of a guyed mast structure, a beam-column element (BCE) is required. The BCE stiffness matrix is also generated in the local element system $(\bar{x},\bar{y},\bar{z})$ defined in Section 2.1, and includes both the axial and geometric stiffness contributions (as described for the CE) plus the flexural stiffness in the $\bar{x}$-$\bar{y}$ plane. The bending stiffness is obtained by assuming a fifth-order $\bar{v}(\bar{x})$ expansion in terms of the transverse displacements $\bar{v}$, rotations $\bar{\varphi}$ and curvatures $\partial\bar{\varphi}/\partial\bar{x}$ at the end nodes, the latter two degrees of freedom being eliminated by static condensation. Elements with variable section and inertia may be specified.

The BCE mass discretization results from static lumping of the element mass at both end nodes.

The complete structure can be idealized as an assembly of both cable and beam-column finite elements. The stiffness matrix, nodal force vector and lumped mass matrix of the discretized structure are obtained by direct superposition of the stiffness matrices, applied nodal forces and lumped masses, respectively, of the individual elements, after a transformation to common or global coordinate systems at all interconnecting nodal points.

In this investigation, the guyed mast structure was assumed to be symmetric and symmetrically loaded with respect to a vertical X-Y plane, where Y is the

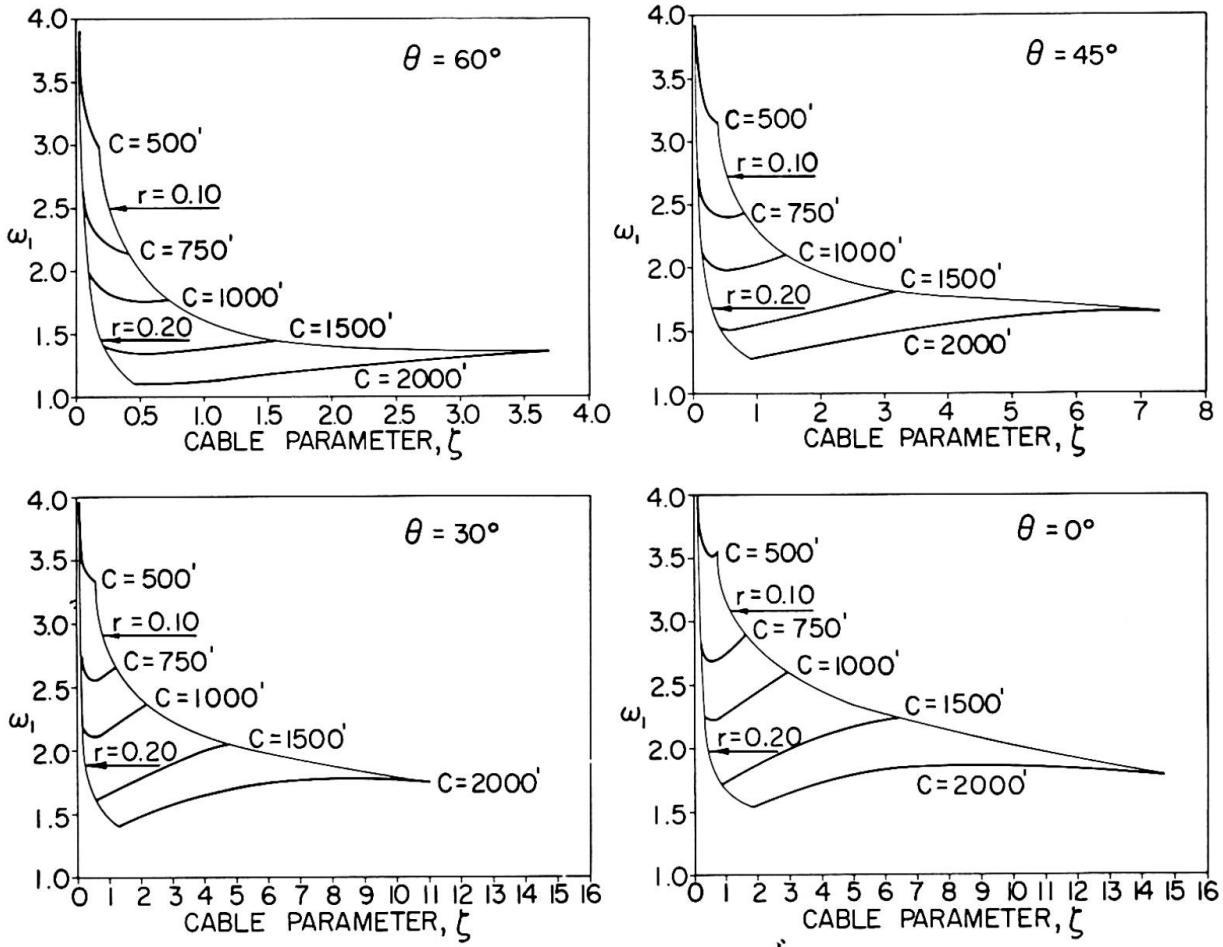

FIG. 4 FIRST NATURAL FREQUENCY ω_1 (rad/sec) OF GUY CABLES INCLINED AT $\theta°$, CROSS-COUPLING BETWEEN MODES INCLUDED

vertical shaft axis. A finite element may represent either a single structural component in the X-Y plane, or two members initially located in two vertical planes X'-Y and X"-Y symmetrically placed with respect to the X-Y plane, and which remain symmetrically located after deformation. Thus the actual three-dimensional problem is reduced to a two-dimensional problem.

3.2 Loading Actions

Static Loading: In the static analysis, the structure is subjected to its own weight and the mean or steady wind pressure. The dead load is converted to nodal forces by static lumping at the nodal points. The wind forces are calculated by assuming that the wind acts in the direction of the horizontal X axis defined in Section 3.1, and that the mean velocity $\bar{V}_X(Y)$ at any height Y is given by the well-known power law (10). The wind pressure on each finite element is assumed to be uniform and determined by the velocity at the midheight and the geometric and aerodynamic properties of the member (exposed width and drag-lift coefficients). The resultant element wind forces are then lumped at the end nodes. In addition, concentrated wind forces intended to represent certain concentrated areas such as insulators, reflectors, etc., may be specified at any nodal point.

Gust Loading for Deterministic Dynamic Analysis: The deterministic gust analysis requires the specification of a wind velocity history from a set of digitized velocity records $V_X(t,Y_i)$ taken at several heights Y_i. This input can be conveniently reduced to a dimensionless or "reduced" pressure fluctuation

$$\mu_x(t,Y) = \frac{q_x(t,Y)}{\bar{q}_x(Y)} - 1 \qquad (3\text{-}1)$$

where q_x is the dynamic pressure corresponding to V_x and $\bar{q}_x$ is the average over the sample used. Interpolation may be used if $Y \neq Y_i$. In order to simplify the analysis procedure in the present case, however, a reduced pressure fluctuation $\bar{\mu}_x(t) = \mu_x(t,Y_m)$ computed from a sample taken at height Y_m was used over the entire structure as a multiplier on the actual static wind force distribution. This assumption is probably conservative, since the vertical correlation decay is neglected.

Gust Loading for Non-deterministic Dynamic Analysis: The following assumptions were made for the non-deterministic gust analysis:

(a) The horizontal gust component $V_{gx}(t,Y) = V_x(t,Y)-\bar{V}_x(Y)$ is a stationary Gaussian random variable and small with respect to $\bar{V}_x$.
(b) The cross-spectral density function proposed by Danvenport (10) and described by Ferry Borges in the theme paper (11) represents the vertical correlation of horizontal gustiness.
(c) The drag and lift coefficients are independent of the vibration frequencies.
(d) The peak intensity level (σ-level) of the response components is a function of both the response spectra and the wind sample duration, as proposed by Davenport (12), but extended for multi-degree of freedom systems.

3.3 Analysis Procedure

This Section describes briefly the main steps of the computer analysis of the discretized structure.

Static Solution: Because of the presence of the guy cables, the structure is geometrically non-linear. The static equilibirum position (SEP) under the static loading is determined by a matrix iterative procedure of Newton's type. A typical linearized step includes the following sequence of operations:

(a) Calculate the external nodal forces on the present geometry and the internal nodal force resultants from the element forces (axial forces and bending moments) determined at the previous step (in the first step, the only internal element forces are the initial cable tensions specified on the initial geometry). The unbalanced nodal forces are the difference of the external and internal forces.
(b) Evaluate the tangent structural stiffness and solve for incremental nodal displacements, which, when added to the previous displacements, define the new structure configuration.
(c) Calculate the internal element forces in the new geometry (for each cable element, the cubic equation (2-1) must be solved for T). Then repeat steps (a) through (c).

The convergence to the SEP can be conveniently measured by the magnitude of the unbalanced nodal forces corresponding to the unconstrained nodal displacements. Usually 4 to 6 iteration cycles are found to be sufficient for most problems.

Frequency-mode Analysis: For the dynamic analysis, the structure is assumed to oscillate linearly about the SEP. This assumption permits standard matrix mode-superposition techniques to be used for both the deterministic and the non-deterministic cases. A set of "m" significant lowest frequencies ω_r and associated vibration modes $\{\Phi_r\}$ is obtained by solving the vibration eigenvalue problem:

$$[K]\{\Phi_r\} = \omega_r^2 [M]\{\Phi_r\} \qquad (r = 1,2...m) \qquad (3\text{-}2)$$

where $[K]$ is the tangent stiffness matrix at the SEP and $[M]$ the lumped mass matrix. This is accomplished by reducing (3-2) to a standard eigenvalue problem form after elimination of all rotational degrees of freedom.

Deterministic Gust Analysis: The normal response amplitudes $Y_r(t)$ are obtained by solving the modal response equations

$$\ddot{Y}_r(t) + 2\gamma_r\omega_r\dot{Y}_r(t) + \omega_r^2 Y_r(t) = P_r\,\bar{\mu}_x(t) \qquad (r = 1,2,\ldots m) \qquad (3\text{-}3)$$

where $P_r = \langle R_w^T \rangle \{\Phi_r\}$ are the static generalized wind forces calculated using the static wind forces $\{R_w\}$ at the SEP, and γ_r are the modal damping coefficients. The time history of any desired quantity $z(t)$ about its SEP value is given by

$$z(t) = \sum_{r=1}^{m} B_{zr}\, Y_r(t) \qquad (3\text{-}4)$$

where B_{zr} are the modal influence coefficients of z. The program generates time response plots of nodal displacements, nodal accelerations and internal element forces, as well as the peak or envelope values.

Non-deterministic Gust Analysis: The gust response spectra of the discretized structural model are evaluated for each contributing vibration mode using standard random vibration techniques (13). This procedure requires a double integration to be performed over the structure, the integration being reduced to a double summation over the model elements using a Gauss-Legendre numerical quadradure formula for a set of conveniently spaced frequencies (from $\omega = 0$ to $\omega = 2\omega_r$). The modal variances σ_r^2 are then computed by numerical integration of the response spectra over the significant frequency range. A program option allows the cable elements to be excluded from the analysis for the purposes of comparison.

The variance or mean square oscillation σ_z^2 of any desired quantity $z(t)$ is easily calculated by mean square superposition of the modal variances weighted by the modal influence coefficients B_{zr}. Finally, σ_z is multiplied by the peak value or σ-level of $z(t)$, which is computed as proposed by Davenport (12).

4. GUYED MAST EXAMPLE

4.1 Description

A tall guyed mast having four sets of three-way guy cables and a cantilever antenna was chosen for the present example. The dimensions and structural properties of the system, see Fig. 5, were based on the CFPL mast described by Hartmann and Davenport (8) with certain modifications.

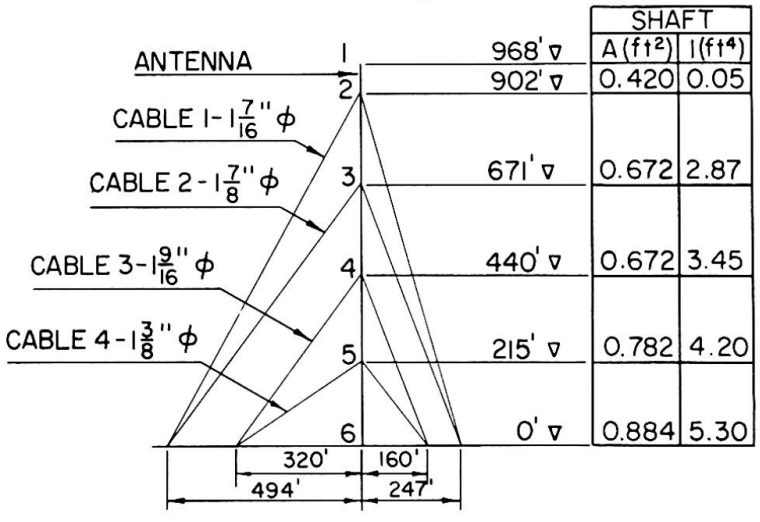

SHAFT	
A(ft²)	I(ft⁴)
0.420	0.05
0.672	2.87
0.672	3.45
0.782	4.20
0.884	5.30

FIG.5 MAST PROPERTIES AND GEOMETRY

The fluctuating wind velocities used in the deterministic dynamic studies were obtained from the NASA 150-meter meteorological tower located at the Kennedy Space Center (KSC) in Florida. The data was recorded on magnetic tape and then digitized at 10 records per second (14), although in the present investigation data intervals of 0.5 seconds only were used, the velocity at

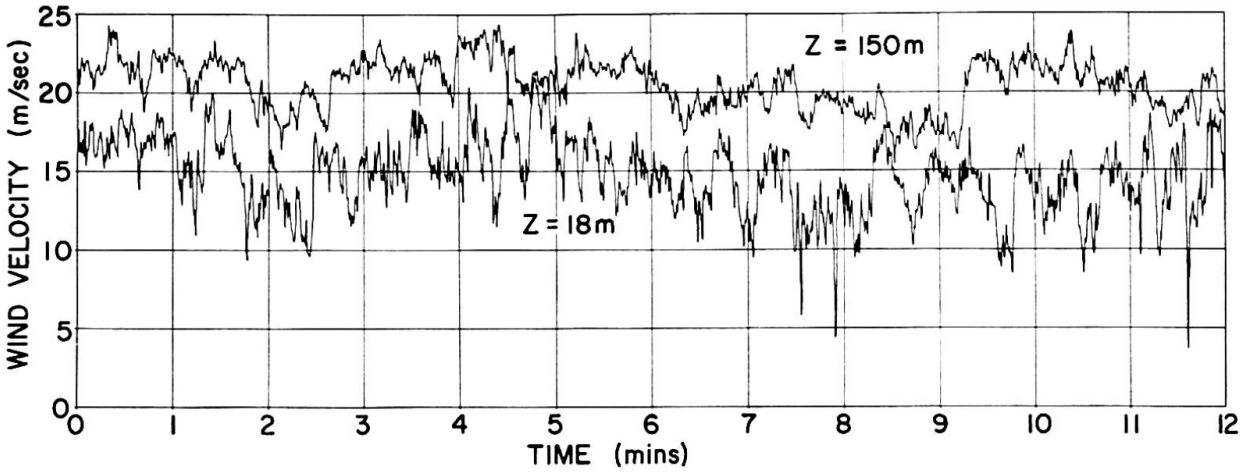

FIG. 6 WIND VELOCITY RECORD FROM 18m AND 150m KSC MET. TOWER

each interval being the average of five digitized values. A plot of a 12 minute segment of the wind velocity record measured at the 18- and 150-meter levels is shown in Fig. 6, which clearly indicates the increase of the mean velocity with height and the randomly fluctuating nature of the gusts. It is also noted that the fluctuations are somewhat more intense at the lower elevation, and, for this reason, the wind records used to evaluate the system responses were taken from the 150-meter level, corresponding to about mid-height of the mast. Wind velocity inputs of about 2 minutes deviation were considered sufficient to give estimates of the responses, since the longest periods of the system rarely exceed 5 seconds.

The mast was assumed to be located in open country, for which the mean wind velocity was taken to follow a 1/7th power law variation with height. The parameters required to completely define the cross-spectral density of the horizontal wind velocities proposed by Davenport (10), namely the ground drag coefficient and exponential decay coefficient, were taken to be 0.001 and 7, respectively.

4.2 Refinement of the Guyed Mast Model

To avoid excessive computer analysis time, tests were made to determine the least refined model, which still gives uniform responses compared with more refined models. Three models were considered, see Fig. 7, with the properties shown in Fig. 5 and also with the shaft elements considerably stiffened. The initial cable tension level was taken to be about 11.5% (standard) of the breaking strengths for each test, and the mean wind velocity +75 mph at the 10-meter elevation. The viscous damping of the system in this and subsequent tests was taken to be 0.6% of critical for all modes.

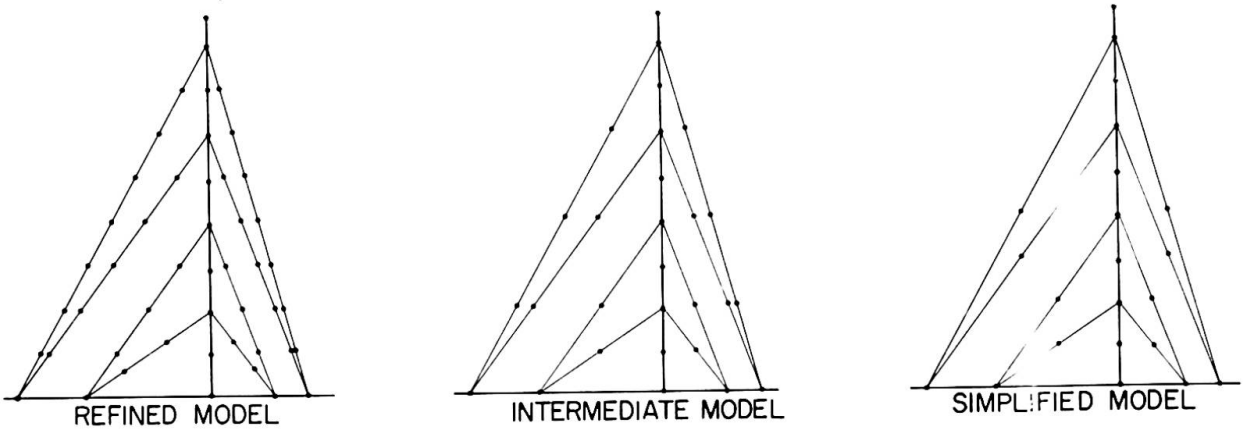

FIG. 7 NODAL POINT ARRANGEMENTS FOR GUYED MAST MODELS

The results of the static and deterministic analyses showed that the intermediate model responded in a uniform manner compared to the refined model (which should be used to obtain the responses in the final analysis of a real problem), whereas the simplified model responses suffered considerable variability. The intermediate model was then used to study the influence of a number of parameters on the system responses, with a saving in computer time of the order of 60% for a full static and frequency-mode analysis, and up to about 35% for a deterministic dynamic analysis. The parameters studied include shaft stiffness, initial cable tensions, the mean and fluctuating wind velocities, and the wind on the cables.

4.3 Results of the Guyed Mast Studies

Static Responses: The results of numerous tests on the intermediate model for the influencing parameters outlined above indicate that the shaft responses are controlled largely by the cable sizes and spatial arrangements, and, once these have been selected, the shaft displacement and bending moments are little influenced by changes in the initial cable tensions or the shaft stiffness. Increasing the cable sizes by 50% resulted in reductions in the shaft displacements of up to 30% for identical initial tensions. The shaft moments in this case were redistributed, but still little changed in magnitude, indicating that the flexural behavior of the shaft is a relatively unimportant design parameter for a given cable arrangement. For initial tensions between 10-20% of the breaking strengths it was also found that, although the guy cables exhibit nonlinear properties locally, the overall guyed mast behavior is closely linear for wind velocities up to about 60 mph, beyond which linearity is lost.

In the above tests the $\bar{z}$-displacements (see 2.1) of the CE were neglected, and further tests using a revised program to include these effects showed that the shaft displacements had been underestimated for positive winds and overestimated for reversed winds, resulting in a loss of linearity of the system for positive winds. The influence of the $\bar{z}$-displacements of the CE emphasizes the importance of including the wind on the cables in any analysis.

Deterministic Dynamic Responses: Increasing the shaft stiffness was found to have little effect on the cable modes of the system, since the static cable tensions at the SEP are themselves unaffected, but has a direct influence on the predominant shaft mode frequencies, which results in some increase in the shaft displacements and a rapid increase in the shaft bending moments. Increasing the initial cable tensions, however, had the opposite effect and the predominant cable modes only were influenced. The result in this case was a slight overall reduction in the shaft displacements and moments, although these effects were somewhat variable, particularly for the antenna cantilever, which tends to act as an independent appendage and has a considerable influence on the shaft modes.

As stated earlier, a two minute fluctuating wind input taken from the 150-meter level of the KSC met. tower was used to evaluate the deterministic dynamic responses in the tests to study the various influencing parameters. The responses due to records of one, two and three minutes duration taken from the 150-meter level are listed in Table 1 for comparison, since it may be postulated that, for a record of duration less than 20 minutes or so, the probability of higher intensity wind gusts occuring in the record increases with increased length of the record. To illustrate the effect of the apparent increased gustiness at lower elevations of the KSC tower data, the responses due to a two-minute input taken from the 30-meter level are also tabulated. In each case the responses are based on the SEP due to a +75 mph mean wind velocity at 10-meters, with the $\bar{z}$-displacements neglected. Effective "gust factors" based on response are presented for comparison with the non-deterministic results and the quasistatic procedures commonly used in design offices. Shaft axial force and cable tension responses are not tabulated, since the dynamic

contributions were found to be generally small, usually less than 30% of the corresponding static maxima.

Table 1

Response	KSC met. wind record (duration/elevation)			
	2 min/30m	1 min/150m	2 min/150m	3 min/150m
x-acceleration				
*Node 1	0.71g	0.27g	0.31g	0.35g
2	0.29g	0.09g	0.10g	0.10g
x-displacement (ft)				
Node 1	3.93	1.29	1.77	1.94
2	1.48	0.59	0.76	0.88
3	0.92	0.28	0.57	0.59
4	0.81	0.24	0.42	0.47
Gust factor on x-displacement				
Node 1	2.88	1.62	1.85	1.93
2	2.11	1.45	1.57	1.66
3	2.16	1.35	1.72	1.74
4	2.59	1.47	1.82	1.92
Bending moment (kft)				
Node 2	355.0	128.5	161.0	171.5
3	530.5	230.5	271.0	291.9
4	316.0	114.5	127.0	194.0
5	441.5	119.0	201.5	222.9
Gust factor on bending moment				
Node 2	4.64	2.32	2.65	2.76
3	2.16	1.50	1.60	1.64
4	2.68	1.61	1.68	2.03
5	2.76	1.47	1.80	1.89

*See Fig. 5

Due to the coupling between the system modes and the dependence of modal sequence on the overall system stiffness, it is difficult to preselect the important modes influencing the responses. Further tests to study the modal contributions showed that the choice of modes for the dynamic response calculations can be made on the basis of the magnitudes of the modal generalized forces, and this procedure was adopted for the non-deterministic analyses.

Non-deterministic Dynamic Responses: The non-deterministic responses of the intermediate model listed in Table 2 were evaluated from the SEP's due to the +75 mph basic mean wind velocity, first with the $\bar{z}$-displacements of the cables neglected, for comparison with the deterministic results in Table 1, and then with the $\bar{z}$-displacements included. Also tabulated are the mean peak intensity levels (see 3.2) and the effective "gust factors" for each response. The axial force responses are again omitted, due to the relatively small dynamic influences involved.

The effect of ignoring the $\bar{z}$-displacements of the cables is seen to overestimate the system responses by up to about 20%, although it was found in further tests that the corresponding responses may be underestimated by as much as 40% if the wind pressure on the cables is ignored completely in both the static and dynamic analyses. It is noted from Table 2, however, that the shaft acceleration responses are not affected by the $\bar{z}$-displacements of the cables, since they are mainly influenced by the predominant antenna-shaft modes.

The shaft displacement responses obtained by neglecting the $\bar{z}$-displacements of the cables are seen to compare fairly closely with the corresponding deterministic responses due to the 30-meter wind record, which is clearly conservative since the same gustiness is assumed over the full height of the

mast. The average gustiness of the 150-meter record provides the more realistic deterministic responses, which tend to maximum values somewhat less than the non-deterministic responses.

Table 2

Response	z-displacements neglected	P*	z-displacements included	P*
x-acceleration				
Node 1	0.57g	4.42	0.57g	4.42
2	0.26g	4.49	0.26g	4.50
x-displacement (ft)				
Node 1	3.60	4.35	3.28	4.37
2	1.62	4.34	1.34	4.37
3	0.41	4.44	0.37	4.45
4	0.33	4.45	0.31	4.46
Gust factor on x-displacement				
Node 1	2.73		1.95	
2	2.22		1.55	
3	1.52		1.33	
4	1.65		1.52	
Bending moment (kft)				
Node 2	280.7	4.42	278.5	4.42
3	458.5	4.42	375.0	4.40
4	221.0	4.52	209.0	4.51
5	228.5	4.49	229.5	4.49
Gust factor on bending moment				
Node 2	3.88		3.81	
3	2.00		1.58	
4	2.18		2.02	
5	1.91		1.84	

*P = peak intensity level (sigma level)

5. CONCLUSIONS

The finite element model is shown to provide a suitable representation of the guyed mast and allows detailed static and dynamic analyses to be performed on a fully integrated system. Several hitherto ignored factors, such as the wind effect on the cables and concentrated areas, and the use of the deflected static equilibrium position as the mean dynamic configuration, can be naturally included. The behavior of the actual structure can be arbitrarily approximated by a mesh refinement process limited only by the capacity of the computer program, and the incorporated static and kinematic assumptions.

The computer program has been used in the analysis of a number of complex guyed mast systems, but can also treat arbitrary two dimensional structures, including suspension bridges. Moreover, the methods described in this paper can be extended to include any conceivable structural system by constructing the appropriate finite element models.

The deterministic responses due to a single wind record sample depend on the duration of the sample, as well as the atomospheric conditions at the time and place of measurement. These observations suggest that wind record samples are not a useful means of determining the probable maximum responses, unless an ensemble of such samples is used and the resulting responses evaluated on a statistical basis. This procedure is tedious and uneconomic, and, due to the random nature of the wind gusts, the use of stochastic procedures is clearly the more rational approach. Deterministic methods, however, do have useful

applications in providing time-histories of response, particularly if used in conjunction with actual response measurements.

REFERENCES

(1) Walmsley, T., "Length, tension, and sag of stay ropes." Proc. I.C.E., No. 19, 1924 (paper 4481).

(2) Routh, R. J., "Advanced rigid dynamics" (Macmillan 1st edn. published 1860).

(3) Rohrs, J. H., "On the oscillations of a suspension chain." Trans. Cam. Phil. Soc., 9, 1851.

(4) Kolouŝek, V., "Solution Statique et dynamique des pylones d'antennae haubanes." Pub. IABSE, Vol. 8, 1947.

(5) Cohen, E. and Perrin, H., "Design of multilevel guyed towers." ASCE Journ., Vol. 83, ST5, Sept. 1957.

(6) Dean, D. L., "Static and dynamic analysis of guy cables." ASCE Journ., Vol. 87, ST1, Jan. 1961.

(7) Davenport, A. G. and Steels, G. N., "Dynamic behavior of massive guy cables." ASCE Journ., Vol. 91, ST2, April 1965.

(8) Hartmann, A. J. and Davenport, A. G., "Comparison of the predicted and measured dynamic response of structures to wind." Eng. Sc. Res. Report ST-4-66, Univ. Western Ontario, London, Canada, 1966.

(9) Shears, M., "Static and dynamic behavior of guyed masts." Univ. of California Structural Engineering Lab. Research Report No. 68-6, 1968.

(10) Davenport, A. G., "The application of statistical concepts to the wind loading of structures." Proc. Inst. Civil Engrs., Vol. 19, 1961.

(11) Ferry Borges, J., "Dynamic Loads." Theme VI paper. VII Congress of IABSE, New York, Sept. 1968.

(12) Davenport, A. G., "Note on the distribution of the largest value of a random function with application to gust loading." Proc. Inst. Civil Engrs., Vol. 28, 1964.

(13) Crandall, S. H. and Mark, W. D., "Random vibrations in mechanical systems." (Academic Press) 1963.

(14) Scoggins, J. R., "Some properties of low altitude atmospheric turbulence at Cape Kennedy, Florida." NASA TMX-53640, July 1967.

SUMMARY

This paper reports detailed computer studies made using a suitable discretized model to investigate the response characteristics of guyed masts under the action of turbulent wind influences. The actual structure is idealized in the form of a finite element model, which is fully integrated geometrically and structurally. Estimates of the dynamic responses of a tall, guyed mast are evaluated deterministically using actual wind velocity records and non-deterministically using the theory of random vibrations and incorporating available wind velocity spectra. A comparison between the deterministic and non-deterministic responses, and a discussion of the relative merits of the two procedures is presented.

RÉSUMÉ

On présente ici une technique detaillée d'analyse sur ordinateurs de la réponse de mâts haubannés sous l'action du vent turbulent. La structure est représentée par un modèle discret d'éléments finis qui tient compte de tous les paramètres géométriques et structuraux actuels. La réponse dynamique d'un mât haubanné élevé est obtenue de deux façons: par une méthode déterministique utilisant des vitesses du vent réellement enregistrées; et par un modèle statistique qui utilise la théorie des vibrations aléatoires et des spectres de réponse au vent probables. On compare les solutions obtenues par les deux méthodes et l'on discute leurs mérites respectifs.

ZUSAMMENFASSUNG

Dieser Bericht enthält detaillierte Computer-Analysen des charakteristischen Verhaltens abgespannter Maste unter dem Einfluss von turbulentem Wind. Das eigentliche Bauwerk ist durch endliche Elemente idealisiert, das alle geometrischen und baulichen Parameter enthält. Das dynamische Verhalten von hohen abgespannten Masten wurde mit zwei Methoden ermittelt: Die erste basiert auf eigentlichen Windgeschwindigkeitsmessungen und die zweite verwendet statistische Methoden unter Zuhilfenahme von vorhandenen Windgeschwindigkeitsverteilungen. Ein Vergleich dieser beiden Verfahren mit ihren jeweiligen Vor- und Nachteilen wird erläutert.

Leere Seite
Blank page
Page vide

VI

Wind Resistant Design of a Cable-Stayed Girder Bridge

Le calcul de la résistance au vent pour le pont à haubans

Über den Windwiderstand der seilverspannten Brücke

EIICHI MURAKAMI
Dr. Eng., Manager
Japan Highway Public Corporation
Japan

TADAYOSHI OKUBO
Chief, Structure Section
Public Works Research Institute
Ministry of Construction
Japan

1. Introduction

Because of the development of structural analysis methods, computation measures, available materials and construction technique, dimensions and flexibility of recent bridges have been increased and the damping capacity of them has been decreased. As a result of these, recent bridges are liable to be subjected to not only static wind effects but dynamic ones. Cable-stayed girder bridges are one of the examples of them.

The authors consider that structures have to be designed against wind effects shown in Table-1. When a structure is rigid enough, only the aerodynamic wind forces shall be considered; but for a flexible structure, dynamic effects together with the static instability phenomena shall be considered. In the case of cable-stayed girder bridges, aerodynamic wind forces, aeolian vibration, galloping and/or torsional flutter among the wind effects listed in Table-1 will have a prime importance.

Table - 1 Wind Effects on Structures

Wind effects	Static effects	Aerodynamic wind forces	Drag, lift, pitching moment
		Static instability problem	Divergence
			Lateral buckling of girder
	Dynamic effects	Forced vibration	Random vibration
			Aeolian vibration
		Self-excited vibration	Galloping
			Torsional flutter
			Coupled flutter

As pointed out by J.F. Borges in his introductory report on the subtheme "Dynamic Loads", the estimation of wind velocity is a fundamental problem for the wind-resistant design of structures. The life time and height of structure, the local condition of structure site and the turbulence in wind mainly govern the estimation of wind velocity.

Among these factors wind turbulence will have two aspects in its influence on the estimation of wind velocity. The first is the spatial distribution of turbulence and the second is the structural response caused by turbulence. By considering the spatial distribution of turbulence, wind velocity on shorter bridges shall be greater than those on longer ones. The relation between wind velocity and the dimension of structures has already been derived in the tentative design criteria against wind effects for proposed Honshu-Shikoku bridges (1). On the other hand, effects of random vibrations excited by wind turbulence may be substituted by increasing the wind velocity so as to represent the expected maximum stress conditions in the structure, but, so far as the authors know, the quantitative modification of wind velocity has not yet been obtained.

In this contribution, the authors describe the wind-resistant design process of the Onomichi Bridge, including the estimation of wind velocity, results of the wind tunnel model tests and the vibration tests on the completed bridge. It is already shown that cable-stayed girder bridges not always possess a satisfactory stability against dynamic wind actions (2) (3). The wind tunnel model tests for the original design of Onomichi Bridge showed an unsatisfactory aerodynamic stability, too. However, fabrication of the bridge had been simultaneously progressed during the model tests and only a limited change in the sectional shape of girder was possible. Among several alternatives, a plan to install a lane of open grating at the center of bridge floor showed an improvement in increasing the critical wind velocity and was adopted.

Vibration tests on the dynamic characteristics of the completed bridge such as natural frequencies, vibration modes and structural damping were conducted. The measured structural damping was comparatively low which showed the possibility of wind excited vibration.

In the conclusion, the authors emphasize the necessity of the thorough investigation by wind tunnel model tests in the designing process of cable-stayed girder bridges.

2. Outline of the Onomichi Bridge

The Onomichi Bridge, which is located in the Seto-Inland Sea and spans a sound of about 200 meter wide between Onomichi City and Mukaijima, is a cable-stayed continuous girder bridge of 215 meters center span and 85 meters two side spans. The continuous girder of the bridge consists of two plate girders 3.2 meter high and steel plate deck 10.4 meter wide.

As shown in Figure-1, the girder is stayed at both sides by locked coil ropes in a fan shape. The ropes are supported by two towers of 72.6 meter high and are fixed at the girder ends and tower ends.

Natural frequencies of the bridge are approximately calculated as shown in Table-2. The ratio of fundamental natural frequencies in torsional mode and flexural mode is about 2.93.

Table - 2 Natural Frequencies of the Onomichi Bridge

(c/s)

Mode	Symmetric Mode			Asymmetric Mode		
Order	1st.	2nd.	3rd.	1st.	2nd.	3rd.
Vertical flexural vibration	0.581	1.385	1.795	0.914	1.562	2.249
Torsional vibration	1.706	3.942	4.536	3.055	3.978	5.543

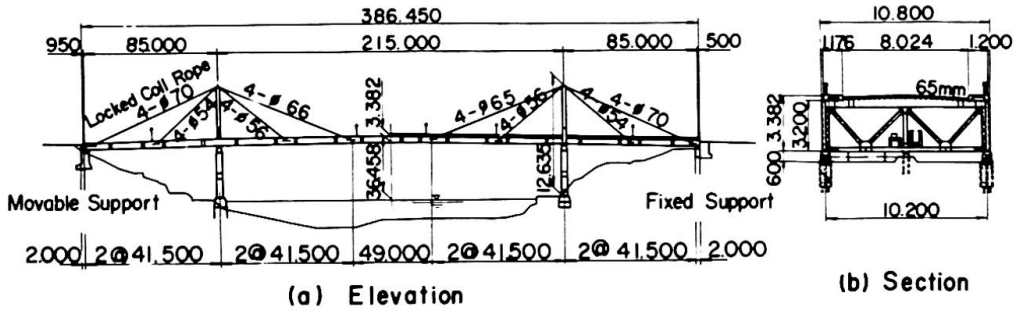

Figure-1 Elevation and Section of Onomichi Bridge

3. Estimation of expected wind velocity

By reason of the importance and the life time of the Onomichi Bridge, 100 years period was chosen as the return period for estimating wind velocity.

About 5 kilometers apart from the bridge site, a meteorological observatory station exists and observed wind velocity data of 10 minutes duration after 1942 are available. Assuming the double exponential distribution of probability density of the annual maximum wind velocity, the return values in period of 50 and 100 years at the station are estimated as 21.5 and 22.8 m/s, respectively. The values should be modified by considering the difference of topographical condition between the bridge site and the station.

On the other hand, in connection with the meteorological survey for the proposed Honshu-Shikoku bridges, multi-regression analysis upon return values of wind velocity in the area of Seto Inland Sea were conducted. In the analyses, the influences of local topographical conditions such as the openness and undulation of topography, rate of sea area and others were taken into account. As the estimated values at the bridge site, 29.6 and 31.8 m/s for 50 and 100 years return periods were obtained by this method. However, because the multi-regression analyses were conducted for applying the wide area of Seto Inland Sea and it was not so sufficient to apply for the estimation of wind velocity in the local area, the values obtained by this method were ignored and 22.8 m/s was chosen as the fundamental value for estimating wind velocity at the bridge site.

By taking into account of the effect of convergence of wind in a narrow channel and other topographical conditions, wind velocity at the bridge site was estimated 1.2 times of those at the station, that was 27.4 m/s. It was considered that the comparatively low value of wind velocity was resulted from the greater roughness of ground surface around the bridge site. Therefore, 1/4 was assumed as an exponent of the power law for the vertical profile of wind velocity, which resulted in the modification factor of 1.377 at the altitude of the bridge girder of 36 meters.

As described in the introduction, wind velocity should vary according with the dimension of structure. The modification factor for the span length of 215 meters is 1.208 according to the design criteria for the proposed Honshu-Shikoku bridges.

As the result of modification of wind velocity mentioned above, 45.5 m/s was obtained. The aerodynamic stability of the bridge was judged by this value.

4. Wind loads and calculated critical wind velocities

In design of the Onomichi Bridge, horizontal wind loads of 1680 kg per linear meter of the girder and of 300 kg per unit area (m^2) of towers were taken into account according to the "Design Specifications for Steel Highway Bridges". As shown later, the wind tunnel model tests showed smaller value of drag acting on the girder than the above mentioned value.

The critical wind velocity for the lateral buckling was calculated by a formula derived by Hirai and Okauchi (4). In the calculation, values of drag and lift coefficients obtained by the wind tunnel model tests were used. The calculated value was 148.5 m/s and was far beyond the above mentioned wind velocity of 45.5 m/s.

Also, the critical wind velocity for the coupled flutter was calculated by introducing aerodynamic forces on the flat plate derived by Theodorsen, for the purpose of reference, though the air flow around the bridge girder usually separated from the surface of structure and the theory based on the potential flow could not be applied. The calculated value was 78 m/s and exceeded the above mentioned value of 45.5 m/s.

5. Wind tunnel model tests

Measurements of three components of aerodynamic forces and instability tests were conducted on section models of 1/25.6 scale. A wind tunnel of Göttingen type was used for the tests, which had the test section of 3.0 meter high and 1.8 meter wide. The maximum wind velocity of the tunnel was 23 m/s. A detailed description of the tunnel is shown in the reference (5).

In the measurements of aerodynamic forces, an electrical beam balance was used. In the instability tests, the model was mounted horizontally on a spring system with its spanwise axis normal to the wind flow. The model was allowed vertical and/or pitching motions separately or in coupled motion.

The polar moment of inertia and the mass of model per unit span were simulated to those of the prototype. No reliable value of structural damping of the actual bridge was available for the authors, those of the prototype in flexural and torsional motion were assumed to be 0 06 and 0.05, respectively. Damping of the model were kept as low as possible and, for the model of modified final design, an additional damping was given by a set of electromagnetic dampers. The ratio of torsional frequency to the flexural ones of the prototype in the fundamental mode was about 2.93, but because of the installation mounting the model, the ratio of the model was about 2.

The similitude on the reduced velocity was used in the conversion of wind velocity from model to prototype. In other words, the value of reduced velocity V/NB, in which V, N and B were the wind velocity, the frequency of vibration and the representative linear dimension of model and prototype, was assumed same for model and prototype.

As the wind tunnel model test on the original design progressed, it was revealed that a negative slope of lift coefficient curve was found in the measurement of aerodynamic forces and galloping vibration started in comparatively low wind velocity in the instability test; so, changes in external shape of the bridge girder were required. However, at that time, fabrication of the girder was simultaneously progressed and only a slight change was possible.

Several alternative plans were proposed and tested in the wind tunnel and finally a plan to install a lane of open grating at the center of girder was adopted. Table-3 shows the required and actual values of models for the original and modified final design. For the brevity, results of the model tests only for the original and modified final design are shown in this contribution.

Aerodynamic coefficients of the girder sections are shown in Figure-2. The negative slope of lift coefficient appeared in the original design could not be diminished even in the modified final design. However, as seen in Figure-3, the dynamic behavior of model was improved. Figure-3 (a) shows relations between amplitude and wind velocity in flexural vibration when models were subjected to horizontal wind. Conditions of models were different, so wind velocity converted to the prototype is shown in the figure.

Table - 3 Values of Model

Model	Weight		Polar moment of inertia		Structural damping	
	required	actual	required	actual	flexural	tortional
	gr.	gr.	gr-cm-s^2	gr-cm-s^2	δ_h	δ_α
Original	7667	7648	3620	3430	0.060	0.022
Modified final	7667	7679	3620	3650	(0.029 0.065*	(0.008 0.050*

Frequency		Frequency ratio	
flexural Nh	torsional Nα	required	actual
c/s	c/s		
1.55	3.48	2.93	2.25
1.80	3.90	2.93	2.17

* With additional damping by electromagnetic damper units.

In the case of original design, vertical vibration of restricted amplitude set on at 9.6 m/s wind velocity and held out to the wind velocity more than 30 m/s. Beyond 35 m/s, the amplitude grew rapidly and the vibration became catastrophic. The predicted critical wind velocity of the prototype was about 38 m/s The tests on modified final design were conducted with two different damping values as shown in Table-3. The value of logarithmic decrement in vertical mode with additional damping were almost same with the test on original design. However, in the modified design, a restricted vibration set on at the wind velocity of about 13 m/s and lasted until 16 m/s. Beyond the wind velocity of 48 m/s, a vertical flexural vibration occurred again and the vibration became catastrophic with the increase of wind velocity. Thus, the critical wind velocity of 48 m/s was predicted for the modified design. The restricted vibration in the modified design seems to be an aeolian vibration and the catastrophic one a galloping. In the case of original design, it can be considered that overlaping of aeolian vibration and galloping have occurred.

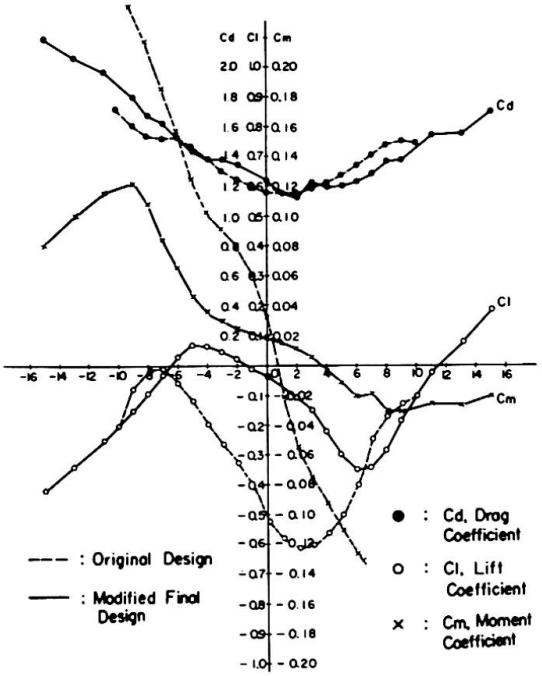

Figure –2 Aerodynamic Coefficients of Girder Section

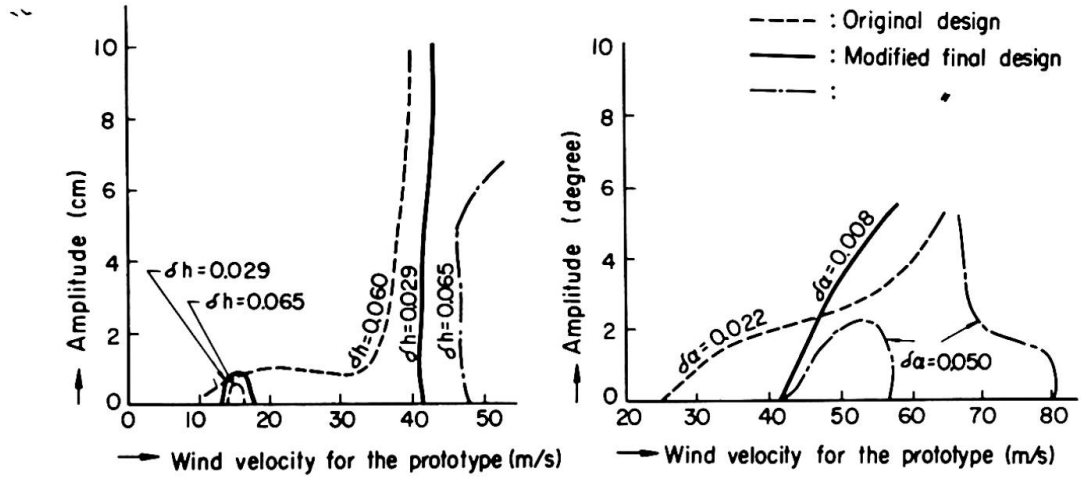

Figure – 3 Amplitude and Wind Velocity of Model Vibration

Figure-3 (b) shows relations of torsional amplitude and wind velocity. In this case, too, the manner of vibration was similar to those of flexural vibration. But the model of modified design with $\delta\alpha$ = 0.050 showed a noteworthy behavior in the range of wind velocity 67 to 80 m/s. In this range, when a small disturbance less than 2 degrees was given to the model, then the vibration died out, but when the initial disturbance exceeded 2 degrees, then the vibration diverged.

As seen in Figure-3, the value of structural damping influences the aerodynamic behavior of bridge. So the necessity of measuring the value of prototype was acutely felt and the vibration test of the Onomichi Bridge after its completion was scheduled during the model tests were progressed. For serving the prediction of aerodynamic behavior of the bridge after finding the value of structural damping of the completed bridge, a special analysis was applied to the records of wind tunnel model tests on the modified final design.

In general, the value of damping consists of structural damping and aerodynamic one and the aerodynamic damping varies according to wind velocity, amplitude of vibration, sectional shape of the structure and incidental angle of wind. From the diagrams showing the amplitude and numbers of vibration, we can obtain the values of damping corresponding to each amplitude and each velocity and can draw contour lines which show the relation among the values of damping, amplitude and wind velocity. Figure-4 shows such contour lines of flexural and torsional vibrations for the model of modified design with and without additional damping.

In Figure-4, (a) and (b) show contour lines in flexural motion without and with additional damping, respectively. The structural damping, which means the damping in still air, of the former is 0.029 and that of the latter is 0.065. The difference is about 0.035. If the superposition of structural damping was possible, zero contour in (b) must coincide with - 0.035 contour in (a). The comparison of (a) and (b) shows that this is correct qualitatively but not in the strictly quantitative meaning.

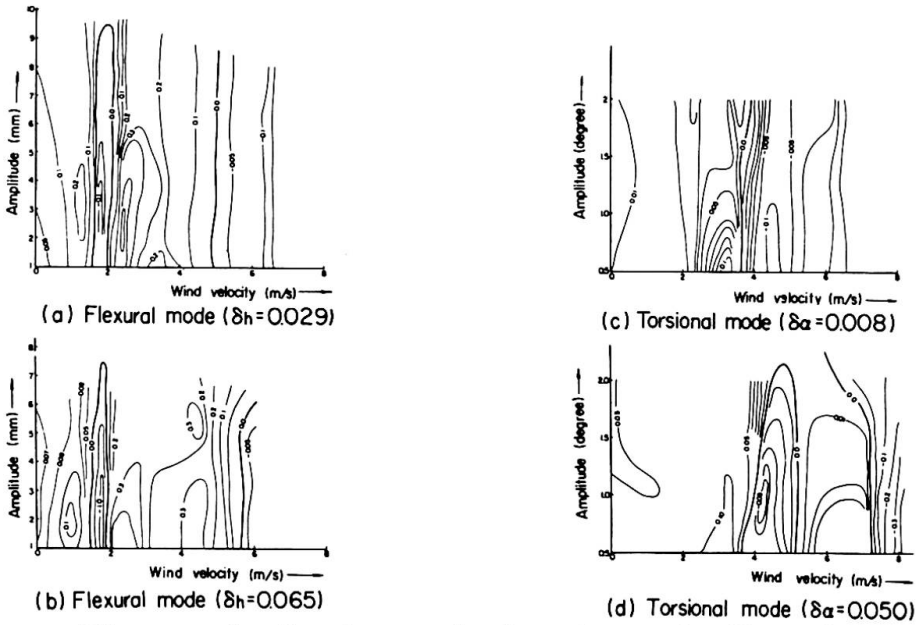

Figure-4 Contour of Aerodynamic Damping

Figure-4 (c) and (d) show contour lines in torsional motion. The structural damping of the former is 0.008 and that of the latter is 0.050 and the difference is about 0.04. In torsional vibration, too, zero contour line in (d) roughly coagree with - 0.04 contour line in (c). From the above facts,

the authors consider that these contour lines offer an effective supplementary measures for predicting the aerodynamic behavior of prototype.

6. Vibration tests of the completed bridge

After the completion of the bridge, vibration tests for surveying mainly structural damping were conducted. In the tests, the bridge was vibrated by specially devised twin excitors which were able to generate reciprocating forces in phase or out of phase and thus able to excite the bridge in any of flexural and torsional motions. Figure-5 shows a plan of twin excitors. The exciting frequency is variable from 0.2 to 10 c/s. The maximum exciting force per each unit at 10 c/s is 15 tons. A remarkable feature of the excitors is that the position of unbalanced weights can be changed during the operation so as to keep constant exciting forces regardless of frequency. The other remarkable feature of them is that the exciting forces can be eliminated within short period by moving unbalance weights into zero output position. The former is useful for recording resonance curves and the latter for causing a damped free vibration.

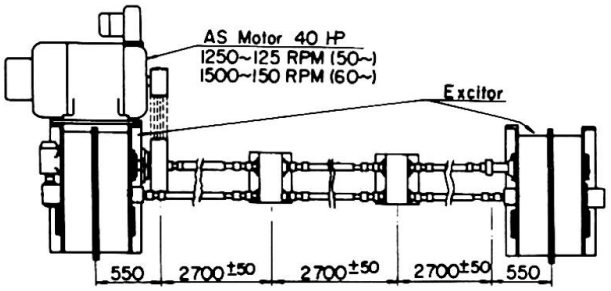

Figure-5 Plan of Twin Excitors

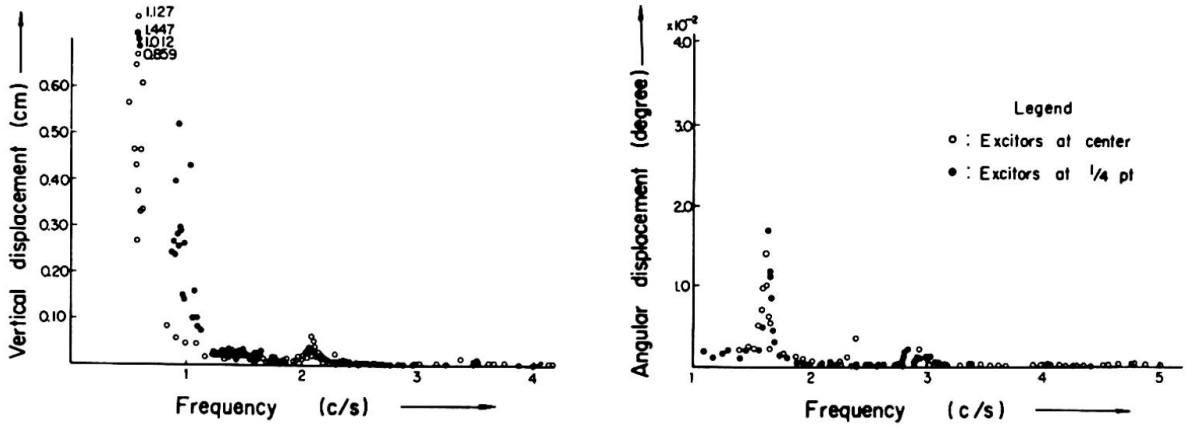

(a) Flexural Vibration (b) Torsional Vibration

Figure-6 Resonance Curve

Table - 4 Measured Natural Frequencies (c/s)

Mode	Symmetric mode		Asymmetric mode	
	First	Second	First	Second
Vertical flexural	0.58	1.38	0.92	1.62
Torsional	1.66	-	2.94	-

The excitors were installed at the center or at the quarter point of the center span. Motion of the bridge at every 1/8 point in the center span, every quarter point in the side spans and at the top of the tower were measured by using temporary installed accelerometers. Figure-6 (a) shows a resonance curve in vertical flexural vibrations and (b) shows those in torsional vibrations. Figure-7 shows modes of vibration in the fundamental symmetric and asymmetric modes of vertical flexural and torsional vibrations. Table-4 shows measured values of natural frequency. The comparison of Table-4 and 2 shows good coincidence of the calculated frequency and measured ones.

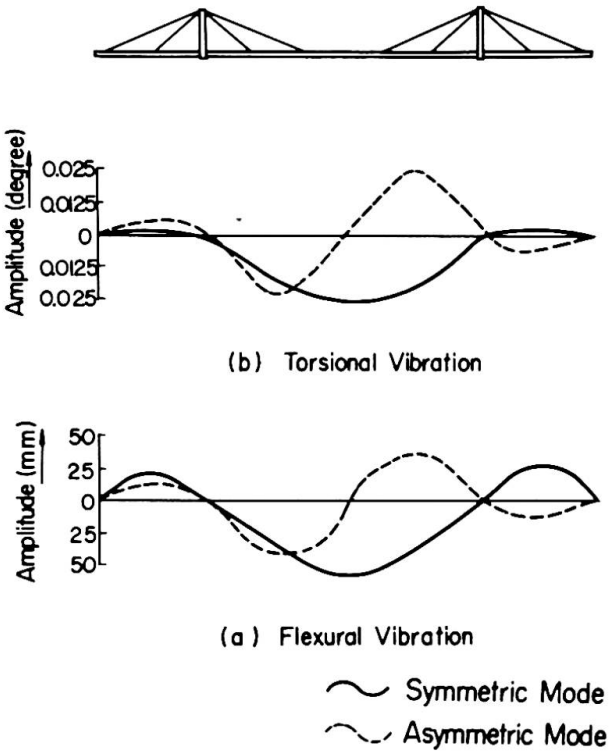

Figure-7 Modes of Vibration

Figure-8 shows diagrams of amplitude and number of vibration cycle in the damped free vibration of the bridge. The logarithmic decrements of the bridge were obtained by averaging the slopes in the diagram and were 0.05 for the vertical flexural motion and 0.035 for the torsional motion. The measured values are somewhat smaller than those assumed in the wind tunnel model tests.

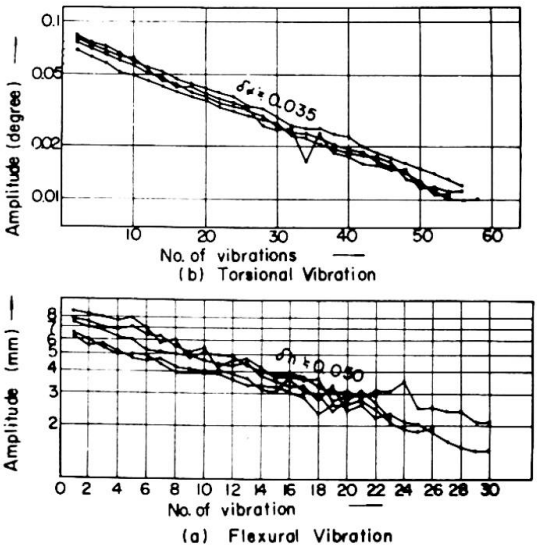

Figure-8 Decrement of Amplitude

7. Observation

As the results of wind tunnel model test show, the critical wind velocity of the Onomichi Bridge for the aerodynamic instability is not so high and possibly the restricted vibration occurs in low wind velocity. In fact, during the vibration tests, the bridge was subjected to wind velocity of about 13 m/s and a vertical flexural vibration of about 20 cm/s² acceleration, which was stationary, was caused by wind and was recorded. The observed frequency was almost equal to the natural frequency of vertical flexural vibration in the first symmetric mode.

For inspecting the dynamic behavior of the bridge under the wind action, two anemometers and ten accelerometers have been installed. One of the anemometers has been installed at the top of tower and the other at the center of main span. When wind velocity exceeds a certain amount, say 20 m/s, recording papers of these run fast and wind velocity of every two or three seconds can be obtained. Accelerometers are coupled with the anemometer at the center of main span, and when wind velocity exceeds the above amount, they start to record vibrations of the bridge. Vertical flexural, torsional and swaying vibrations can be observed.

Also, accelerometers can start to record vibrations caused by earthquake when ground acceleration exceeds a certain amount, say 5 cm/s^2.

8. Conclusion

In the introduction, the authors have classified wind effects on structures as shown in Table-1. The wind tunnel model tests on the Onomichi Bridge in steady wind have shown that aeolian vibration, galloping and torsional flutter of the bridge girder possibly occur and that cable-stayed girder bridges are liable to vibrate under wind actions as similar as other flexible structures.

When a structure is rigid enough, static wind loads such as drag, lift and pitching moment are enough to be taken into account in designing it. On the contrary, when a structure is flexible, not only static wind loads but dynamic wind effects on it should be considered. So it can be concluded that two major problems in the wind resistant design of structures are to estimate the design wind velocity and to consider dynamic wind effects on them.

There are several methods for estimating wind velocity, to which structures are subjected, but sometimes return values obtained by different methods differ from each other. The difference is considered to be mainly caused by the evaluation of influences of the local topographical condition at the structure site. On the local distribution of mean wind velocity, multi-regression analyses on return values, numerical calculation method based on the fluiddynamic equations, wind tunnel tests for topographical models and instrumental observation of the actual distribution are the evaluating methods. Studies for establishing an effective method of statistically estimating return values of maximum wind velocity taking into account the local topographical conditions of the structure site will be necessary.

At present, it is very difficult to represent dynamic wind effects on structures in terms of wind loads. In the near future, dynamic wind effect causing aeolian vibration on structures may be represented by a stationary external force acting on them and those causing random vibration (buffeting) may be represented by the equivalent increase of wind velocity. However, it would be essentially impossible to represent the dynamic wind effects causing self-excited vibrations in terms of wind loads, even in the case of soft flutter. Therefore from the

view point of wind resistant design of structures, especially flexible ones, "wind effect" instead of "wind loads" shall be considered.

The value of critical wind velocity, which governs the dynamic instability of structures, should be investigated for self-excited vibrations. Only the wind tunnel model test is the measures for predicting the critical wind velocity for the prototype. Besides the critical value of wind velocity, dynamic responses of structures such as the amplitude and frequency of vibration can be revealed by the model test.

From a functional point of view, Selberg (6) proposed three kinds of critical wind velocity in the soft flutter problems according to their torsional amplitudes. In this case, prediction of vibratory amplitude of structures is indispensable for evaluating the critical wind velocity of them. Because the vibratory amplitudes in the soft flutter are governed by the value of structural damping, contour lines of aerodynamic damping related to amplitude and wind velocity as shown in Figure-4 offer an effective measures for predicting the critical wind velocity.

From the reasons mentioned above, the authors conclude that the design of flexible structures such as cable-stayed girder bridges or suspension bridges should be investigated by the wind tunnel model tests in the region located in zone of strong wind like our country.

In addition, measurements of structural damping, especially those in torsional mode, of completed bridges have an important meaning on the aerodynamic stability of structures and are desirable. Those values obtained in our test on the Onomichi Bridge were considerably low. The accumulation of values of structural damping measured on presenting structures is quite necessary.

Finally, the author emphasize that the observation on the dynamic behavior of structures under wind action contributes to the progress in wind resistant design method of them as same as it contributes to the inspection of structural safety.

References

(1) A. Hirai and T. Okubo: On the Design Criteria Against Wind Effects for Proposed Honshu-Shikoku Bridges. Symposium on Suspension Bridges, Lisbon, Nov. 1966.
(2) D.E. Walshe: The Aerodynamic Investigation for the Proposed Kniebrücke, Düsseldorf. NPL Aero Rep.1149, June 1965.
(3) D.E. Walshe and N. Narita: The Aerodynamic Investigation for the Proposed Lower Yarra Bridge. NPL Aero Spec. Rep.008, Feb., 1968.
(4) A. Hirai, I. Okauchi and T. Miyata: On the behaviour of suspension bridges under wind action. Symposium on Suspension Bridges, Lisbon, Nov., 1966
(5) T. Takata, T. Okubo and N. Narita: The performance of a wind-tunnel for bridge testing. J. of Res. Public Works Res. Inst. (unpublished)
(6) A. Selberg: Aerodynamic Stability of Suspension Bridges. IABSE. 17, Zürich, 1957.

SUMMARY

This paper describes the design considerations of the Onomichi Bridge against wind effects such as the estimation method of design wind velocity, results of wind tunnel model test, vibration tests of the Bridge and installations observing the aerodynamic response of bridge. Basing on their classification of wind effects, the authors point out the possibility of causing a cable-stayed girder bridge aeolian vibration, galloping and torsional flutter and the necessity of considering dynamic wind effects besides wind loads in the design.

RÉSUMÉ

Cet article décrit les considérations de dimensionnement faites pour le pont Onomichi contre les effets du vent: Méthodes d'estimation de la vitesse du vent, résultats d'expériences faites sur modèle au tunnel aérodynamique, tests vibratoires sur le pont et installations observant le comportement aérodynamique du pont. Se basant sur leur classification des effets du vent, les auteurs relèvent la possibilité d'obtenir des vibrations sur un pont à haubans, des galoppades et des flottements tordants. Ils montrent la nécessité de considérer les effets dynamiques à côté des charges de vent dans le dimensionnement.

ZUSAMMENFASSUNG

Der Beitrag beschreibt die notwendigen Betrachtungen über den Windeinfluss, die bei den Studien der Onomichi-Brücke gemacht wurden, wie Schätzungsmethode für die in die Berechnung einzusetzende Windgeschwindigkeit, Modellversuche im Windkanal, Vibrationstests an der Brücke und Einbauten zum Beobachten des aerodynamischen Verhaltens der Brücke. Die Autoren stützen sich auf ihre Klassifizierung der Windeinflüsse, um die Möglichkeit von Schwingungen, Galoppieren und Torsionsschlingern an seilverspannten Brücken zu betonen. Sie weisen auf die Notwendigkeit hin, bei der Bemessung neben den ruhenden Windlasten auch die dynamischen Einflüsse zu berücksichtigen.

VI

Earthquake Forces Acting on Tall Concrete Chimneys

Charges sismiques sur des chemineées en béton de grande hauteur

Erdbebenkräfte auf hohe Betonschornsteine

W.S. RUMMAN
Associate Professor of
Civil Engineering

L.C. MAUGH
Professor of
Civil Engineering

University of Michigan
Ann Arbor, Michigan, USA

SCOPE OF THE STUDY

This investigation is based on studying the response of ten actual reinforced concrete chimneys varying in height from 352 ft. to 1200 ft. The physical properties of these ten chimneys are tabulated in Table 1. Accelerograms for the three actual earthquakes tabulated in Table 2 have been selected for the analytical study. All tabulated results are based on the average values obtained from the response due to these three accelerograms. It should be mentioned that the average response due to the three earthquakes has been found to be very close to the average response due to seven strong motion earthquakes which include the three used in the paper [1].

METHOD OF SOLUTION

The modal analysis techniques are used in finding the response of a chimney to the earthquake accelerations at the base of the chimney. The steps will be stated very briefly.

1. Determine the mode shapes and the shears and moments associated with each mode. The Stodola process combined with numerical integration is used [1] , [2]. For practical purposes three or four modes of vibration will be enough.
2. The displacements, $Y(x,t)$, in the chimneys as well as the shears, $V(x,t)$, and bending moments $M(x,t)$ at any section and at any time are then computed by the following equations [2], [3]:

$$Y(x,t) = \sum_{j=1}^{n} \phi_j(x) \cdot q_j(t) \qquad (1)$$

$$V(x,t) = \sum_{j=1}^{n} V_j(x) \cdot q_j(t) \qquad (2)$$

$$M(x,t) = \sum_{j=1}^{n} M_j(x) \cdot q_j(t) \qquad (3)$$

Table 1 - Data for Chimneys Used in Study

Chimney No.	Height (ft.)	Outside Diameter (ft.)		Total Weight (kips)	Period (seconds per cycle)	E (kips/ sq.in.)	Remarks
		Top	Bottom				
1	352	23.58	30.90	4532	1.74	3500	Corbel supported brick lining
2	450	16.33	35.79	6743	2.12	3500	Corbel supported brick lining
3	534	18.67	35.03	8374	2.26	3500	Independent liner
4	622	23.33	47.26	12526	2.33	4000	Independent liner
5	707	19.98	69.14	26236	2.91	3500	Corbel supported brick lining
6	797	31.33	62.50	23392	3.29	3625	Steel liner
7	825	25.00	63.96	22970	3.44	3625	Steel liner
8	840	41.66	74.42	40976	3.33	3630	Three steel liners
9	997	33.67	83.00	42440	3.64	3625	Steel liner
10	1200	37.00	95.29	65955	4.68	3820	Steel liner

Table 2 - List of Earthquakes

Designation	Location	Date	Direction
A	El-Centro, Cal.	May 18, 1940	West
B	Olympia, Wash.	April 13, 1949	N 10° W
C	Taft, Cal.	July 21, 1952	S 21° W

in which x is the distance along the chimney, t is the time, $\phi_j(x)$ is the mode shape in the j^{th} mode and $V_j(x)$ and $M_j(x)$ are the shears and moments associated with the j^{th} mode.

The value of $q_j(t)$, which is a multiplier for the modal displacements, shears and moments, is obtained from the following equation:

$$\ddot{q}_j(t) + 2\beta\omega_j\dot{q}_j(t) + \omega_j^2 q_j(t) = \frac{-a(t)\int_0^H m(x)\phi_j(x)\,dx}{\int_0^H m(x)\phi_j^2(x)\,dx} \qquad (4)$$

in which β is the fraction of critical damping, ω_j is the frequency in radians/sec., a(t) is the acceleration of the earthquake and m(x) refers to the mass per unit length.

Equation (4) is solved numerically [1] using a third order Runge-Kutta process.

3. Although the solution of equations (1), (2), and (3) will give displacements, shears and moments at all intervals of time, yet the maximum values at any section are the only ones that are of interest. These maximum values are computed for each earthquake and the average is then obtained.

RESULTS

Base Shear

Many codes express the value of the maximum shear at the base of a chimney due to earthquakes as a function of the first mode period and of the total weight of the chimney. For this reason the maximum base shear has been computed for each chimney due to earthquakes A, B, and C and the average of these three maximums has been plotted as a ratio of base shear to total weight in Figure 1. It should be emphasized that the maximum base shear (Figure 1) is the maximum of the algebraic sum of four-mode responses.

Base Moment

A dimensionless plot of the maximum base moment, M_b, is given in Figure 2. The ratio of M_b divided by the product of the base shear times the height, H, is plotted against the first mode period of the ten chimneys considered in this study.

Shear Distribution from Accelerograms

The distribution of the maximum shears along the chimneys is presented in Figure 3 in normalized form for five of the ten chimneys considered. The numerical value of the maximum shear for any height above the base can be calculated from the value of the base shear recorded in the Figure.

Maximum Bending Moment Curves

The maximum bending moments in five of the ten chimneys are presented graphically in normalized form in Figure 4. These bending moments are the average value of the maximum moment curves due to earthquakes A, B, and C.

PROPOSED ACI EARTHQUAKE PROVISIONS [4]

1. Base shear. In the proposed chimney code of the American Concrete Institute, the base, V_b, is given by the empirical equation:

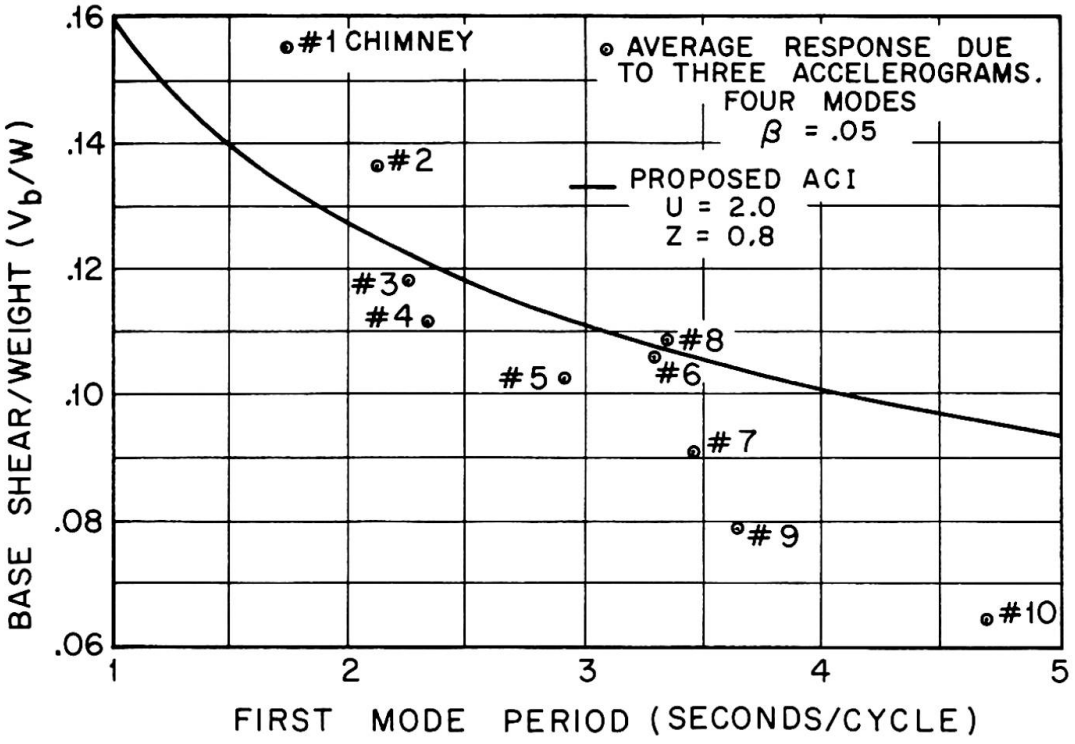

Figure 1 Base Shear/Weight Vs. First Mode Period

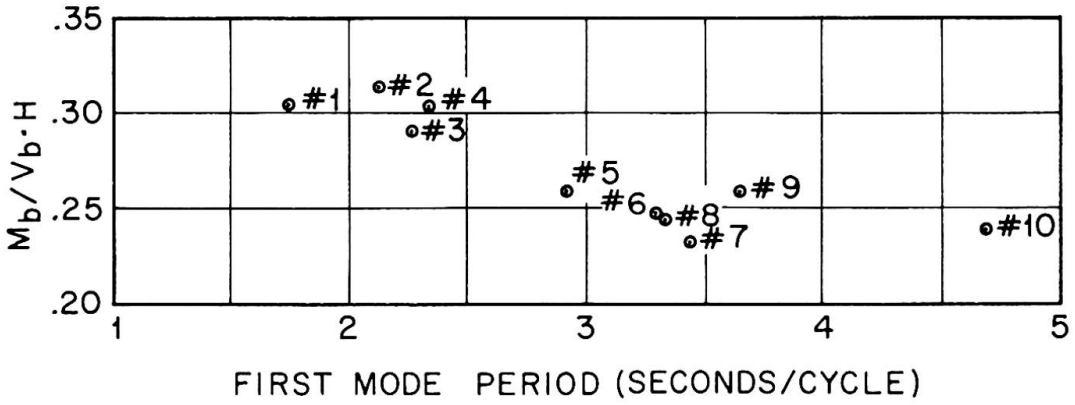

Figure 2 Base Moment/Base Shear Times Height Vs. First Mode Period

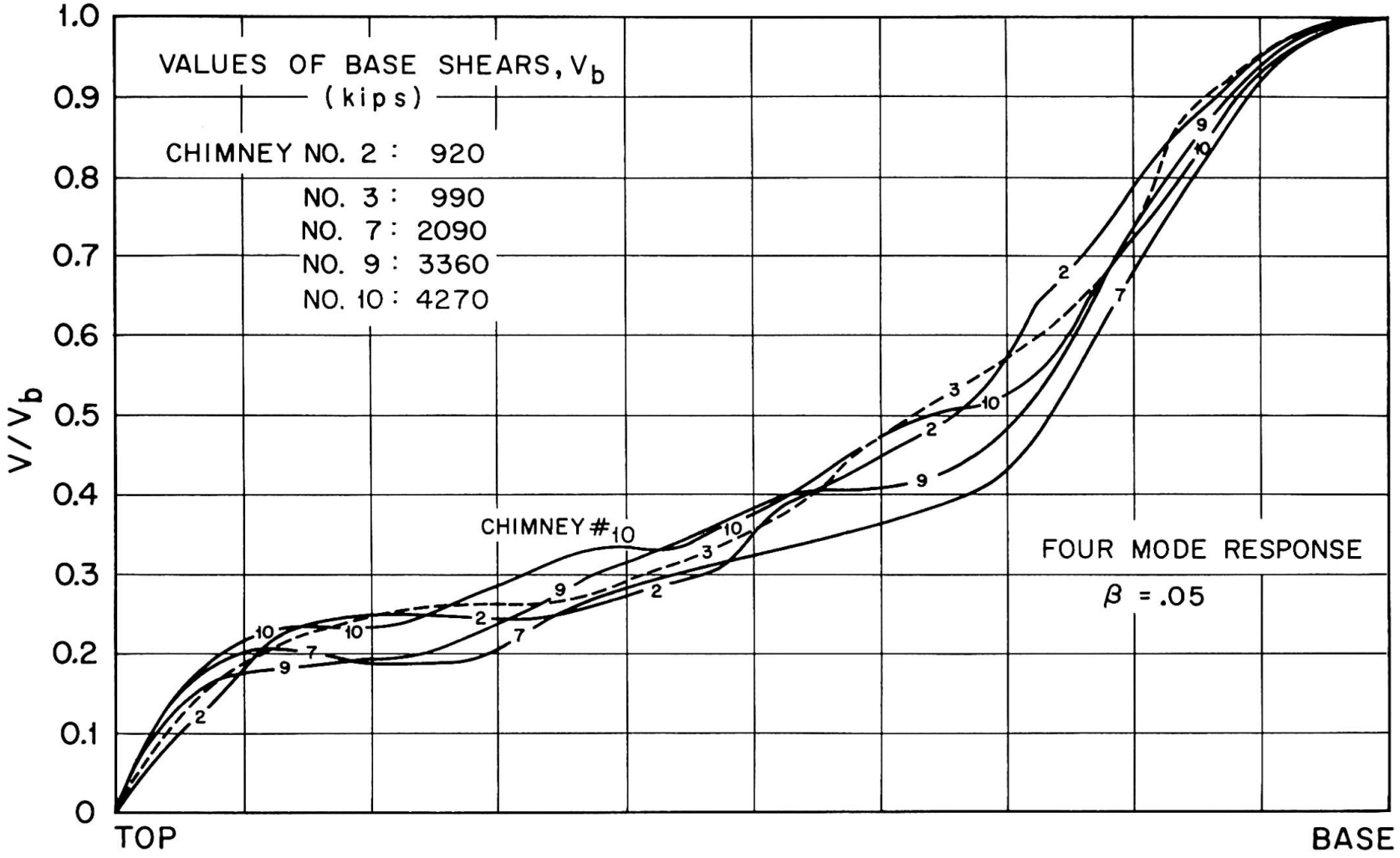

Figure 3 Normalized Maximum Shear Curves
(Average Response Due to Three Earthquakes)

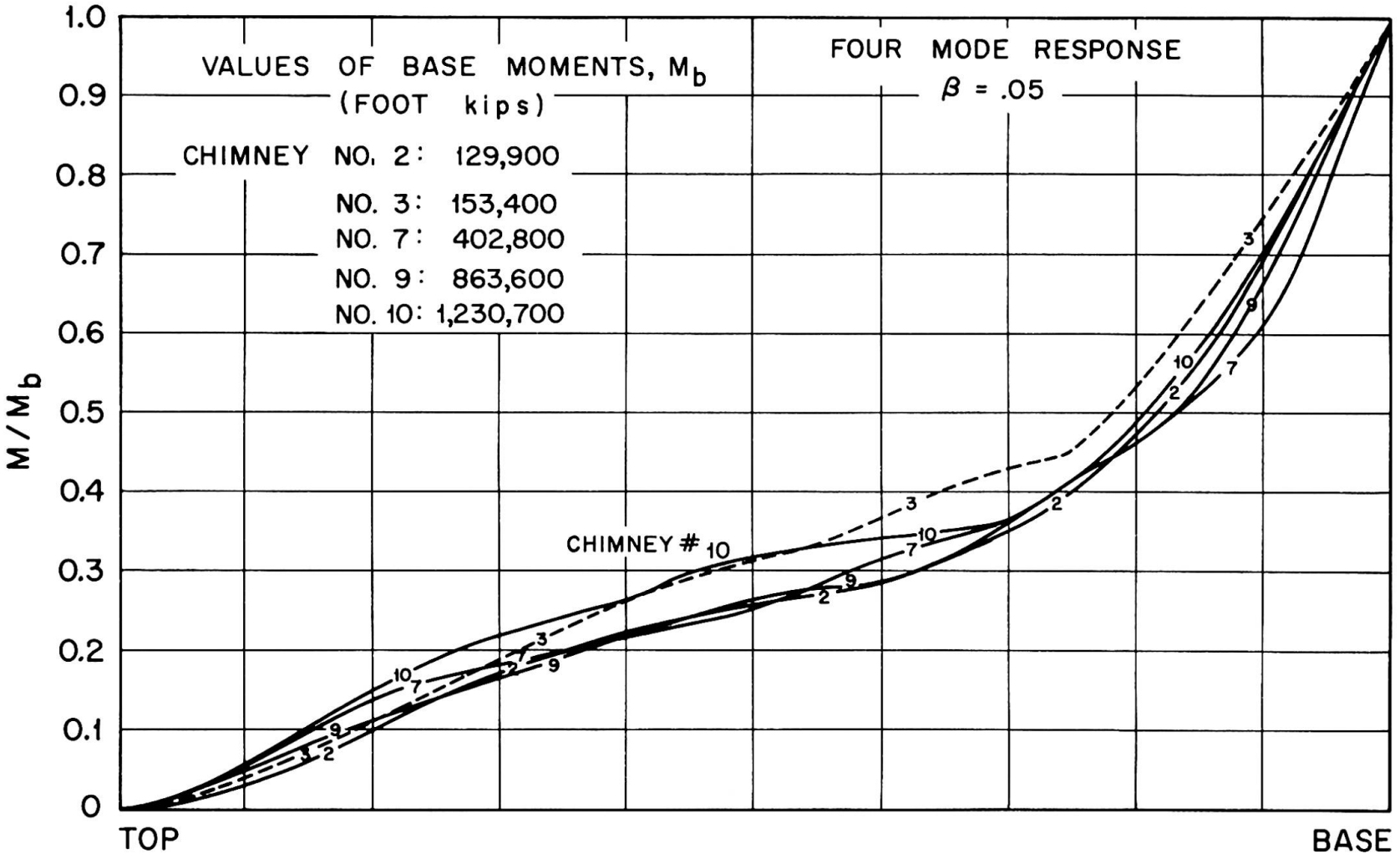

Figure 4 Normalized Maximum Moment Curves
(Average Response to Three Earthquakes)

$$V_b = ZUCW \text{ or } V_b = ZUCW_1 \quad (5)$$

where

Z = a zone factor which shall not be less than 0.30 for Zone 1, 0.5 for Zone 2 and 1.0 for Zone 3. Zones are indicated on a map for the United States Uniform Building Code.

U = Use factor varying from 1.3 to 2.0.

W = Total weight of chimney without lining

W_1 = Total weight of chimney with lining

$$C = \frac{0.1}{\sqrt[3]{T}}$$

The period, T (secs. per cycle), may be approximated by:

$$T = \frac{1.8\ H^2}{(3D_1 - D)\sqrt{E}} \cdot \sqrt{\frac{W_1}{W}} \quad (7)$$

H = Height of chimney in feet

D_1 = Outside diameter of chimney shell at base (ft)

D = Outside diameter of chimney shell at top (ft)

E = Modulus of elasticity of concrete (lbs./sq./in.)

2. Distribution of Lateral Forces. Fifteen percent of the base shear, V_b, is considered concentrated at the top of the chimney and the remainder is distributed in accordance with the following requirement:

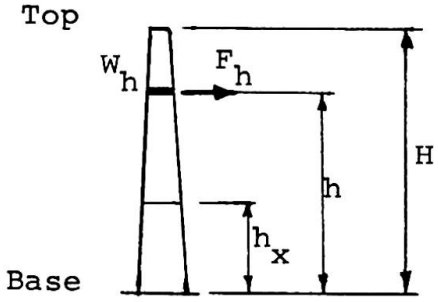

$$F_h = 0.85\ V_b \frac{w_h h}{\sum w_h h} \quad (8)$$

3. Bending Moments. The bending moment at any level as provided by the proposed code is:

$$M_x = J_x \left[0.15\ V_b (H - h_x) + \sum_{h=h_x}^{H} F_h (h - h_x)\right] \quad (9)$$

where

$$J_x = J + (1 - J)\,(h_x/H)^3 \quad (10)$$

$$J = 0.6/\sqrt[3]{T} \quad \text{(But not less than 0.45 nor more than 1.0)} \quad (11)$$

COMPARISON OF PROPOSED ACI PROVISIONS WITH THE ACTUAL RESPONSE DATA

The comparison with the proposed ACI Code will be presented under three parts:

(a) First Mode Period T

Both the computed values and those obtained from the ACI formula (equation 7) are tabulated in Table 3.

Table 3 - Comparison of the Computed First Mode Period, T (secs. per cycle), with the ACI T

Chimney No.	Height	Computed T	ACI T
1	352	1.74	1.98
2	450	2.12	2.34
3	534	2.26	3.18
4	622	2.33	2.94
5	707	2.91	3.03
6	797	3.29	3.92
7	825	3.44	4.02
8	840	3.33	3.86
9	997	3.64	4.43
10	1200	4.68	5.38

(b) The Base Shear or Total Lateral Force

The shape of the proposed ACI curve for base shear is plotted in Figure 1 to compare it with the data obtained from the mathematical analysis. This curve is a plot of Equation (5) for Z = 0.8 and U = 2.0.

(c) The Bending Moment Curves

To compare the ACI bending moment curve with the computed curve it is necessary to use the same base shear. Therefore the maximum base shear that was obtained by the actual response is distributed according to the ACI provisions and the ACI bending moment curve is obtained from such distributions by using Equation (9). These ACI moments are compared with those obtained from the actual response in Figures 5, 6, and 7 for chimneys #4, #7, and #10 respectively.

IMPORTANCE OF MAXIMUM STRESS INVESTIGATION

The non-linear variation of the stress in the reinforcing steel of a typical reinforced concrete chimney with respect to the change in the bending moment is clearly shown in Figure 8. The values given have been calculated for a cross-section with a center line diameter, d, and thickness, t, of 51.97 ft. and .833 ft. respectively. The variation is affected considerably by the percentage of reinforcing steel. Procedures for design have been presented in a previous paper by the authors [3] and will not be repeated here. However, it is recommended that a load factor of at least 1.5 times the working load bending moments be used in the maximum stress design with upper stress limits of o.8 f'_c for concrete and F_y for steel. The value of f'_c is the specified compressive strength of the concrete and F_y is the yield strength of the steel. The above remarks do not apply to an ultimate strength design.

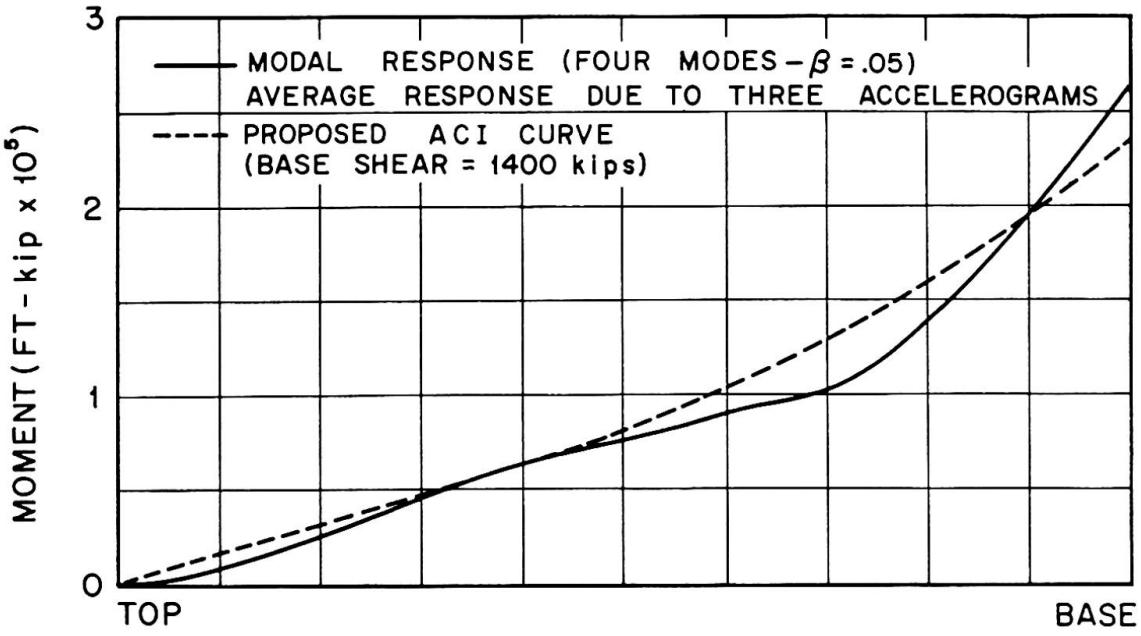

Figure 5 Comparison of Moment Curves – Chimney #4
(Actual Response Vs. Proposed ACI)

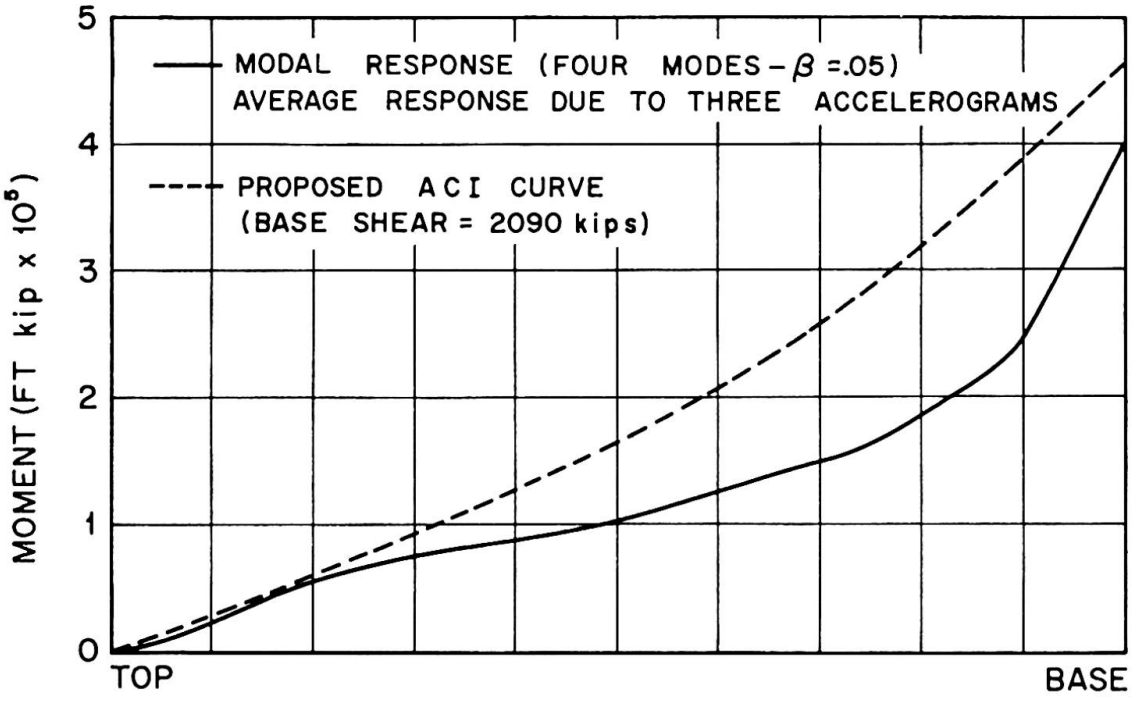

Figure 6 Comparison of Moment Curves – Chimney #7
(Actual Response Vs. Proposed ACI)

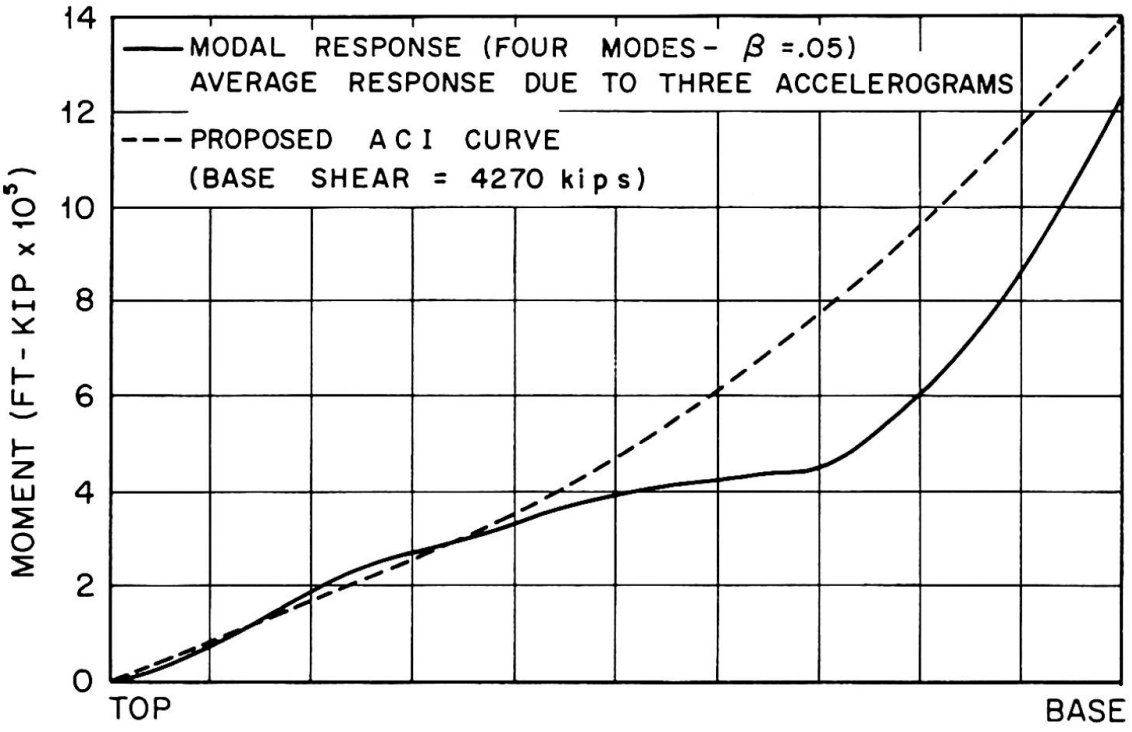

Figure 7 Comparison of Moment Curves-Chimney #10
(Actual Response Vs. Proposed A C I)

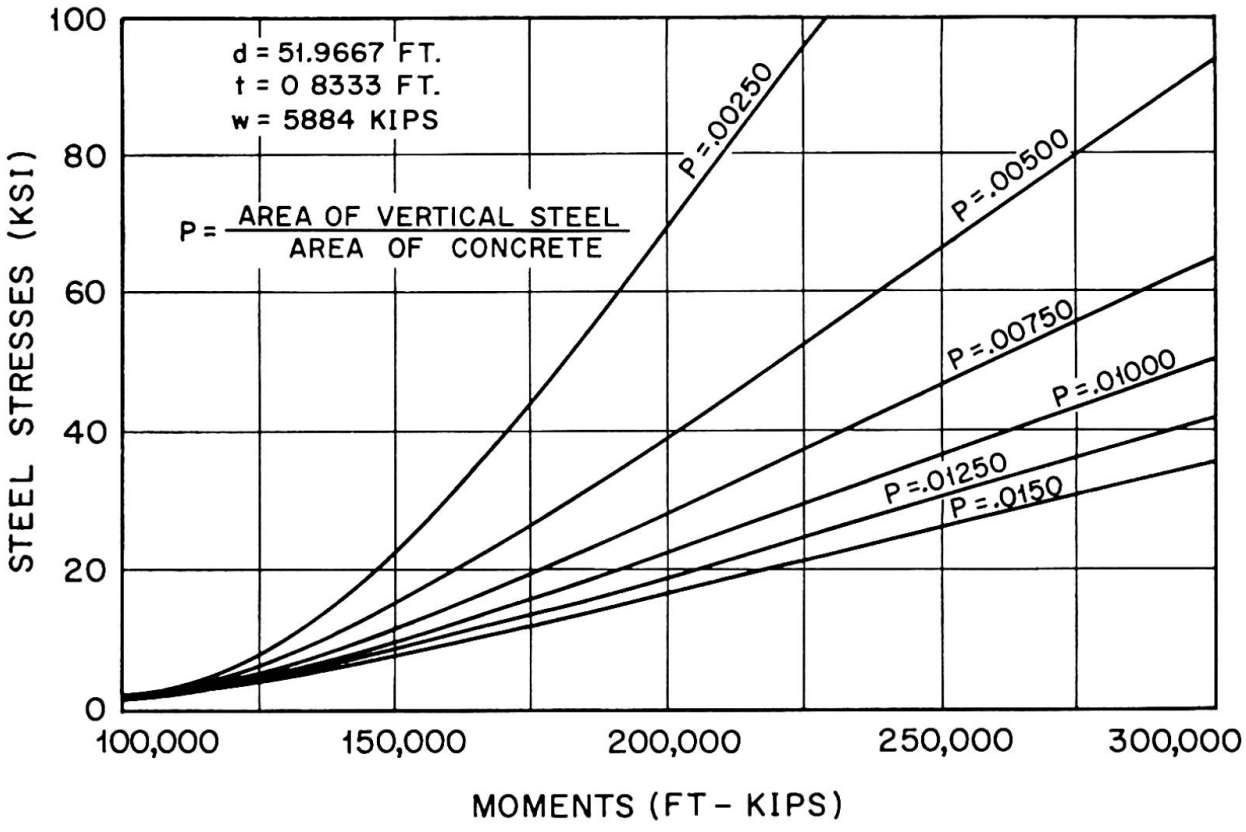

Figure 8 Steel Stresses Vs. Moments for Steel Ratios P

CONCLUSIONS

Only certain pertinent facts of reinforced concrete chimney design for earthquakes have been presented in this paper. From the data given it seems reasonable to draw the following conclusions:

1. Although procedures that are presented in chimney codes are useful for preliminary designs they are not always sufficiently accurate for a final design.

2. A response analysis in which from three to seven carefully selected accelerograms are used is recommended for investigating the final design.

3. Both a working stress and a maximum stress investigation of the stresses should be made.

4. Although not discussed in this paper maximum shearing stresses should also be determined. These stresses may occur in the upper one-fifth of the chimney.

REFERENCES

1. Rumman, Wadi S., "Earthquake Forces in Reinforced Concrete Chimneys", Journal of the Structural Division, ASCE, Vol. 93, No. ST6, Proc. Paper 5650, December 1967, pp. 55-70.

2. Rumman, W. S., "Vibrations of Steel-Lined Concrete Chimneys," Journal of the Structural Division, ASCE, Vol. 89, No. ST5, Proc. Paper 3661, Oct., 1963, pp. 35-63.

3. Maugh, L. C., and Rumman, W. S., "Dynamic Design of Reinforced Concrete Chimneys", ACI Journal, Proceedings, Vol. 64, No. 9, September, 1967, pp. 558-567.

4. These provisions have been approved by ACI Committee 307 in March 1968 but as yet have not been finally approved by ACI. It is expected that they will be published in the American Concrete Institute Journal in September 1968 as a Proposed Code.

BIBLIOGRAPHY

1. Housner, G. W., and Keightley, W. O., "Vibrations of Linearly Tapered Cantilever Beams", Journal of the Engineering Mechanics Division, ASCE, Vol. 88, No. EM2, Proc. Paper 3101, Apr., 1962, pp. 95-123.

2. Berg, G. V., and Housner, G. W., "Integrated Velocity and Displacement of Strong Earthquake Ground Motion," Bulletin, Seismological Society of America, Vol. 51, No. 2, Apr., 1961, pp. 175-189.

3. Alford, J. L., Housner, G. W., and Martel, R. R., "Spectrum Analysis of Strong-Motion Earthquakes," California Institute of Technology, Pasadena, Calif., Aug., 1951.

4. Housner, G. W., "Earthquake Resistant Design Based on Dynamic Properties of Earthquakes," Journal, American Concrete Institute, Vol. 28, No. 1, July, 1956.

SUMMARY

This paper is primarily concerned with presenting some results of the response of actual reinforced concrete chimneys to recorded accelerograms of actual earthquakes. The results are based on an elastic response using the first four modes with a damping coefficient of .05 of critical.

The analytical results are then compared with those proposed by the American Concrete Institute Code (1968) for Earthquake Design of Chimneys. The provisions of this Code are summarized in the paper.

The last part of the paper emphasizes the necessity of designing reinforced concrete chimneys for both a working stress and a maximum stress condition as the stresses, especially in the steel, do not vary linearly with the bending moments.

RÉSUMÉ

Cette rédaction présente quelques résultats de réactions de cheminées en béton précontraint sur les accélérations mesurées de plusieurs tremblements de terre.

Ces résultats analytiques sont comparés avec le Code de l'Institut Américain du Béton, dont les prescriptions sont résumées ici. Enfin, la rédaction démontre la nécessité de dimensionner les cheminées en béton précontraint et pour une charge de service et pour des conditions de charge maximales, vu que les tensions ne varient pas linéairement avec le moment, surtout dans l'acier.

ZUSAMMENFASSUNG

Dieser Beitrag ist hauptsächlich bemüht, einige Ergebnisse zu zeigen, die man aus der Aufzeichung der Beschleunigungen von Erdbeben als Wirkung auf Stahlbeton-Schornsteine erhält.

Die Ergebnisse stützen sich auf elastische Bestimmung, die ersten vier Fälle benützend, mit einem Dämpfungsbeiwert von 0.05 des kritischen. Die analytischen Ergebnisse sind dann mit denjenigen verglichen worden, die durch die Normen des amerikanischen Betoninstitutes für den Entwurf von Schornsteinen bei Erdbeben vorgeschlagen wurden. Der letzte Teil des Beitrags betont ausdrücklich die Notwendigkeit, Stahlbetonkamine für Gebrauchs- und maximale Spannungsbedingungen zu entwerfen, da die Spannungen, insbesondere jene des Stahles, nicht linear mit dem Biegemoment ändern.